Effects of Low Intensity Light Therapy On Cancer Cells: *in vitro* Evaluation

A thesis submitted in fulfillment of the requirements for the degree of

Doctor of Philosophy in Engineering

PANTEA PEIDAEE

B.Sc, M.Eng, M.Sc., M.Eng

School of Electrical and Computer Engineering

College of Science, Engineering and Health

RMIT University

February 2014

Abstract

According to statistics from World Health Organization (WHO), cancer is the second cause of death in developed countries and top ten cause of death in developing countries. The economic impact of cancer on society due to human toll and associated medical costs is disproportional and depends on demographics and medical facilities patients have access to. Despite significant breakthroughs in medical technologies, advanced treatments and research efforts to combat cancer, burden of cancer remains devastating on human life.

Recent advancements in medical science and health care technologies, and development of innovative medical instruments proved to enhance cancer treatment; however, there is still no substantial slowdown in mortality rate and treatment costs. The significant socio-economic impact of cancer and shortfalls of currently available conventional treatment methods motivate scientists and engineers to scavenge for novel cost-effective cancer treatment approaches with less severe side-effects and enhanced efficacy.

In most cases, cancers arise from genetic alterations in the DNA of a somatic

cell. Small coding sequences along a strand of DNA, genes, control all functions of human body. The genes are codes that "tel" a cell how to make different proteins, which are building blocks of cells that control their behaviour. Although all genes are present in all cells of a body, not all are active at the same time. Genes that control cell growth are active at certain times of life. Proto-oncogene is one of those genes that have many different functions in a cell; some provide signals that lead to cell division, while others regulate programmed cell death (apoptosis). An oncogene, a permuted proto-oncogene, contributes to the growth of a tumor. In order to control oncogenes, the correlation between its coding sequences and its biological activity needs to be unravelled. Hence, there are numerous attempts to model this complex correlation. Among these models, the Resonant Recognition Model (RRM) has demonstrated and proved to be a reliable computational approach to modelling structure-function relationships between biomolecules (proteins and DNA) as well as their interaction with external electromagnetic fields (EMFs). The RRM theory proposes that an external electromagnetic field at a particular activation frequency will produce resonant effects on a protein biological activity, and this activation frequency can be determined computationally. According to the RRM model implementation for oncogene and proto-oncogene proteins, wavelengths of external irradiation in the range of 3500nm-6500nm will demonstrate effects on the functionality of oncogene proteins.

External electromagnetic radiation (EMR) of low intensity light mainly in the

visible and near infrared wavelengths demonstrated to induce therapeutic effects on various medical conditions, including wound healing. It was shown that the induced EMR effects are dependent on a particular wavelength, intensity and duration of EMR exposures. There are studies that showed that applied EMR in the visible and infrared light range can modulate protein and cellular activity.

This research project evaluates experimentally cytotoxic effects of external exposures of low intensity light in the wavelength range of 3500nm to 6500nm (the range predicted computationally by the RRM) on selected cancer and normal cells. For this purpose, an exposure device is designed and fabricated to irradiate cells at the selected far infrared wavelength range. The exposure system is used for external *in vitro* irradiation of human and animal normal and cancer cells. The effects of applied irradiation are evaluated quantitatively and qualitatively, with the findings are being presented and discussed in the thesis. The structure of this thesis is as follows.

Chapter 1 - comprehensive overview of cancer: its development and effects on human life; socio-economic impact of cancer on society; cell cycle and cell cycle control mechanisms; interruptions and erroneous processes in cell cycle progression that lead to cancer development; Current conventional treatment methods and their long- and short-term side effects; and finally complementary and novel cancer treatment methods.

Chapter 2 - a comprehensive literature review relevant to the project scope is presented : various applications of low intensity light therapy and other similar new medical radiation techniques are described.

Chapter 3 - exposure system design and development: different design proposals including their limitations due to imposed experimental conditions are presented and discussed. After selection of the appropriate design for the device fabrication, the enforced experimental limitations from biological and electrical point of view are discussed in this section. Finally, the scope and boundaries of this project are clearly indicated.

Materials and methods used in this project are explained in Chapter 3. The choice of culture medium, cell types, exposure LEDs, experimental set ups and quantitative and qualitative cell-based assessment assay procedures are also described in details.

Chapter 4 - presents the quantitative analysis of experimental evaluation of different EMR exposures on selected cancer and normal cells. The results obtained from implementation of the quantitative cell based assays (LDH, MTT, PrestoBlue^{TM}) on animal and human cancer and normal cells are presented and discussed.

Chapter 5 - presents the results of far infrared exposures on cell morphology of cancer and normal cells. These qualitative assessments are conducted by phase

contrast microscopy and confocal laser scanning microscopy (CLSM) on animal and human cancer and normal cells.

Future work and further possible extensions of this experimental work is recounted briefly in Chapter 6.

Finally, Chapter 7 - summarizes and concludes the findings of the experimental *in vitro* evaluations of the effects of low intensity light radiation on animal and human cancer and normal cell lines.

Declaration

I, Pantea Peidaee, declare that the PhD thesis entitled "Effect of Low Intensity Light Therapy On Cancer Cells: *in vitro* Evaluation" is no more than 100,000 words in length including quotes and exclusive of tables, figures, appendices, bibliograph, references and footnotes. Except where due acknowledgement has been made, the work is that of the author alone; the work has not been submitted previously, in whole or in part, to qualify for any other academic award; the content of the thesis is the result of work which has been carried out since the official commencement date of the approved research program; and, any editorial work, paid or unpaid, carried out by a third party is acknowledged.

PANTEA PEIDAEE

12/02/2014

Acknowledgements

I would like to acknowledge and appreciate the invaluable contributions of the following individuals through out these four years of my PhD studies.

- My senior supervisor Dr. Elena Pirogova, for her direct supervision, support and assistance that helped me to successfully complete this project,
- My second supervisor Dr. Ravi Shukla who helped me immensely in tissue culture experimentation of this project,
- My husband, Amirabbas Rezaee, who has always been there for me academically and emotionally through my PhD roller coaster ride,
- My parents, especially my mother, who taught me to be tough and enduring individual during difficult times and the most important of all, to never give up my goals, and
- All my great friends at RMIT University, who morally supported me through out these years.

I would also like to thank:

- RMIT University for providing me with the RMIT Scholarship;
- School of Electrical and Computer Engineering, RMIT University for financial support purchasing materials and consumables required for my experiments and travel funding for conference attendance;
- School of Applied Sciences and Medical Sciences, RMIT University, Bundoora Campus for their facilities used during my experimental work;
- RMIT Library for providing valuable books, journal publications and other learning materials.

Publications

Journal Publications:

- **Peidaee, P.**, Almansour, N., Shukla, R. and Pirogova, E. (2013). 'The Cytotoxic Effects of Low Intensity Visible and Infrared Light on Human Breast Cancer (MCF7) cells', *Computation Structural Biotechnology Journal (CSBJ)*, 6(7), e201303015.

- **Peidaee, P.**, Almansour, N., Shukla, R. and Pirogova, E. (2013). 'In Vitro Evaluation of Visible, Near and Far Infrared Light Radiation on Cancer and Normal Cells', *G.MD-Medical Data*, 5(1), 2013, pp 007-013.

Peer-Reviewed Conference Papers:

- Hu, J., **Peidaee, P.**, Elshagmani, E., Istivan, T. and Pirogova, E. 2013, 'The Effects of Synthetic Azurocidin Peptide Analogue on Staphylococcus Aureus Bacterium', In *13th IEEE International Conference on BioInformatic and BioEngineering (BIBE)*, Chania, 10-13 November.

– **Peidaee, P.**, Istivan, T., Shukla, R. and Pirogova, E. 2013, 'Experimental Evaluation of Cytotoxicity Effects in Cancer and Normal Cells Exposed to Far Infrared Radiation', In *The 33rd Proceedings of Progress in Electromagnetic Research Symposium (PIERS)*, Taipei, Taiwan, 25-28 March 2013.

– **Peidaee, P.**, Shukla, R. and Pirogova, E. 2013, 'Influence of Far Infrared Radiation on cytotoxicity of Human Breast Cancer (MCF7) cells: experimental evaluation', In *Proceedings of International Work-Conference on Bioinformatics and Biomedical Engineering (IWBBIO)*, Granada, 18-20 March.

– **Peidaee, P.**, Cosic, I. and Pirogova, E. (2012). 'Low Intensity Light Therapy Exposure System', In *World Congress on Medical Physics and Biomedical Engineering(IFMBE Proceedings)*, Beijing, 26-31 May, Volume 39, pp 1648-1651.

Journal Publications in Preparation:

– **Peidaee, P.**, Almansour, N., Shukla, R. and Pirogova, E. Determination of Cell Cytotoxicity Effect of Low Intensity Light on Human Breast Cancer cell line using the MTT Assay and Confocal Microscopy, IEEE Transaction on Biomedical Engineering, 2014.

– **P. Peidaee**, N. Almansour, R. Shukla and E. Pirogova. In vitro Analysis of

Selected Low Intensity Light Exposure Wavelengths on Murine Melanoma (B16) Cells, Annals of Biomedical Engineering Journal, 2013, Submitted.

Contents

List of Figures

List of Tables

Chapter 1

Introduction

The aim of this project is to experimentally evaluate a theoretical hypothesis proposed within the Resonant Recognition Model (RRM) [1–3], which states that external electromagnetic radiation (EMR) of far infrared (3500nm to 6500nm) wavelengths would induce cellular apoptotic effects in cancer cells that will lead to therapeutic effects in cancer. This project attempts to evaluate the validity of the proposed hypothesis in the controlled experimental conditions. Hence, *in vitro* irradiation of normal and cancer cells at the proposed wavelengths range is conducted for different cell lines and different regimes of exposure. The effects of EMR on cancer and normal human and animal cell lines are measured using three standard cell-based quantitative assays along with two qualitative assays. Moreover, for the completeness of the analysis, irradiation of cells at other wavelengths outside the proposed far infrared range is conducted as well with the induced effect being compared and discussed.

To achieve this goal an exposure device is designed to bias the far infrared range LEDs to perform at their optimum efficiency. LEDs working at the optimum efficiency, radiate the electromagnetic radiation at the required wavelengths with the maximum nominal optical power. The exposure device is then used to radiate a number of animal and human cancer and normal cells with the proposed far infrared LEDs as well as other LEDs in the visible and near infrared range. All experiments are conducted inside the incubator to be as close as possible to the conditions of a living organism.

The experimental work in this project thrive to test the theoretical hypothesis proposed by RRM approach implementation [1–3]. The ultimate aim of this project is to test an alternative approach toward cancer treatment. Furthermore, this novel approach might be able to pave the way for development of a non-invasive and cost-effective cancer therapy method that is not only effective in cancer treatment but also addresses the limitations of the current cancer treatment methods in terms of cost of treatments.

The chapter 1 starts with the definition of cancer and different classification. After that, a brief history regarding the first appearance of cancer in human's ancient literature will be narrated. Then, a brief insight into cancer causes, which can result in development and spread of cancer in human-beings, is provided. Subsequently, statistics of cancer regarding its diagnostics and mortality rate as well as its impact on our societies economically and socially is explored. In order

to propose a novel cancer treatment method, a comprehensive insight into the development and progression of cancer is critical in understanding of how cancer develops and spread biologically and what can be done to break this vicious circle. After that, deterrent procedures and check points that human body has in order to inhibit or combat the progression of cancer is presented.

1.1 Definition of Cancer

Like all other living organisms, human body consists of cells. The average number of cells that make our body is approximately about 60 trillion cells [4]. Genes, inside the nucleus of a cell, are responsible for this tightly regulated cell reproductions and cell deaths [4]. Out of billions of cells that are created each day, there are sometimes abnormal cells being created. Typically, these abnormal cells are detected, repaired or eliminated by the immune system [5]. This process is very routine for human body and it is believed that everyone can develop precancerous cells during their life time but only less than half of human population develop cancer [4].

Generally, damaged cells stop reproducing on their own and they would form a tiny, harmless lumps. However, there is a chance that these faulty cells could not be repaired or eliminated. Long before the appearance of a tumor (lump) that can be tested and diagnosed by physician/oncologist, cancer cells start with

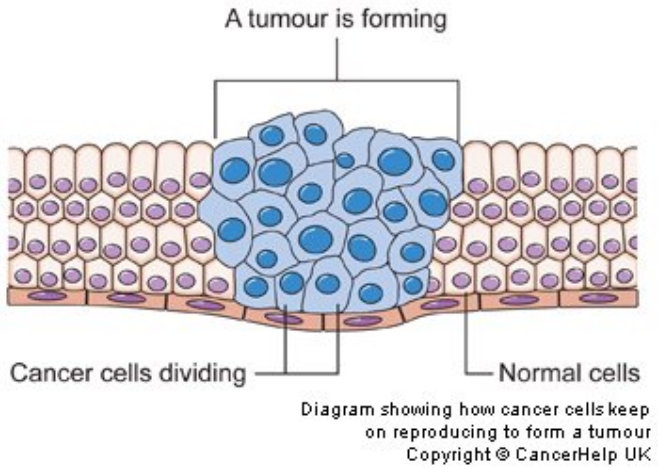

Figure 1.1: Development of Cancer [6]

changes in one cell or a small group of cells. Then, they grow uncontrollably into aggressive tumors that is being called cancer [4]. These tumors can affect the health of an individual by blocking the digestive system or blood vessels, by pressing against nerves or even by releasing hormones that can affect normal function of the body [4].

Tumors are generally categorized into two forms: benign (noncancerous) and malignant (cancerous). Benign tumors are those that usually grow quite slowly and do not spread to other parts of the body. These tumors usually are covered by normal cells. Benign tumors become problematic only when they grow very large, become uncomfortable by taking space or pressurizing body organ, or when they release hormones that interfere with normal body works. In contrast to benign tumors, malignant tumors grow rapidly, damage and destroy surrounding normal tissues and spread throughout the body [4].

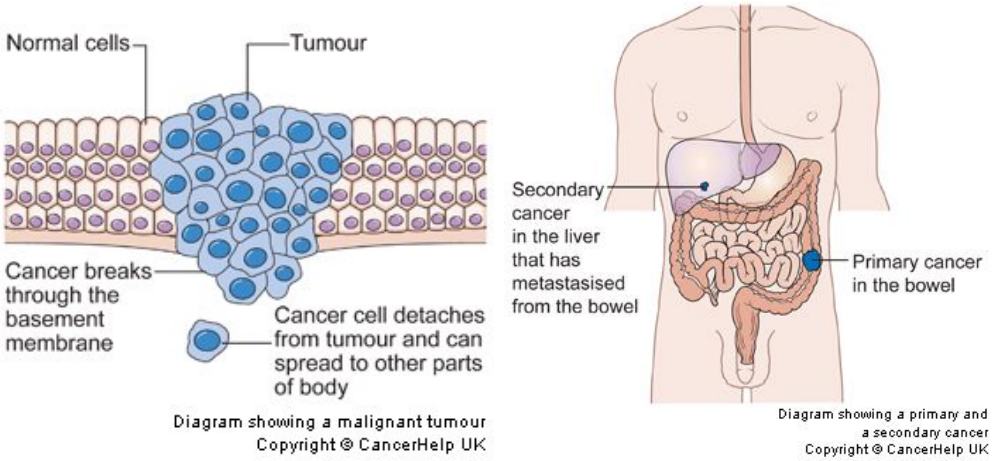

Figure 1.2: Development of Primary and Secondary Cancer [6]

The spreading ability of cancer cells makes it very aggressive and harmful. The tumor that appeared first is called "primary tumor". These cancerous cells can travel through blood (circulatory system) or lymphatic system to form secondary tumors. Malignant tumors can be locally invasive, so they can only damage surrounding tissues and turn normal cells into cancer cells. Or, the metastatic form of tumors, which means that faulty cancerous cells spread around and invade other organs and tissues of the body to form tumors all over the body [5, 6].

Cancers are classified into different categories according to the type of fluid or tissue they originate from or according to the body organ, in which they develop first. There are five broad classifications of cancers depending on the tissue and blood categorization [5].

Carcinoma is a type of cancer found in epithelial body tissues that cover or line surfaces of organs, glands or body structures. These type of cancers account

for 80 to 90 percent of cancer cases.

Sarcoma is a malignant tumor, which grows in connective tissue type cells such as fat, cartilage, muscle, tendons, and bones. This type of cancers usually affect young adults.

Lymphoma is originated from the nodes or glands of the lymphatic system or in organs such as brain and breast. Lymphoma has two categories of Hodgkin's and non-Hodgkin's lymphomas.

Leukemia, which is also known as blood cancer, is a cancer of bone marrow. This type of cancer inhibits bone marrow from the production of normal red and white cells and platelets which are needed to resist infection and prevent anemia respectively.

Myeloma develops in plasma cells of bone marrow. When myeloma cells are collected in one bone and form tumor, it is called plasmacytoma. And, the collection of myeloma cells forming many tumors in many bones is called multiple myelomas.

Despite distinctive characteristic differences exhibited in various categories of these group of diseases, *in vivo* and *in vitro* studies have shown that certain traits are common along all types of cancer cells. The main common characteristic of cancer cells is uncontrolled growth in the body or on culture dish [7]. Genetic

changes in DNA promote cell proliferation uncontrollably, which will result in generating malignant tumors that invade surrounding healthy tissues.

The other common characteristic of cancer cells is morphological changes in cytoplasm, which make cancer cells less adhesive to other cells and non-cellular substrates. This loss of adhesiveness allows cancer cells to detach from a tumor mass and move to other organs of the body. If these tumors do not spread through other organs of body, they usually can be removed by surgical procedure. However, malignant tumors tend to separate from the parent mass and spread to distant sites where they establish the lethal tumors that are no longer removable or curable [7].

Another common feature of cancer cells is the fact that they are not following the apoptosis process, a natural cell cycle process destroying damaged cells. In normal condition, when chromosome content of normal cells becomes disturbed, a signaling pathway is usually activated for self-destruction (apoptosis) of a cell. However, this process is not followed in cancerous cells. Generally, the chromosomes' content of cancerous cells are highly disturbed but this natural self destruction process does not take place in these cells.

One more common feature of cancer cells is ignoring neighboring cells signal and moving over to other cells. Thus, they form a much higher cell density than normal cells. When normal cells are surrounded by other cells, they stop their

proliferation. They do not move over to another cell; therefore, a mono layer on the bottom of a culture dish is formed.

The formation of blood vessels is another common characteristic of cancer cells. These vessels provide a steady supply of oxygen and nutrient to the faulty cells. Thus, they are responsible for the growth of cancer cells because the absence of these nutrition supplies can stop or slow down the spread of cancer cells. In general, the circulatory system grows a network of new blood vessels into and around the tissues during growth or repair process. This process is called angiogenesis. Cancerous cells employ similar technique and send chemical signals called activator molecules to the neighboring healthy cells to promote the growth of new blood vessels.

To combat development and spread of cancer, human body has several defensive mechanisms. Human natural defensive systems to fight against cancer are lymphatic system, leukocytes (white blood cells), and antibodies (activated when immune system detect antigen, and Natural Killer (NK)) [4]. However, cancer develops when these natural defensive mechanisms are not performing properly.

1.2 History of Cancer Diagnosis

Recorded history shows that cancer has always been part of human and animal existence. The earliest evidence of cancer is found in fossilized bones and human

mummies. For instance, a type of bone cancer is detected in human mummies of ancient Egypt. The oldest discovered cancer description document dates back to 3000 BC in Egypt. This manuscript is called Edwin Smith Papyrus and is part of Egyptian textbook on surgery. This document describes 8 cases of tumors and it says that "There is no treatment" [5].

However, Greek physician Hippocrates, the "Father of Medicine", is the first physician who named this disease. He described non-ulcer forming tumors as "carcinos" and ulcer forming tumors as "carcinoma". The name means "Crab" in Greek which describes the finger-like spreading of cancer cells. Later on, a Roman physician, Celsus, is the first physician who coined the name "cancer" instead of carcinos, a Latin word for crab. After that, another Roman physician named cancer as "oncos" (Greek for swelling), which is now used for the specialists of cancer, oncologists [8].

Prior to twentieth century revelation, tumors were perceived as foreign viruses that are taken root in the body of affiliated patients similar to HIV and Flu mechanism. The biological revolution of mid twentieth century triggered by Watson and Crick's discovery of the DNA double helix, changed the perception of biological processes and their underlying science [5]. The discipline of molecular biology that starts its existence following mid-twentieth century discovery explained intimate details of genetics and heredity. This molecular foundation explained how cells grow and divide, how the tissues develop under the control of specific genes

and how does genetic constitution of a cell and organism determine its appearance and functionality. Without this foundation, modern cancer research could not be developed this far [8].

According to advancement of biological science in mid twentieth century, unrestrained growth of cancer cells form a lump of tissue called a tumor. Except leukaemia, all other types of cancer form tumors [5, 8]. This new knowledge also revealed that tumors, like normal tissues, are composed of masses of cells. In contrary to earlier virus approach for cancer, it is proven now that tumors are often derived from normal cells rather than invading from outside of the body. Tumors are cells that lost the ability to assemble and create tissues of normal form and function. Cancer is considered a genetic disease of cellular control mechanism. It is defined by a group of genetically permuted cells forming invasive tumors, which ceased to respond to normal growth control signals. Furthermore, cancer tumors tend to travel across patient's body and reside in a new position at quite a distance from where the tumor first appeared.

1.3 Cancer Causes

An in-depth view along a strand of DNA reveals small coding sequences called genes along a strand of DNA (often referred as "molecule of life"). All the functions of body are led by genes. Genes are the codes that tell a cell how to make

different proteins that control cell behavior [9]. Thus, anything that damages cell's DNA can potentially lead to tumor development. In cancer cells, some of these genes found to be mutated, so they cannot perform their normal functions. In order to develop cancerous tumor, a number of genes in a cell need to be damaged [6].

Cancer arises from genetic alterations in the DNA of a somatic cell. These genetic mutations in DNA result in out of control cell behavior and lead to tumors. Genetic mutations sometimes happen in the germline, which result in inherited cancers or predisposition to cancer. Most often these mutations occur in somatic cells. These somatic mutations are accumulated over lifetime. In general, cancers are caused by multiple genetic mutations. Currently, there are 70 genes associated with germ line mutations and 342 genes associated with somatic mutations [10, 11].

To shed some light into the cause of gene mutation, contributing factors are examined and investigated. These factors are age, human habits and lifestyle, medical history, genetic heredity factor, environmental conditions, hormonal and virus influences, past treatments and other external factors.

The following risk factors and mechanisms are considered to contribute to cancer development:

1. Age is considered as the largest risk factor for cancer since majority of cases

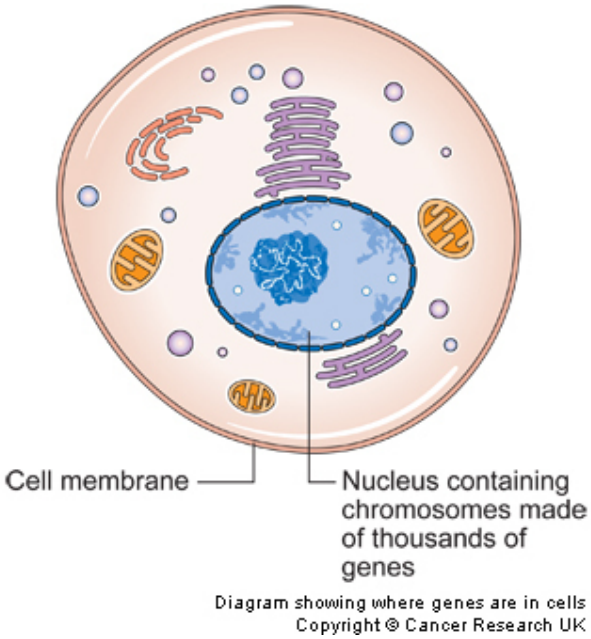

Figure 1.3: Structure of a Cell [6]

of cancer are diagnosed in people over 65 years old.

2. The other major risk factor is lifestyle. High-fat diet, working with toxic chemicals and smoking are the most recognized lifestyle elements contributing to cancer development. In fact, tobacco was the first recognized contributing factor for gene mutation. The findings by a clinician in London came hundred fifty years after the first trials of tobacco by Japanese scientist. He classified tobacco as a carcinogen (a substance believed or known to cause cancer in human) [4, 5].

3. The next contributing risk factor is family history, inheritance of genetic mutations. Genetic factors play important role in childhood cancers. However, genetic predisposition does not necessarily mean that an individual

will develop a certain type of cancer. It was found that genetic factor contributes to upto 10% of all cancers. The other 90% are caused by lifestyle and environmental factors [4].

4. The existence of some genetic disorder is another risk factor. For instance, Wiskott-Aldrich and Beckwith-Wiedemann syndrome are known to alter the immune system. One theory suggests that when cells in the bone marrow, the stem cells, become damaged, they make abnormal or cancer cells [5].

5. Another contributing factor can be exposure to certain viruses. This does not mean that cancer can spread from person to person but those infected with these diseases have increased risk of developing cancer later on. Some of these viruses are human papilloma virus (HPV), Hepatitis B and C viruses, Epstein-Barr virus, and HIV virus. The latter two viruses have been linked to development of Hodgkin and non-Hodgkin lymphoma in childhood cancers [5, 6].

6. Environmental exposure to carcinogen chemicals and substances are believed to cause cancer. Till date, pesticides, fertilizers and possibly power line are considered to have direct effect in development of childhood cancers [5]. The search for the environmental causes of genetic mutation in cancer led to the classification of many other specific substances as carcinogens such as coal tars and their derivatives (i.e. benzene), some hy-

drocarbons, aniline, asbestos, and ionizing radiation sources including sun, radon gas and X-ray [8]. As of 2012, more than 100 chemical, physical and biological carcinogens were identified by World Health Organization's International Agency [12]. Moreover, high dosage of chemotherapy and radiotherapy may contribute to the development of a second malignancy later in life [5].

Even though several hypotheses are considered to contribute to DNA permutation, there is no concrete single reason identified for gene mutation that result in cancer development. A risk factor does not necessarily cause the disease, but it may, in fact, increase the chances of cancer incidents since it makes the body less resistant to it [13].

1.4 What are the impacts of cancer?

Cancer has maintained its position as the second cause of death in developed countries and among the top ten cause of death around the world [7, 13, 14]. One out of every two men and one out of 3 women develops cancer in their lifetime based on American Cancer Society data in 2008 [7, 13]. Thirty years after the declaration of the global fight against cancer, the most recent mortality and incident rates of cancer in 2008 do not reflect any significant slow down in these numbers. According to statistics, every year 12.7 million people are diagnosed

with cancer and 7.5 million dies from the disease [14, 15].

American cancer society provides comprehensive information on financial and economic impact of cancer on society. The economic burden of cancer on a society is assessed in two categories of direct medical costs and indirect costs. Indirect medical cost is the cost of productivity loss due to premature death. In the United States alone, the cost of direct medical cost in 2008, according to National Institute of Health, was $77.4 billion and indirect mortality costs associated with cancer was $124 billion [16]. All in total, the monetary burden of cancer on American health system and people was $201.5 billion for that year alone.

A joint study of American Cancer Society and LIVESTRONG [17] estimates the economic toll of cancer as the highest economic loss. This comparison conducted on all causes of death globally, including communicable, non-communicable diseases. The research is based on death and disability from 17 forms of cancer in 188 nations who are member of World Health Organization (WHO). According to the 2010 report [18], the total global economic impact of cancer due to premature death and disability is calculated to be $895 billion in 2008. This figure is 1.5 percent of world's gross domestic product (GDP). This figure for financial loss due to cancer is 19 percent higher than a loss caused by the heart disease. According to statistics, heart disease with the cost of $753 billion is the second leading cause of death [17]. The cancer treatment costs mentioned in these stud-

ies exclude direct medical cost associated with cancer treatment. Inclusion of cancer direct medical costs further increases its overall economic impact [17].

At human level, cancer is taking an enormous human toll around the world and this number is on the rise for developing and third world countries. According to the report [16], every year in the United States 580,350 individuals dies from cancer. Majority of these people who develop cancer do not have proper health insurance. Moreover, they develop cancer later in their life time which brings immense hardship and affect their quality of lives [16]. On the global scale, death and disability from lung, colon and breast cancer has the highest economic loss, while other types of cancer impose considerable economic burden especially on underdeveloped countries.

Apart from death and disability resulted from cancer, the profound social psychological and financial pressure that individuals and families go through should not be ignored. These conditions are especially more profound in developing and underdeveloped countries where loss of income due to illness or death of family member quickly undermines family's finances. According to the findings of the American Cancer study and other similar studies, cancer is projected to be the leading cause of death worldwide, followed by heart disease and stroke. In 2008, sixty percent of total cancer death of 7.6 million took place in developing country [18]. In addition, out of 12.4 million global cancer diagnosis cases, more than half of these are diagnosed in developing countries. These alarming figures

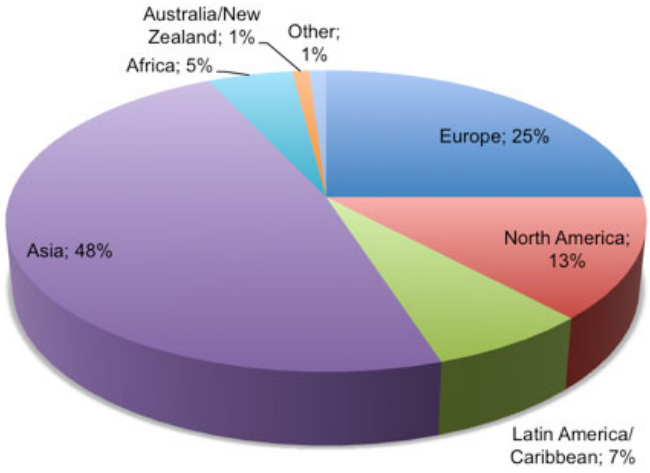

Figure 1.4: Distribution of new diagnosed cases of cancer [12]

demonstrate the fact that preventable forms of cancer are taking disproportionate human toll [18].

This disproportionate human toll and economic loss in middle- and low-income countries is an indication that the impact is not evenly distributed. For instance, Unites States has the highest economic loss from cancer in terms of actual dollar sign but this money loss is 1.73 percent of its Growth Domestic Product (GDP). A country such as Hungary, with much smaller population, is losing 3.05 percent of its GDP [18]. This study further confirms the "silent pandemic" of cancer is penetrating into underdeveloped and developing countries. If a substantial global response is not established soon, this problem can overwhelm the health systems, threaten social structures and finally challenge economic development efforts [18]. These statistical results are clear indication of socio-economic inequalities of can-

cer survival rate [19]. Thus, WHO and global health experts believe that more cost effective and targeted interventions could mitigate the human and financial toll of cancer worldwide [18].

Australia has the highest incident rate of melanoma in the world due to its environmental problem related to ozone layer depletion. Sun exposure is responsible for 95 to 99 percent of skin cancers in Australia. Skin cancer accounts for 80 percent of newly diagnosed cancer cases and over AUD $1 million is billed by GPs for skin cancer consultation. Melanoma, the most dangerous form of skin cancer, is the fourth most common form of cancer in Australian men and women. While melanoma makes up only 2.3% of all skin cancers, it is responsible for 75% of skin cancer death [20].

Figure 1.5: Skin cancer mortality rate [16]

In 2009, there were over 11,500 new diagnosed cases of melanoma, which is approximately 10 percent of all cancer type diagnosis. In 2011, 1544 deaths resulted from melanoma [21]. Melanoma mostly affects men and women in their 80s. The risk ratio for men is 1 in 14 and for women the risk ratio is 1 in 23, approximately twice the rate of Unites States, Canada and United Kingdom. For instance, United States statistics of 2013 shows 76,690 newly diagnosed melanoma cases from which 9,480 people are expected to die. The risk of melanoma for

whites is about 2 percent, 0.1 percent for blacks and 0.5 percent for Hispanics [16]. The conventional methods of treatment increase five year survival rate by 91% for melanoma detected before spreading and at early stages of cancer. This rate decreases dramatically for more advanced stages of melanoma.

1.5 Cell Cycle and Cancer

The cell division process depends on tightly regulated sequence of events taking place in orderly fashion. These chains of events depend on the proper level of transcription and translation of certain genes. Disturbance in the order of this crucial process results in unregulated cell growth. Fundamental alteration in the genetic control of cell division leads to unrestrained cell proliferation that is called cancer. Out of approximately 30,000 genes exist in the human genome, a small subset of these genes is crucial for prevention, development and progression of cancer [22, 23].

Cell cycle irregularity associated with cancer occurs through mutation of proteins that are important at different stages of the cell cycle. Mutations in gene encoding of CDK, cyclins, CDK-activating enzymes, CKI, CDK substrates, and checkpoint proteins [24] are observed in cancer [25]. Mutations in cells led to cancer occurrence in two categories of genes: genes whose protein products promote cell division or inhibit cell death; and genes whose protein products directly

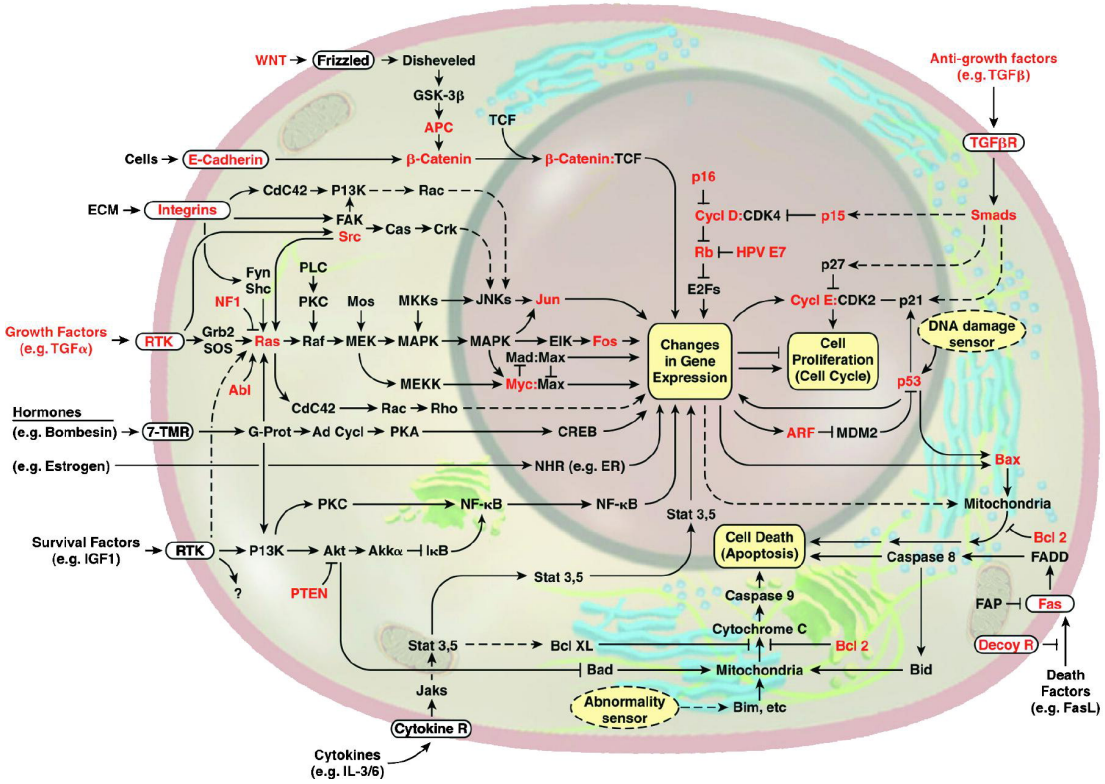

Figure 1.6: Comprehensive Cell Cycle Control and Signalling pathways [22]

or indirectly prevent cell division, promote cell death, or repair the damaged genes [6, 26]. In other words, two types of genes are responsible for turning a normal cell into a cancerous one. These genes are Oncogenes (unrestrained cell proliferation) and Tumor suppressor genes (prevention of cell apoptosis and gene repair).

1.5.1 Oncogenes

Proto-oncogenes promote cell division in a regulated manner. They include growth factors, growth factor receptors and cyclins [22, 23, 27]. They play an important role in early stages of human life by stimulating cell growth and proliferation as an organism develops. They usually control the rate of cell division and growth in the body. Once the process completed, proto-oncogenes go to dormant state or turned "off" state. Later in the life when proto-oncogenes are inappropriately turned "on" by changes or mutation, it randomly multiplies the cell and eventually causes cancer [9]. Thus, the products of proto-oncogenes at different stages of cell cycle stimulate cell proliferation, while its mutated version or oncogenes lead to tumor growth [11]. When gene mutation takes place, the cells replicate at a rate that far exceed cell loss [28].

For instance, cell cycle progression from a G(gap) phase to either S-phase (DNA replication) entry or M-phase (mitosis or DNA split) entry is controlled by four factors; i) mass factor for somatic cells, which is the accumulation of a specific

cellular mass; ii) growth rate factor, which is a specific growth rate requirement for M-phase entry of some cells; iii) time factor, which is mainly important for embryo cells to control the timing of successive M-phase by timer or oscillator genes; and iv) replication factor, which ensures the completion of proper DNA duplication at S-phase [29, 30]. Proto-oncogenes, in their normal state, code for the normal proteins controlling these critical processes. However, permuted proto-oncogenes (oncogenes) code the proteins to facilitate cell cycle progression forward uncontrollably. Usually, oncogenes are responsible for unregulated progression of cell cycle from G-phase to either S-phase or M-phase which contribute to uncontrolled cell division and tumor growth. In addition, oncogenes can save cells from programmed cell death or apoptosis. It is believed that oncogenes alter receptors at the cell surface to give a wrong "on" position signal [31]. Receptors are responsible for signaling the cell to divide. These receptors bind to growth factors, proteins that interact with DNA to initiate duplication, and signaling molecules to initialize DNA duplication through various pathways [31, 32].

Genetic alteration of proto-oncogene leads to different irregularities in a cell cycle. Sometimes, mutations permanently activate proteins that normally switch between activation and inactivation state. This type of mutation results in unlimited cell proliferation. Another type of mutation causes chromosomal translocation where broken DNA is reattached. This mutation type leads to altered regulation of protein expression or formation of fusion proteins. Moreover, the

presence of multiple copies of a proto-oncogene rather than its permutation version is another form of gene alteration.

Oncogenes that promote unregulated cell growth are considered one of the most important discoveries in cancer research [33]. Recent study of proto-oncogene mutation of 1000 cancer samples representing 17 types of cancer showed that the permutation of 14 proto-oncogenes with diverse cellular functions is associated with a high propensity for cancer [32–34]. Oncogenes activation is believed to be induced by a number of factors such as radiation, viruses, certain chemical in the environment, changes in genes, mutation of DNA molecule and break or rearrangement of chromosomes.

1.5.2 Tumor suppressor genes

In contrary to cell proliferation-stimulating function of proto-oncogenes and oncogenes which drive the cell cycle, tumor suppressor genes code for proteins that generally impose cell cycle arrest, repair DNA errors and restrict cell growth and division [22, 23]. In some circumstances, these genes promote programmed cell death or apoptosis. Due to their functionality, tumor suppressor genes are mainly involved in maintenance of cell cycle checkpoints and proteins required for apoptosis induction. In normal cell cycle progression, any damage to cell's DNA is detected by tumor suppressor genes. Then, they react according by inducing cell apoptosis. When cell cycle is supposed to continue its progress, these genes are

switched off by other proteins in the cell cycle before the growth phase of cell can grow. If they are not switched off, they inhibit cell growth. Mutation or damage of tumor suppressor genes lead to dysfunction of proteins inhibiting the progression of cell cycle [25, 31]. When tumor suppressor genes are permuted, they do not work properly. Thus, cell growth and division continues uncontrollably resulting in tumor development. Two of the most notable tumor suppressor genes are p53 and pRb.

p53

This gene is located on human chromosome 17 and expresses tumor suppressor activities. p53 is one of the most important and the best known and studied tumor suppressor gene [22, 23]. This gene was discovered in 1979 through research into the viral etiology and the immunology of cancer [35]. p53 tumor suppressor is a sequence-specific DNA-binding protein that plays a crucial role in determining whether a cell needs to undergo cell arrest or cell apoptosis at the cell cycle checkpoints after detection of abnormalities such as DNA damage, hypoxia and the activation of oncogenes [27, 31].

p53 consists of 393 amino acids. Any substitution of p53 amino acid sequences results in loss of its tumor suppressor functionality. While mutation of amino acids 175, 248 and 273 leads to loss of functionality, changes in amino acid 273 is the most common [27]. Reproduction of damaged DNA cell results in uncontrolled

cell growth. Inactivation of p53 result in loss of p21 regulation in response to DNA damage. One of the mechanism that prevents cancer progression is to stop cell division until the damaged DNA is repaired [25].

p53 is the most commonly mutated tumor suppressor gene in human cancer [31]. Around 50% of human cancers are associated with mutations in p53. In addition, cancers that are associated with p53 mutations are more aggressive and have higher mortality rate. p53 mutations are confirmed to contribute to the development of bladder, breast, cervix, colon, lung, liver, prostate and skin cancers [30].

pRb

This gene is located on human chromosome 13 and is another gene with tumor suppressor activities. Retinoblastoma protein (pRb) and its corresponding gene, RB1, the first identified tumor suppressor, are the well-studied factors of cell cycle arrest or apoptosis [22, 23]. It is the most important CDK substrate during G_1 phase. pRb interacts with a protein called E2F. E2F is a nuclear transcription factor involved in cell replication during the S phase. Interaction of pRb with E2F prevents progression of cell replication. For this interaction to occur, pRb should not be phosphorylated by a kinase. In case of mutation, pRb is always found to be phosphorylated by a kinase. When phosphorylated by kinase, pRb becomes inactive and unable to regulate E2F. Hence, control of cell division at

the S phase does not occur [22, 23, 30, 31].

The inhibitory activity of CKI for induction of growth suppression is conducted through activation of pRb. The functionality of pRb is interconnected with p16 and CDK-cyclin D, so perturbation of any of these cell cycle regulators affect cell cycle regulation. In fact, deletions and mutations lead to non-functional or complete absence of pRb, which can result in binding of certain tumor virus proteins such as human papillomaviruses (HPV) [25]. Thus, absence or functionality loss of pRb is closely associated with unrestrained cell cycle progression. This condition is common in acute lymphoblastic leukaemia [36]. Mutations of pRb in human leads to retinoblastoma (a juvenile eye cancer) and lung cancer. Mutations or abnormalities in some component of pRb pathway have been found in approximately 90% of human cancer [37].

Chapter 2

Literature Review

One out of every two men and one out of three women develop cancer in their lifetime based on American Cancer Society data published in 2008 [13]. Statistically, cancer is the second cause of death in developed countries [7]. Due to its impact on the human well-being, immense scientific effort is dedicated towards finding a cure for cancer. These efforts led to the development of treatments such as chemotherapy and medical radiation. However, these treatments have limited success [15]. Therefore, there is still a need for novel methods and approaches as interventional treatments. Substantial progress in understanding the molecular basis of cancer led to development of three broad categories of cancer treatment methods: conventional treatment methods, complementary and alternative treatment methods, and interventional treatments.

The following section comprehensively describes currently available cancer treatment methods, their side effects, as well as their short comings. Then, closely

related techniques with therapeutic applications are discussed. Subsequently, medical applications of different forms of wave and light therapy as well as low intensity light therapy approach are presented as these techniques are closely relevant to the novel hypothesis of this project. This study aims to experimentally investigate the effects of theoretically proposed far infrared range radiation on cancer cells. Lack of similar experimental and clinical research as well as publication resources in the literature arise from the novelty of this approach for cancer treatment. However, this chapter provides literature review of available external low intensity radiation techniques for various other medical conditions.

2.1 Conventional Treatment Methods

Conventional methods of cancer treatment are mainly based on western medicine and generally conducted by trained and licensed medical professionals in medical facilities. These treatments are based on established scientific principles and have been proven effective in most cases. Conventional treatment methods are categorized as follow: surgery, radiotherapy, chemotherapy, Hormone therapy and immunotherapy (also known as biotherapy). Among them, surgery, radiotherapy, and chemotherapy are the most widely practiced treatment methods.

In early 20th century, small and localized tumors that could be completely removed by surgery were considered curable cancer types. Later on, radiation

therapy introduced as a supplement to surgery treatment for controlling small tumors that were not removable surgically. At last, chemotherapy was discovered to cure small tumors that could not be removed by surgeon or radiotherapist.

Among these conventional cancer treatment methods, surgery is known to be the most effective and acceptable method used for treatment of many cancers. Although chemotherapy and radiation are less invasive therapies, complication and severe long term side-effects associated with these methods make them less optimum methods.

2.1.1 Surgery

Surgery is one of the oldest, most efficient and common medical procedure. Surgery has been performed since the beginning of human civilization. Ancient Hindus believed to be the first people used surgery to remove tumors. Ancient surgeon and physician such as Celsus, Hippocrates and Galen acknowledged reappearance of cancer tumors once they have been surgically removed. There are numerous cases reporting that when a tumor is surgically removed, the disease has returned later when a scar was formed [8]. Reports of re-occurrence tumors led to the misconception that considered cancer as an incurable disease. Misconceptions about cancer and complications and primitive procedures involved in cancer surgery led to a slow development progress in cancer treatment. Despite significant progress of medicine in some ancient civilizations, no considerable

progress in cancer treatment is observed in literature [8].

This approach towards cancer was prevailed until 19 and 20th centuries when advancement of human knowledge and technology introduced new materials and techniques reducing risks, complications and recovery time of surgery. Discovery of anesthesia in 1846 by John Hunter, Astley Cooper and John Warren, raised the popularity of surgery as a swift and precise procedure. Three surgeons who contributed immensely to cancer surgery were Bilroth in Germany, Handley in London, and Halsted from John Hopkins University in Baltimore. Through the efforts of these surgeons and their followers for development of cancer surgery, limitations of cancer surgery have been recognized [8].

Further innovations of 20th century in design and development of more sophisticated and advanced medical instruments, reduced the side effects of surgery. Hence, surgery becomes one of the most effective and popular cancer treatment. The type of surgery, recommended for cancer treatment, differs for every patient depending on the type of cancer and patient's health. Therefore, several types of surgery are known to be beneficial for cancer patients [8]. Some of these surgeries are used in combination with other conventional methods of treatment such as chemotherapy and radiotherapy. The following is a list of these surgeries [4], [5]:

- **Curative Surgery** is used to remove tumors that are localized and have not yet been spread beyond its original site. However, this treatment is not

used as the only treatment method. Generally, this method of surgery is used in conjunction with radiotherapy either after or before the surgery.

- **Preventive Surgery** is used to remove precancerous, abnormal and normal tissues and lumps that may develop into cancers later on.
- **Diagnostic Surgery** takes a sample for biopsy from a tissue that is suspected to have cancer cells developed.
- **Staging Surgery** is used to remove parts of a tissue to be examined for the degree of cancer's spread in the body. Laparoscopy is a special tube with camera and biopsy function that is inserted through a small incision to inspect the extent of the disease.
- **Debulking or Cytoreductive Surgery** is used to remove parts of, not all, a tumor when removal of the entire tumor may damage or endanger an organ or the body. This treatment method is used in combination with radiotherapy or chemotherapy after the surgery to kill the rest of cancer cells.
- **Palliative Surgery** is not a curative treatment but rather relief of cancer symptoms. This method of treatment is used for advanced stages of cancer spread to relieve discomfort or remove problems created by cancer or cancer treatment methods.
- **Reconstructive Surgery** is used to restore the function or appearance of

a body part that is deformed or damaged by cancer or cancer treatment methods [4], [5].

During tumor removal surgery, some tissues surrounding the tumor are removed by a surgeon as a margin. These margins are categorized into two margins; i.e. clean margin and positive margin. Clean margin is the margin that does not contain any cancerous cells. This margin indicates that all cancerous cells are removed. Positive margin is the margin containing cancer cells. These cancerous cells in positive margin can be removed by additional surgery or other conventional treatment methods [4].

Advances in imaging techniques such as ultrasound (sonography), Computed Tomography (CT) scans, Magnetic Resonance Imaging (MRI) scans, and Positron Emission Tomography (PET) scans enable surgeons to have a detail understanding of the type, location and size of a tumor. These imaging modules help surgeons to conduct surgeries with high precision. Among these imaging techniques, CT scans and ultrasound are used to guide biopsy needles into tumors [8].

In addition, advancement of medical devices utilized in fiberoptic technology, endoscopy and other special surgical instruments facilitate minimal opening of a skin during the surgery. This minimal incision for surgery reduces the recovery time and complications. Fiberoptics are usually used for abdomen (laparoscopic) surgery or chest (thorascopic) surgery. Endoscope is used to remove tumors in

colon, esophagus or bladder cancers [8].

There are currently even less invasive ways of destroying tumors inside the body and removing them. Cryosurgery (cryotherapy or cryoablation) freezes the tumor with liquid nitrogen spray. This method is mainly used to kill abdominal cancer cells. Laser is another technology used for cutting through tissue (instead of a scalpel) or vaporizing (burn or destroy) tumors. This method is used for cervix, larynx, liver, rectum, skin and other organs. Apart from laser, radio frequency ablation is used to kill cancer cells by heating cells with radio waves through the antenna placed in a tumor [8].

Utilization of the above mentioned advanced medical instruments and techniques reduces the side effect of cancer surgery but it does not completely eliminate it. Issues associated with cancer surgery include the following [5]:

- Damaging or deforming organs or part of the body;
- Blood loss or clots;
- Allergic or adverse reaction to medicines;
- After surgery pain and discomfort;
- Infections from surgical procedure;
- Other illnesses such as pneumonia.

2.1.2 Radiotherapy

Radiation therapy also known as therapeutic radiology or radiation oncology utilizes high energy waves or particles to combat disease. In radiotherapy for cancer treatment, high energy is delivered to the area of the body affected by cancer. It is evident that certain levels of radiation work to destroy cancer cells and prevent normal and cancer cells from growing and dividing. Radiotherapy usually utilizes X−rays (a form or subset of ionizing radiation) to kill cancer cells and stop their growth and division. These radiations damage DNA and other structural aspects of cancer cells. This damage either kills the cells immediately or weaken them to the degree that they cannot be reproduced [4]. Cancer cells radiated with this high energy beam are less able to recover and repair themselves compared to normal cells.

In late 19th century, a German physicist, Wilhelm Conrad Roentgen, discovered a new kind of ray named as "X-ray". Four years later, he was awarded the Nobel Prize in physics for this discovery. Within months, X-ray was utilized as a diagnostic tool (X-rays) and a few years after that its therapeutic effects for cancer treatment (radiotherapy) was proposed [6, 8]. Initially, radiation therapy was performed with low-voltage diagnosis machine using radium.

Interestingly, in early 20th century, it was discovered that radiation could cause cancer development. It was also discovered that cure of cancer depends on the

strength of radiation emitted by the radiotherapy machines. In those days, many radiologists used the skin of their arms to obtain pink reaction or "erythema dose" for the proper daily dose of radiation for patients. There is no surprise that many of them developed leukemia later on [8]. With advancements in technology, more complex and precise radiation machines were developed. Nowadays, advanced radiotherapy machines expose cancer affected areas with a very high precision beam, which lead to reduction of side-effects of radiatheraoy on normal surrounding tissues.

Advancements in molecular biology enabled development of more complicated treatment protocols and integration of radiation treatment with surgery or chemotherapy. Some types of cancers are cured completely by using radiotherapy alone, but some others require a combination treatment of radiotherapy with surgery or chemotherapy for a more effective healing response. In recent years, about 50 percent of recently diagnosed cancer patients benefited from these treatment protocols. About 40 to 60 percent of all cancer patients, whether they have primary or advanced cancer, use radiotherapy as part of their treatment plans. Radiotherapy is also used to control cancer by stopping cancer from spreading, when cure is not possible or to relieve symptoms of cancer to reduce pain and prolong patients life expectancy [5, 38]. There are two main broad categories of radiotherapy radiation: external radiation (external beam radiotherapy or EBRT) and internal radiation (brachytherapy, implant radiation).

External therapy uses X-ray (photon), cobalt irradiation, electrons, and rarely other particles such as protons. External radiation is delivered through a machine called linear accelerator, which directs the radiation beam to the tumor site with a minimum damage to the surrounding normal tissues. External radiotherapy is the preferred method of treatment for most types of cancers including brain, head and neck cancers, larynx, breast, lung, cervix, bladder, prostate, vagina and rectum cancers [6,8]. In external radiotherapy, different machines are utilized with different characteristics and techniques for delivering high beam radiation. The two major types of radiation beams are photons (X-ray) and electrons. Electrons have shorter wavelengths and can generally penetrate a tissue to a certain depth. The choice of using photons or electrons mainly depends on the location of a tumor inside the body. In addition, protons beam causes a little damage to organs and tissues when passing through but it is very effective in killing cells at the end of its path [5, 8].

- **Conformal Radiation Therapy (CRT)** uses CT images and special computers to map the location of tumor sites precisely in three dimensions. It is particularly useful for conducting radiotherapy on tumors near vital organs that are sensitive to medical radiation effects.
- **Intensity-Modulated Radiation Therapy (IMRT)** works similar to CRT in locating tumors in 3D space. However, in IMRT, photons beams are delivered in different directions. Conformal protons beam radiation

therapy uses a similar approach to IMRT, but instead of using X-ray, this radiation technique utilizes protons beams. It is especially useful in prostate and head and neck cancers.

– **Stereotactic radiation therapy or radiosurgery** is a radiotherapy technique delivering large precise radiation dose to a small tumor. Unlike what its name is suggesting, no incision is made for this technique. The beam is delivered through a especially designed linear accelerator called Gamma Knife or CyberKnife. Its main application is for therapy of brain tumor.

Internal radiation is another type of medical radiation radiotherapy. These types of radiotherapy techniques are used to conduct medical radiation for internal organs and tissues that are hard to reach by usual external radiation techniques due to tissue penetration limits. In this technique, medical radiation dosage is delivered orally as a pill or liquid absorbed by cancer cells or by placing radioactive implant inside, or close to, the tumor through an intravenously (IV) or catheter. In some types of internal radiation techniques, chemical modifiers are used before the external radiation. Chemical modifiers are substances prompting cancer cells to develop agents that make tumors more sensitive to medical radiation. This method protects normal cells from absorbing radiation [4, 5, 38].

Two main internal radiation methods are **intraoperative radiation therapy (IORT)** and **chemical modifiers or radiosensitizers**. IORT is a form

of treatment that delivers radiation in the middle of surgery. In this approach, higher radiation beam is given directly to tumors or to their nearby tissues after removing the cancer to prevent cancer reoccurrence. This method is very common in abdominal or pelvic cancers and minimizes the amount of normal tissues exposed to the radiotherapy [4, 6].

Brachytherapy is another internal radiation therapy commonly used to treat localized tumors by implanting radioactive device inside a body cavity. This method is mainly used for treatment of bronchus, cervix and vagina cancer. In other cases, radioactive "seeds" are placed into the tumor through needles and these radioactive seeds lose their radioactivity within a short period of time [5]. This method is mainly used for prostate, breast, head and neck cancers. Since it is placed inside the body close to the tumor, it is a very effective treatment with less side effects that EBRT [4, 38].

However, as was mentioned above, radiotherapy methods not only kill or damage cancer cells but also they damage or kill the surrounding normal tissues. These cancer radiotherapy methods lead to short-term and long-term side effects. Depending on the area treated with radiotherapy, some potential side effects are mentioned below:

- Fatigue
- Hair loss can be permanent if radiation is for head or neck cancer

- Nausea, vomiting, abdominal pain
- Eating disorder and loss of appetite
- Mouth ulcers, gum destruction
- Skin irritation, dry skin and photo sensitivity
- Constipation, diarrhea
- Decrease in blood cell counts
- Abdominal or bladder pain
- Swelling
- Infertility
- cough or shortness of breath

2.1.3 Chemotherapy

Chemotherapy is one of the most common treatment methods prescribed by oncologist to combat cancer. It is a drug-based treatment method used to slow down or stop the growth of cancer cells. Depending on the type of cancer, patient's health condition and other prescription drugs taken, there is a large number of different chemotherapy drugs. This treatment is usually given in the form of injection into the muscle or fat tissue, drip (intravenous (IV) infusion) into the

bloodstream through a vein, topically (applied to the skin), directly into a body cavity or sometimes even in the form of tablets or capsules [38], [4].

The idea of using chemical drugs for cancer treatment started during World War II. At that time, changes of bone marrow cells into blood cells were reported for naval personnel who were exposed to mustard gas during military action. Simultaneously, US Army was studying a number of chemicals aiming at developing more effective agents and as a protective measure. One of the chemicals studied for that purpose is called *nitrogen mustard*. It demonstrated to work effectively against lymphoma cancer [8]. This discovery led to the development of a series of more effective agents (called alkylating agents) that have therapeutic effects on cancer. They damage DNA of rapidly growing cancer cells. Soon after, Sidney Farber of Boston demonstrated that nitrogen mustard has therapeutic effects on children with acute leukemia. Further investigation of the biological processes led to therapeutic effects revealed that aminopterin produced by this chemical blocks a critical chemical reaction needed for DNA replication. This chemical is the predecessor of today's drug used for cancer treatment, methotrexate. The discovery of drug that can block cell functions led to the beginning of chemotherapy era [8].

From 1956, when the first tumor, called choriocarcinoma, was treated by methotrexate, chemotherapy became one of the main cancer treatment method. Till date, different groups of drugs have been developed and used in different ways to fight cancer cells [6]. To optimize their efficiency for cancer treatment, chemotherapy

may be used alone for some type of cancer or in combination with other treatment methods such as surgery or radiotherapy [5]. When chemotherapy is received before surgery or radiotherapy to shrink the tumor before chemotherapy, it is called neo-adjuvant chemotherapy [8]. Patients may receive post-operative or adjuvant chemotherapy after surgery to eliminate undetected cancer cells and to decrease the chance of reoccurrence [4]. These different methods of using chemotherapy result in complete or partial remission of cancer for many types of cancers.

Chemotherapy drugs have the common ability of damaging cells as they grow or divide by damaging the genes inside the nucleus of cells. Different chemotherapy drugs damage cells at different stages of cell division. Some drugs damage cells at the point of splitting, while some others destroy cells when they are making copies before splitting. These drugs can be categorizes as following [4]:

- **Alkalyting**- agents bind to DNA in the cell to prevent cell division.
- **Antimetabolites**- replace nutrients needed for DNA replication with an inactive substances.
- **Antitumor antibiotics**- interfere with DNA structure and prevent DNA from uncoiling.
- **Hormonal drugs**- suppress hormone processes required for cell growth.
- **Plant alkaloids**- interfere with internal cell structures aiming to prevent

cell division.

From the mechanisms of actions of chemotherapy drugs, it can be deducted that chemotherapy interrupts chemical processes involved in normal and abnormal cell division. Thus, chemotherapy drugs kill not only cancer cells but also normal cells that are constantly growing and dividing such as skin, bone marrow producing blood cells, hair follicles and lining of digestive system continuously renewing themselves [6]. Thus, a variety of mild to severe short-term and long-term side effects from chemotherapy drugs on individuals are inevitable. Depending on the types of drugs used for the treatment, some of the following immediate and early side effects can be seen [4, 38]:

- Allergic reaction
- Flu-like symptoms
- Nausea, vomiting, abdominal pain, dizziness
- Pain or swelling at the injection site
- Red/orange color urine
- Bone and joint pain
- Loss of appetite and changes in sense of smell and taste
- Mouth ulcers

- Skin rashes, dry skin and photo sensitivity
- Constipation, diarrhea
- Decrease in red blood cell counts
- Increase risk of infection and bleeding
- Numbness and tingling feeling in fingers and toes.

To date, the known long-term side effects of chemotherapy are listed below [5, 38]:

- Hair loss (reversible)
- Secondary malignancies (rare)
- Early menopausal symptoms and infertility impairment
- Weakness and fatigue
- Liver, lung, kidney, bladder and heart damage
- Seizure

Among presented above conventional cancer treatment methods, surgery is considered the most effective and leading method for a variety of cancers. Although chemotherapy and radiation are less invasive therapies, there are well known complications and severe long-term side-effects associated with these therapies. These

draw backs of existing cancer therapies prompted cancer researchers to look for new approaches and methods for cancer therapy that are more cost-effective with less severe side-effects and better healing effect [8].

2.2 Complementary and Alternative Methods (CAM)

Complementary and Alternative Methods are two different approaches used in cancer treatment. However, these two approaches are generally classified in one category since they are not considered as conventional methods. Complementary treatments are used concurrently with mainstream conventional treatment methods, while alternative treatment methods are used instead of the conventional treatment. Generally speaking, complementary methods do not aim to induce healing effects. They are mainly concerned with patients' sense of well-being by uplifting general or mental health of patients [6]. In addition, these cancer treatment methods help to relieve pain and symptoms of cancer, or side effects of cancer treatment. In the past, complementary treatment was referred to as supportive care. Examples of complementary therapies include acupuncture, aromatherapy, herbal medicine, massage therapy, meditation and yoga [8].

On the other hand, alternative methods are complete systems of theory and practice developed separately from and/or in parallel with the conventional treatments [39]. These methods claim to induce therapeutic effects on cancer, even

though they are not scientifically approved yet either due to a long process of testing or lack of clinical or theoretical support. Examples of these treatment methods include naturopathy, immune therapy, homeopathy, chinese herbs and megavitamins. *Homeopathic* and *naturopathic* treatments are developed in Western culture, while Chinese medicine and Ayurveda are based on Eastern religious beliefs [39].

2.3 Interventional Treatment Method

Although some types of cancers are clinically managed quite effectively with conventional methods, the most invasive and common cancers such as breast, lung and melanoma cancers are not handled efficiently with these conventional methods [40]. Some other cancer types, such as prostate cancer, are resistant to the conventional methods [41, 42]. These treatment methods are used cautiously due to their long-term and short-term significant side effects. Excessive use of conventional methods may result in deterioration of patient's health considerably and cause secondary severe health conditions [8]. With progress in cancer research and new knowledge of cancer development and progression, new therapies are being developed that target specific tumor cells or inhibit their growth. These new promising methods on their own or in combination with the conventional methods are reported to either reduce the size of tumors or alleviate their symptoms [4]. Some of these new treatment methods are laser therapy, electromagnetic

radiation (EMR), photodynamic therapy (PDT), cryotherapy and hyperthermia. Most of these treatment methods are a form of radiation. A brief description of these method along with its therapeutic applications are presented in this section.

2.3.1 Electromagnetic Field (EMF) and Electromagnetic Radiation (EMR)

According to definition, Electromagnetic Field (EMF) is a physical field produced by charged objects. Electromagnetic field is generated from the interaction of electric field produced by stationery charged particles and the magnetic field produced by moving charged particles. The interaction between electromagnetic field, charges and currents are defined by Lorentz force law and Maxwell's equations shown in Table 2.1 and Equation (2.1).

$$F = q(E + v \times B) \tag{2.1}$$

where the force

$$F$$

enforce on a particle of electric charge

$$q$$

with instantaneous velocity

$$v$$

.

$$E$$

Name	Integral equations	Differential equations
Gauss's law	$\oiint \partial\Omega \mathbf{E} \cdot \mathrm{d}\mathbf{S} = \frac{1}{\varepsilon_0} \iiint_\Omega \rho \, \mathrm{d}V$	$\nabla \cdot \mathbf{E} = \frac{\rho}{\varepsilon_0}$
Gauss's law for magnetism	$\oiint \partial\Omega \mathbf{B} \cdot \mathrm{d}\mathbf{S} = 0$	$\nabla \cdot \mathbf{B} = 0$
Maxwell-Faraday equation (Faraday's law of induction)	$\oint_{\partial\Sigma} \mathbf{E} \cdot \mathrm{d}\boldsymbol{\ell} = -\frac{d}{dt}$	$\iint_\Sigma \mathbf{B} \cdot \mathrm{d}\mathbf{S} \nabla \times \mathbf{E} = -\frac{\partial \mathbf{B}}{\partial t}$
Ampére's circuital law (with Maxwell's correction)	$\oint_{\partial\Sigma} \mathbf{B} \cdot \mathrm{d}\boldsymbol{\ell} = \mu_0 \iint_\Sigma \left(\mathbf{J} + \varepsilon_0 \frac{\partial \mathbf{E}}{\partial t}\right) \cdot \mathrm{d}\mathbf{S}$	$\nabla \times \mathbf{B} = \mu_0 \left(\mathbf{J} + \varepsilon_0 \frac{\partial \mathbf{E}}{\partial t}\right)$

Table 2.1: Maxwell's Equation

is electric field,

$$B$$

is magnetic field.

The main difference between these two concepts is the fact that electromagnetic radiation is the wave propagation of energy through the space. Electromagnetic Radiation (EMR) is a particular form of the more general electromagnetic field, where a form of energy emitted and absorbed by charged particles as it travel through the space in wave form. EMR is associated with electromagnetic field that moves away from its source. EMR has both electric and magnetic field components oscillating with 90^o degree phase difference from each other perpendicular to the direction of wave propagation or energy.

2.3.2 Electromagnetic Spectrum

Electromagnetic Radiation is a type of energy transmitted in the form of waves. These waves correspond to spatial and time variations of the electric and magnetic field. Electromagnetic fields are divided into different categories (called spectra) depending on their frequency (measured in cycles per second (Hertz)), wavelength (measured in meters), and certain characteristics and applications that each division has. The electromagnetic spectrum is generally divided into 7 broad categories of Radio, Microwave, Infrared, Visible, Ultraviolet, X-ray, Gamma ray [43]. Some of these classifications are further divided into subcategories as shown in Table 2.1.

Electromagnetic radiation is described as a stream of mass-less particles called photons. Each photon has a certain energy level and is traveling in a wave-like pattern at the speed of light in vacuum (3×10^8). The energy level of each type of photon is defined through oscillation rate in Hertz. Rate of oscillation is inversely proportional to the distance each photon travels in meters. Higher photon energy means higher frequency of oscillation and shorter wavelength. Thus, radio waves contain photons with the lowest energy level, while Gamma rays have the highest energy level in the spectrum [44].

Radio waves are generally used by radio stations for broadcasting and in space emitting by stars and gases [43]. These radio wave radiations have long been sus-

Category		Frequency (Hz)	Wavelength (m)
Long Wave	ELF (Extremely Low Frequency)	$3 - 30$	1×10^{8}-1×10^{7}
	SLF (Super Low Frequency)	$30 - 300$	1×10^{7} - 1×10^{6}
	ULF (Ultra Low Frequency)	$300 - 3 \times 10^{3}$	1×10^{6}-1×10^{5}
	VLF (Very Low Frequency)	$3 \times 10^{3} - 3 \times 10^{4}$	1×10^{5}-1×10^{4}
RadioWave	LF (Low Frequency) or Long Wave (LW)	$3 \times 10^{4} - 3 \times 10^{5}$	1×10^{4}-1×10^{3}
	MF (Medium Frequency) or Medium Wave (MW)	$3 \times 10^{5} - 3 \times 10^{6}$	1×10^{3}-1×10^{2}
	HF (High Frequency) or Short Wave (SW)	$3 \times 10^{6} - 3 \times 10^{7}$	1×10^{2}-1×10^{1}
Microwave	VHF (Very High Frequency)	$3 \times 10^{7} - 3 \times 10^{8}$	1×10^{1}- 1
	UHF (Ultra High Frequency)	$3 \times 10^{8} - 3 \times 10^{9}$	1 - 1×10^{-1}
	SHF (Super High Frequency)	$3 \times 10^{9} - 3 \times 10^{10}$	1×10^{-1}-1×10^{-2}
	EHF (Extremely High Frequency)	$3 \times 10^{10} - 3 \times 10^{11}$	1×10^{-2}-1×10^{-3}
Infrared	Far Infrared	$3 \times 10^{11} - 3 \times 10^{12}$	$1 \times 10^{-3} - 1 \times 10^{-4}$
	Mid Infrared	$3 \times 10^{12} - 3 \times 10^{13}$	$1 \times 10^{-4} - 1 \times 10^{-5}$
	Near Infrared	$3 \times 10^{13} - 3 \times 10^{14}$	$7 \times 10^{-5} - 1 \times 10^{-6}$
Visible	red, orange, yellow, green, blue, violet	$3 \times 10^{14} - 7.5 \times 10^{14}$	$4 \times 10^{-9} - 7 \times 10^{-7}$
	Ultraviolet	$7.5 \times 10^{14} - 3 \times 10^{16}$	$1 \times 10^{-7} - 4 \times 10^{-7}$
	X rays	$3 \times 10^{16} - 5 \times 10^{19}$	$1 \times 10^{-11} - 1 \times 10^{-8}$
	Gamma rays	$5 \times 10^{19} - 3 \times 10^{20}$	$> 3 \times 10^{19}$
	Cosmic rays	$3 \times 10^{20} - 3 \times 10^{22}$	1×10^{-10}-1×10^{-12}

Table 2.2: Approximate wavelength, frequency of each region of the electromagnetic spectrum [43].

pected and tested for their negative effects on biological system, while a number of other number studies investigate their healing effects [45, 46].

Microwave radiation is used by astronauts to learn about the structure of galaxies in their vicinity. Microwave radiation is used in bioelectromagnetic radiation for therapeutic applications. [47] investigates the biological effects of microwaves for extremely high frequency range [millimeter waves (MMWs)] at non-thermal power intensities on *Escherichia coli* (*E. coli*) cells and rat thymocytes. The findings of this experimental work demonstrate interaction of microwaves with cell-to-cell communication. This study uses low intensity linear, right and left polarized waves in the frequency range of 30-300 GHz with two different cell densities of 4×10^7 and 4×10^8. This *in vitro* study reveals several factors contributing to the effects of low intensity microwaves on the chromatin conformation in cells. These factors are frequency dependencies of resonance type, dependence of the resonance effects on polarization, "window" dependence of Power Density (PD), narrowing of the resonances, and rearrangement of action spectra frequency with decrease in the PD. In addition, this study shows that at the cellular level certain parameters affect the final result. These parameters are the genotype of *E. coli* cells, the growth stage of the bacteria culture, the cell density, static magnetic field during exposure, and the time interval between exposure and start of analysis process. Depending on the affecting parameter, MMWs inhibits or stimulates the growth functions [47].

Infrared waves have long been utilized in night vision goggles to pick the heat wave emitted from objects. In space, they are used to map the dust between stars. Due to its nature, this range of waves is considered the safest range for human body. Thus, it is considered as an interesting range for various therapeutic applications [44]. This range of electromagnetic radiation is further subdivided into three ranges of Near Infrared (760nm - 1500nm), Mid Infrared (1500nm - 4000nm), Far Infrared (4000nm - 10^6nm). In fact, this research project investigates the applicability of this radiation range as an alternative treatment for cancer. This range is discussed extensively in later sections.

The most well-known visible light in the space is the light emitted from the stars in the sky. Visible light is detectable by human eye so it has been utilized extensively in day-to-day life of everyone as a source of light, alarm systems and etc. Visible light consists of all rainbow colors (in the range of 400nm to 700nm) violet, blue, green, yellow, orange and red.

Due to its visibility to human eye, this range of light is used by early medical science for treatment of different medical conditions [49]. The effects of *in vitro* radiation of light on cancer and normal cells is investigated here for comparing the effects of the proposed far infrared irradiation range and other ranges.

The most well-known ultraviolet radiation is emitted from the Sun. These rays are mainly famous for skin tans and burns which is proven to have harmful effect

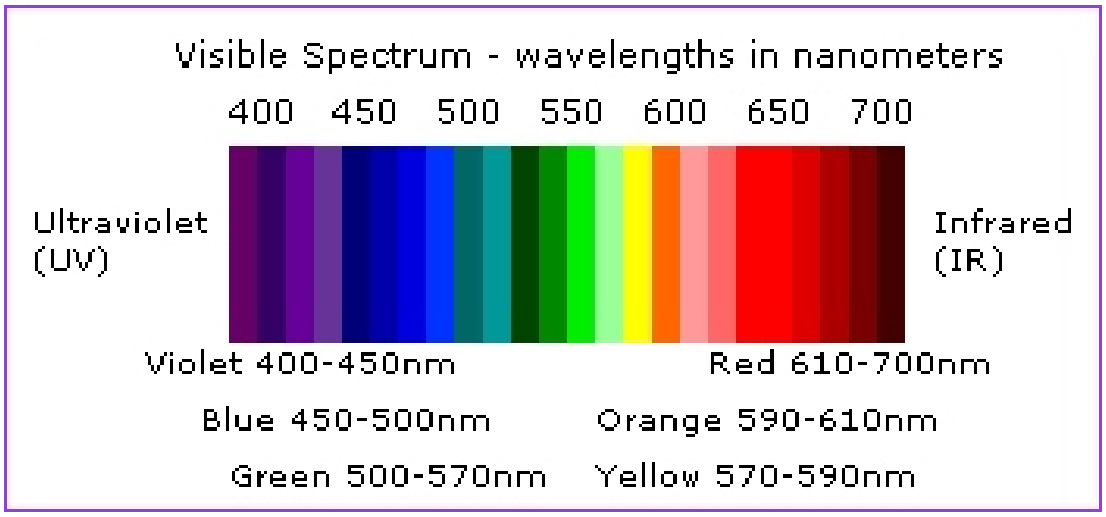

Figure 2.1: Visible light range [48]

on human skins. The known harmful effects of these waves are related to skin cancer and premature skin aging.

X-rays have very high frequency range and low wavelength which enable these rays to pass through the objects. Thus, they are mainly used in medical imaging of teeth and body parts. They are also used for security purposes in scanning bodies or objects.

Gamma rays have the highest photon energy implying that they travel the shortest distance of all rays in the spectrum. Thus, Gamma rays characteristics make deep tissue imaging a possible reality.

Due to the higher energy level of Gamma and X-rays, they are used in two forms of ionizing and non-ionizing radiation. Ionizing radiation is when light particles carry enough energy to liberate an electron from a molecule or atom. Gamma

and X-rays and some of UV are ionising radiation because the photon energy is high enough to remove electrons from atoms. Non-ionising radiation would be anything with hν of less than 14eV. These ionising radiations have various application in medical imaging.

2.3.3 Electromagnetic Field (EMF) Therapy

Bioelectromagnetics is the term used to describe interaction of non-ionizing electromagnetic fields with biological systems. There are a number of studies demonstrating that low level electromagnetic fields induce non-thermal therapeutic effects. For instance, [50] reports of non-thermal biological effects of electromagnetic field exposures in microwave frequencies. Pulsed electromagnetic field (PEMF) has gained popularity as a therapeutic agent over the last forty years, following the promising evidence that electric currents accelerate bone formation [51, 52]. Electromagnetic field is used in two different ways for therapeutic purposes. The first therapeutic application of PEMF is on high frequencies which the opposite side of low frequencies in magnetic spectrum. High rate of changes in PEMF induce significant biological currents in tissue. This induced current leads to a greater biological effect depending on the magnitude of the induced current. However, the high frequency nature of this field induces heat effect in biological organisms [51, 53].

The second and the most popular therapeutic application of PEMF is extremely

low frequency (ELF) which is at low end of electromagnetic spectrum from 0 Hz up to 300 Hz. [54] investigates the underlying electrical properties of tissues, cell membranes from ELF wavelength range in microwave range and in sinusoidal waveform. This work discusses and evaluates the possible mechanism for thermal and non-thermal weak interaction between the induced energy and tissues. Authors concluded that slow rate of changes in ELF do not induce any biological current in the tissue. PEMF at extremely low frequency fields are either inducing no significant heating to the tissue or thermal effect is in the range of naturally occurring thermal fluctuation in tissue [55].

PEMF stimulation gained credibility as a therapy following the observation that physical stress on bones induces small electric current enhancing bone formation. In this process, electrical stimulation of chondrocytes promotes the synthesis of proteogylcans, the major component of cartilage matrix. The experimental therapies for extremely low frequency are emerged in recent years for a variety of medical conditions such as non-union bone fractures [56, 57], joint disorder, skin ulcers [58], migraines [59], degenerative nerves [60], pelvic pain, neurological disorders and etc. [51].

While majority of ELF sources of electromagnetic field stimulation are sinusoidal waveforms, they can have various shapes such as asymmetric, biphasic, and quasi-rectangular or quasi-triangular [51, 61]. It is established that specific types of low-level electromagnetic fields induce specific biological functions depending

on wave magnitude, frequency, and form of the field [51, 55]. For instance, in 1979, the United States Food and Drug Administration (FDA) approved the use of quasi-rectangular and quasi-triangular waveforms as efficient forms of treatment for disorders associated with fractures [62]. Moreover, it has been established that intermittent use of PEMF provides better outcome that its continuous use [63–65].

In some studies, ELF-EMF exposure is associated with carcinogenesis [66], while more recent studies shows that ELF-EMF induces therapeutic effect on cancer tumors. One of the more recent experiment published in 2011 [67] demonstrates that ELF-EMF induces positive effect on enhancement of immune system to fight against cancer. The patients in this clinical work were exposed to low intensity coherent electromagnetic fields for 8 hours per day and 6 days a week for 4 weeks. The results from this human trial study show that the coherent exposures of electromagnetic field on end-stage cancer patients result in significant increase of cancer cytotoxicity in all treated patients [67].

Recently, *in vivo* animal study [68] investigated the hypothesis of using ELF-EMF as an anti-proliferation method for treatment of cancer cells. Among all experiments using ELF-EMF, there are a number of research studies dedicated to the effects of various field strengths measured in Tesla and different frequency of time varying magnetic field on cancer [69–71]. [72] presents a thorough study of therapeutic effects and analysis of amplitude modulations as well as tumor

corresponding frequencies ranging from 0.1 Hz to 114 KHz of electromagnetic field exposures on thyroid, lung, pancreatic and leiomyosarcoma cancers. The authors concluded that cancer-related frequencies appear to be tumor specific and they observed better treatment outcome for advanced cancer patients.

The effect of this electromagnetic exposure at cellular level is also investigated in several other publications such as [73]. In this work enhancement of p53 inhibitor as a result of LF-EMF exposure is explored. Furthermore, [74] demonstrates therapeutic changes in cell cycle kinetics and G_1 phase protein resulted from low frequency electromagnetic field radiation. In addition, *in vitro* experiments in [75] report that exposures by ELF-EMF on BEL-7402 cell line induced therapeutic effects. In [76], the effect of both time varying and static magnetic field is reported to enhance apoptosis and tumor growth inhibitors. Authors used 1mT of electromagnetic field with Extremely Low Frequency (ELF) at 50Hz used on MCF7 cells and MRC-5 lung fibroblast.

Furthermore, a recent paper [77] reported the findings of a clinical study where very low levels of amptitude-modulated electromagnetic fields induce therapeutic responses in cancer patients. The study is conducted on advanced hepatocellular carcinoma (HCC). In their approach, HCC is exposed to 27.12 MHz electromagnetic field using *in vivo* exposure system. In addition, breast cancer cells are exposed to tumor-specific modulation frequencies with in the same 100Hz-21kHz range as cancer-specific frequencies. Their tumor-specific modulation frequen-

cies are obtained by biofeedback method. This clinical study confirmed a significant reduction in HCC and breast cancer cells proliferation by exposure of HCC-specific and cancer-specific modulation frequencies, respectively.

2.3.4 Photodynamic Therapy (PDT)

Photodynamic therapy, photoradiation therapy or photochemotherapy are all different names for a method that is used as an experimental treatment method for some types of cancer. PDT is a form of light therapy [78] or phototherapy that consists of exposure of cancer cells to a specific wavelengths of light in the presence of an active drug in the target area. In this method, a special drug, called photosensitizing agent, is used to make cancer cells sensitive to a specific wavelength of external light.

When a photosensitizing drug is exposed at a particular wavelength, it reacts and produces a form of oxygen that kills nearby cells [79–81]. These photosensitizer agents that are concentrated in cancer cell absorb the light and destroy a tumor through production of a form of oxygen resulting from the agents' activation [8]. Each photosensitizer is activated by a light exposure at the specific wavelength [81, 82]. Thus, activation wavelengths determine the penetration distance that each light source travels into the body [81, 83].

Photosensitizer agent is injected into the bloodstream or, in case of non-melanoma

skin cancer, is applied on the skin as a cream. The photosensitizer agent is absorbed by all cells in the body but stays longer in cancer cells than normal cells. After that (24 hours to 72 hours after the injection), when the drug is removed from normal cells but is still active in cancer cells, the tumor is exposed for about 45 minutes to a specific wavelength of light that activates the drug [79]. The time intervals between the drug injection and light exposures is called *drug-to-light interval*, which depends on the type of a drug used. PDT can not only be used directly to destroy cancer cells but also it can be used to shrink or destroy tumors by activating immune system to attack cancer cells and by damaging the blood vessels in the tumor, which blocks the supply of nutrient [79–82].

The light source used in PDT is mainly generated by laser or Light Emitting Diodes (LEDs) [80, 83]. The laser light can be directed to the tumor site(s) through fiber optic cables, when internal organs are affected by cancer (lung or esophagus cancer). Argon laser is used in PDT as it penetrates for about an inch through the tissues without damaging them [5]. LEDs are usually used for surface tumors such as skin cancer.

A clinical report published in 2010 [84] provided a significant incentive for application of LEDs in PDT cancer treatment. This study was a clinical research conducted on a patient with nevoid basal cell carcinoma syndrome (NBCCSI), a genetic disorder characterized by multiple basal cell carcinomas (BCCs) along with skeletal abnormalities. Patients were treated with PDT using blue light

(approx. 475nm) radiation and 20% e-aminolevulinc acid.

In [85], non-melanoma skin cancer cell lines such as basal cell carcinoma (BCC) and squamous cell carcinoma (SCC) were irradiated by light (LED) at five different wavelengths of 460, 525, 630, 730 and 850 nm. Each LED had a spectral bandwidth of 10-15 half width, half maximum (HWHM). These LEDs were selected from the visible and near infrared light range in order to quantify their exposure effects on the concentration of oxygenated and deoxygenated hemoglobin. In this study, the light sources were computer controlled and the exposure system was designed to illuminate $40.5mm \times 30mm$ area of tissue [85]. In addition, an image acquisition technique was incorporated to quantitatively measure and monitor a tissue oxygenation supply. This system was applied in the preliminary clinical study of nine skin cancer lesions [85]. It was observed that for superficial BCC and SCC *in vivo* measurements, there were significant spatial and inter-subject variations. Volume maps demonstrated three times greater concentration of hemoglobin in the lession than in a normal tissue by visible light irradiation at the wavelengths of 460, 525, and 630nm targeting tissue volume penetration within approximately 1 mm in tissue. Specifically, the findings discussed in this paper provide spatially resolved insight into light penetration in tissue and oxygenation. Therefore, this approach provides a more quantitative and controlled dosimetry specific to the lesion. The authors conclude that the developed methodology has a potential to positively improve treatment outcomes

by optimizing the execution of PDT for its various intensities and duration.

Furthermore, there is a number of photosensitizer agents approved by U.S. Food and Drug Administration (FDA) to be used in PDT. These are porfimer sodium (Photofrin), Aminolevulinic acid (ALA or Levulan), and Methy ester of ALA (Metvixia cream) [8]. To date, PDT is approved to be used for the following cancers: vocal cord, cervical, skin (non-melanoma), lung, head and neck, vaginal, vulva, penile, and esophageal cancers [5, 86, 87]. Concurrently, PDT is a progressive research area where a number of research and clinical studies are underway to apply PDT for brain, prostate, tonsil, pancreatic, mouth, gallbladder, bladder and peritoneal cavity cancers [86–88]. Simultaneously, there is a strong focus on development of a more effective light source and photosensitizer agents [79–81, 83, 87, 89].

However, penetration of the light used in PDT is limited by the wavelength, which makes PDT applicable for certain types of cancers [90]. This technique is used to treat cancers on the lining of internal organs or cavities such as head and neck area, oesophagus or bronchus [6]. In addition, PDT is not efficient for treatment of large tumors because the light cannot penetrate deep into the tumor [80,81,91]. Moreover, it is not effective in advanced stages of cancer, where tumors is spread to different parts of the body [92].

Implementation of this treatment method usually does not require hospitaliza-

tion and is performed as an outpatient procedure [91]. To increase its efficiency, PDT is used in conjunction with other methods such as chemotherapy, radiotherapy and surgery. PDT provides less invasive treatment option compared to other treatment methods. There is no known long-term side effect associated with PDT. However, its short-term side effects are well known and presented here [8, 92]:

- Photosensitivity reactions for up to 6 weeks;
- Skin changes;
- Swelling and burn of nearby healthy tissue;
- Allergic reaction.

2.3.5 Hyperthermia Therapy

Hyperthermia or heat therapy is another method used for cancer treatment [93, 94]. Therapeutic heating effect in hyperthermia is induced by different forms of radiations (electromagnetic fields), by placing patients in a strong magnetic field, and by planting electrodes to transfer heat via perfusion process. According to the National Cancer Institute (NCI), hyperthermia helps to shrink the size of tumors by damaging cells due to excessive induced heat or by depriving cells from their vital nutritions [5]. Hyperthermia is applied in three different ways: local, regional and whole body hyperthermia (depending on the spread of disease).

However, the aim of this project is not to induce any heating effect. This project aims to test the hypothesis that a specific range of far infrared wavelengths can induce therapeutic effects on cancer cells. Thus, extra measures are taken into consideration to remove any heat effect on cancer cells being exposed to low level infrared radiation in the range of 3500nm to 6500nm.

2.3.6 Light Therapy

Light, a sub set of electromagnetic radiation, in the form of both artificial and natural light, is utilized for different medical applications. Hippocrates, founder of bioelectromagnetism, prescribed sun exposures for breast cancer in ancient Greece [61]. The concept of using light for medical purposes is a centuries-old concept. This concept was employed in ancient Egypt, Greece, China and India. This old therapy method was used historically by Egyptians as solar therapy. In their healing practices, direct sunlight was utilized. Avicenna used light for healing diseases as well as a diagnostics tool for different physical conditions of patients [95].

Two thousand years after its first usage by Hippocrates, Luigi Galvani tried to treat tumors, aneurisms and hemorrhages by applying electricity to the affected tissues [95]. Even in 1840, Pravaz and Recamier demonstrated a method for killing cancer cells in uterus by using electricity [95]. However, in the nineteenth century, the focus of science shifted toward the matter rather than energy

which resulted in advancement of medical applications in surgery and antiseptic. Interest in healing using light radiation sources declined in the nineteenth century.

In 20th century, research discoveries in light and chromotherapy changed the perception of scientific society toward the use of light for medical purposes. One of these discoveries was in 1951, when Takkata studied the effects of direct sunlight exposures on menstrual cycles [95]. This idea gradually attracted more interest and attention, when more experimental results corroborated the fact that light radiation induces changes in the biological processes of human body. Although the basis of such effects was not well perceived until recently, the experimental results were showing biological effects to occure upon light exposures.

In later nineteenth and early twentieth centuries, EMR in the form of electricity current or light exposure was used as a common practice for simple and complicated medical conditions. For instance, sun exposure was a common prescription for different medical conditions such as seasonal disorder. In fact, during World War II, sun rooms were built in hospital for treatment of such disorder [61]. In 1904, Nils Finsen won the Nobel prize for his Ultraviolet (UV) therapy [96]. [97] is a comprehensive review of psychiatric clinical study of light therapy. It presents the fact that light therapy has long been used as a psychiatric intervention for seasonal affective disorder (SAD) [98] and sleep disorders [99]. In recent years, light therapy demonstrates to be able to induce therapeutic effects on a num-

ber of other illnesses such non-seasonal depression [100], bipolar depression [101], attention deficit hyperactivity disorder (ADHD) [102], Alzheimer's disease [103], parkinson's disease and dementia [104].

During 1960s, when laser (Light Amplification by Stimulated Emission of Radiation) invented, investigations of EMR side-effects became a hot research topic. Endre Mester, a scientist at Semmelweis University in Budapest, tried to explore whether laser exposures lead to cancer by testing the effect of laser exposures on two groups of mice [105]. The dorsal hair of both groups mice were shaved for the experiment. Then, one group was exposed to low power ruby laser (694nm) light, while the other group was not exposed. At the end of the experiments, no sign of cancer development, as a result of laser exposures, was recorded but surprisingly the treated group grew the shaved hair quicker than the unexposed one. This was the first demonstration of "laser biostimulation". Since then, in the last fifty years, numerous research projects have been conducted with mainly coherent (laser) light exposures, while growing interest is recently shifted toward non-coherent (LED) light applications.

In terms of cancer treatment, light in the forms of laser or LED is used to provide a non- or less- invasive treatments. Light has medical applications in two general categories: high intensity and low intensity light. Each category has therapeutic applications that are very different in their concepts and applications. High intensity light therapy usually uses a different type of laser beam as its source

of light. Due to its concentrated form of light, it is a very powerful and precise tool. These types of lasers are used to remove small tumors as a surgery tool, to apply heat to tumors to shrink them or as diagnostics tool in cancer. For instance, one application of laser in cancer therapy is known as laser therapy. This method utilizes high intensity laser light to shrink or destroy tumors due to the high energy transferred into and absorbed by a tumor. The major benefit of laser therapy is the fact that it causes less bleeding and damage to surrounding tissues. While high intensity or high beam laser therapy is not a new approach for cancer treatment, the concept of using low intensity light for cancer treatment is a novel approach that is of interest to this project.

2.3.7 Low Intensity Light Therapy (LILT)

The idea of using light radiation to control biological function has always been fascinating to scientists. This approach is long been implemented in plants research extensively [106, 107]. As an example in [108], authors presented a system, called a promoter system, that induces a gene promotion by irradiating short pulses of light. This system is based on red light irradiation that modulate the activities of two chimeric proteins to select a gene promoter. The authors also demonstrated that this induced gene promoter is reversed by far-red light exposure. In this paper, the extent of induction is precisely controlled with the number of photons delivered to cells by the light pulses.

To expand the methodology of using LILT in other living organism motivated researchers to investigate the underlying mechanisms that lead to changes in biological function of cells. This approach invigorates the possibility of controlling and using cellular signaling pathways to induce a biological function for therapeutic purposes by programming and engineering biological networks [31, 109–113]. For instance, in [113], the authors utilize the light exposures at the wavelength of 650nm and 750nm to control a cellular behavior. The authors propose the use of a new genetically encoded light-control system based on reversible protein-protein interaction from the phytochrome signaling network of *Arabidopsis thaliana*. It is also demonstrated that this system can translocate the target proteins precisely and reversibly to the membrane [113]. This process is used to reshape and direct the cell morphology of mammalian cells. The outcomes of this research lead to opportunity of designing diverse light-programmable reagents that enable a new generation of perturbative, quantitative experiments in cell biology. The study [112] provides a modification for the current strategies of stimulating intracellular signal transduction pathways.

A recent study [31] provides a different strategy and approach to designing new signaling pathways. The authors explained the molecular mechanism of cell signaling networks in eukaryotes. This paper discusses the possibility of exploiting cell signaling mechanisms to engineer cells to perform new functions. Although this study mainly look in cell signaling at molecular level, it is evident that their

system can be used to induce or precisely control cell signaling for therapeutic purposes. Subsequently, in [114], the authors utilize the cell mechanism concepts for signaling pathways and demonstrate the frequency dependence of signal transduction in the osmo-adaptation pathway of *Saccharomyces cervisiae*. In this study, a negative feedback is used to infer a concise predictive model.

Side Effects of LILT

As discussed in a number of studies and due to the low intensity nature of LILT exposures, the energy transferred through these methods of exposures is not high enough to break the molecular bonds between cells or tissues. According to [115,116] no detectable temperature rise in the tissue and no macroscopic changes in the tissue structure were observed by the authors. Furthermore, [117] and [118] investigated the effect of LLLT for wound healing and pain relief. No changes in the structures of the tissues are reported by the authors. In [119], the authors tried to determine the optimum wavelength and power for lipoplasty without altering macroscopic structure of the tissue.

Low intensity light (laser or LED) therapy (LILT) is widely believed as a benign treatment modality. Even though this method is not considered to impose any severe side effects, it is still at its early experimental stages [120–123]. To firmly confirm that low intensity light exposure does not induce substantial side-effects, a number of research studies are being dedicated to this cause. For instance, [124]

thoroughly investigates any possible DNA or protein damage in B14 cells after low intensity laser irradiation of near infrared range (810nm). This paper could not establish any cytotoxic or genotoxic effect as result of the exposures. The authors also showed that LILT exposures do not lead to direct damage in DNA.

Therapeutic Application of LILT

Several recent studies concluded that biological signaling processes correspond to electrical properties of radiation such as frequency (Hz), intensity of exposure or exposure power (mW), duration (s), and amplitude modulations [95, 125–129]. Effectiveness of this treatment approach highly depends on their proposed energy transferred (measured by duration and intensity of exposure) and the wavelength of light irradiation. Any changes in these two crucial variables (energy transferred and wavelength) mitigate the therapeutic effect predicted by different research study [97]. For instance, in [119, 130–135], the authors found that the optimum therapeutic effect for bio-modulation is observed at the wavelengths between 630nm and 640nm. Any variation to the wavelengths or total transferred energy other than their specifically predicted parameters reverses the effect or results in a negative outcome [136, 137].

Research has shown that low intensity (in mW/cm^2) of light irradiation induces therapeutic effects compared to the higher level light radiation [138]. According to the research result from [138], intensities higher than 1000 mW/cm^2 introduce

heat energy that is not safe for medical applications such as exposure of human eye. The authors in [138] also describe that different intervals of light in wavelength range of 600nm to 900nm is known and proven to induce certain therapeutic effect. The importance of this parameter is discussed and demonstrated by a number of *in vitro* and *in vivo* studies in humans [139] and animals [140]. Thus far, studies have shown that low intensity (less than 100 mW/cm^2 range) laser or light therapy (LILT) is confirmed to have positive effect in pain reduction [141–143], promotion of wound healing [144–149], tissue repair [150–152], tissue growth and post-surgical healing [115, 153–155], inflammatory response reduction [156–158]. In addition, LILT is confirmed to induce therapeutic effect on tissue damage prevention and regeneration of diseases in neurology [159], ophthalmology in [160], cardiology in [161], and otolaryngology in [162], relief of neurogenic pain and neurological problems and some other medical conditions [138, 163–168]. It has also received market clearance by FDA for reducing pain for breast augmentation surgery [169].

Moreover, a very recent study [170] showed that low intensity laser (light) therapy used in fat reduction and lipoplasty to avoid the side effects and risks of current use of ultrasound and laser lipoplasty method [171–173]. This technique can be used as a substitute to the current methods by a non-invasive alternative modality for fat reduction [174]. For instance, in this experiment, the authors confirmed that 14mW of 635nm wavelength exposure results in significantly improved

liposuction procedure. This review study mainly focuses on current research that have reported on the effect of LLLT for liposuction [115, 153–155], non-invasive body contouring and fat reduction [175–182], cellulite reduction [175, 176, 180] and serum cholesterol and triglyceride level reduction [183, 184]. The main principle of LILT lies beneath the fact that changes in energy state of bio-molecules by external electromagnetic radiation (EMR) lead to changes in a particular biological function [185, 186]. Although these cellular changes are often difficult to predict, it is inferred that depending on the intensity level of external EMR as well as absorption level of such irradiation at cellular level, a particular cellular effect would be induced.

In [187], a comprehensive overview of therapeutic application of far infrared radiation is presented. The wavelength range explained in this literature review is from 5.6 μm to 1000 μfm. This recent study showed that clinical application of far infra-red therapy as a non-invasive and convenient therapeutic modality could improve access flow, inflammatory status and survival of the artreiovenous fistula (AVF) in hemodialysis (HD) patients through both thermal and non-thermal effect. The non-thermal effects of far infra-red application were endothelial-improving, anti-inflammatory, antiproliferative and antioxidative effect. The authors proposed that the anti-inflamatory effect of FIR therapy is maximized for 4, 6 and 24 hours of FIR radiation. It is also stated that FIR energy transfers as 2-3 cm into subcutaneous tissue without irritating or overheating

effect on skin. The authors recorded the steadily increase in skin temperature to around 38-39°C during FIR treatment for 30 to 60 minutes when radiation source was more than 20cm away from the skin.

Using LED or Laser as a Light Source in LILT

According to an argument presented in [188] by Tiina Karu, a well-known scientist in LILT, low intensity light/laser radiation conducted with laser, a coherent non-ionizing form of light, or LED, a non-coherent non-ionizing form of light, induces the same effects on cells. Although early studies used lasers as the source of light radiation, it is now believed that non-coherent light emitting diodes [153] are as effective as coherent laser light [189–191]. Professor Karu in [188] explained that the characteristic differences of LED, non-coherent light source, and laser, coherent light source, do not affect their therapeutic outcomes. The authors demonstrated that wavelength, intensity and duration of low intensity visible monochromatic light radiations are responsible for induction of therapeutic effects on biological systems of *E. coli*, yeast and HeLa, not the type of exposure light source. These parameters are considered as the most significant elements in therapeutic effects of light radiation. Following the experimental findings of Karu [188], a growing number of experiments are being conducted with LEDs instead of laser [192].

The motivation to use LED for LILT is analyzed and discussed in [170]. The

authors discuss a number of research studies utilized LEDs rather than laser for cellulite reduction at red (660nm) and near-infrared (950nm) wavelengths [153,175,193]. Furthermore, authors in [194] investigate the intra-cellular changes induced by irradiation of visible and near infrared wavelength light. In this analysis a series of low intensity LEDs with different wavelengths is used to obtain the maximal stimulation. The study found that central wavelength of 590nm±14 nm stimulate Cytochrome c oxidase (Cco)/nitric oxide (NO) synthesis at physiological nitrite concentration which exerts beneficial effects on cells and tissues.

In fact, [195] provides a comprehensive review of all known clinical and experimental therapeutic effect of low intensity light therapy for near infrared LED exposures. This research reported that LED exposures in the far red to near infrared region of the spectrum (630nm-1000nm) modulated a number cellular functions including wound healing acceleration, improvement in recovery of heart injury, attenuation of injured optic nerves. The study reviewed current research on the use of far red to near infrared wavelength in *in vitro* and *in vivo* models. The authors demonstrated that NIR-LED light stimulates mitochondrial oxidative metabolism *in vitro*, while accelerating cell and tissue repair *in vivo*. Review of these *in vitro* and *in vivo* effects of NIR-LED led to the conclusion that NIR-LED light exposure is potentially a novel, non-invasive, therapeutic intervention for a range of diseases linked to mitochondrial dysfunction such as age-related macular degeneration, Leber's hereditary optic neuropathy, Parkin-

son's and Alzheimer's disease.

Application of LILT in Cancer Treatment

LILT is increasingly gaining popularity for various medical conditions due to its non-invasive, non-ionizing and non-thermal effects approach on cells and tissues. These characteristics of LILT are attracting researchers to apply low intensity laser or light exposure as an alternative cancer treatment in the last couple of years. Despite the recent shift in the focus of international oncology research toward LILT, this topic is not yet reached its adolescence [196] to be qualified as an approved cancer treatment modality. However, extensive amount of research is conducted on inter cellular changes and pathways induced by exposure to low intensity light [49, 197–209].

There is a growing number of experiments in the visible and near infrared wavelengths range attempting to implement the novel approach of LILT for cancer or cancer symptoms treatment [85, 210–216]. For instance, [210] used low level laser therapy to stimulate lymphangiogenesis, encourage lymphatic motility, and reduce lymphostatic fibrosis for treatment of lymphedema after breast cancer. The authors observed that low power laser exposure reduced limb volume. However, the risk of recurrence of cancer or metastasis is not evaluated here.

Study [217] investigates the effects of low level laser therapy on murine melanoma

cells, B16F10. The experiments are conducted *in vitro* and *in vivo*. The cells for *in vitro* investigation were examined 24, 48 and 72 hours post irradiation with Tripan Blue, MTT and cell quest histogram tests. The results showed that a significant increase in the hypodiploid melanoma cells was observed at 72 hours post irradiation. In the *in vivo* examinations, the mouse models were irradiated once every day for three days with laser at frequency of 660nm and intensity of 50mW laser for 60 seconds and 420 seconds. The volume and histological characteristics of tumor were examined for possible effects of exposures. The treatment with longer duration of irradiation (420s) demonstrated significant increase in tumor volume, blood vessels and cell abnormalities compared to other treatments that did not show significant changes in tumor's morphology. This research concluded that longer duration of radiation (420s), indicating higher transferred energy, significantly increased melanoma tumor growth *in vivo*, while shorter radiation time demonstrated negative effect [217]. The authors concluded that shorter duration of in vivo exposure induces more therapeutic effect on B16F10 than a much longer exposure duration of 420s.

Furthermore, study [218] evaluates the effect of LILT at molecular and cellular level. In this paper, MCF7 (breast cancer) cells are exposed to 366 nm He-Ne laser with different low intensity levels (5, 28.8, and 1000 mJ/cm^2). Changes in cell viability of MCF7 cells is measured by Trypan Blue, a cell based assay. The relevant biochemical alterations and vibrational spectra of experiments are ob-

tained by micro-Fourier transform infrared technique. These experimental results demonstrate that the degree of the cell metabolism influence (RNA, phosphate and serine/threonine/tyrosine bands) depends on the intensity of light exposure. Lowest intensity of laser exposure on MCF7 cells showed bio-inhibition with decrease in metabolic rates, while the highest intensity led to bio-stimulation with the increase in the metabolic rates. The middle intensity surprisingly, showed elevation in the metabolic rate without any cell proliferation being noticeable.

Moreover, in [219] authors used low level laser therapy concurrently with radiotherapy of head and neck cancer patient to reduce the pain and complications. The most common complication from the radiotherapy treatment of head and neck cancer is the oral mucositis. The authors used 10mW He-Ne laser at the wavelength of 632.8nm simultaneously with radiotherapy for oral cavity carcinoma patients with the stages II-IV cancer progression. In the 6 week period of observation, they observed the effective treatment results in preventing and healing mucositis in cancer patients.

One of a very few studies that can relate to this research project partially is [220]. In this study near infrared irradiation of a light source similar to solar irradiation is used. The non-thermal effect of this irradiation on doxorubicin in xenografts in nude mice is investigated. The authors introduced a pre- and parallel-irradiational cooling to exclude any thermal effect on their experiments. The aim of this research was to measure any induced non-thermal cytocidal effects

in cancer cells. In their earlier publication, this group of authors demonstrated that NIR penetrates the skin and induces non-thermal affect on dermis [221–224]. To explore the non-thermal effect of NIR radiation, changes in cell viability of cells, DNA damage response pathways, and the percentage of mitotic cancer cells after the treatment is measured and reported. Then, anti-cancer effects of external NIR irradiation in nude mice is measured and compared with docorubicin in xenografts. This evaluation and comparison is conducted by measuring a tumor volume and immunoblot analysis of protein phosphorylation. According to their analysis, the results of the *in vitro* experiment with A549 lung adenocarcinoma cells irradiation using NIR light with the intensity of 2 mW/cm^2 demonstrated a reduction in cell viability of lung adenocarcinoma cells. Promotion in phosphorylation of ataxia-telangiectasia mutated (ATM) in A549 cells is observed as a result of this treatment. Additionally, mitotic percentage of A549 cells points to a significant reduction due to this treatment. Nude mice experiments on tumor growth of MDA-MB435 melanoma cell xenografts exhibit the inhibition due to both NIR and doxorubicin. The paper concluded that NIR irradiation induced non-thermal cytocidal effects in cancer cells as a result of activation of DNA damage response pathway [220].

Chapter 3

Exposure Device Design, Materials and Methods

In this chapter, a complete technical overview of the project and the detailed explanation of the experimental setup and considerations are provided. This chapter also outlines the exposure system design and its limitations, materials and methods used for *in vitro* experimental evaluations. To experimentally evaluate the theoretical hypothesis proposed in [1–3], a radiation device is fabricated and tested on normal and cancer cells.

The design of the exposure system requires several considerations to be addressed first. The selection of the radiation source and the limitations that would be enforced by such decision are discussed in the first section. This section also presents input and output signal characteristics of different radiation sources. After that, Section 3.1 provides a few different design proposals based on the constraints imposed by the environmental factors as well as experimental con-

ditions, and the choice of the radiation exposure light. Then, the final design proposal is presented in the next section. This section also points out certain limitations that are imposed on the project's scope. These restraints are inherent to the nature of experimental *in vitro* evaluation of the proposed theoretical hypothesis.

In section 3.2 of this chapter, a detailed description of cell lines, cell culture materials, experimental setup are presented. Afterward, different regimes of exposure and post exposure incubation and their selection methods are explained. Finally, a description of the qualitative and quantitative assays employed here to evaluate and measure the effects of different wavelengths and exposure regimes on cancer and normal cell lines is provided.

3.1 Exposure System Design

The first critical factor taking into account in design of the exposure system is the light source used for irradiation of cells. The selection of light source energy is between coherent light of Light Amplification by Stimulated Emission (Lasers) and non-coherent light of Light Emitting Diodes (LEDs). Hence, the next section is concerned with the characteristic differences between LED and Laser. The following section outlines specifications of selected far infrared LEDs as well as the their optical intensity provided by LEDMicrosensors, Russia.

Then, three different design proposal based on the choice of the particular light source and experimental environmental condition are proposed and discussed along with their advantages and disadvantages. Subsection 3.1.4 presents the final design specifications of the developed prototype used in this project. Subsequently, final subsection expresses scope constraints imposed by the design, implementation and characteristic limitations that arise from the *in vitro* experimental evaluation of the proposed theoretical hypothesis.

3.1.1 LED versus LASER

LEDs are combination of two different semiconductors n-doped and p-doped. N-doped semiconductors have excess of electrons while p-doped electrons have holes or lack of electrons. When a voltage is applied, electrons from the n-doped region move toward the p-doped region. As a result of this movement, a light of the specific wavelength will be emitted. The color of the light emitted form LEDs depends on the chemical composition of semiconductor combination used in the LED [164].

Low intensity light therapy exposure system can be designed with either lasers or LEDs, but their characteristic differences should be considered when designing such system. Some of the main differences for the design purposes will be named here. In terms of the structures, they both require a double hetero structure for better carrier and optical confinement. Lasers provide coherent light in contrast to

LEDs that provide non-coherent light. Although there have been lots of interest in using laser for healing purposes, there is no reason to believe that coherent Laser light is any better than LEDs [138].

Lasers are dominated by the stimulated emission, while LEDs are by the spontaneous emission. Power and spectral characteristics in Lasers are sensitive to temperature fluctuations, despite the fact that LEDs are indifferent to temperature fluctuations. As a result of this sensitivity, Lasers require expensive drive electronics for temperature stabilization. LEDs have low intensity noise, while Lasers have high intensity noise [225–227].

In addition to that, one of the most recognized researcher in LLLT, Professor Tina Karu, demonstrated in her research with various types of radiation sources that lasers do not have better therapeutic effect than LEDs. Coherent properties of light are not reflected when it interacts with biological tissues at the molecular level. In fact, the absorption of low-intensity light in biological systems is incoherent [202, 228].

Therefore, Laser or coherent light is not any better than LEDs or non-coherent light in terms of its penetration or action. In fact, the benefits are based on each photon action which is the same in both lights [138, 229, 230]. Moreover, LEDs are much cheaper than Lasers [138].

The reason that it has been more research in Low Laser Light Therapy (LLLT)

for healing than LEDs is for the fact that "Laser" has a superior marketing appeal and sound mysterious. However, lasers are costly, means that patients can not do the treatment at home. Karu concluded [228, 231, 232] that under physiological conditions the absorption of low-intensity light by biological system in purely non-coherent. It goes on to the conclusion that at cellular level coherent and non-coherent light with the same wavelength, intensity and irradiation time provide the same biological effects [228,231,232]. It was shown that at the cellular level coherent and non-coherent light with the same wavelength, intensity and irradiation time provide the same biological effects [232].

3.1.2 Visible, Near Infrared (NIR) and Far Infrared (FIR) LEDs

According to the proposed hypothesis presented in the RRM, external radiation of the wavelength range 3500nm to 6500nm is expected to have effect on the biological function of oncogenes and proto-oncogenes [1–3]. And thus, this irradiation is expected to induce therapeutic effects on cancer cells. In this project, LEDs are chosen as the exposure light source over Lasers for the following reasons.

First, according to the earlier discussion in Section 3.1.1, non-coherent light of LEDs and coherent light of Lasers induce the same biological effect on biological systems. In addition, therapeutic effects of LEDs on a number of medical conditions are proven, so the use of LEDs as a light source for exposures is an

emerging, novel idea that it is gaining popularity in medical research. LEDs exposure does not require expensive medical setup, since it is safer to work with and they are generally cheaper to be used in exposure systems. Moreover, no experiments could be found in the literature that LEDs are used as light source for exposure of cancer cells. Hence, here LEDs are chosen over Lasers for the novelty of the proposed method and their identical effects on living organisms.

To comprehensively evaluate the proposed hypothesis, a number of LEDs in and outside the proposed range are selected for external *in vitro* irradiation. The main idea behind this selection is to measure whether the proposed far infrared range induce cytotoxic effects on cancer cells; or this effect can be seen at other wavelengths outside that range, too. Hence, apart from the selected six LEDs in the far infrared range, three low intensity LEDs in the visible range and three LEDs in the near infrared range are chosen for this *in vitro* experimental project. In the following paragraphs, the characteristic specifications of each LED are presented consecutively in the ascending wavelengths:

Visible Range LEDs

The visible range LEDs, also called colored LEDs, are 466nm (Super Bright Blue Color LED) manufactured by Kingbright, 585nm (Yellow Color LED), and 626nm (Red Color) manufactured by HEWLETT PACKARD. The biasing and performance characteristics of these LEDs are shown in Table 3.1.

LED	Peak Wavelength (nm)	Dominant Wavelength (nm)	Package Size (mm)	LED Color	Viewing Angle (°)	Luminous Intensity (mcd)	Forward Voltage, V_F (v)		Capacitance, C(pF)	DC Forward Current I_F(mA)
							type	max		
466nm	430	466	5	Blue	± 8°	150	4.0	4.5	65	30
585nm	583	585	5	Yellow	± 12.5°	96.2	2.1	2.6	15	20
626nm	635	626	5	Red	± 12°	125	1.9	2.6	11	20

Table 3.1: Characteristics of Visible Light LEDs

LED	Package Size (5mm)	Viewing Angle	Radiant Intensity (mW/sr)		Forward Voltage, V_F (v)		Rise/Fall time (ms)	Forward Current I_F(mA)
			typ	max	typ	max		
810nm	5	±12	70	135	1.4	1.9	20	100
850nm	5	±10	120	140	1.5	1.8	20	100
950nm	5	±10	20	40	1.3	1.9	20	100

Table 3.2: Characteristics of Near Infrared LEDs

*Note: Power of the light source is measured by the luminous intensity. It is directional and is measured in Candela (cd). Candela(cd) is the SI base unit of luminous intensity in a specific angle from a light source.

Near Infrared Range LEDs

Three near infrared LEDs are chosen for this project: 810nm, 850nm, and 950nm wavelengths. These LEDs are purchased from Power Light System, Vishay Semiconductors, OSRAM(Opto Semiconductors) in consecutive order. The biasing requirements and radiation specification of these LEDs are demonstrated in Table 3.2.

Far Infrared Range LEDs (Theoretically Proposed Range)

Six LEDs in the computationally calculated far infrared wavelengths range are selected and purchased from LED Microsensor. The wavelengths of the purchased LEDs are: 3400nm, 3600nm, 3800nm, 3900nm, 4100nm, 4300nm. Each LEDs has characteristics that is shown in Table 3.3.

Standard LED models (LED chip with circular or ring top contact) - LEDXX																	
LED Wave-length, nm	Peak emission wave-length, μm			FWHM of the emission band, μW			Power, mW					Voltage, V	Maximum operat-ing current, mA		Switching time, ns			Operating tempera-ture range, $^{\circ}C$
							QCW mode			Pulse mode								
	min	Typ	max	min	Typ	max	min	Typ	max	min	Typ	max		QCW mode	Pulse mode	min	Typ	max	
LED3400	3.30	3.40	3.49	400	500	600	25	35	45	320	400	480	0.2-0.5	250	2000	10	20	30	-200 ... +50
LED3600	3.60	-	3.70	400	-	600	20	-	40	180	-	220	0.2-0.4	250	2000	10	20	30	-200 ... +50
LED3800	3.70	3.75	3.84	500	600	700	20	30	40	180	200	220	0.5-0.8	250	2000	10	20	30	-200 ... +50
LED3900	3.85	3.90	3.94	550	650	750	15	20	30	180	200	220	0.2-0.8	250	2000	10	20	30	-200 ... +50
LED4100	3.95	4.05	4.09	700	850	1000	15	20	30	180	200	220	0.5-0.7	250	2000	10	20	30	-200 ... +50
LED4300	4.10	4.15	4.30	700	850	1000	8	10	12	180	200	220	0.2-0.8	250	2000	10	20	30	-200 ... +50

Table 3.3: Far Infrared LEDs characteristics [233]

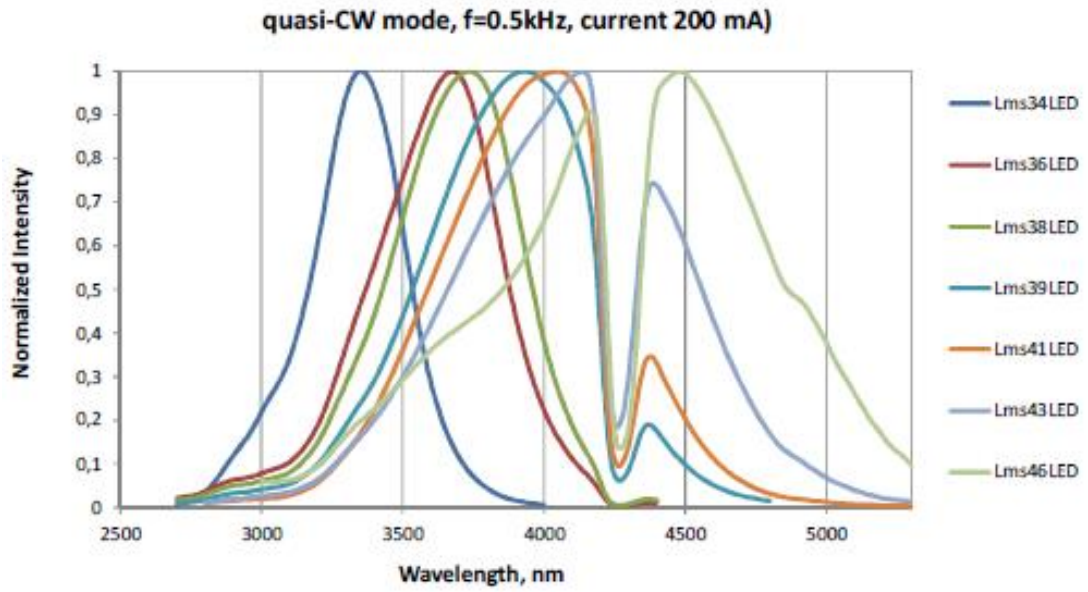

Figure 3.1: Intensity vs. Wavelength for far infrared LEDs [233]

Figure 3.1 shows the maximum optical intensity for LEDs in the far infrared wavelengths. The images (demonstrated the peak wavelengths) show that each LED is operating at it's maximum nominal optical intensity.

Then, the optical angles at which different types of LEDs are irradiating, are shown in Figure 3.2.

The purchased LEDs are with the parabolic reflectors, therefore the electromagnetic wave radiation is conducted with a narrow optical angle. The optical angle for these LEDs is between -10° and +10° or in other words its viewing angle is ±10°. Narrow viewing angle indicates a minimum dispersion of the radiated light and the maximum possible optical intensity.

Voltage and current characteristics of these far infrared LEDs are provided in

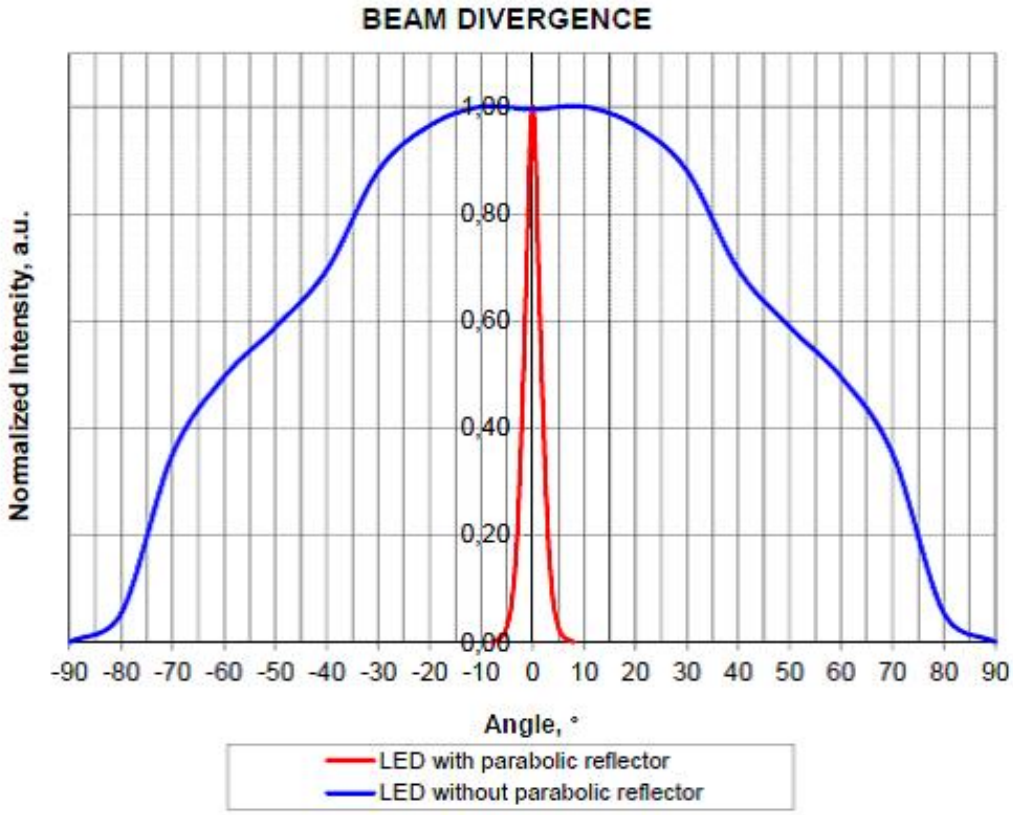

Figure 3.2: Angle vs. Optical Intensity for far infrared LEDs [233]

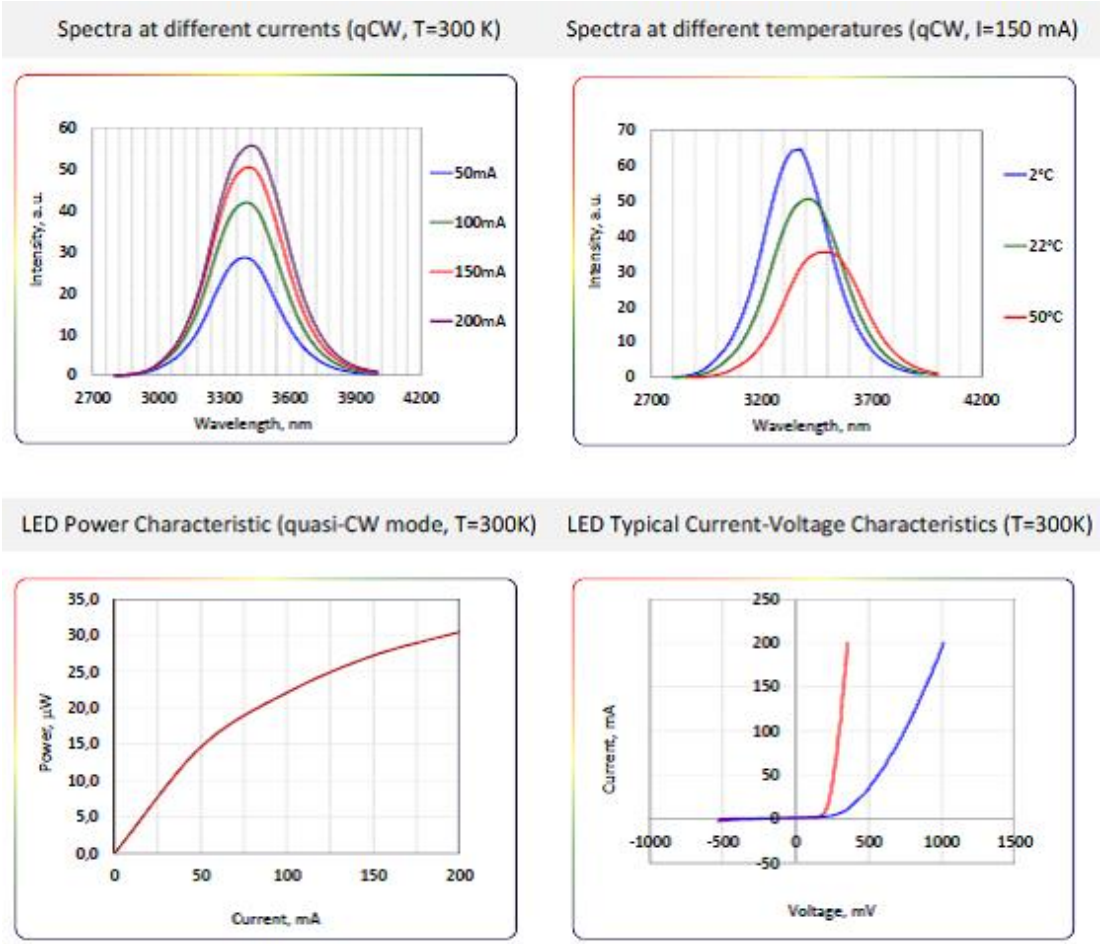

Figure 3.3: Specifications of 3400nm LED [233].

the following figures. Figure 3.3 depicts current-voltage, power, current, and temperature characteristics of 3400nm LED.

Figure 3.4 demonstrates current-voltage, power, current, and temperature characteristics of 3800nm LED.

In Figure 3.5, characteristics of 3900nm LED are shown with current-voltage, power, current, and temperature graphs.

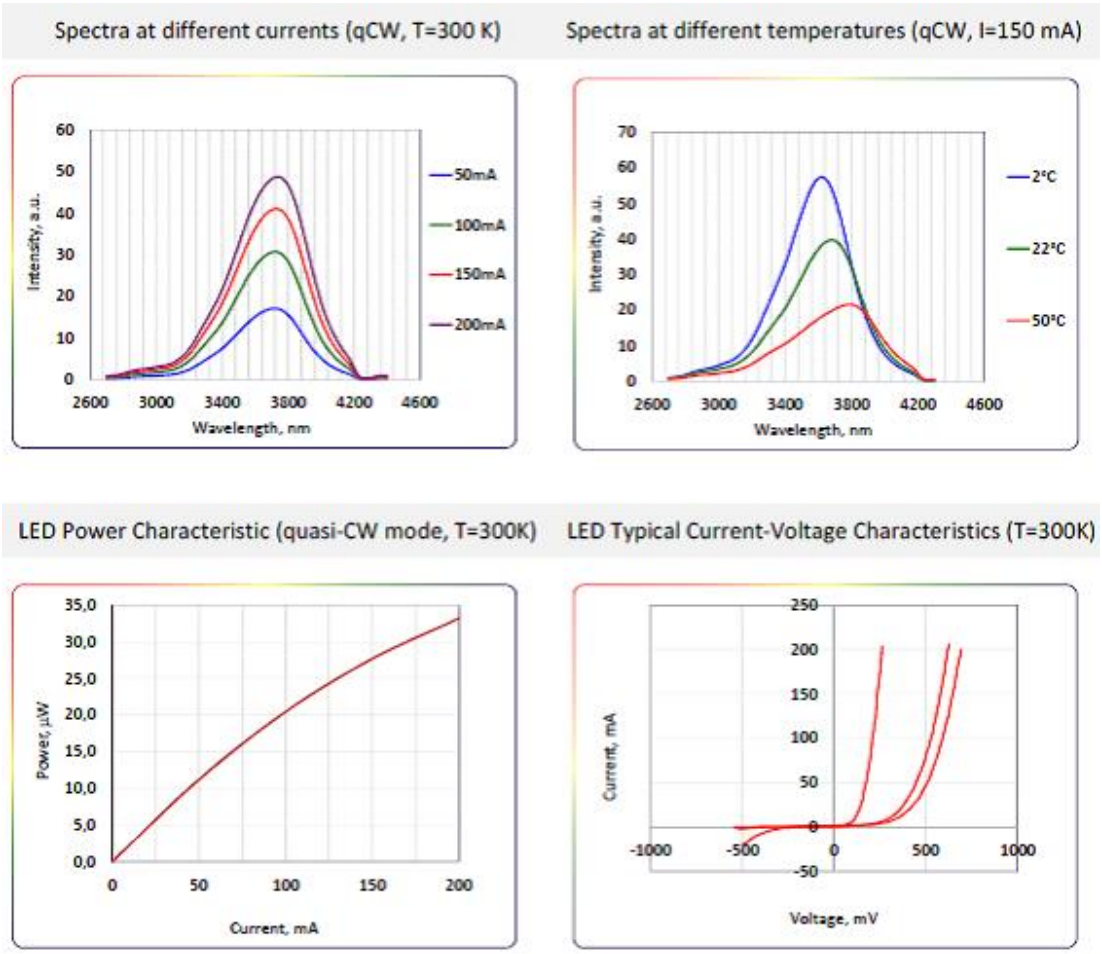

Figure 3.4: Specifications of 3800nm LED [233].

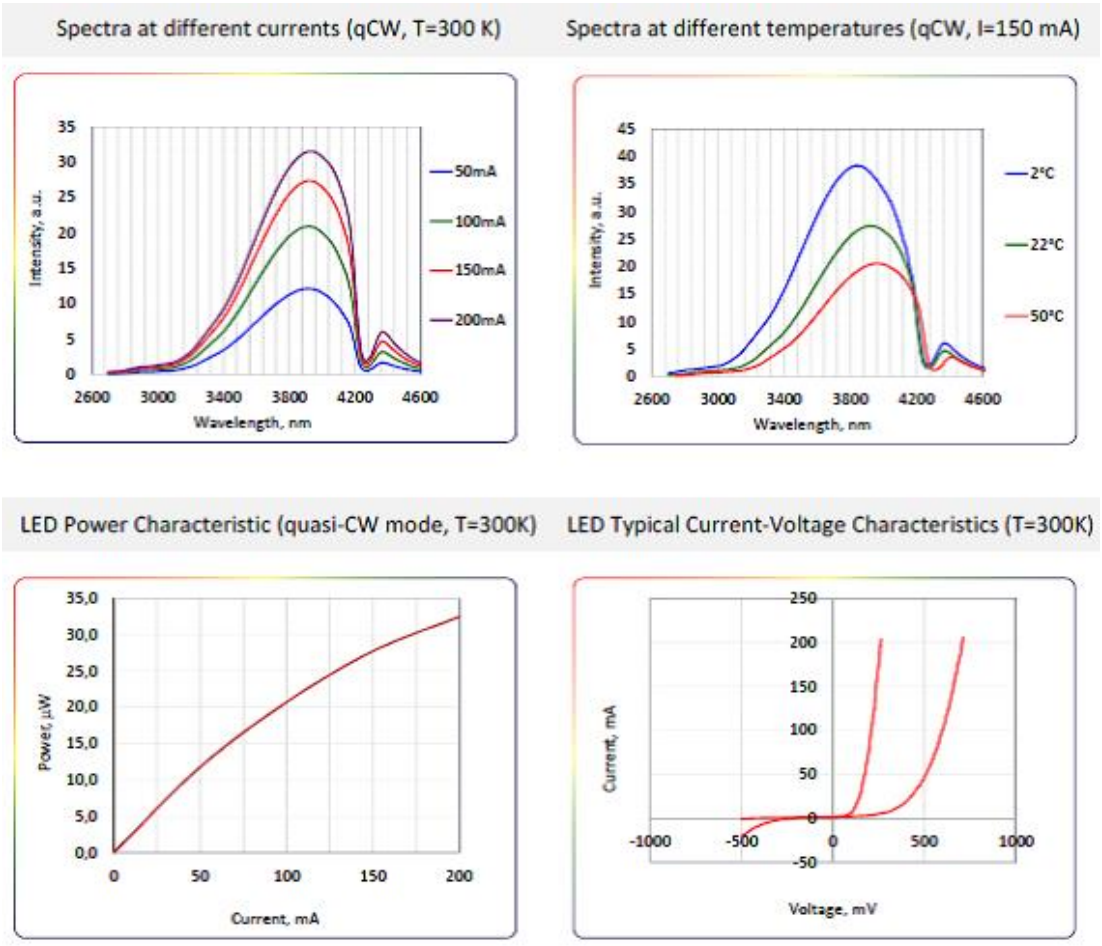

Figure 3.5: Specifications of 3900nm LED [233].

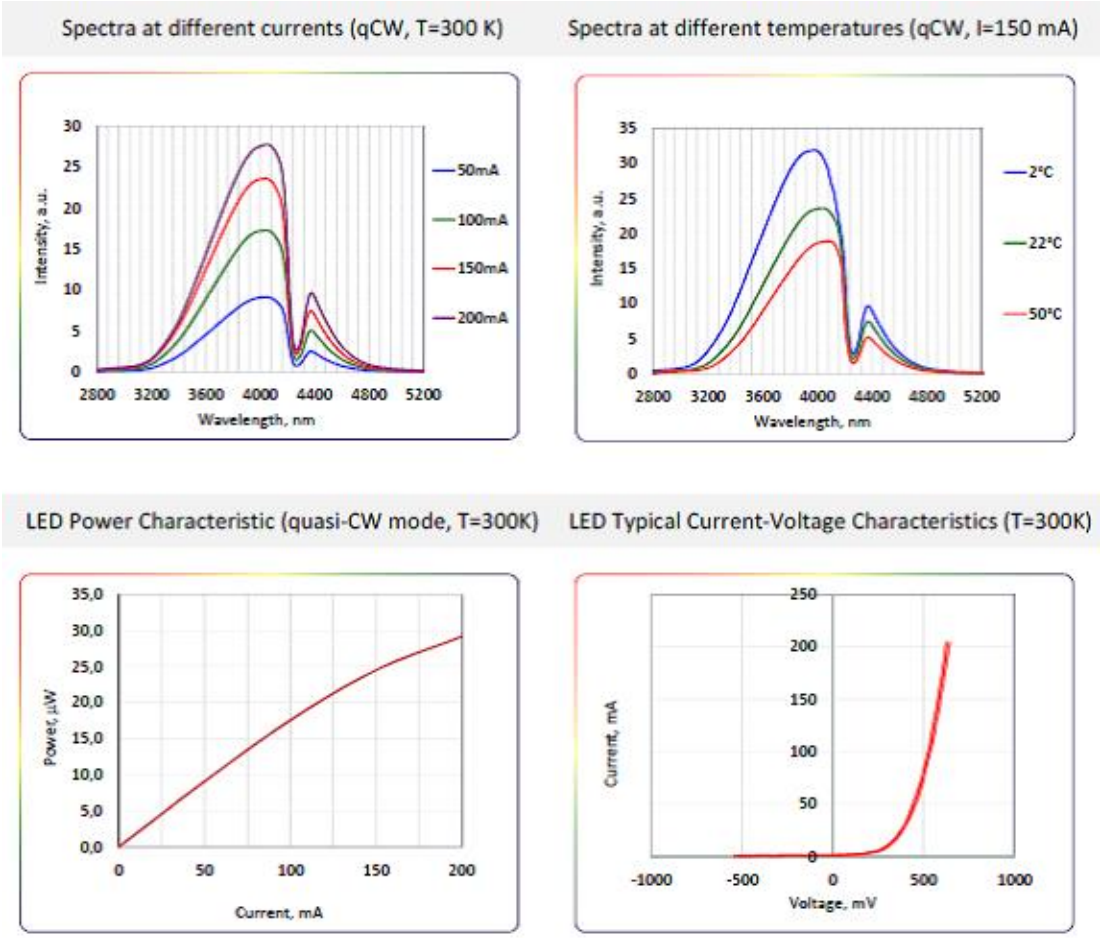

Figure 3.6: Specifications of 4100nm LED [233].

The following images (Figure 3.6) show the current-voltage, power, current, and temperature characteristics of 4100nm LEDs in the far infrared range.

Finally, Figure 3.7 illustrates current-voltage, power, current, and temperature characteristics of 4300nm LEDs used for *in vitro* experiments in this project.

Now, Table 3.4 represents the optical powers per steradian for all LEDs used in this project, according to the measurement provided by LED Microsensor. Since low intensity light radiation is the main scope of this project, the LEDs are

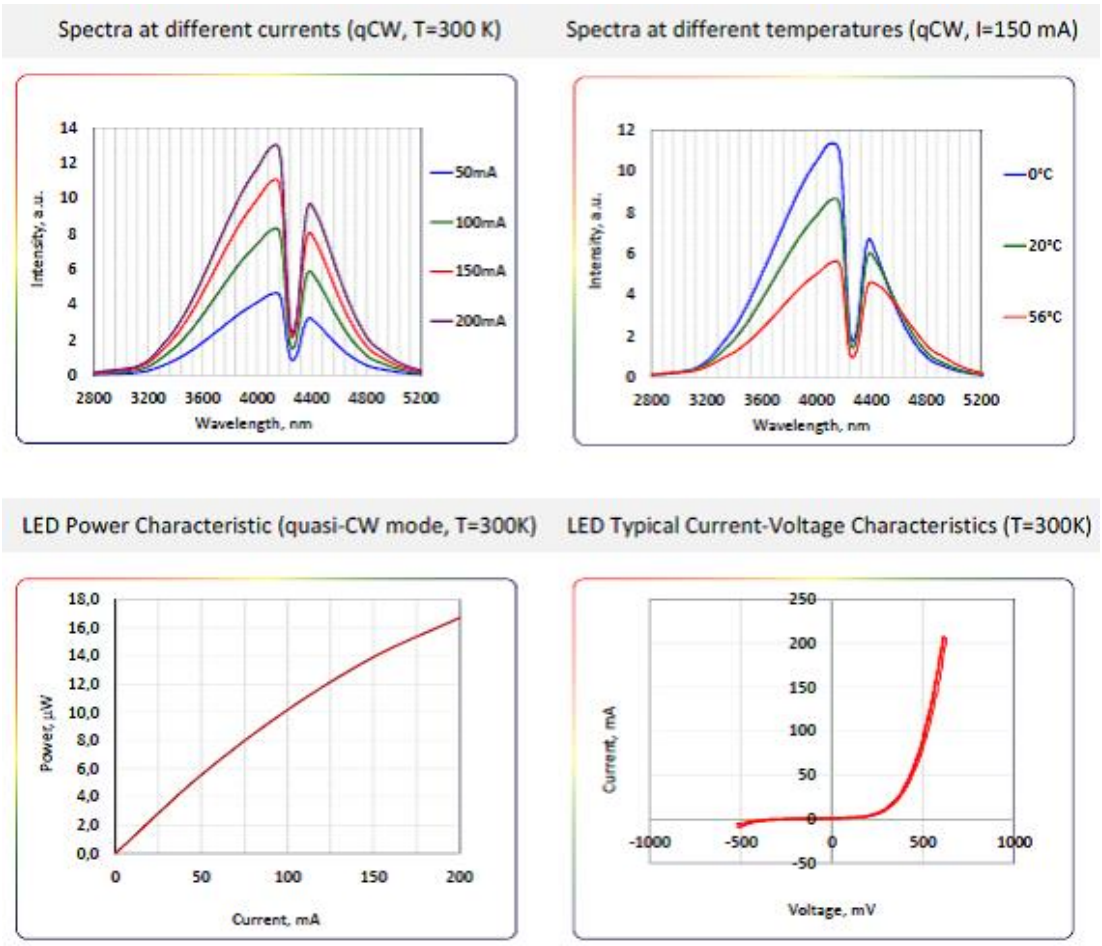

Figure 3.7: Specifications of 4300nm LED [233].

selected based on their low intensity [187, 217].

Optical Power

The LED mechanism of light emission is due to a release of a quantum of energy, called a photon, when the excited electron from a higher energy level moves to a lower energy band gap. The energy of each photon is measured as follow:

$$E_p = \frac{hc}{\lambda} \tag{3.1}$$

where E_p is the photon's energy and λ is the wavelength. Since LED is emitting a number of photons depending on its forward current, then the light power (P) is energy per second which equivalently means the number of photons multiplied by the energy of each photon. This statement is demonstrated in Equation 3.2.

$$P = N\eta_{int}E_p/t \tag{3.2}$$

where N is the number of electrons. P is the light power and measured in mW. η_{int} is internal efficiency and t is time. N can be replace with current (I) multiply by time (t) divided by electron charge (e). That is, $N = \frac{It}{e}$. Thus, Equation 3.2 can be rewritten as:

LED Wavelength	sample	#	optical power (at 200mA, qCW)		#	optical power (at 200mA, qCW)	
			μW	μW per steradian		μW	μW per steradian
3400nm	Lms34LED-R	# 1	26.7	5.9	# 2	30.8	6.8
3600nm	Lms36LED-R	# 1	39.9	8.8	# 2	36.7	8.1
3800nm	Lms38LED-R	# 1	22.5	5.0	# 2	22.3	4.9
3900nm	Lms39LED-R	# 1	21.0	4.6	# 2	21.5	4.7
4100nm	Lms41LED-R	# 1	15.4	3.4	# 2	18.2	4.0
4300nm	Lms43LED-R	# 1	8.8	1.9	# 2	8.3	1.8

Table 3.4: Measured Optical Intensity of each far infrared LED used in this project [233].

$$P = \frac{\eta_{int} E_p}{I} \qquad \text{Or,} \qquad P(mW) = \frac{\eta_{int} E_p(eV)}{I(mA)} \tag{3.3}$$

where light power (P) is measured in mW, E_p is measured in electron Volts (eV) and current (I) in mA.

Depending on the LEDs intrinsic design characteristics including optical irradiation angle and design structure, a radiant intensity is commonly measured in power per area (mW/cm^2) or power per steradian (mW/sr). The SI standard for the radiant intensity measurement is power per steradian. However, the difference between these two units of measurement comes from their methods of measurement. LED light is irradiated in a cone shape angle as shown in Figure 3.8.

If this area is measured as cone shape and considering a sphere contains 4π steradians, then a zone area is $A_z = 2\pi R(h = R - d)$. And, if a detector is used for measuring the intensity, the area of the detector would be $A_D = \pi r^2$. Thus, the solid angle of the cone is calculated as follow:

$$\omega = \frac{4\pi A_z}{A_s} = \frac{2\pi h}{R} \tag{3.4}$$

The conversion of power per area to power per steradian is:

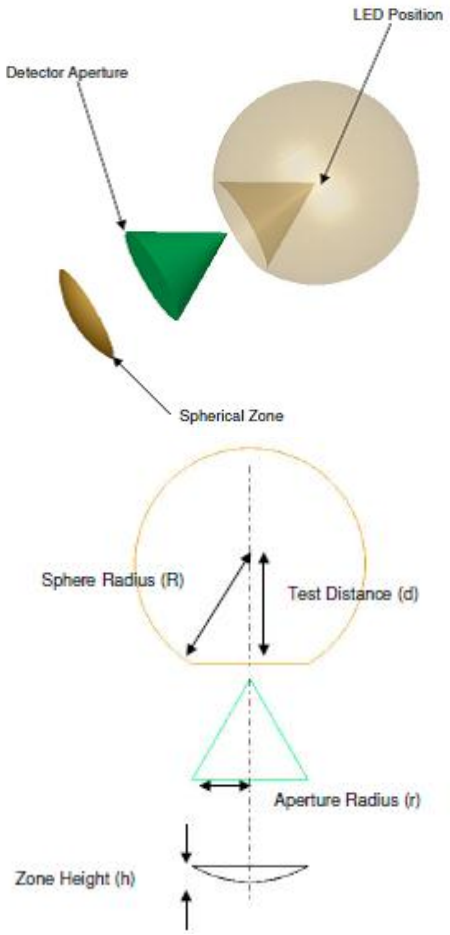

Figure 3.8: Solid angle measurement [234]

$$
\begin{aligned}
E_{e,sr}\omega(mW/sr) &= \text{Power/Intensity} = E_{e,area}A_D(mW/cm^2) \\
E_{e,sr}\omega &= E_{e,area}A_D \\
E_{e,sr} &= \frac{E_{e,area}A_D}{\omega}
\end{aligned} \tag{3.5}
$$

Moreover, a luminous intensity of a monochromatic light source with a specific wavelength λ is calculated as follow:

$$E_v = 683.002 \times \bar{y}(\lambda) \times E_e \tag{3.6}$$

where E_v (I_v) is the luminous intensity in candelas (cd = lm/sr). E_e (I_e) is the radiant intensity in watts per steradian (W/sr). And, $\bar{y}(\lambda)$ also known as $V(\lambda)$ is the standard luminosity function. This function is dimensionless and describes an average spectral sensitivity of human visual perception of brightness for different wavelengths. Even though the numbers are not perfectly accurate, they are good evaluations for experimental purposes. Commission Internationale de $I'\acute{E}$clairage (CIE) established a standard $\bar{y}(\lambda)$ function to be used for conversion of the radiant energy into the luminous energy. A particular value corresponds to each wavelength, which is normalized to a peak value of unity at 555nm. If a monochromatic wavelength is used, a corresponding $\bar{y}(\lambda)$ function value (a constant) is replaced in Equation 3.6. In case of multi-wavelength, sum or integrate

over the spectrum of present wavelengths should be used for luminous intensity calculation.

$$E_v = 683 \int_0^{\inf} \bar{y}(\lambda) \frac{dE_e(\lambda)}{d\lambda} d\lambda \tag{3.7}$$

Moreover, in these calculations, a luminous flux or luminous power is measured by lumen (lumen(lm)= candela(cd).steradian(sr)).

3.1.3 Different Exposure System Designs

In this section, three different types of the proposed exposure system are described and presented. These design proposals are based on the proposed theoretical hypothesis investigated experimentally in this project. According to the wavelengths obtained from the RRM calculations [1–3], some effect on functionality of oncogenes and proto-oncogenes in regard to cell growth are expected to be observed. The far infrared wavelength range proposed by the theoretical implementation of the RRM approach is between 3500nm and 6500nm. Hence, the selected LEDs in the mentioned wavelength range are required to be biased appropriately to work in their optimum range. Various environmental and physical constraints such as humidity, size of the incubator shelves, robustness of the device, the maximum number of LEDs to be biased, and the stability of the biased current imply a meticulous design consideration. To address different aspect of these constraints,

three different types of the design are proposed for this *in vitro* far infra-red exposure system to be tested on human and animal cancer and normal cell lines. Each design has its own advantages and disadvantages. Then, a combination of these design proposals are used for the final design in this research project.

Detailed description of each design is presented in the following section: 1) the first one is a fully digital circuit; 2) the second: a semi-digital circuit; followed by 3) a fully analog circuit.

Digital Circuit Design

The first design is the most optimal one and it utilizes a micro controller to provide a more accurate tunable pulse as well as different levels of intensity. In this circuit design, a micro controller (ATMega 32) and 3 Gals (v2500c) is used as the main component of the circuit. In addition, a key pad is used to take the frequency and peak to peak amplitude current pulse as input of micro controller. Then, the entered current frequency is shown through 4 seven segments assigned as part of this design. The frequency of the pulse is obtained by manipulating the clock of micro controller through a command in the program of micro controller.

The advantages of this system are as follow:

First, the system provides a sharp and accurate pulse for different current intensity.

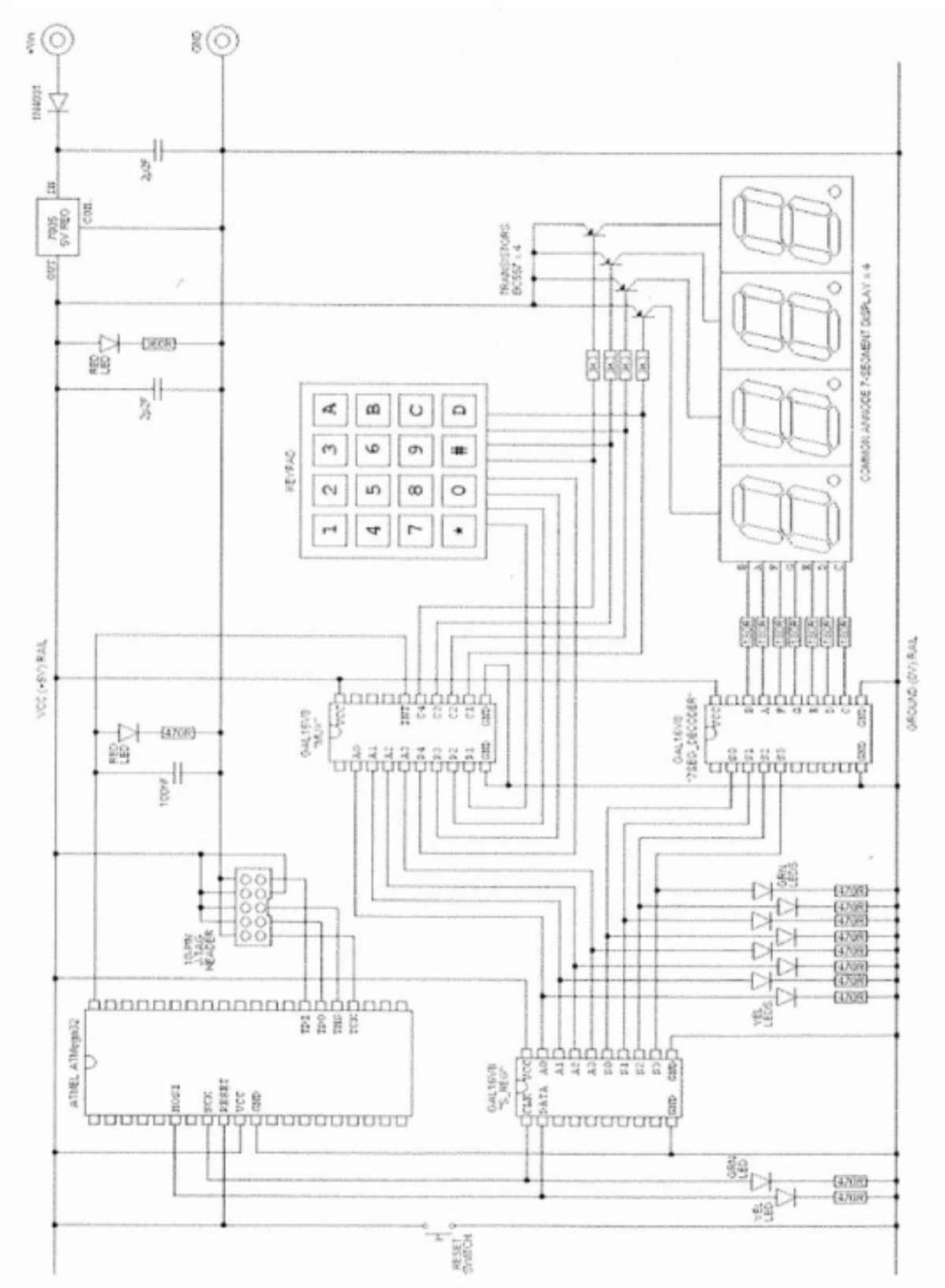

Figure 3.9: Digital Design Proposal

Second, this design provides the identical input current frequency, modulation and peak to peak amplitude for up to 6 LEDs.

Third, the frequency of the current pulse is tunable, since it can be adjusted from the keypad.

Fourth, different Pulsed Width Modulation (PWM) of the output current is obtained by a small adjustment in the command of the micro controller program.

The disadvantages are:

First, for any modification to the system, a good knowledge of the computer architecture, assembly language, C/C++ and gal programming are required. So, it is a complex system in terms of trouble shooting and adjustments.

Second, any shock to the circuit due to any accidental fall of the board requires the micro controller and/or gals to be programmed again since the system is fully digital. Thus, it is sensitive to physical shocks.

Third, the proposed system is susceptible to moisture and heat. The experiments are conducted inside the incubator of $37^{\circ C}$ with 5% CO_2. Therefore, this circuit is not able to perform well in the humid environment of the incubator.

Fourth, due to its complexity, any small glitches in the system require the expertise of an electrical engineer to handle it.

Semi-digital Circuit Design

Figure 3.10 is the second optimum design proposed for this project. In this design, Integrated Circuit (IC) 555 is used to reduce the digital complexity of the system. The current output pulse is regulated and stabilized through analogue element such as resistors, diodes and transistors. This circuit accommodates 1 far infrared LED only.

The advantages of this semi-digital circuit are:

First, working with IC 555 timer does not require a complex computer programming knowledge.

Second, the output pulse current generated by this design is accurate.

Disadvantages are:

First, the circuit is not able to provide a stable input bias for various intensities and different numbers of LEDs. Changing peak to peak current, modulation and frequency input required for the optimum operation demands hardware adjustments in the system.

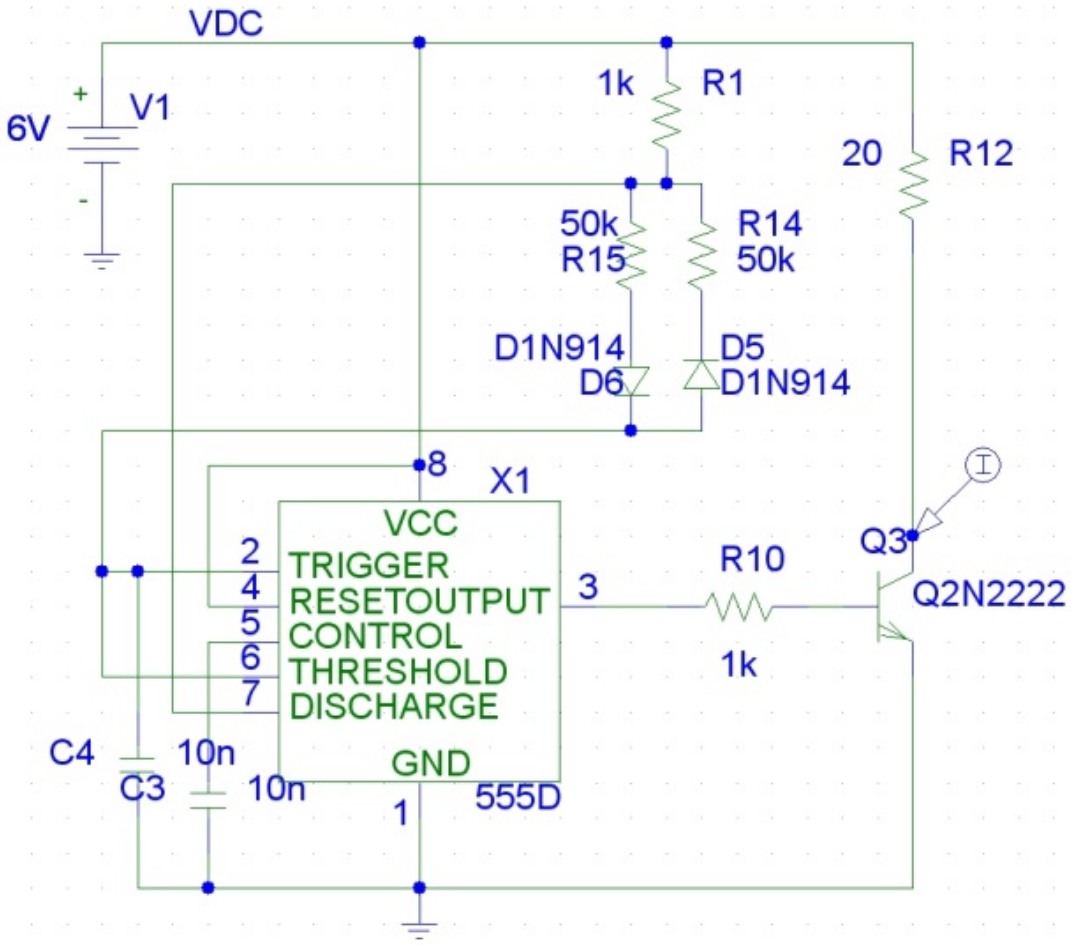

Figure 3.10: Semi-analog Design Proposal

Second, changing the number of active LEDs changes the amplitude of the current pulse. Thus, by adding extra LED, the output biased current for LEDs is deteriorated.

Third, IC 555 output signal is very unstable in humid environment such as incubator.

Fourth, duration of exposure affects the output current pulse accuracy. This means that if the circuit runs for a longer time, the current pulse deteriorates further.

Fifth, the output of the circuit is so unstable that it cannot accommodate to drive more than one LED without significant changes in the hardware design part.

Analogue Circuit Design

Figure 3.11 represents the third optimum design. To overcome the shortcoming of digital and semi-digital designs for a humid environment, a fully analog circuit is proposed. In this circuit, resistors, capacitors, diodes and transistors are used to bias far infrared LEDs that can irradiate cells inside the incubator. The final version of the circuit in figure 3.11 is modified during the board printing (PCB) to accommodate more LEDs and incorporate some advantages of other design proposals.

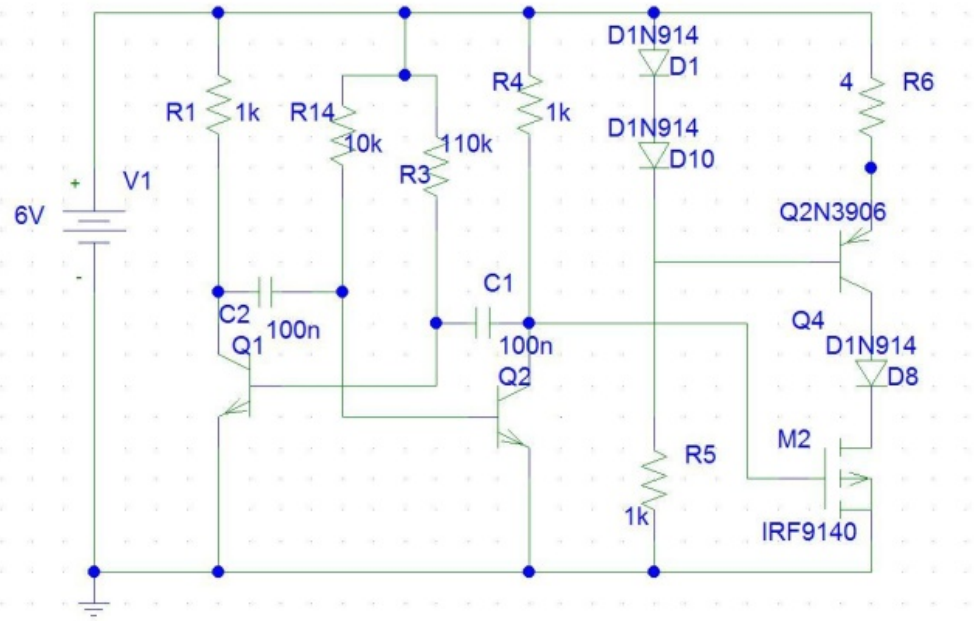

Figure 3.11: Analog Design Proposal

Here are the advantages of this design:

First, the outcome of the system is very reliable and accurate since the design is analog.

Second, this design is less affected by physical shock, moisture or heat compared to the other two designs.

Third, the complexity of this design is less than the other two. By not using a micro controller immensely reduces the design complexity. In case of physical shock, a user does not face programming problems in assembly and C/C++ language for GALs and a micro controller.

Fourth, unlike the second design, this circuit does not encounter current in-

stability that requires hardware adjustment for different number of used LEDs.

The only drawback of this system is lack of sharpness in rising edges of the current pulse compared to the other two digital designs. However, as indicated in their specifications, these far infrared LEDs are generally sensitive to the current pulse level and its frequency, not the sharpness of current rising edge. Thus, this issue does not present a huge obstacle for the optimum performance.

The following images in Figure 3.12 and 3.13 demonstrate a printed circuit board (PCB) of the exposure system and the final fabricated exposure system used for *in vitro* experimentations in this project.

The exposure system is placed upside down on 96-well plate, shown if Figure 3.14, for the quantitative assays and 24-well plates for the qualitative assays. Far infrared LEDs placement in this device is as follow: three LEDs on the first row from the top of the image and on the left hand side are 3400nm, the second row from the top has three 3600nm LEDs, the third row has three 3800nm, the fourth row has 3900nm, the fifth row contains three 4100nm LEDs, and the sixth row has three 4300nm LEDs.

It is worth to mention that the area of each hole drilled for each LED is approximately identical to the area of each well in 96-well plate as it is shown in Figure 3.14

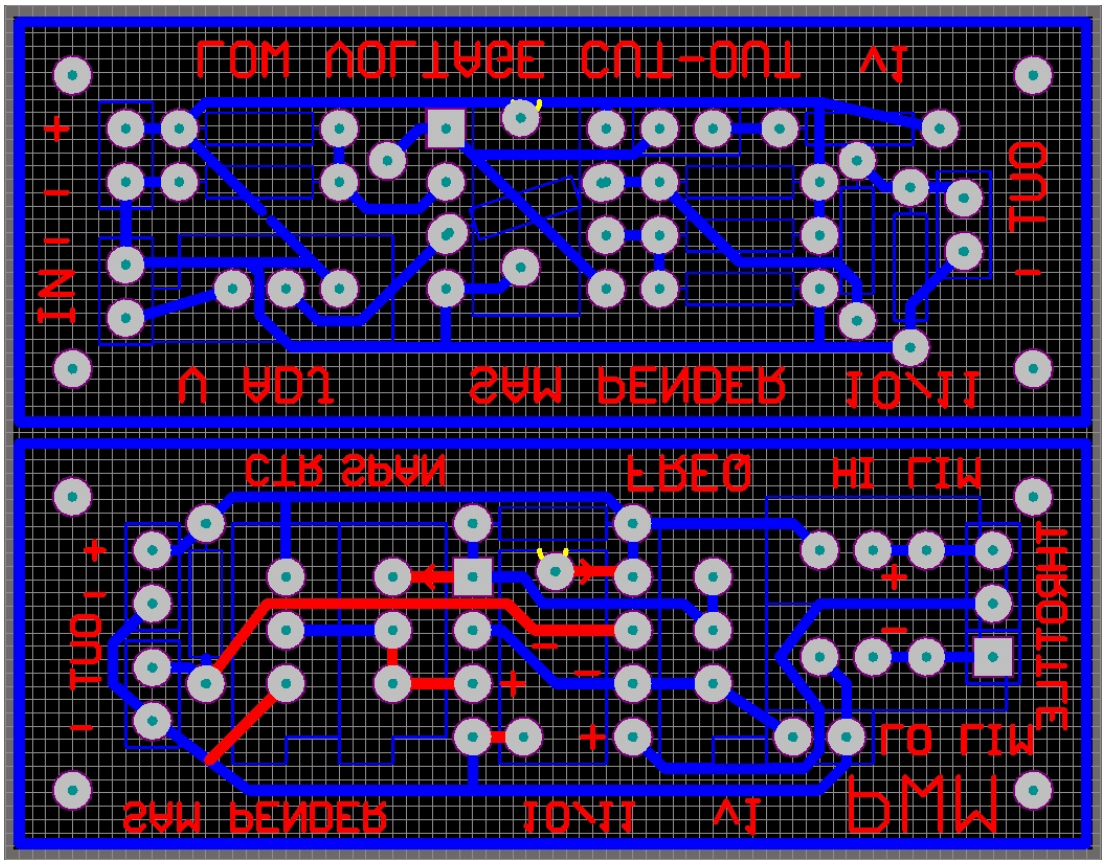

Figure 3.12: Printed Circuit Board (PCB) for the exposure system biasing one far infrared LED. Scale of 1:1

Figure 3.13: Final fabricated exposure system used for external *in vitro* irradiation of cancer and normal cells in this project.

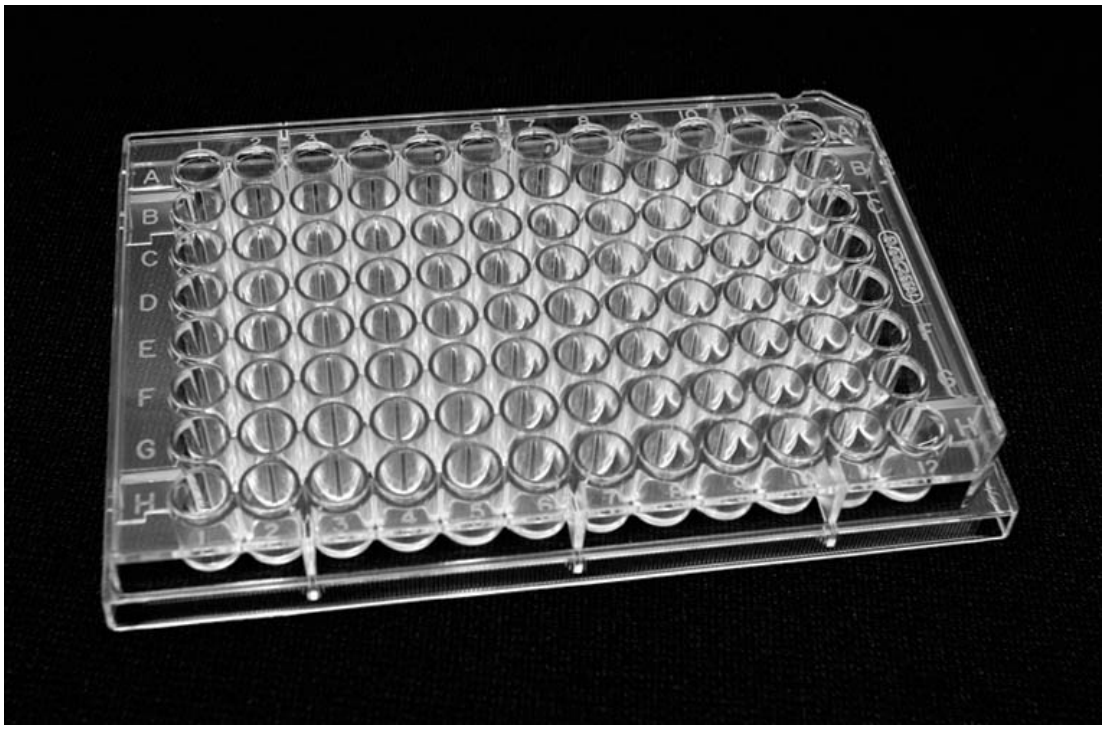

Figure 3.14: standard flat bottom corning 96-well plate image from the internet.

3.1.4 Proposed Design Specifications

As explained earlier, the idea of using low intensity light is considered to be a newly developed concept gathering more popularity as an innovative approach for different medical conditions other than cancer research. The use of this approach for cancer treatment is an innovative approach and novel attempt. Theoretical hypothesis, from implementation of the RRM concepts, predicts that far infrared wavelength range 3500nm-6500nm can induce changes in biological activity of oncogenes and proto-oncogene proteins. These genes play crucial role in spreading and development of cancer. According to the prediction, the external exposures of the proposed wavelength range is expected to instigate therapeutic effects on

cancer cells. To evaluate this theoretical hypothesis, experimental evaluation is the first necessary step. Thus, an external exposure system that can emit light in the proposed wavelength range is developed for in vitro experiments on normal and cancer cell lines.

The proposed exposure system is expected to bias a selected number of frequencies in the range of 3500nm-6500nm simultaneously. Each LEDs irradiates a particular wavelength monochromatically. Since six LEDs are selected in the far infrared range and three of each frequency are needed for triplicate of the experiments, the input current for eighteen far infrared LEDs thus should be accommodated in a single electrical board.

Scope Limitation

The hypothesis of this project falls into the category of the electromagnetic radiation therapy for cancer treatment with the use of Low Intensity Light Therapy (LILT). Specifically, this project is mainly concerned with *in vitro* experimental radiation of the selected normal and cancer cells using Light-Emitting Diodes (LEDs).

The first scope limitation is the types of cancer tumors that this hypothesis, if validated experimentally, can induce therapeutic effects on cancer cells. These constraines come from the intrinsic nature of the far infrared wavelengths pen-

etration into a patient's body. The penetration depth of the infrared radiation depends on its wavelengths, and can reach up to some centimeters, while the near infrared light has the deepest penetration rate [235–238]. Thus, the infrared radiation can penetrate through the body for two to three centimetres and human body absorbs most of its energy in contrary to strong reflection of the visible light. Hence, our hypothesis and design are proposed for the surface and near the surface tumors. The fabricated exposure device is expected to induce therapeutic effects on cancer cells such as melanoma, breast cancers and other skin cancers. As a result of this limitation, mouse melanoma cell line (B16F10) and human breast cancer cell line (MCF7) are used for the *in vitro* experimental evaluation due to their availability and compatibility to the types of cancers that the fabricated exposure system is designed for.

The other limitation is related to the far infrared wavelength LEDs used in this project. Far infrared wavelength LEDs are not readily available in the market due to their limited and specialized functionality such as gas sensing. Therefore, conducting the experiments for each wavelength within the computationally predicted wavelengths range is almost impossible. There are only a handful of wavelengths (in the RRM predicted range) that are available for purchase and they are very expensive.

3.2 Materials and Methods

In this section, materials and methods used for the *in vitro* experimental evaluation are described in details. This section begins with description of cell lines used for the external irradiation and continues with cell culture medium used for cellular subculture, storing and resuscitation. Then, different quantitative and qualitative assays conducted in this work are explained in details.

3.2.1 Cell Lines

Four cell lines are used as the primary cells for the *in vitro* experiments. Two of the cell lines are animal cells and the other two cell lines are human cell lines. These cell lines are provided by the Biotechnology Lab, School of Applied Science, RMIT University, Australia. Due to the limitation of the proposed device and hypothesis, only near surface tumors are tested and evaluated. Therefore, mouse melanoma and human breast cancer cells are used here, since both are regarded as the near surface tumors.

Murine Melanoma Cell line (B16F10) is a murine melanoma cell line used extensively in cancer research. The species of the cell line is Mouse and it is skin tissue. The morphology of the cell line is categorized as Fibroblast-like characteristics and their growth mode is adherent [239]. Thus, these cells represent animal cancer cell line in this work.

Chinese Hamster Ovarian Cell line (CHO) is a cell line derived from the ovary of Chinese Hamster. CHO is used in medical and biological research extensively. CHO cells are categorized as epithelial cells and have relatively rapid growth in culture. This cell line is grown as a cultured monolayer with adherent growth mode.

Human Breast Cancer Cell line (MCF7) is a breast cancer cell line which was taken from human breast tumor at Michigan Cancer Foundation-7 in 1970. The cell line is an invasive breast ductal carcinoma. Growth mode of MCF7 is adherent and the morphology of the cell line is categorized as epithelial cell type. MCF7 is used in this research as a human cancer cell line [240].

Human Epidermal Melanocyte Cell line (HEM) is human primary cell line isolated from human neonatal foreskin. The cell morphology of HEM is categorized as Epidermal with the growth mode of adherent. This cell line represents human normal cell line. It is also used as a comparison for human breast cancer cell line in the evaluation of far infrared exposure effect hypothesis in this research work.

3.2.2 Cell Culture Medium

Medium solution used for cell culture and subculture of B16F10, Chinese Hamster Ovarian (CHO), MCF7 and HEM cell lines consists of the following items:

DMEM (Dulbecco's Modified Eagle Medium) is purchased from Invitrogen life technologies, Australia. DMEM is a widely used basal medium for supporting the cell growth in mammalian cells. According to invitrogen webpage, variety of cells can grow in DMEM including primary fibroblasts, neurons, glial cells HUVECs, and smooth muscle cells. The DMEM medium used in this project is the invitrogen modification with high glucose, L-glutamine, Phenol Red, and Sodium Pyruvate.

HEPES (4-(2-hydroxyethyl)-1-piperazineethanesulfonic acid) purchased from Invitrogen life technologies, Australia. It is a zwitterionic organic chemical buffering agent. Addition of HEPES to cell culture medium provides supplemental buffering at pH level of 7.2 to 7.6. HEPES does not provide nutritional benefit to cells. The presence of HEPES in the media is solely for the extra buffering capacity.

FBS (Fetal Bovine Serum) is purchased from Bovine Serum Biological, Australia. FBS serum supports consistent cell growth over time because of its high content of embryonic growth promoting factors. The serum is manufactured from fetal bovine blood collected from government approved abattoirs. It consists of $\leq$ 25mg/dL hemoglobin and $\leq$ 10EU/mL endotoxin

At first, HEPES is added to the DMEM with the ratio of 0.2 to 10. This means HEPES added to DMEM is 2% of the total volume of DMEM. Then, FBS is added to the solution with the ratio of 1 to 9 which means FBS

amount added to the solution was 10% of the total solution volume [241].

Penicillin-Streptomycin is also purchased from Invitrogen life technology, Australia. The ratio of 0.1 to 10 was added to the cell culture medium which is around 1% of the solution to prevent cell culture contamination. The combination of antibiotics penicillin and streptomycin are used to prevent bacterial contamination of cell culture with gram-positive and gram-negative bacteria [241].

0.05% Trypsin-EDTA (1X) with phenol red is used for cell dissociation during the routine cell culture passaging. Trypsin is purchased from Invitrogen life technology, Australia. Trypsin is an irradiated mixture of proteases derived from porcine pancreas [241].

Cells are sub-cultured at 70-80% confluency. The sub-cultured passages, used in this work, are all passage numbers less than 15 to avoid any cell culture deterioration and distortion of proper reaction to the treatments. Cells are also seeded at the initial density of 1×10^4 for quantitative analysis and initial density of 2×10^5 is used in qualitative assays. Furthermore, cells are incubated inside the incubator at $37^{\circ C}$ with humidified atmosphere containing 5% CO_2.

3.2.3 Experimental Setup

The regimes of exposure and post exposure are determined after a number of preliminary experimental tests for the optimum regime. To find the optimum exposure and post exposure incubation, the effects of irradiation starting from 30 minutes of exposure and 30 minutes of post exposure incubation are recorded and compared. Then, at each consecutive step, duration of exposure or post exposure incubation are increased alternatively. Since the changes in cell viability or cell morphology are not significant for 30 minutes of exposure, the timing of exposure irradiation and post exposure incubation are increased alternatively to reflect its exposure effect visibly. Hence, 30, 60, 90, 120 and 180 minutes of irradiation with different post exposure incubation of 30 minutes, 3 hours, 6 hours, 18 hours and 24 hours of post exposure incubation are studied for possible biological effects. Then, after a number of experiments, the following three regimes of exposure and post exposure incubation reveal to induce the most visible effect that were qualitatively and quantitatively assessed.

Exposure Regime 1 consists of 1.5 hours of exposure irradiation with no post exposure incubation.

Exposure Regime 2 consists of 1.5 hours of exposure irradiation with 24 hours of post exposure incubation.

Exposure Regime 3 consists of 3 hours of exposure irradiation with 24 hours

of post exposure incubation.

These exposure regimes are determined to clarify whether the exposure irradiation or post exposure incubation induce more significant biological effect. The experimental setup for conducting EMR exposures and cell-based quantitative and qualitative assays are explained in the following sections.

3.2.4 Plates Setup

Irradiation of cells for quantitative analysis of all experiments is conducted in 96-well plates. Plates are sterile, flat bottom 96-well plates from Corning Life Sciences, NY, USA. The specification of the 96-well plates is presented in Table 3.5 and their image is shown in Figure 3.14. The shape and diameter size of LEDs and their place in the exposure system are very closed to the diameter of each well in the 96-well plates. In order to avoid the cross talk between and interference from different wavelengths in the exposure system, experiments are conducted in wells surrounded by empty wells. Hence, the 2^{nd}, 4^{th}, 6^{th}, 8^{th}, 10^{th} and 12^{th} column of these plates and rows B, D, F are filled with 100μL of the medium with cells (as indicated with black color in Figure 3.15). In addition, before the start of experiments these sterile plates are UVed for 1.5 hours to remove any contamination threat.

For qualitative assays, 24 well plates are used. These 24 well cell culture plates

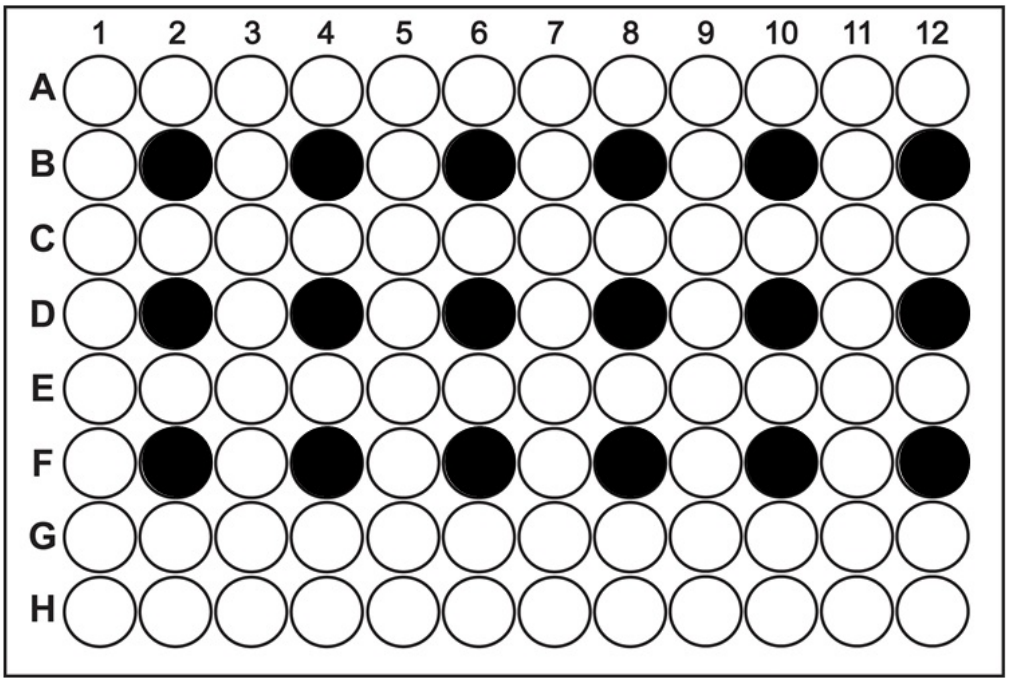

Figure 3.15: 96-well cell culture plate template for *in vitro* experiments.

are sterile, flat bottom plate from Corning Life Sciences, NY, USA. In phase contrast microscopy each well of the second row (row B) is exposed to different wavelength in the far infrared range. The same structure of the exposure is repeated on the third row (row C). Sham exposed wells are the first row (row A) as it is shown in Figure 3.16.

3.2.5 Heat Shield Gel

As it is evident, exposures at the far infrared wavelengths may induce heating effects in cells. Although there is a 2mm gap between LED exposure and the cell medium, extra measures are put in place to remove any heating effect. Heating effects may cause hyperthermia in the experiments. The mechanism of hyper-

Figure 3.16: Image of 24-well cell culture plate from the internet.

Type of Plate	Well Volume (μ L)	Well Depth (mm)	Well Diameter (top/bottom) (mm)	Plate Length (mm)	Plate Width (mm)	Plate Height (mm)	Well Bottom Thickness (mm)
96 well flat bottom	360	10.67	6.86/6.35	127.8	85.5	14.2	1.27
24 well flat bottom	1900	17.4	16.26/15.62	127.89	85.6	19.69	1.27

Table 3.5: Microplate Dimension for Corning 96 Well and 24 Well Microplates from Corning Life Sciences

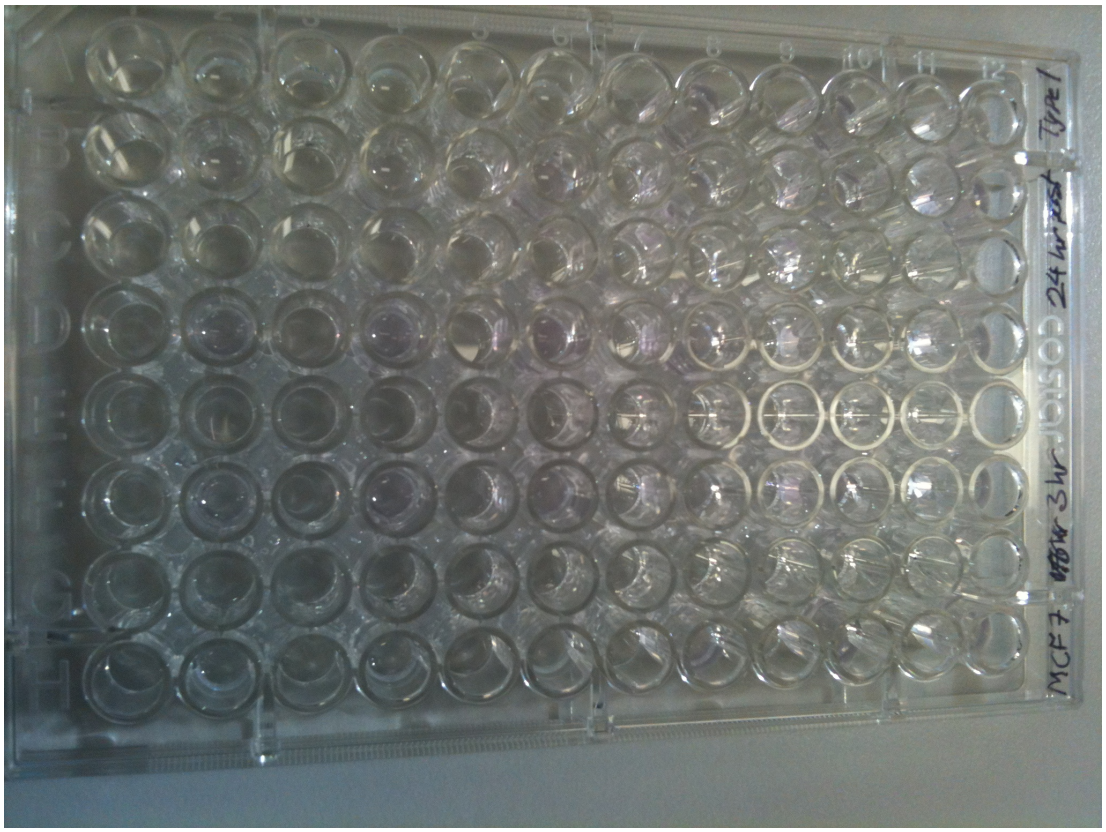

Figure 3.17: Image of 96-well plate with heat shield gel.

thermia is a completely different mechanism from the mechanism of low intensity light exposure, which present a main interest in this research project. To conduct the experiments in a closely controlled environment for evaluating the effects of proposed low intensity light on cancer cells, a heat shield gel is purchased and used throughout the experiments. This heat shield gel is purchased from Inventables, USA and dissipates any heat generated from far infrared exposures. According to the specification, this gel shield up to $4100^{\circ C}$. It also shields transfer of heat from other wells. The gel is placed in the gaps between the wells and around each well conducting the experiments as shown in the Figure 3.17.

3.3 Cell-based Assays

To measure the effect of far infrared exposure irradiation, a number of cell-based quantitative and qualitative assays are used. These assays are used to reveal any biological effect that irradiation at the different regimes of visible, near infrared and far infrared wavelengths may induce in normal and cancer cell lines. Additionally, for human cancer cells an extra quantitative assay is used to further evaluate the effect of far infrared exposure irradiation. To conduct this comprehensive study, the effects of external electromagnetic irradiation was first evaluated quantitatively with LDH, MTT or PrestoBlue^{TM} assays. Upon significant detection of cellular apoptosis or cytotoxicity from implementation of quantitative assays, two qualitative assays are used to detect any cellular morphology changes, cellular apoptosis and necrosis. The following section describes the quantitative assays and processes used for quantification of treated cells reaction to external LED irradiation.

3.3.1 Quantitative Assays:

The three standard quantitative assays used in this project were Lactate Dehydrogenase(LDH) and 3-(4,5-dimethyl thiazol-2-yl)-2, 5-diphenyl tetrazolium bromide(MTT) Assay and PrestoBlue^{TM}.

Lactate Dehydrogenase (LDH) Assay

LDH or Cytotoxicity Assay measures LDH activity release from damaged cells and is performed by assessing LDH released into the media as a marker of lysed or dead cells. LDH is a stable cytoplasmic enzyme present in all cells. Upon plasma membrane damage, LDH is quickly released into the cell culture supernatant. Basically, the assay determines the degree of plasma membrane damage in *in vitro* cell systems. Different ways of conducting this measurement is explained in details in [242, 243]

LDH is an enzymatic cell assay of cell death or apoptosis detecting and quantifying cell-mediated cytotoxicity in two steps. In the first step, LDH-catalyzed conversion of lactate to pyruvate reduces NAD^+ to $NADH/H^+$. In the second step, H/H^+ from the $NADH/H^+$ is transferred by catalyst (diaphorase) to tetrazolium salt INT which is reduced by formazon. This process increases the amount of dead or plasma-membrane-damaged cells which result in increase of LDH enzyme activity in culture supernatant. Then, escalation in the amount of enzyme activity increases the amount of formazon forming. The amount of formazons is proportionally related to the number of lysed cells. The formed formazons are water-soluble and show broad absorption maximum at about 500nm where tetrazolium salt INT does not show any significant absorption [244].

In this work LDH kit from Roche Applied Science, Australia has been purchased

and used for the LDH activity measurement. Here is the step by step procedure for LDH Assay analysis:

Step 0 Cells are counted with Countess Cell Counter machine and cell concentration of 1×10^4 cells per mL are deposited in 96-well plate. Template of LDH assay is shown in Figure 3.18. Three wells are deposited with the medium only as a background control for any possible medium effect on the result, as shown in light green color in Figure 3.18. Three wells are assigned as low control (no exposure) shown in blue color. Then, three more wells are assigned as high control, where lysis is used for those to quantify the maximum cell death possible, and are shown in red color. Low and high control wells are not exposed to irradiation. After that, the plates are incubated over night.

Step 1 - Each well is irradiated according to the regime of exposure and post exposure incubation being tested.

Step 2 - The following two mixture are prepared for testing:

Catalyst Mixture: Catalyst bottle is mixed thoroughly with 1mL of double distilled water for 10 min.

Reaction Mixture: 250μL of Catalyst Mixture is mixed with 11.25mL of Dye solution for 100 LDH tests.

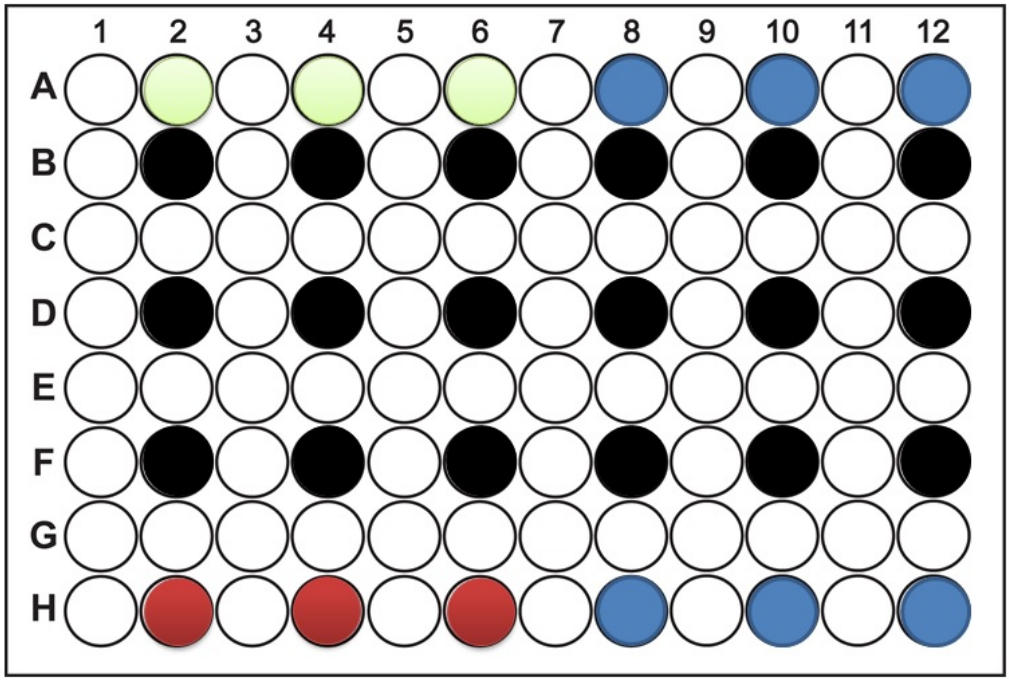

Figure 3.18: Image of 96-well plate template for LDH assay.

Step 3 5μL of Lysis solution is added in each of the 3 wells assign for high control activity in LDH Assay.

Step 4 The plates are incubated for 15 minutes and then the rest of the process is conducted in darkness due to the sensitivity of dye solution to light.

Step 5 100μL of Reaction Mixture to each irradiated well includes low Control. After that the plates are covered by aluminium foils.

Step 6 The plates are then incubated for 5-10 minutes.

Step 7 50μL of Stop solution are added to each well to disrupt the process.

Step 8 The plates are shaken for 10 second.

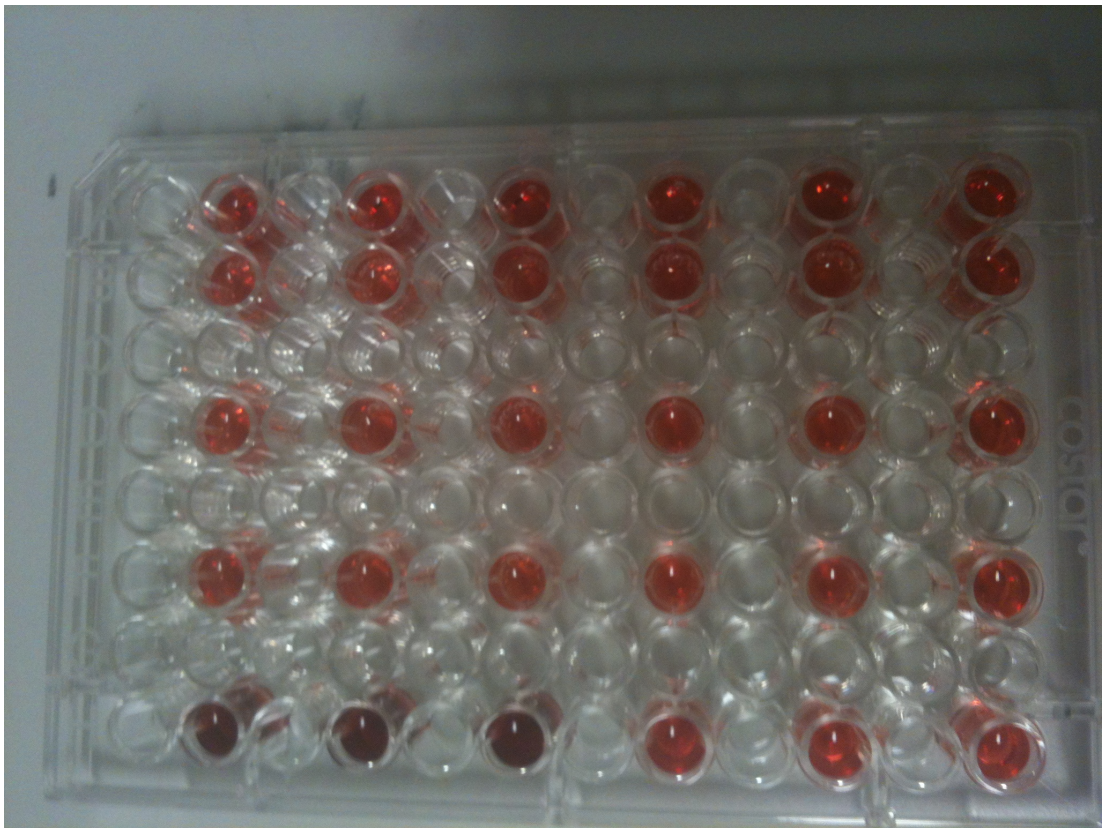

Figure 3.19: A sample of 96-well plate conducted with LDH assay.

Step 9 Reading of ELISA plate reader is conducted with 492nm filters.

Figure 3.19 demonstrates a sample of LDH assay analysis conducted on 96-well plate.

Thiazolyl Blue Tetrazolium Bromide (MTT) Assay

In general, 3-(4,5-dimethyl thiazol-2-yl)-2, 5-diphenyl tetrazolium bromide(MTT) is a chromogenic indicator and is used for *in vitro* assay of cells population's response to external factors. This colorimetric cell proliferation assay also provides large scale assays. MTT is among one of the most popular and versatile as-

says developed by Mossman [245]. The principle of this method is to measure the amount of tetrazolium salts reduction. Measurement of tetrazolium salts is widely accepted as a reliable way to examine cell proliferation.

The main process, involved in MTT assays, is to convert the water soluble MTT (3-(4,5-dimethyl thiazol-2-yl)-2, 5-diphenyltetrazolium bromide) into insoluble formazans. MTT solution then enters the undamaged cells and passes into the mitochondria where its amount is reduced and transformed into insoluble, purple color formazan product. The amount of yellow tetrazolium MTT is reduced by the action of dehydrogenase enzymes in active cells to generate reducing equivalents such as NADH and NADPH. Then, the resulting intracellular dark purple formazons are solubilized with isopropanol and released formazan reagent solution. This solution is then quantified by spectrophotometric means such as ELISA plate reader. Quantification of the results with ELISA reader is measured at a certain wavelength filter around 570nm [246] .

As MTT reduction can only occurs in metabolically active cell, the measured level of activity is that of active cells. MTT measurements from spectrophotometry are cell proliferation rate and viability of the cells. Metabolic events led to apoptosis or necrosis result in reduction of cell viability. The reduction in live cell numbers result in reduction of the amount of MTT formazon forming and reduction in reading from plate readers such as ELIZA. In addition, MTT reagent results in low background absorption values in the absence of the cells. However,

physiological state of cells and variations of mitochondrial dehydorgenase activity in different cell types impose limitation for the use of MTT. Despite these limitations, MTT method is useful for the measurement of cell growth in response to mitogens, antigeic stimuli, growth factors, other cell growth promoting reagents, cytotoxicity studies, and in the derivation of cell growth curves [247].

In this project, Vybrant MTT Cell Proliferation Assay kit from Invitrogen, Life technologies, Australia is purchased and used. Step by step process used to evaluate changes in cell proliferation by MTT Assay is explained below.

Step 0 The cells are prepared and deposited in 96-well plate with the concentration of 1×10^4. 100μL of the prepared cells are placed in columns 2,4,6,8,10 and 12 and rows B, D, and E. Three repeats for each frequency was assigned in the plate. Then, 3 wells in rows A were placed 100μL of media only without cells. The other 3 wells on row A are used for low control which contained 100μL of the cell concentration without a treatment. The last row of the plate was also used as control. Figure 3.20 shows the order of MTT experiments are being conducted. The black filled wells are those deposited with the prepared cell concentrations. The blue filled wells are low controls and light green filled wells are cell-less mediums. After that, the plates are incubated over-night before irradiation starts the next morning.

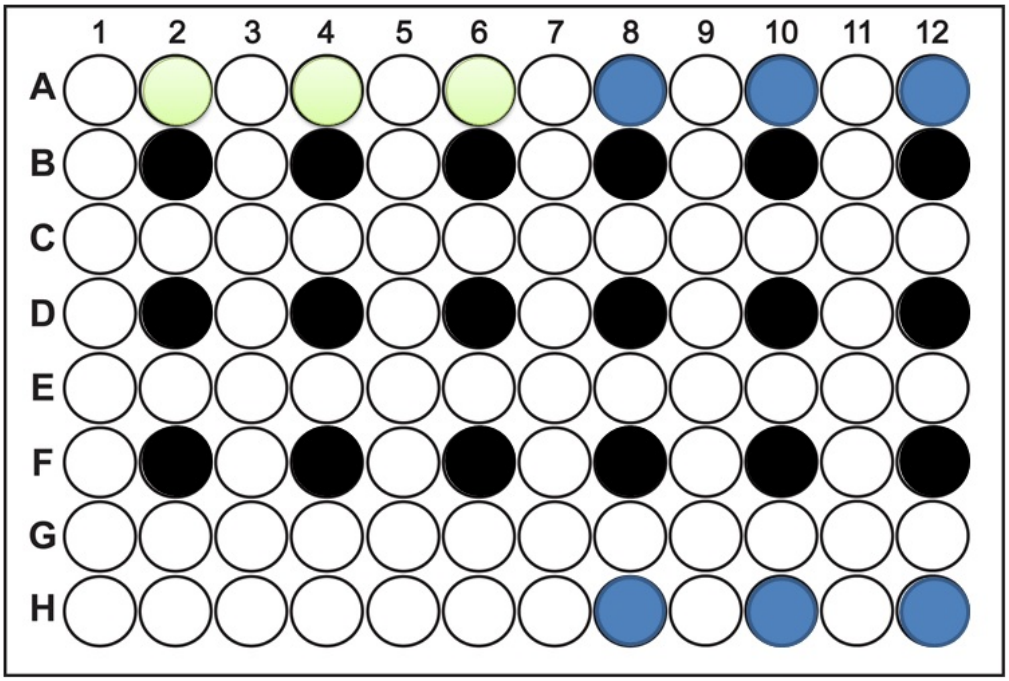

Figure 3.20: Image of 96-well plate template for MTT assay.

Step 1 The cells are irradiated the next day. Each plate is tested for one exposure regime and this process is repeated three times for each experiment.

Step 2 After elapse of post exposure incubation time, the following two MTT preparation steps are taken.

MTT Solution: 10mg/mL of MTT mixed with distilled water. Solution filtered and sterilized after adding MTT. The solution can be kept for 6 months in $-0^{\circ C}$ and stored for 4 days at $4^{\circ C}$.

MTT Solvent: Isopropanol.

Step 3 10μL of MTT solution is deposited into each well and wrapped with

aluminium foil to avoid light exposure.

Step 4 The plates are then left in the incubator at $37^{\circ C}$, 5% CO_2 for 4 hours.

Step 5 After 4 hours, cells are checked under microscope for the purple formazan crystals. The process is conducted very quickly due to the sensitivity of formazan crystals to the microscope light.

Step 6 Then, the media is removed from each well and replaced by 100μL of MTT solvent (Acidified Isopropanol or DMSO) into each well in order to solve the formazan crystals. These processes are all completed in darkness.

Step 7 The plate are shaken for 10 Seconds.

Step 8 The ELISA reader is used for OD reading with 595nm filters.

A sample of MTT assay conducted in 96 well plate is shown in Figure 3.21.

PrestoBlue^{TM} Assay

PrestoBlue^{TM} is a cell viability assay that evaluates the viability and proliferation of a wide range of cell types. This assay is described extensively in [248]. PrestoBlue^{TM} reagent is a resazurin-based solution performed as a cell viability indicator by utilizing the reducing power of living cells to measure cell proliferation quantitatively. PrestoBlue^{TM} reagent is quickly reduced by metabolically

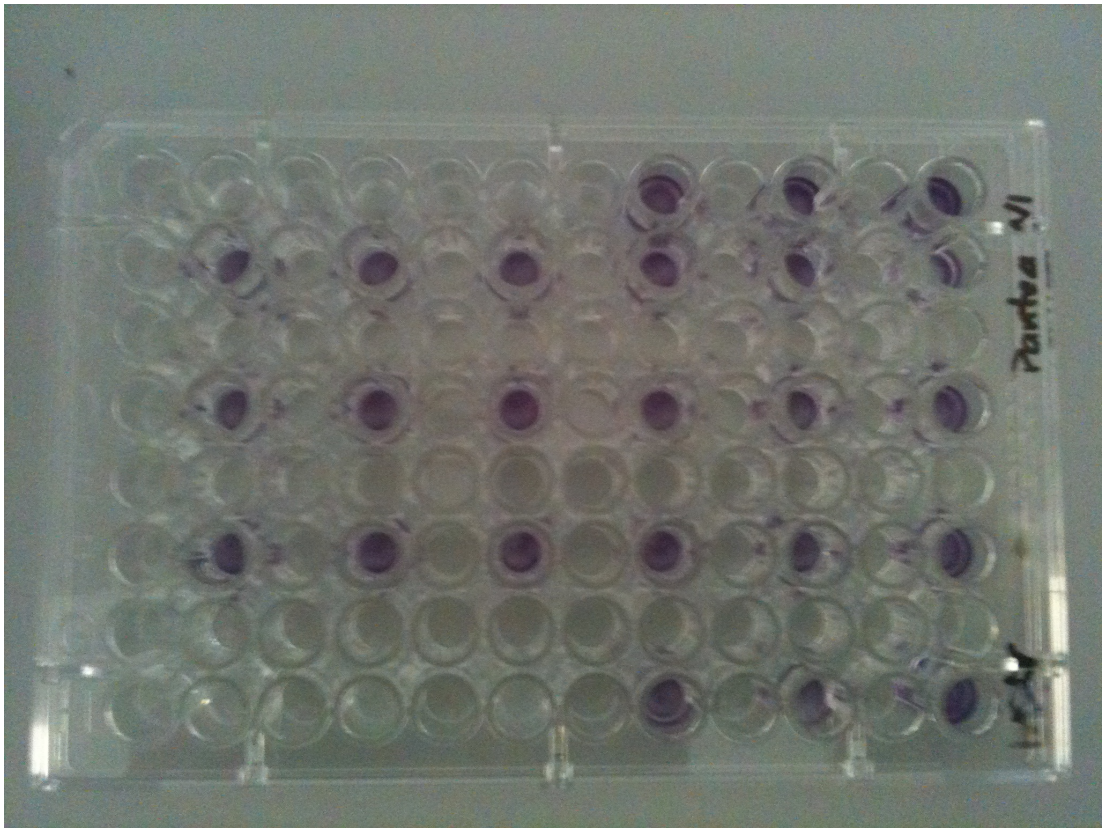

Figure 3.21: A sample of 96-well plate conducted with LDH assay.

active cells and provides a quantitative measurement of cell viability and cytotoxicity. This reagent is (a cell-permeant compound) blue and nonfluorescent. When reagents are added to the cells, they are modified by reducing the environment of the viable cell. As a result of this modification, PrestoBlue^{TM} reagent turns red in color and becomes highly fluorescent. These changes are monitored using fluorescence or absorbance measurements [249].

PrestoBlue^{TM} cell viability reagent protocol by Invitrogen (Life technology, USA) is purchased and used for evaluating changes in cell viability as a result of external exposures. Here is a step by step process used to evaluate changes in cell proliferation by PrestoBlue^{TM} cell viability assay.

Step 0 The cells are prepared and deposited in 96-well plate with the concentration of 1×10^4. 100μL of the prepared cells are placed in columns 2,4,6,8,10 and 12 and rows B, D, and E. Three repeats for each frequency are assigned in the plate and the whole process is repeated three times. Then, three wells in the rows A are placed with 100μL of media only without cells. The other three wells on row A are used for low control, and contain 100μL of the cells concentration without treatment. Afterward, the plates are incubated over night before irradiation the next day.

Step 1 After irradiation and elapse of post exposure incubation time, 10μL of PrestoBlue^{TM} reagent are added to each well.

Step 2 The plates are incubated for around 30 minutes at 37C with 5% CO_2.

Step 3 After the incubation, the plates are taken to ELISA reader for OD reading with 595nm filter.

3.3.2 Qualitative Assays:

To comprehensively investigate and detect any morphological changes as a result of irradiation in the far infrared, near infrared and visible range, two standard qualitative assays are used: light microscopy and confocal microscopy.

Phase Contrast Microscopy

Phase contrast microscopy is an optical microscopy technique that works based on the principle that different cellular components have different refractive index. Thus, the reflected light ray from different biological elements show phase differences for the reflected light. Then, phase contrast microscopy transform these phase differences into amplitude difference of light. The transformation technique was discovered in 1950s by Zernike. The technique of transforming phase differences to amplitude differences is also known as positive or dark phase contrast [250].

The phase contrast microscopy is employed to study the effects of irradiation on morphological changes in human breast cancer and normal cells. Cells are

seeded at a density of 2×10^5 cells per mL in a 24-well plate and incubated overnight. The next day, cells are radiated using the designed exposure device by visible, near-infrared, and far-infrared wavelengths for 3 hours, and then further incubated for 24 hours. After 24 hours of incubation, they are washed carefully with phosphate-buffered saline (PBS). Phase contrast microscopy images for each wavelength are taken at 100X magnifications using Nikon Eclipse Ti-E microscope (Nikon Instruments Inc, Japan).

Confocal Laser Scanning Microscopy

The principle of this technique of imaging was developed by Marvin Minsky in 1953. However, it took thirty years for laser to be developed and utilized in confocal microscopy. Toward the end of 1980s, confocal laser scanning microscopy became a standard imaging technique. Laser scanning confocal microscopy uses a pair of pinhole aperture to confine the volume of the sample focal plane size to approximately a micron. To image a relatively thick sample, a series of successive volume sections along the optical (z) plane of the microscope is acquired.

Laser scanning or confocal microscopy scans an specimen sequentially point by point, line by line or multiple points at once. Then, these pixel information are reconstructed with a computer into one image. In addition, confocal microscopy is able to provide images at different layers of a sample. The main feature of confocal microscopy is its ability to construct a blur-free images of thick sample

at the different depths. Confocal microscopy, multiphoton excitation and deconvolution techniques utilize a process known as optical sectioning to enable detailed observation of thick specimens without artifacts that can accompany specimens by physical sectioning [251].

This imaging modality is utilized here to determine the apoptosis and necrosis effects of far infrared irradiation by the apoptosis and necrosis assay. In this assay, cellular staining with the Annexin V-Alexa Fluor 488 (AF488) conjugate and Propidium Iodide (PI) is followed closely by the manual provided by Vybrant Apoptosis Assay kit II (Invitrogen, USA) with some minor modifications. Early stages of cell apoptosis stained by Annexin V can be detected using a filter designed for florescence detection (excitation/emission = 485/535). Moreover, dead cells stained by Propidium Iodine display strong fluorescent intensity which can be detected with excitation and emission at 560nm and 595nm, respectively [252].

Cells are seeded at a density of 2×10^5 cells per mL in a 24-well plate and incubated overnight. The next day, cells are exposed to far infrared radiation for three hours, and then are incubated for 24 hours. After 24 hours of incubation, they are washed with cold phosphate-buffered saline (PBS) and labeled with V-AF 488 and PI according to the manufacturer's instructions with slight modifications. To each sample, 5 μL of AF488 and 1.5 μL of PI are added followed by 20 minutes incubation at room temperature before being washed twice and resuspended in a binding buffer (10 mM HEPES, 140 mM NaCl, 2.5 mM CaCl2

at pH 7.4). Afterward, stained cells are protected from the light by aluminum foil until they are examined by confocal laser scanning microscopy (CLSM). CLSM images are taken at 100X magnifications due to a better resolution obtained from this magnification. The pinhole aperture set at 1 using Nikon Eclipse Ti-E A1 laser-scanning confocal system (Nikon Instruments Inc, Japan). Images are then analyzed with the NISElement imaging software.

Chapter 4

Quantitative Analysis of *in vitro* Electromagnetic Radiation

The Resonant Recognition Model (RRM) is a physico-mathematical approach based on digital signal processing methods [253, 254]. The RRM theory states that an external electromagnetic field (EMF) at a particular activation frequency would produce resonant effects on protein biological activity [255]. This hypothesis has been successfully evaluated experimentally [3, 256]. It is confirmed that external radiation of the certain frequencies, which were computationally determined using the RRM, can modulate a protein activity.

It was proposed in the RRM that specific wavelengths in the range of far infrared light can induce changes in biological functionality of oncogenes and proto-oncogene proteins. In particular, it was proposed theoretically that wavelength range of 3500nm to 6500nm can induce resonant effect that will lead to changes in oncogene proteins and affect cancer cells. To test his hypothesis *in vitro*, an

exposure device was designed and fabricated to irradiate light in the proposed wavelengths range (3500nm-6500nm) accordingly [257]. The selected far infrared LEDs' wavelength range is known to be able to penetrate from two to three centimeters into a tissue [235–238] and hence be suitable in application for treatment of surface or near surface tumors.

To experimentally evaluate the RRM theoretical prediction, two surface or near surface cancer cell lines are used in this project to test the hypothesis. Additionally, two normal cell lines are used to compare the effects of such far infrared light irradiation on normal cells. The selected cancer cells are murine melanoma (B16F10) and human breast cancer (MCF7), and normal cells are Chinese Hamster Ovarian (CHO) and Human Epithelial Melanocytes (HEM). The experiments are conducted *in vitro* and the cytotoxic effects of applied irradiation are evaluated using L-Lactate Dehydrogenate (LDH), 3-(4,5-dimethyl thiazol-2-yl)-2, 5-diphenyl tetrazolium bromide (MTT) and PrestoBlue^{TM} assays. In order to validate further the RRM hypothesis, the additional wavelengths of visible and near infrared light were selected for evaluation of their possible effects on cancer and normal cells. Hence, a comparative analysis of cytoxic effects of visible and near infrared light exposures on the same cancer and normal cells is provided here.

The chapter presents quantitative *in vitro* evaluation for visible light, near infrared and far infrared light irradiation on normal and cancer cell lines. The effects

induced by the external irradiation are evaluated on two animal cell lines followed by evaluation on two human cell lines for comprehensive analysis. B16F10 is a mouse melanoma (cancer) cell line, while CHO is the normal animal cell line. MCF7 cells are human breast cancer cells and HEM are human normal cells. Cytotoxic effects of the low intensity light radiation are quantified using three standard cell-based assays: LDH, MTT and PrestoBlue^{TM}. LDH assay is used to quantify the effects of selected wavelengths and three different regimes of exposure and post exposure incubation through out examination of L-lactate dehydrogenase enzyme activity. Subsequently, MTT, another quantitative measurement technique, is used to measure changes in cell proliferation of externally exposed cells. Then, PrestoBlue^{TM} is used only on MCF7 cells to provide a comprehensive quantitative analysis. Thus, the order of this section is as follows.

Section 4.1 discusses and reports any cytotoxic effects as a result of external exposures of different wavelengths and exposure regimes on B16F10, CHO, MCF7, and HEM using the LDH assay. Then, the obtained results for different cell lines are analyzed and compared with each other followed by a short discussion and analysis of the results. In Section 4.2, changes in cellular proliferation of both animal and human cell lines are investigated using the MTT assay. The results are analyzed and followed by a brief discussion. In Section 4.3, the effects induced by light exposures on MCF7 cells are further studied by PrestoBlue^{TM}.

4.1 LDH Cytotoxicity Assay

L-lactate hydrogenate (LDH) assay is used here to study the effects of selected visible, near infrared and far infrared wavelengths for three regimes of exposure and post exposure incubation on B16F10 (Murine Melanoma cell) and CHO (Chinese Hamster Ovarian cells).

Cells are seeded at initial concentrations of 1×10^4 cells per mL in 96-well plate and incubated overnight before the start of experimentation. On each plate, three wells are assigned for background control, where no cell and only the medium is placed. Three more wells are assigned as low control, where the cells are exposed to an external irradiation. Additionally, three wells are assigned as a high control measurement to be lysed during implementation of the LDH assay protocol. Cells are exposed to external light irradiation of 3400nm, 3600nm, 3800nm, 3900nm, 4100nm, 4300nm (computationally calculated wavelength in far infra-red range), 466nm, 595nm, and 626nm (visible light wavelength range); and 810nm, 850nm, and 950nm (near infra-red wavelength range). To measure the effects of each exposure regime for each selected wavelength, LDH assay protocol is conducted and the outcome is measured by ELISA plate reader with OD reading set at 492nm.

Exposures at each particular wavelength and for each exposure regime are repeated three times in three wells on the same plate. Then, each set of experiment

is repeated for different stock of B16F10 and CHO cells with different passage number. Passage numbers used range from 2 to 11. In other words, each test is conducted in three times triplicate. Importantly to note, the area around each well is filled with a heat shield gel purchased from Inventable, USA to **eradicate any thermal effect** due to external LED exposures. Furthermore, wells deposited with cells for *in vitro* experiments are placed in a way that four adjacent wells around it are left empty.

The following figures (from Figure 4.1 to Figure 4.6), first demonstrate LDH activity evaluation of cytotoxic effects in B16F10 and CHO cells induced by three different regimes of exposure. This section starts with the LDH assay readings obtained for 1.5 hours of exposure with no post exposure incubation on B16F10 and CHO cells. Next, LDH activity measurement for 1.5 hours of irradiation followed by 24 hours of post exposure incubation is presented. The experimental evaluation of 3 hours of exposure followed by 24 hours of post exposure incubation quantified by LDH assay is presented in Figure 4.5 and 4.6. The same flow of analysis is followed for two human cell lines, MCF7 and HEM. It is worth to mention that all the results translate the cytotoxicity measurements from LDH assay into cellular viability. Hence, the graphs in this section represent changes in cellular viability due to external irradiation at the selected wavelengths light and exposure regimes. LDH evaluations translation to cell viability is calculated as follow:

$$Cell\,viability\,(\%) = 100 - Cytotoxicity\,(\%) \tag{4.1}$$

4.1.1 Exposure of Animal Cells - B16F10 vs. CHO Cells

The Figure 4.1 and 4.2 show cell viability (%) in box plot. Means and standard errors of three times triplicate of the experimental repeats are observed from this graphical representation of the LDH measurement results. First, cytotoxic effect of 1.5 hours of exposure with no post exposure incubation for different wavelength is evaluated by LDH assay.

As can be seen from Figure 4.1, both cancer and normal cells are irradiated for 1.5 hours at light wavelengths of 3400nm, 3600nm, 3800nm, 3900nm, 4100nm and 4300nm. The cell viability of untreated cells is used as a reference and measured at 100% cell viability. By comparison cell viability of B16F10 and CHO in Figure 4.1, reduction in cell viability of cancer cells can be observed and are apparent for all studied wavelengths of far infra-red range. These results in Figure 4.1 reveal that external irradiation at the selected far infrared wavelengths induce a significant effects on cancer B16F10 cells that led to the high release of LDH and cytotoxicity.

It is apparent from the graph shown in Figure 4.2, that the effects of visible light (466nm, 595nm, and 626nm) for 1.5 hours exposures are not significant on B16F10

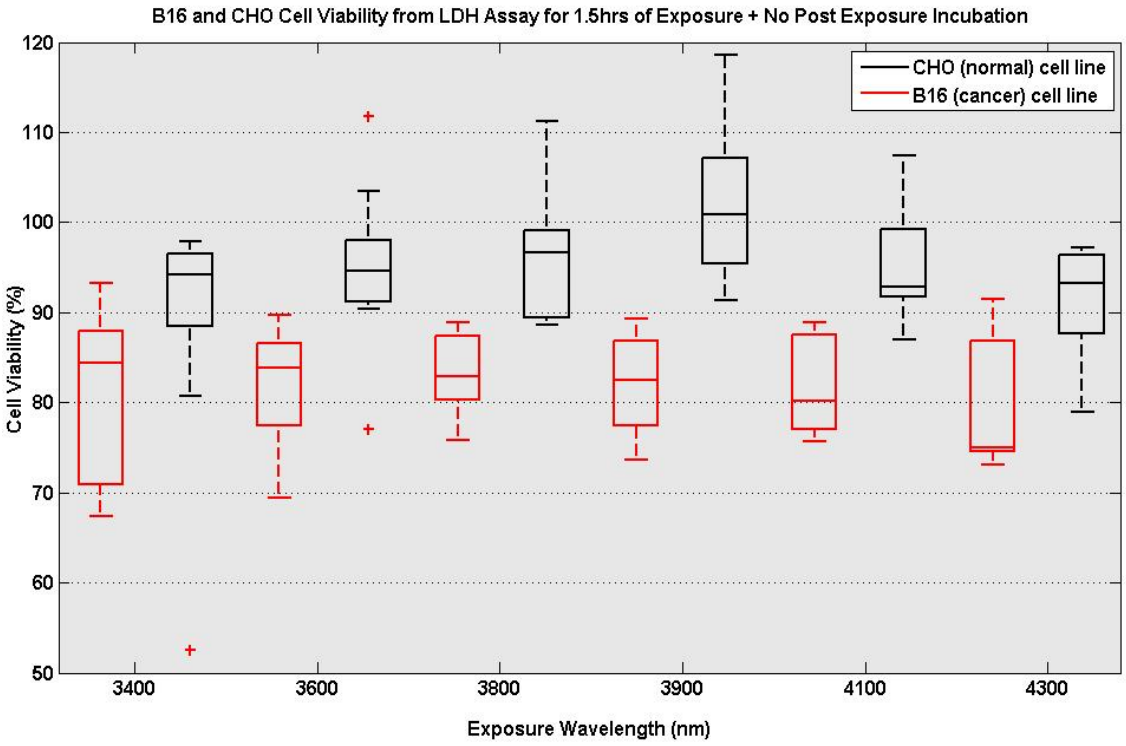

Figure 4.1: External electromagnetic radiation (EMR) of selected far infrared wavelength based on the first regime of exposure. Cells are irradiated for 1.5 hours without any post exposure incubation. The cytotoxic effect of this exposure regime is measured by LDH and the results are recorded by ELISA plate reader with OD reading of 492. The red boxes shown in Figure 4.1 represent LDH results for cancer cells and the black boxes demonstrate LDH result for CHO cells. The horizontal lines in the boxes show the mean value of three times triplicate of the experiment. The lines on the top and bottom of the boxes indicate maximum and minimum values of the experimental repeats.

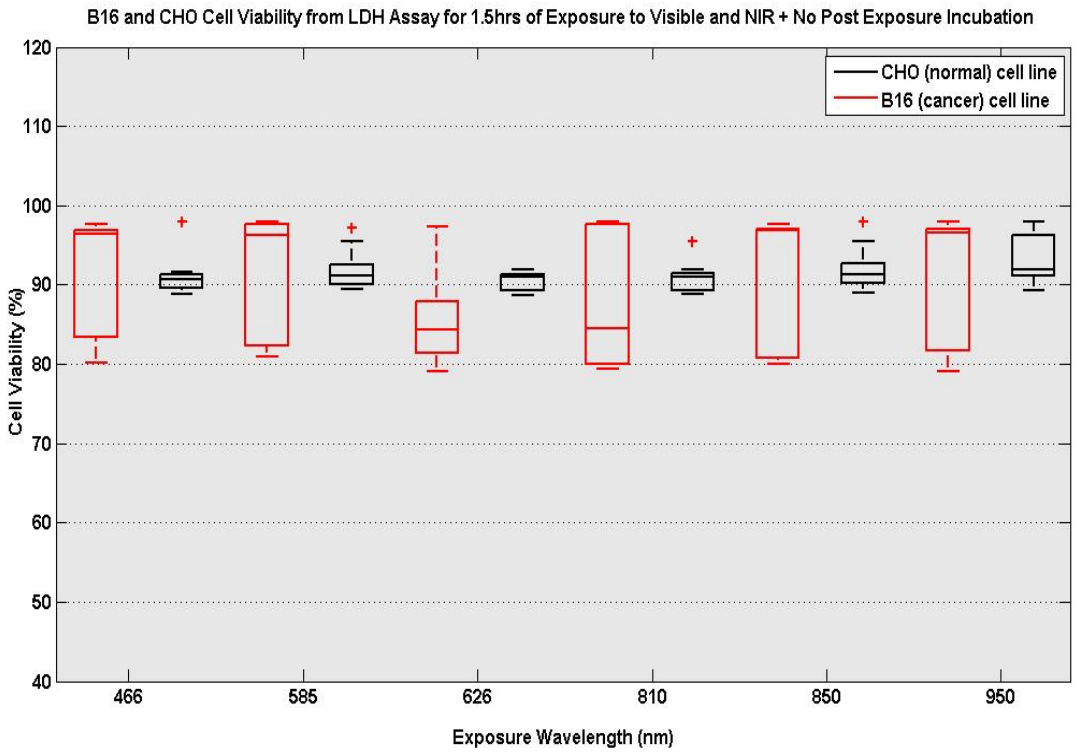

Figure 4.2: Cytotoxicity measurements by LDH assay: B16F10 and CHO cells are irradiated for 1.5 hours by light at 466nm, 595nm, 626nm, 810nm, 850nm, and 950nm (visible and near infra-red wavelength range). The red color boxes represent changes in cell viability induced by external irradiation of animal cancer cells, B16F10. The black color boxes represent cell viability measurement for animal normal cell line, CHO. The horizontal line in the boxes indicate the mean value obtained from all repeat within this particular experiment.

and CHO. Furthermore, assessment of the same exposure regime for selected near infrared wavelength (810nm, 850nm, and 950nm) demonstrates that cell viability of neither of the cell lines are affected considerably. There is no noticeable effect induced by these particular exposures.

In the second experiments, another LDH enzyme activity evaluation of second exposure regime at different wavelengths in visible, near infrared and far infrared ranges is shown in Figures 4.3 and 4.4.

As evident from Figure 4.3 exposure for 1.5 hours by far infrared irradiation with 24 hours of post exposure incubation induce detrimental effects on cell viability of cancer cells shown in red color in Figure 4.3. These red boxes clearly demonstrate the increased LDH activity in B16F10 cells after the exposure and post exposure incubation. In contrary to the cell viability of exposed cancer B16F10 cells, the cell viability of CHO cells (shown in black color) does not indicate any significant deviation from the 100% cell viability of untreated cells. The increased cell apoptosis measured by LDH is translated into the reduction in cell viability of animal cancer cells, while normal cells do not demonstrate any visible effect as a result of this exposure. Moreover, it can be seen that 24 hours post exposure incubation that is added to the second regime of exposure only slightly increases the cytotxicity of the exposed cancer cells.

Figure 4.4 shows changes in cell viability of cancer (B16F10) and normal (CHO)

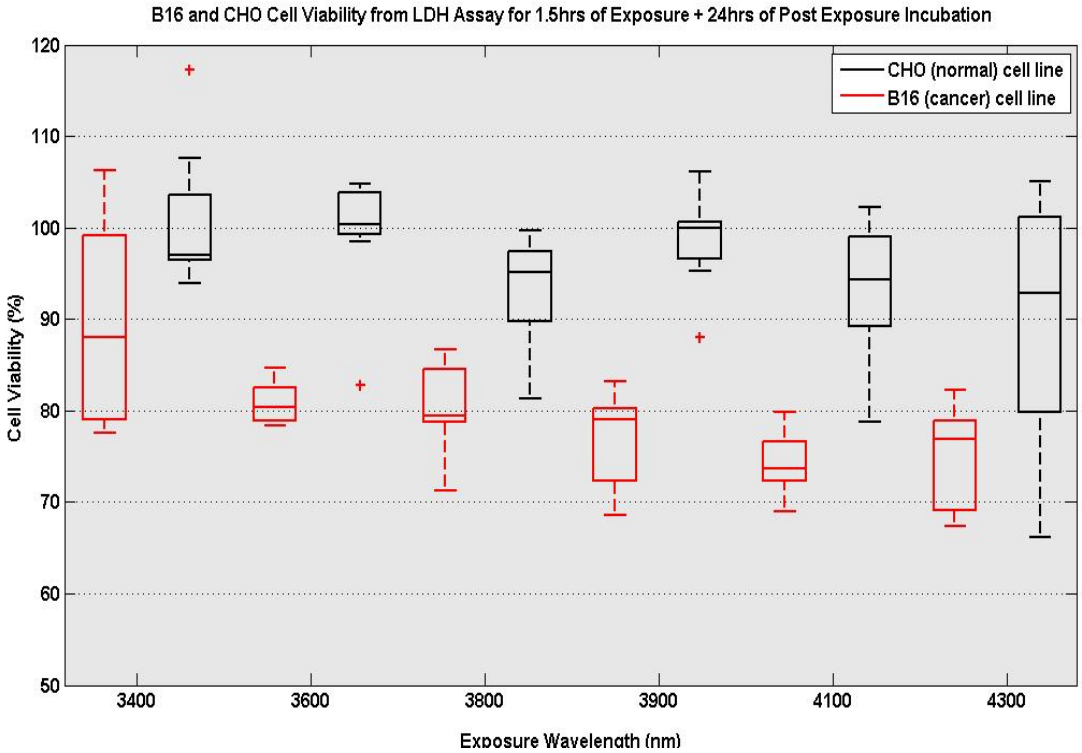

Figure 4.3: External electromagnetic radiation (EMR) of selected far infrared wavelengths based on the second regime of exposure: Cells are exposed for 1.5 hours at far infrared wavelengths and incubated for 24 hours after the exposure. The cytotoxic effects of the exposures are measured by LDH and the results are recorded by ELISA plate reader with OD reading of 492. The red boxes represent LDH results for cancer cells and the black boxes represent LDH results for CHO cells. The horizontal lines in the boxes show mean value of three times triplicate of the experimental data. The lines on top and bottom of the boxes indicate maximum and minimum values of the experimental repeats.

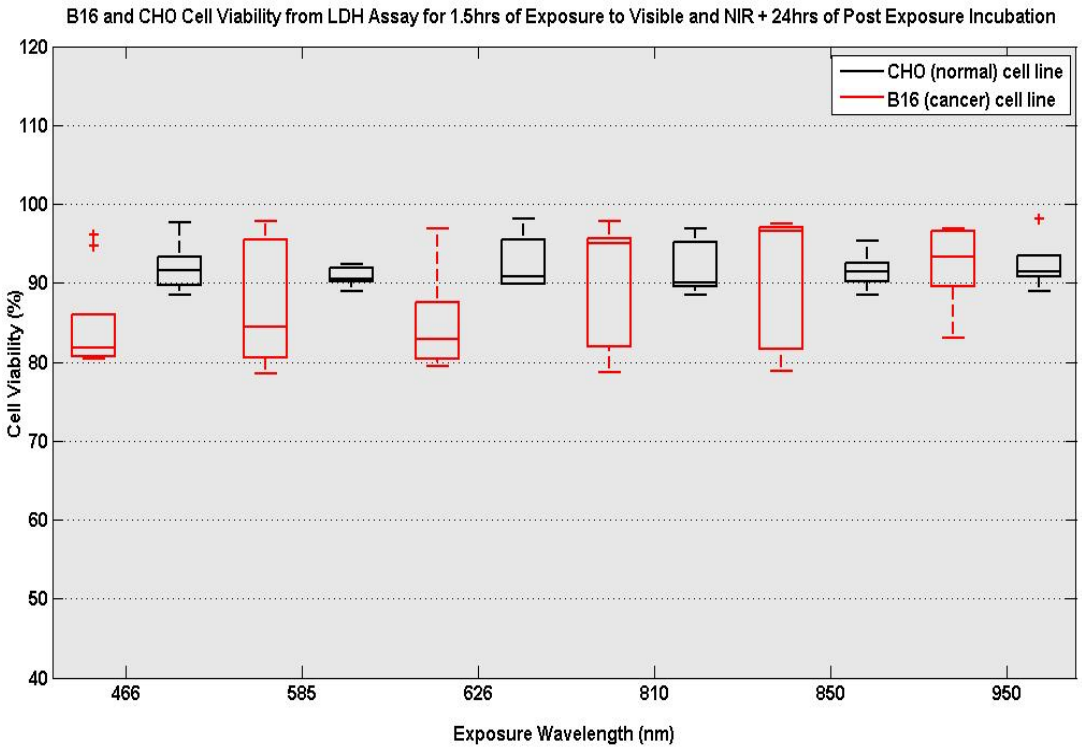

Figure 4.4: Cytotoxicity measurements by LDH assay on B16F10 and CHO cells for 1.5 hours of external electromagnetic radiation (EMR) of 466nm, 595nm, 626nm, 810nm, 850nm, and 950nm wavelengths (visible and near infrared range) followed by 24 hours of post exposure incubation. The red color represents changes in cell viability measured by LDH assay for animal cancer cells, B16F10. The black color represents cell viability measured by LDH assay for normal animal cells, CHO. The horizontal lines in the boxes indicate the mean value obtained from all repeats of that particular experiment.

cell lines for 1.5 hours irradiation at the selected visible and near infrared wavelengths followed by 24 hours of post exposure incubation. The experiments were repeated three times in triplicates with initial cell density of 1×10^4 cells per mL. The red boxes demonstrate LDH analysis of B16F10 cells irradiated by visible and near infra-red exposures, and followed by 24 hours post exposure incubation. The black boxes show LDH analysis of the cells irradiated by three visible and three near infrared exposures and post exposure incubation on CHO cells.

The cell viability measurements for the second exposure regime at 466nm, 595nm, 626nm (the first three visible light wavelengths from left) do not indicate any apparent effect on either B16F10 or CHO cells. Moreover, LDH enzyme activity measurement of the second exposure regime at 810nm, 850nm, and 950nm (the last three wavelengths) of near infrared light demonstrate insignificant cytotoxic effect on both B16F10 and CHO cells. Hence, from LDH enzyme activity analysis of the second irradiation regime of visible and near infra-red exposures, it can be concluded that cellular viability of B16F10 and CHO cells does not alter significantly compared to 100% cellular viability of untreated control cells (unexposed or sham-exposed cells).

Finally, Figures 4.5 and 4.6 represent LDH enzyme activity measurements for another exposure regime: 3 hours external irradiation by visible, near infrared and far infrared wavelengths and 24 hours post exposure incubation of B16F10 and CHO cells.

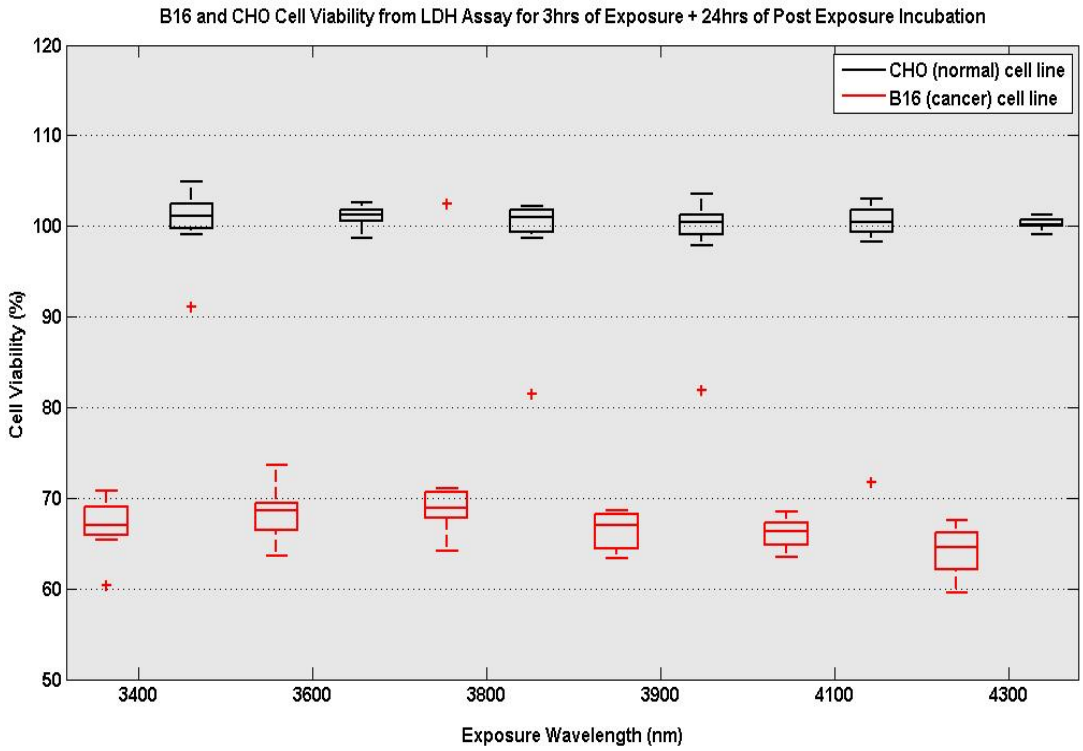

Figure 4.5: External electromagnetic radiation (EMR) at far infrared wavelength for the third regime of exposure: Cells are exposed for 3 hours to selected far infrared wavelengths (3400nm, 3600nm, 3800nm, 3900nm, 4100nm, 4300nm) and then incubated for 24 hours. The cytotoxic effects of exposure are measured by LDH and the results are recorded by ELISA plate reader with OD reading of 492. The red boxes represent LDH results for cancer cells and the black boxes demonstrate LDH results for CHO cells. The horizontal lines in the boxes show the mean values of three times triplicate of the experiment. The lines on the top and the bottom of the boxes indicate maximum and minimum values of the experimental repeats.

As was shown in the previous Figures 4.1 and 4.3, far infrared exposures of CHO cells do not lead to any significant changes in cell viability when it is compared to the 100% cellular viability of untreated cells. In contrast, the irradiated cancer B16F10 cells clearly exhibited changes in cell viability, when compared to the untreated control cells. Moreover, LDH enzyme activity measurements at different regimes of exposures indicate that 24 hours of post exposure incubation only slightly increased cell apoptosis in cancer cells. The effects of 24 hours post exposure incubation compared to that of the exposure duration is not very significant. It can be summarized that far infrared exposures contribute substantially to the cell apoptosis measured by LDH assay.

Figure 4.6 shows changes in cell viability of cancer and normal cells for 3 hours irradiation at selected visible and near infra-red wavelengths followed by 24 hours of post exposure incubation. The experiments were repeated three times and each time the specimen analysis was conducted in triplicate with initial cell density of 1×10^4 cells per mL.

LDH enzyme activity measurements shown in Figure 4.6 for three wavelengths in visible range (the first three wavelengths from left) demonstrate no changes in cellular viability for CHO cells, while B16F10 cells show a minor cellular apoptosis effect.

Additionally, the LDH enzyme activity at the last three wavelengths of expo-

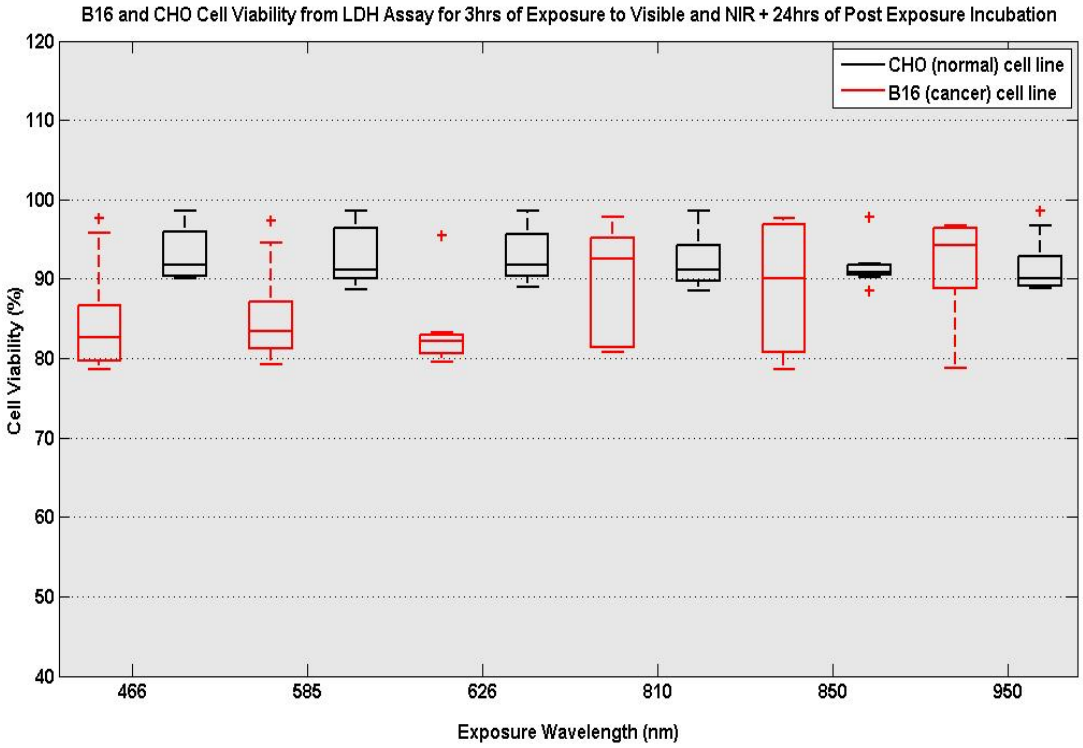

Figure 4.6: Cytotoxicity measurements by LDH assay of B16F10 and CHO cells for 3 hours of external electromagnetic radiation (EMR) at 466nm, 595nm, 626nm, 810nm, 850nm, and 950nm wavelengths (visible and near infrared range) followed by 24 hours of post exposure incubation. The red color represents cell viability measured by LDH assay for animal cancer cells, B16F10. The black color represents cell viability measured by LDH assay for animal normal cells, CHO. The horizontal lines in the boxes indicate the mean value obtained from all repeats of that particular experiment.

sures in the near infrared range shown in Figure 4.6 does not demonstrate any cytotoxic effects induced in either B16F10 or CHO cells. This result is similar to the previous results achieved by the exposures at the first and the second regimes. Figures 4.6 does not indicate significant changes in the LDH enzyme activity of B16F10 and CHO cells.

LDH Assay of B16F10 and CHO Cells - Summary Remarks

Figures 4.1, 4.3, and 4.5 show the effects of three different exposure regimes at the selected **far infrared wavelengths** on B16F10 and CHO cells. Quantitative assessment of these exposures is measured by LDH assay. Comparison the cytotoxic effects induced by different regimes of exposures at far infrared wavelengths on B16F10 and CHO, demonstrates a significant reduction in cellular viability of cancer cells, while normal cells are not being affected significantly. LDH results shown in Figure 4.1, 4.3, and 4.5 indicate that the increased duration of exposures at the far infrared wavelengths followed by 24 hours of post exposure incubation induce more significant effects in cell viability of cancer cells. However, the cytotoxic effects are more evident by the increase in exposure duration rather than post exposure incubation. For instance, irradiation for 1.5 hours at the far infrared wavelengths induce more significant cytotoxic effects in cancer cells compared to the relative increase (%) in cytotoxic effects achieved by 24 hours extra post exposure incubation. This result suggests that longer exposures

can induce more significant cell apoptosis effect in cancer cells.

Figure 4.2, 4.4 and 4.6 show LDH enzyme activities measured by LDH assay for analyzing the effects of the different exposure regimes in the visible and near infrared range of light on B16F10 and CHO cells. The results obtained clearly indicate that three different regimes of light at the wavelengths of 466nm, 595nm, 626nm, 810nm, 850nm, and 950nm do not induce a considerable effect on LDH enzyme activity of either B16F10 or CHO cells. Only third regime (3 hours of exposure followed by 24 hours of post exposure incubation) of visible range exposures on B16F10, which requires a further investigation.

The cell viability reduction in cancer cells (compared to normal cells) due to far infrared exposures can be further pinpointed by the histogram of cancer cell viability and results plane for B16F10 and CHO cells. Figure 4.7 represents histograms of all triple triplicate LDH cytotoxicity assessment for different regimes of exposures and post exposure incubation.

The first histogram is obtained from evaluation of 1.5 hours of irradiation on B16F10 at six far infrared wavelengths (3400nm, 3600nm, 3800nm, 3900nm, 4100nm, 4300nm) of light predicted computationally. As can be seen from the first histogram graph, there is a considerable shift of cell viability can be observed compared to the untreated cell viability of 100%. Subsequently, the second exposure regime (1.5 hours of irradiation with 24 hours post exposure incubation)

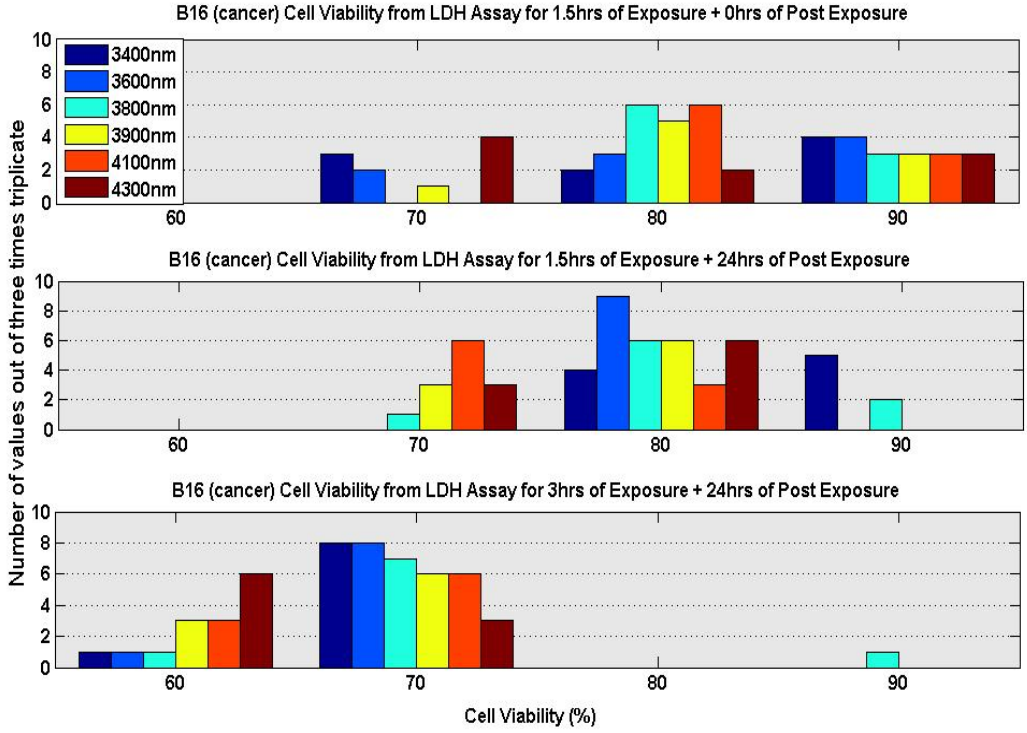

Figure 4.7: Histogram of the evaluated LDH activities for the different exposure regimes on B16F10 cells. The histogram represents evaluated wavelengths at far infrared irradiation for the first regime of exposure (1.5 hours of exposure). The middle graph is the representation of LDH assay results for the second regime of exposure (1.5 hours of exposure + 24 hours of post exposure incubation). The bottom histogram demonstrates the LDH results for the third regime of exposure (3 hours of exposure + 24 hours of post exposure incubation) on B16F10.

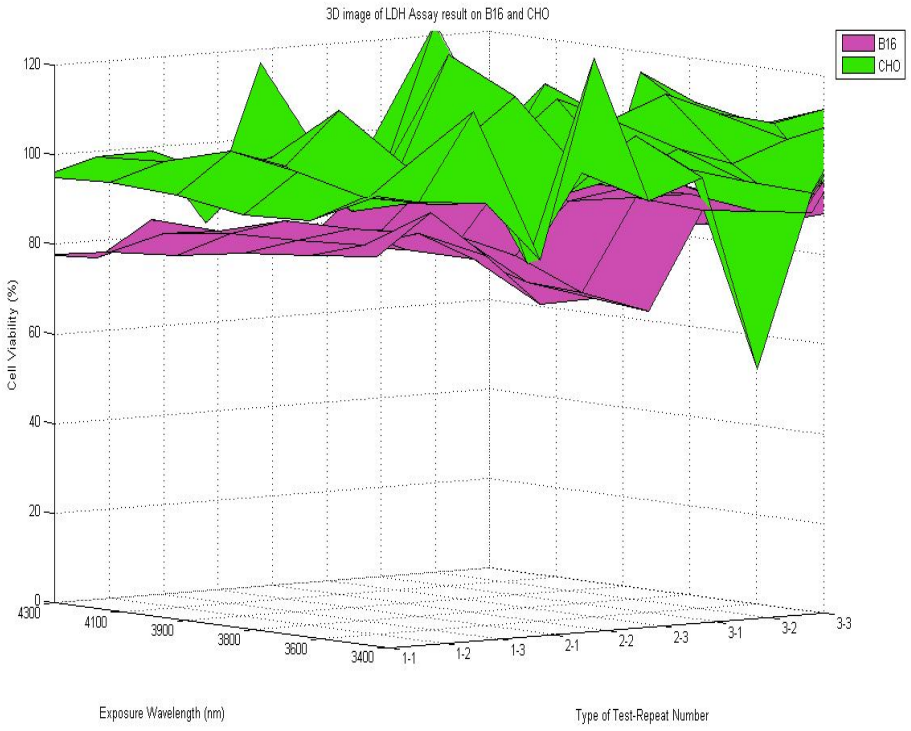

Figure 4.8: LDH enzyme activities measurements by LDH assay are shown for different regimes of far infra-red exposure and post exposure incubation for both cancer (B16F10) and normal (CHO) animal cells.

led to a further reduction in cell viability although it is not significantly different compared to the first graph. As can be seen from the last histogram, the third regime of exposure (3 hours of irradiation with 24 hours of post exposure incubation) resulted in the most substantial overall reduction in cell viability of B16F10 cells.

Figure 4.8 shows further visual clarification of the LDH enzyme activity measurement used for quantifying the effects of different exposure regimes on B16F10 and CHO.

As evident from Figure 4.8, the effects of selected far infrared wavelength LEDs irradiation is exhibited on B16F10 as opposed to CHO cells. From the graph, it can be observed that these two animal cell line react differently to far infrared exposures as their LDH assay are located in two different horizontal planes. LDH results for CHO are around 100% cell viability, while the results for B16F10 cells are in the range of 70 to 90% cell viability.

In summary, comparing results shown in Figures 4.1, 4.3, 4.5, 4.2, 4.4, and 4.6 obtained from LDH analysis of different regimes of external exposures reveals that far infrared wavelengths radiation of animal cells induce significant cytotoxic effects on cell viability of B16F10 cells. Importantly, far infrared frequency range predicted computationally by the RRM is depicted as the most effective wavelength range for cancer cells which was experimentally evaluated here.

4.1.2 Exposure of Human Cells - MCF7 vs. HEM Cells

The following two graphs in Figure 4.9 and 4.10 demonstrate cellular viability of two human cell lines of MCF7 and HEM. The cancer and normal cells are irradiated for 1.5 hours using visible, near infrared and far infrared wavelengths of light. The LDH analysis results are shown as relative changes in cell viability of cells (%).

The graphs in Figure 4.9 show the results evaluation of external far infrared

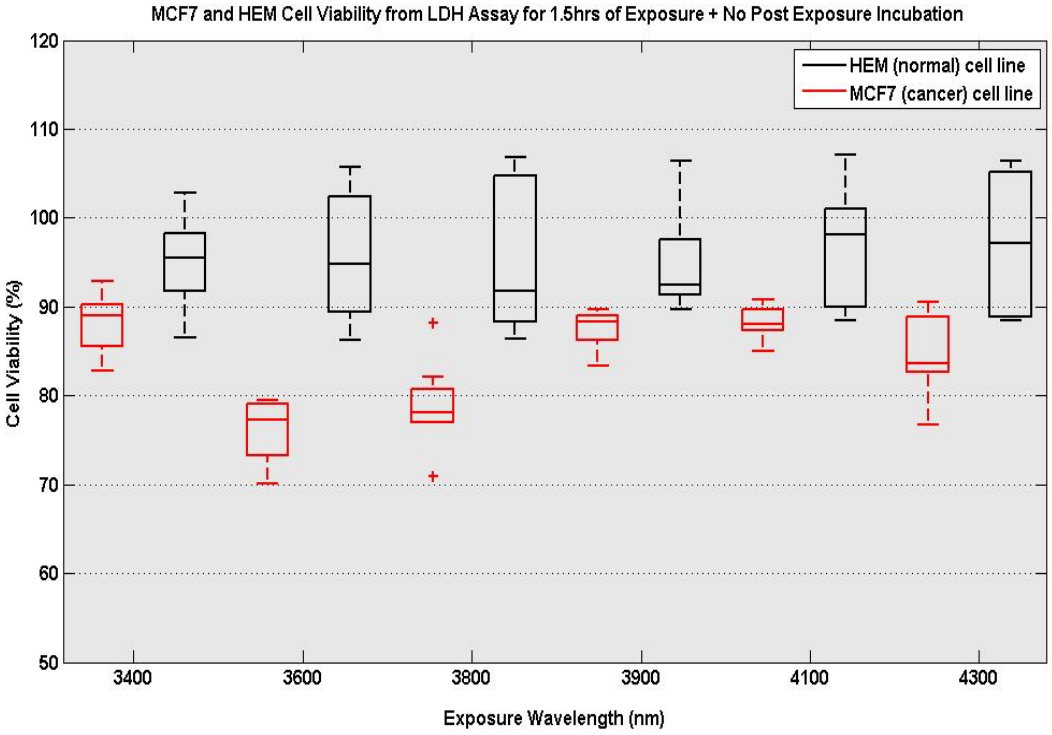

Figure 4.9: External electromagnetic radiation (EMR) at far infrared wavelengths for the first regime of exposure. Cells are exposed for 1.5 hours of the selected far infrared wavelengths. The cytotoxic effects of exposure are measured by LDH and the results are recorded by ELISA plate reader with OD reading of 492. The red boxes in the image represent LDH results for cancer cells, MCF7, and the black boxes demonstrate LDH results for HEM cells. The horizontal lines in the boxes show the mean value of three times triplicate of the experiments. The lines on the top and the bottom of the boxes indicate maximum and minimum values of the experimental repeats.

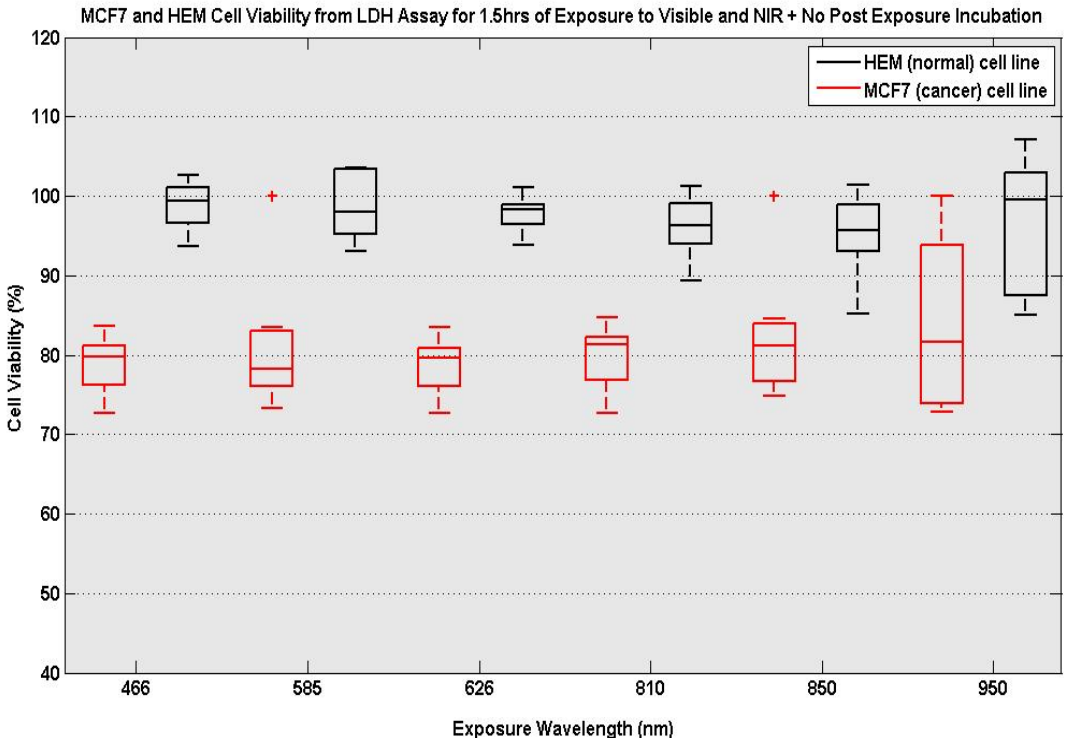

Figure 4.10: Cytotoxicity measurements of MCF7 and HEM cells for 1.5 hours at 466nm, 595nm, 626nm, 810nm, 850nm, and 950nm wavelengths (visible and near infrared range). The results obtained by ELISA plate reader with OD reading of 492nm. The red color represents cell viability measured by LDH assay for MCF7 cancer cells. The black color represents cell viability measured by LDH assay for normal HEM cells. The horizontal lines in the boxes indicate the mean values obtained from all repeats of that particular experiment.

exposures on cell viability of MCF7 cancer cells and HEM normal cells. The LDH results demonstrate that 1.5 hour far infrared exposures induce cytotoxic effects on cancer cells and reduce the cell viability of cancer cells compared to normal HEM cells.

The graph shown in Figure 4.10 reveals the effect of 1.5 hours external irradiation at three wavelengths of visible light (466nm, 595nm, and 626nm) on MCF7 cancer cells (red box plot, the first three wavelengths on left hand side). As seen

from the figure, reduction in cell viability of MCF7 cells indicates that visible range irradiation induces cytotoxic effects on cancer cells. Interestingly, there is significant cytotoxic effect observed for the exposed HEM cells (shown in black box plots).

Near infrared LEDs (810nm, 850nm, and 950nm) irradiation of MCF7 cells, measured by LDH assay in Figure 4.10 induce similar cytotoxic effect obtained from visible range exposures. Moreover, irradiation at the identical exposure regime (1.5 hours of exposure) and wavelengths (810nm, 850nm, 950nm) do not demonstrate any changes in LDH enzyme activity of HEM cells. Thus, it can be inferred that external irradiation at these selected visible and near infrared LEDs do not induce any significant cytotoxic effect on HEM cells.

In Figure 4.11, 4.12, the cytotoxic effects of the second regime of radiation (1.5 hours of exposure followed by 24 hours of post exposure incubation) on human normal and cancer cells are shown and discussed.

Figure 4.11 demonstrates the effects of 1.5 hours of far infrared wavelength external irradiation with 24 hours of post exposure incubation on cell viability of both human cancer cells (in red boxes) and human normal cells (in black boxes). Comparison of the LDH results for both cell lines clearly indicates a significant cytotoxic effect of far infrared exposures on MCF7 cancer cells. Similarly, the exposure effects of the same far infrared wavelengths on B16F10 as described in

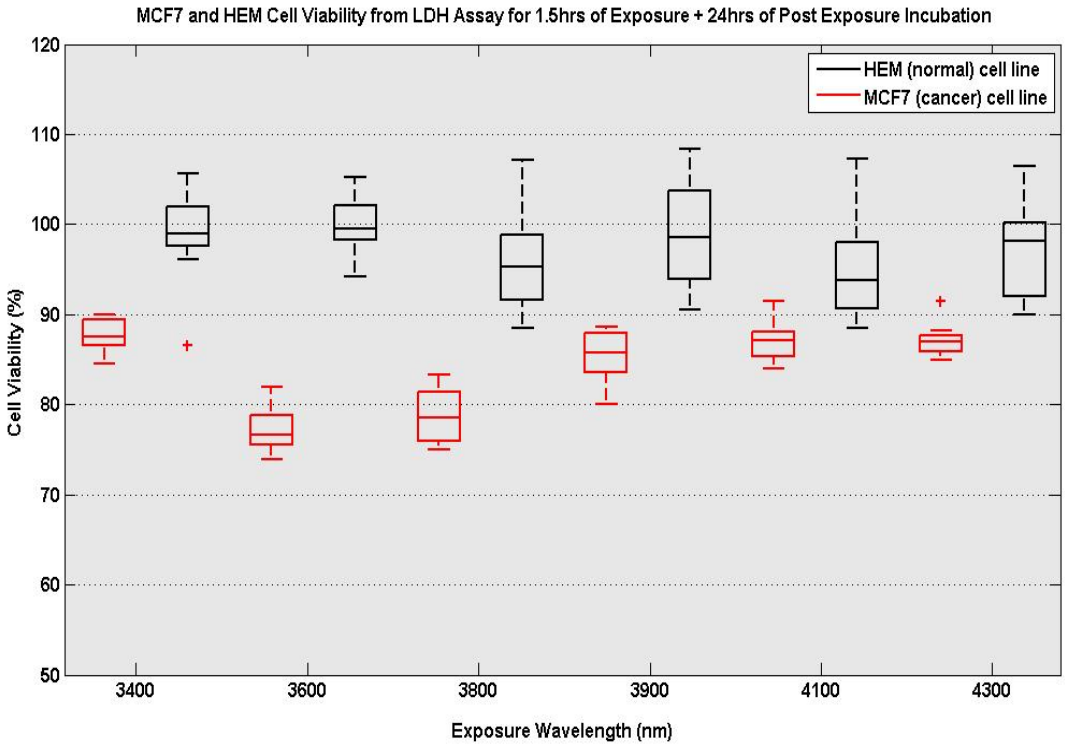

Figure 4.11: External electromagnetic radiation (EMR) of far infrared wavelengths for the second regime of exposure. Cells are exposed for 1.5 hours at the selected far infrared wavelengths followed by 24 hours of post exposure incubation. The cytotoxic effects of exposures are measured by LDH and the results are evaluated by ELISA plate reader with OD reading of 492. The red boxes in the image represent LDH results for MCF7 cancer cells. The black boxes demonstrate LDH result for HEM cells. The horizontal lines in the boxes show mean value of three times triplicate of the experiment. The lines on the top and the bottom of the boxes indicate the maximum and minimum values of the experimental repeats.

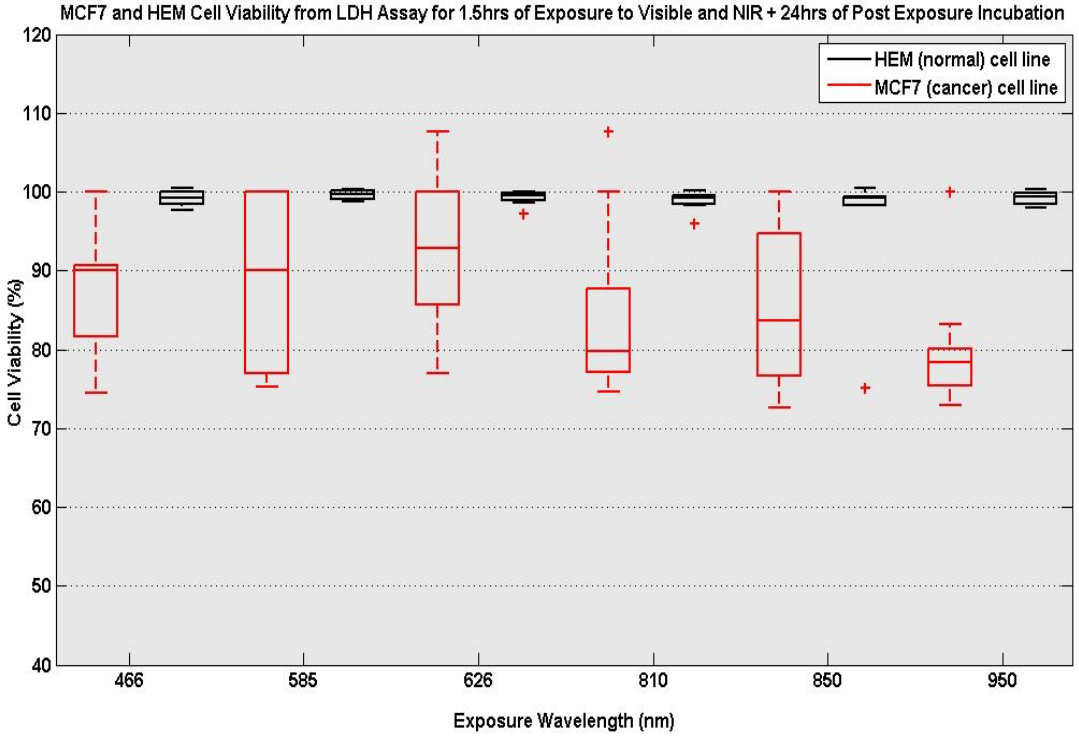

Figure 4.12: Cytotoxicity measurements by LDH assay on MCF7 and HEM cells for 1.5 hours of external electromagnetic radiation (EMR) at 466nm, 595nm, 626nm, 810nm, 850nm, and 950nm wavelengths (visible and near infrared range) followed by 24 hours of post exposure incubation. The LDH analysis results were evaluated by ELISA plate reader with OD reading of 492nm. The red color represents cell viability measured by LDH assay for MCF7 human cancer cells. The black color represents cell viability measured by LDH assay for HEM human normal cell line. The horizontal lines in the boxes indicate the mean values obtained from all repeats of that particular experiment.

subsection 4.1.1, there are cytotoxic effects on human cancer cells when compared to normal cells.

Figure 4.12 shows the results from 1.5 hours of irradiation with visible and near infrared range followed by 24 hours of post exposure incubation. As displayed with black box plots in the graph, LDH analysis of HEM cells in the visible range (the first three black box plots on the left) does not exhibit any considerable

cytotoxic effects as a result of this exposure regime. Similarly, almost no changes in LDH enzyme activity of HEM cells are detected at near infrared range LEDs (810nm, 850nm, and 950nm wavelengths).

The readings from LDH assay analysis for the second regime of exposure and post exposure irradiation on MCF7 cells are illustrated in red box plots. The first three wavelengths on the left hand side show that visible range irradiation induce detrimental effect on cell viability of MCF7 cells. Additionally, the last three wavelengths (in the near infrared range) shown in red boxes demonstrate similar detrimental effect on MCF7 cells. Thus, it can be inferred that visible and near infrared LEDs irradiation can induce cytotoxic effects on human cancer cells, while normal cells were not affected at all.

Figure 4.13 and 4.14 demonstrate the effects of the third regime of exposure (3 hours of exposure followed by 24 hours of post exposure incubation) on cell viability of cancer and normal human cells at the selected LEDs in the visible, near infrared and far infrared wavelengths.

Figure 4.13 shows the changes in cell viability of MCF7 and HEM as a result of 3 hours of far infrared external exposure with 24 hours of post exposure incubation. The LDH analysis shows measurements of LDH enzyme activity indicated as relative changes in cell viability (%) of this exposure irradiation regime. Comparison of the cytotoxic effects induced by exposures on MCF7 (shown in red color)

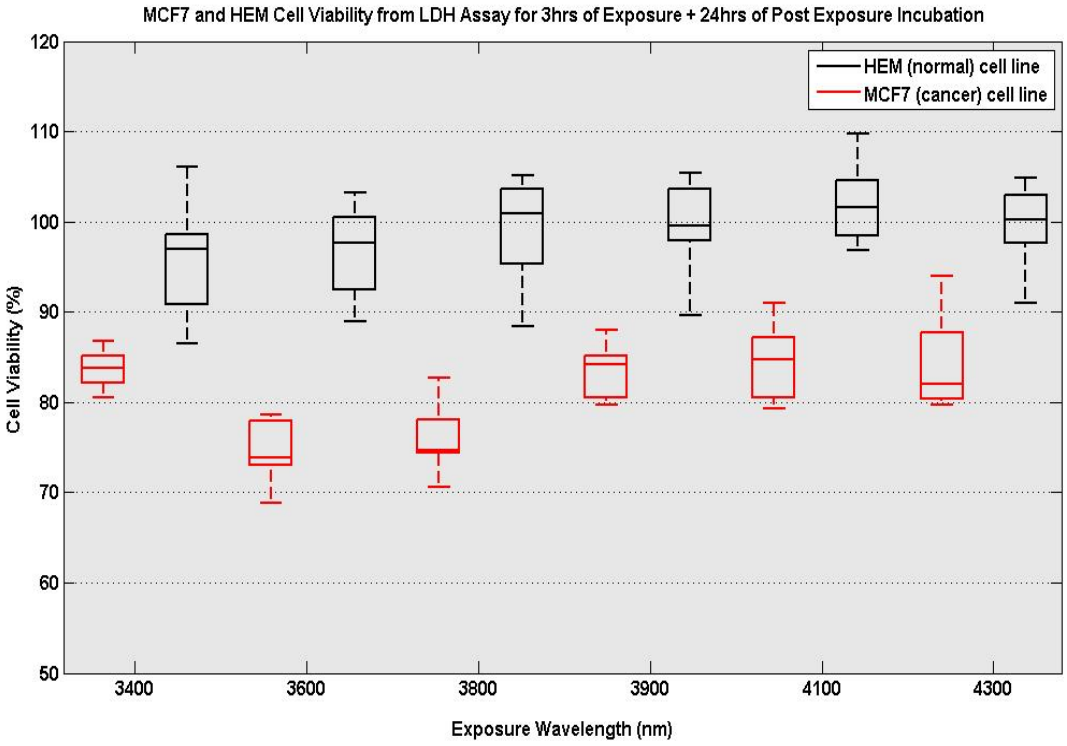

Figure 4.13: External electromagnetic radiation (EMR) of far infrared wavelengths for the third regime of exposure. Cells are exposed for 3 hours at the selected far infrared wavelengths followed by 24 hours of post exposure incubation. The cytotoxic effects of exposures are measured by LDH and the results are evaluated by ELISA plate reader with OD reading of 492. The red boxes in the image represent LDH results for MCF7 cancer cells. The black boxes demonstrate LDH result for HEM cells. The horizontal lines in the boxes show the mean values of three times triplicate of the experiment. The lines on the top and the bottom of the boxes indicate the maximum and minimum values of the experimental repeats.

and HEM (shown in black color) demonstrate a more significant effect induced in cancer cells for identical exposure regime and exposure condition. It seems that MCF7 cells are more responsive to the external irradiation at far infrared wavelengths. The relative changes in cell viability measured by LDH analysis for cancer and normal cells are in accordance with the RRM computational predictions. It was predicted that wavelengths in the range of 3500nm to 6500nm can affect biological functionality of oncogenes and proto-oncogenes, which are crucial elements in cancer origination and development.

Figure 4.14 demonstrate the LDH enzyme activity changes as a result of the third irradiation exposure regime in the visible and near infrared light range on MCF7 and HEM cells. The black box plots represents changes in LDH activity of HEM cells after 3 hours irradiation and 24 hours post exposure incubation. As can be seen from Figure 4.14, there are no effects of these exposures on HEM cells. In contrary, the same exposure regime at six LEDs in visible and near infrared range (shown in red color boxes) demonstrate the detrimental effects on cell viability of MCF7 cancer cells. Hence the exposures at 466nm, 595nm, 626nm, 810nm, 850nm, and 950nm induce cytotoxic effect on MCF7 cells.

LDH Assay on MCF7 and HEM Cells - Summary Remarks

In Figures 4.9, 4.11, and 4.13, the considerable cytotoxic effects are observed for light exposures at the selected far infrared wavelengths on MCF7 human cancer

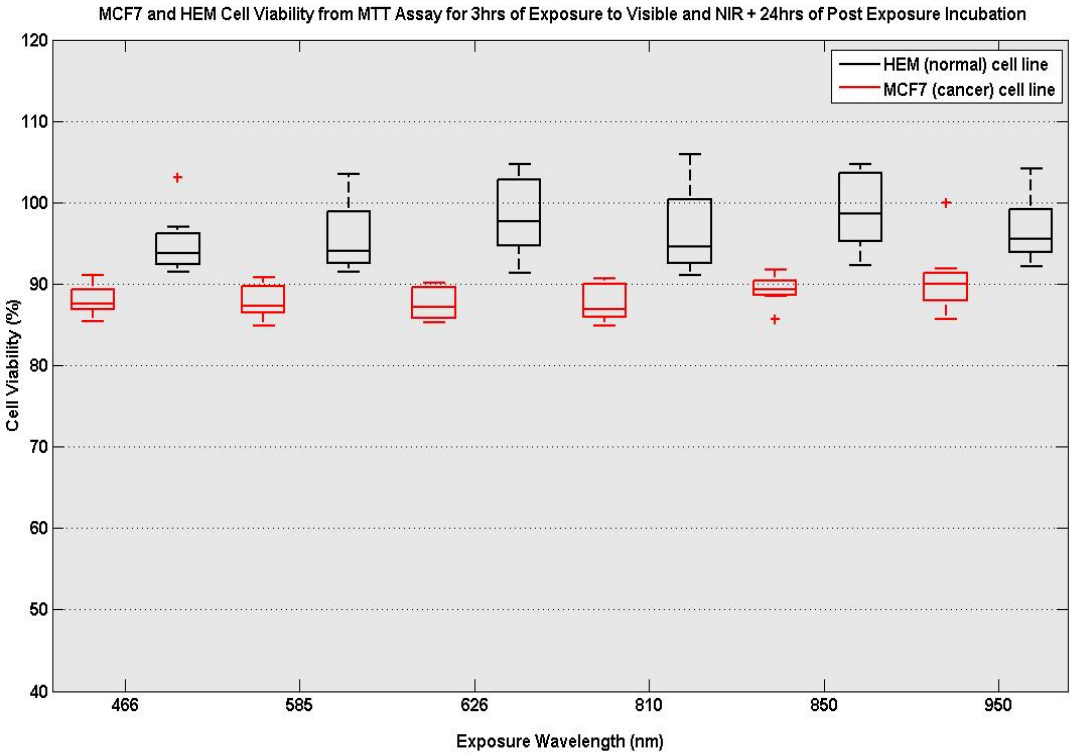

Figure 4.14: Cytotoxicity measurements by LDH assay of MCF7 and HEM cells exposed for 3 hours to 466nm, 595nm, 626nm, 810nm, 850nm, and 950nm wavelengths (visible and near infrared range) followed by 24 hours of post exposure incubation. The LDH analysis results were evaluated by ELISA plate reader with OD reading of 492nm. The red color represents cell viability, measured by LDH assay on MCF7 human cancer cell. The black color represents cell viability of HEM human normal cells. The horizontal lines in the boxes indicate the mean values obtained from all repeats of that particular experiment.

cells. Detrimental effects of this irradiation are demonstrated as relative changes in cell viability of cancer cells for three different exposure and post exposure incubation times. *In vitro* analysis of these far infrared wavelength LEDs on human normal cells does not demonstrate any detectable cytotoxic effects. All three regimes of exposure and post exposure incubation do not indicate any reduction in cell viability of HEM cells compared to the sham exposed HEM cells as opposed to the significant reduction in cell viability of the exposed MCF7 cells.

Figure 4.10, 4.12, and 4.14 present cell viability results of human normal and cancer cells exposed by external visible and near infrared light. LDH enzyme activity measurements of MCF7 and HEM for different regimes of irradiation are illustrated for three LEDs in the visible range and three LEDs in near infrared range. It is evident that visible and near infrared range irradiation have detrimental effects on cell viability of cancer cells, and induced cytotoxic effects on MCF7 cells, while HEM cells are not affected by these exposures even slightly.

Figure 4.15 demonstrates histogram of all triple triplicate repeats of LDH results for relative changes in cell viability of MCF7 cells as a result of far infrared exposures using three different regimes of radiation. Figure4.16 shows the results of far infrared exposures on MCF7 and HEM cells in two different planes.

Importantly, cell viability of MCF7 cancer cells are substantially affected by external irradiation at the far infrared wavelength compared to insignificant effects

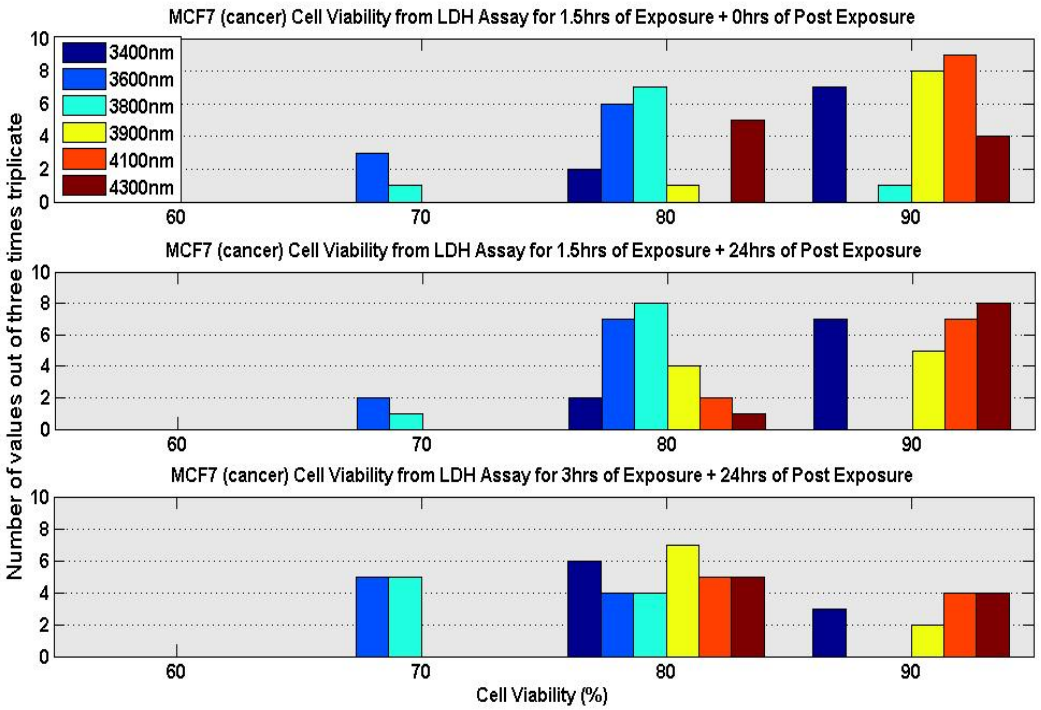

Figure 4.15: Histograms of the evaluated LDH activity for three different exposure regime on MCF7 cells. The top histogram represents all evaluated far infrared exposure for the first regime of radiation. The middle graph is the representation of the second regime of exposure. The bottom histogram demonstrates the result of the third regimes of exposure on MCF7.

of such irradiation on HEM normal cells. The top graph in Figure 4.15 reveals the cytotoxic effects induced by 1.5 hours of irradiation on MCF7 cells. As an be seen, experimental data lies in the range of 80-90% of cell viability. This implies that only a slight reduction in cell viability is recorded for the first regime of exposure. The middle graph displays the results of 1.5 hours of exposure with 24 hours of post exposure incubation on cell viability of MCF7 cells. Cell viability is still in the range of 80-90% hence a second regime of exposure induced only slight effects on cancer cells. Finally, the bottom graph reveals changes in cell viability due to 3 hours of far infrared exposures with 24 hours of post exposure incubation. This graph indicates more significant effects on cell viability reduction in MCF7. This graph clearly indicates the shift in cell viability to the region of 70-80%, which is considered a significant reduction in cell viability, when compared to 100% cell viability of untreated MCF7 cells.

Figure 4.16 further emphasizes on the changes in cell viability or cell apoptosis in MCF7 cancer cells for different regimes of far infrared exposures in comparison to non-cytotoxic effects of the same exposures on HEM cells. The cell viability reduction (%) in MCF7 cells exposed to far infrared wavelengths shown in purple color. LDH assay results for HEM cells are in the z-plane of 100% to 110% cell viability compared to 100% cell viability of sham exposed HEM cells used as control. In comparison, cell viability of the exposed MCF7 cells is overall reduced down to 80% - 90%. Sham exposed MCF7 cells are used as control and

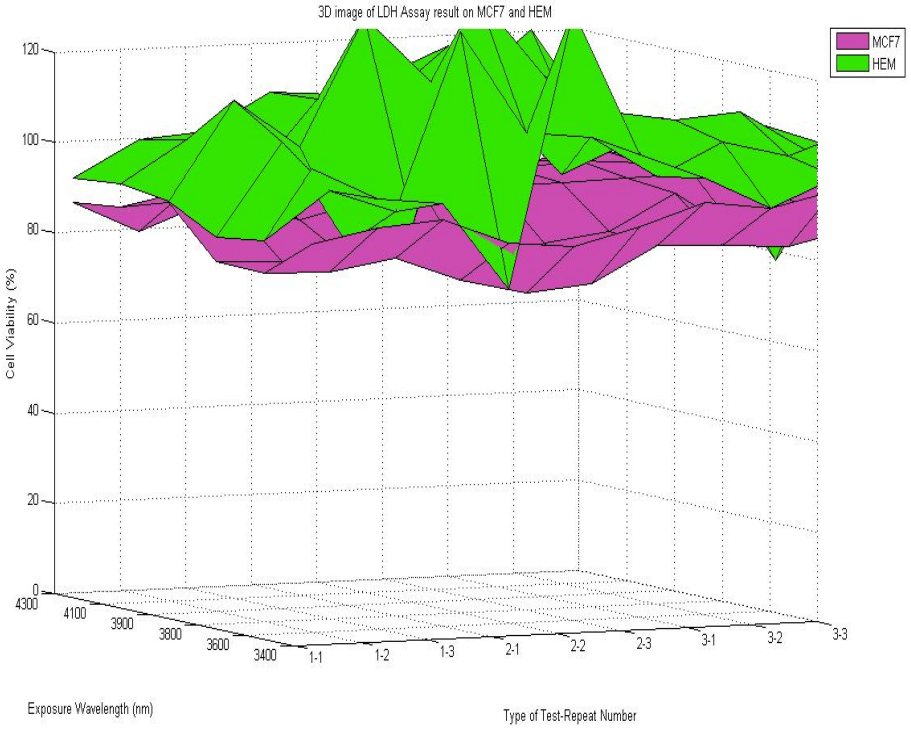

Figure 4.16: LDH enzyme activity measurements by LDH assay are exhibited for different regimes of far infrared exposures and post exposure incubations for both cancers (MCF7) and normal (HEM) human cells.

their cell viability is measured at 100%. Thus, assessment of these two planes for exposed MCF7 and HEM cells strongly suggests that exposures at the selected far infrared LEDs induces a substantial reduction in cell viability of MCF7 cancer cells as opposed to no effect observed in the exposed HEM cells.

4.2 MTT Cell Proliferation Assay

A number of standard quantitative cell-based assays are proposed to be conducted for *in vitro* evaluation of the RRM proposed hypothesis on both animal and human cells. The analysis is conducted using MTT cell proliferation assay, which is used to detect changes in cellular proliferation as a result of external radiation. MTT assay is used to quantitatively measure the effects of external irradiation at the selected wavelengths and different exposure regimes on cell proliferation of B16F10 and CHO cells (cancer and normal animal cell line).

The LEDs used for external electromagnetic radiation in the far infrared range are: 3400nm, 3600nm, 3800nm, 3900nm, 4100nm, 4300nm; in hte visible range are: 466nm, 595nm, and 626nm, and in the near infrared range are: 810nm, 850nm, and 950nm. Cells are irradiated using three different durations of exposures and post exposure incubation.

Cellular proliferation assessments are conducted by MTT assay kit obtained from Invitrogen, Life technologies, Australia. Cells are seeded at initial concen-

tration of 1×10^4 cells per mL in 96-well plate. Then, the plates are incubated overnight before the start of each set of experiments. On each plate, three wells deposited with cell-less medium are assigned for background control. In addition, three more wells are assigned for control, in which cells are not irradiated. After the experiments, MTT cell proliferation analysis results are evaluated by ELISA plate reader with OD reading of 595nm. Experimental exposure of each well is repeated three times on each plate with three different wells. Each set of experiment is repeated three times with different patches of B16F10 and CHO and different passage number. Passage numbers range from 2 to 11.

4.2.1 Exposure of Animal Cells - B16F10 vs. CHO Cells

Figures 4.17 and 4.18 show cell viability measurements obtained from MTT assay conducted on B16F10 and CHO cells for the first regime of exposure (1.5 hours of exposure). In Figure 4.17, cells are exposed to selected far infrared wavelengths range and in Figure 4.18, cells are irradiated with selected visible and near infrared wavelengths LEDs.

The box plots in Figure 4.17 display the MTT cell proliferation analysis for each selected wavelength in the proposed far infrared range. As it is apparent from the box plot graph, 1.5 hours of irradiation at these far infrared range LEDs induces a substantial cytotoxic effect on B16F10 cells (shown in red color boxes). In contrary to the induced apoptotic effects in B16F10, exposures of CHO cells

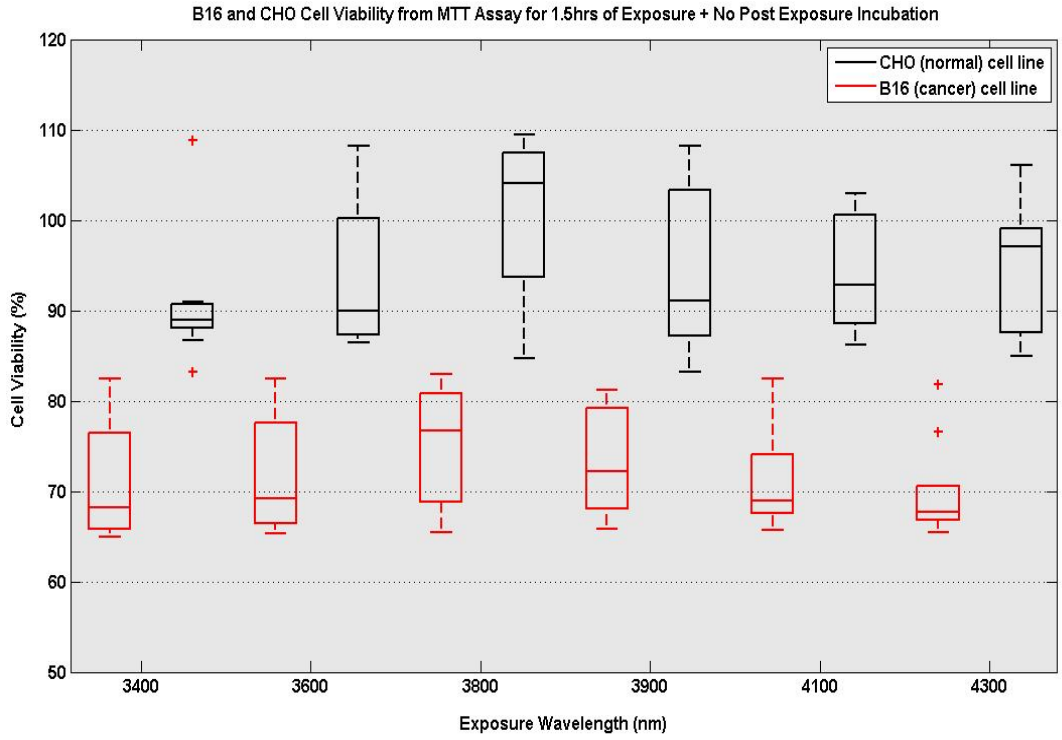

Figure 4.17: External electromagnetic radiation at the far infrared wavelengths for the first regime of exposure. Cells are radiated for 1.5 hours with no post exposure incubation. In this box plot representation, each box represents mean (the middle box horizontal line) and standard errors (vertical lines outside the box) of the repeated MTT results. Data values that are at the significant levels are shown by +. The red color shows cell viability results from MTT assay for B16F10 cells. The black color demonstrates cell viability results for CHO cells.

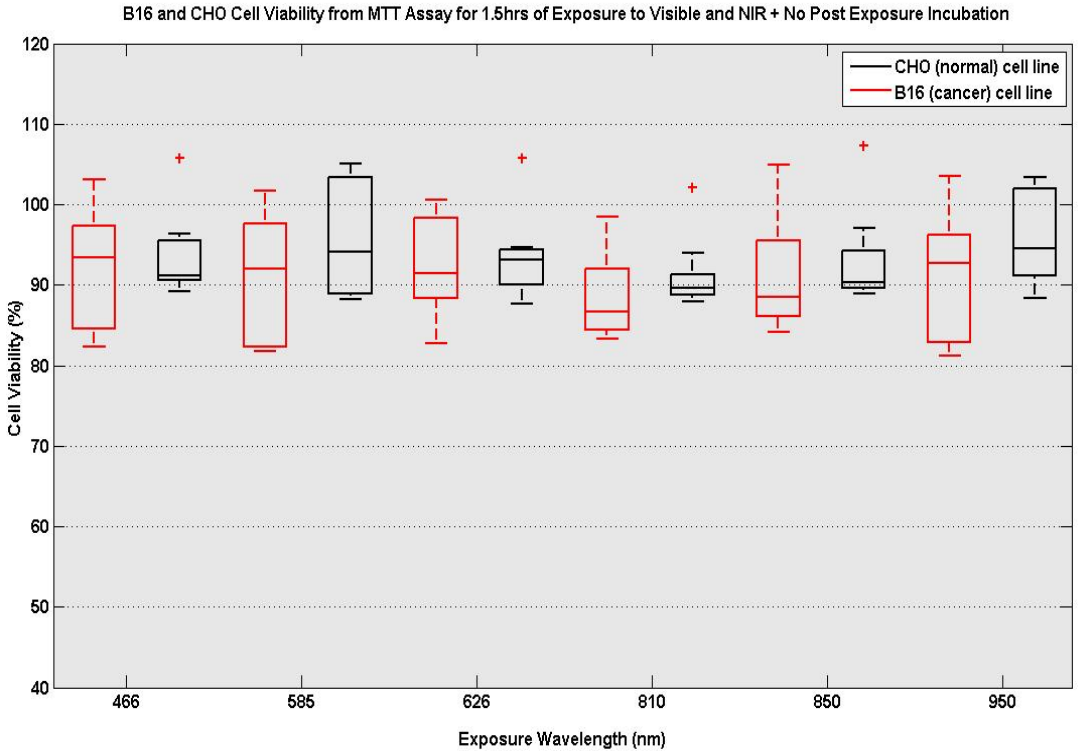

Figure 4.18: Cell proliferation measurements in B16F10 and CHO cell exposed for 1.5 hours at 466nm, 595nm, 626nm, 810nm, 850nm, and 950nm wavelengths (visible and near infrared range). The red color represents cell viability measured by MTT assay for animal cancer cell line, B16F10. The black color represents cell viability measured by MTT assay for animal normal cell line, CHO. The horizontal line in the boxes indicates the mean value obtained from all repeats of that particular experiment.

(shown in black boxes do not demonstrate any significant changes in the cell proliferation in CHO cells.

Figure 4.18 shows the cell viability changes for 1.5 hours of exposures at the selected visible and near infrared wavelengths measured by MTT cell proliferation assay. No substantial cellular apoptosis is induced in B16F10 and CHO cells by the first three visible light wavelengths (466nm, 595nm, 626nm). Similarly, the next three wavelengths representing near infrared wavelengths (810nm, 850nm,

950nm) do not induced any major changes in cell viability of animal cancer and normal cells, B16F10 and CHO cells respectively. The results obtained from MTT analysis for the first regime of exposure is in agreement with the results of LDH analysis on B16F10 and CHO for the same wavelengths of exposures and exposure regimes. In both analyses no substantial cellular apoptosis effects are observed for all three regimes of exposure in the visible and near infrared light.

Figure 4.19 and 4.20 display the cell proliferation effects of far infrared wavelengths as well as visible and near infrared wavelength on B16F10 and CHO cells. These measurements are conducted with MTT assay for the second regime of exposure and post exposure incubation (1.5 hours of exposure and 24 hours of post exposure incubation).

Comparing the results of MTT cell proliferation evaluation for the second regime of exposure on B16F10 cells, a slight reduction in cell viability is observed, while assessment of the same exposure regime on CHO cell does not indicate any effects on cell viability in CHO cells. The graph also clearly demonstrates that the extra 24 hours of post exposure incubation followed the second regime of exposure induces some apoptotic effects on cell viability of cancer cells though the effects are not significant.

Figure 4.20 show the results of cell proliferation analysis of B16F10 and CHO cells that are exposed to visible and near infrared wavelengths. Apparently, no

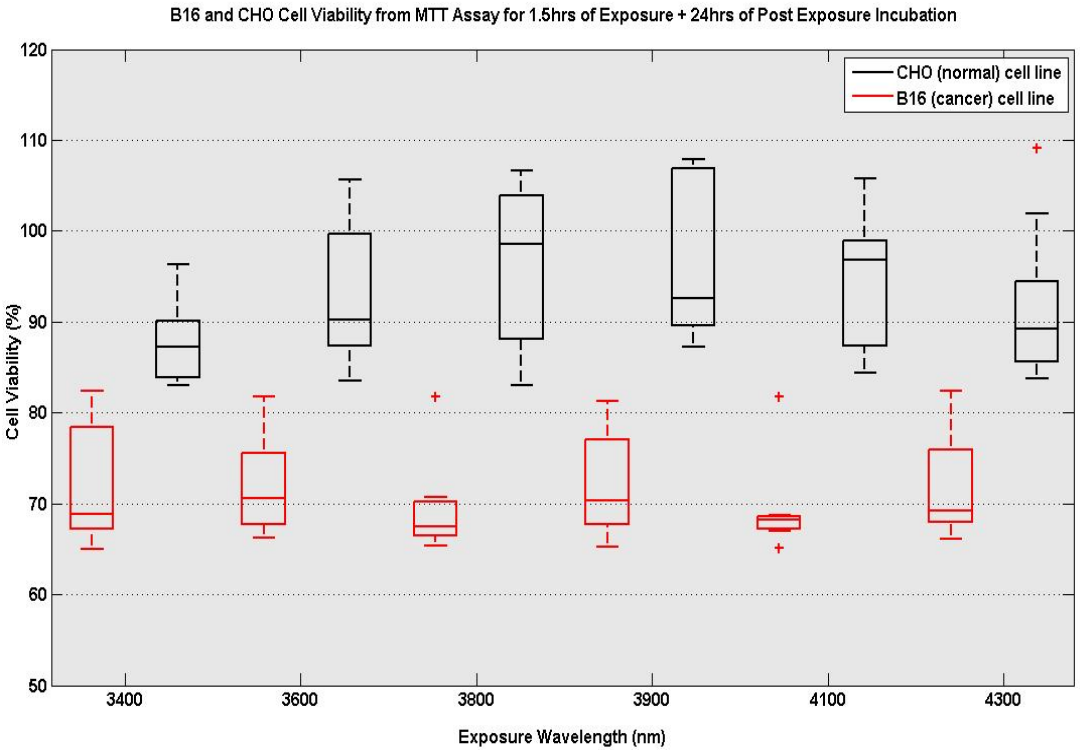

Figure 4.19: External electromagnetic radiation at the far infrared wavelengths for the second regime of exposure. In this regime, cells are exposed at the selected far infrared wavelengths for 1.5 hours and then incubated for 24 hours before the implementation of MTT measurement protocol. In this box plot representation, each box represents mean (the middle box horizontal line) and standard errors (vertical lines outside the box) of the repeated MTT results. Data values that are at the significant levels are shown by +. The red color shows cell viability results from MTT assay for B16F10 cells. The black color demonstrates cell viability results for CHO cells.

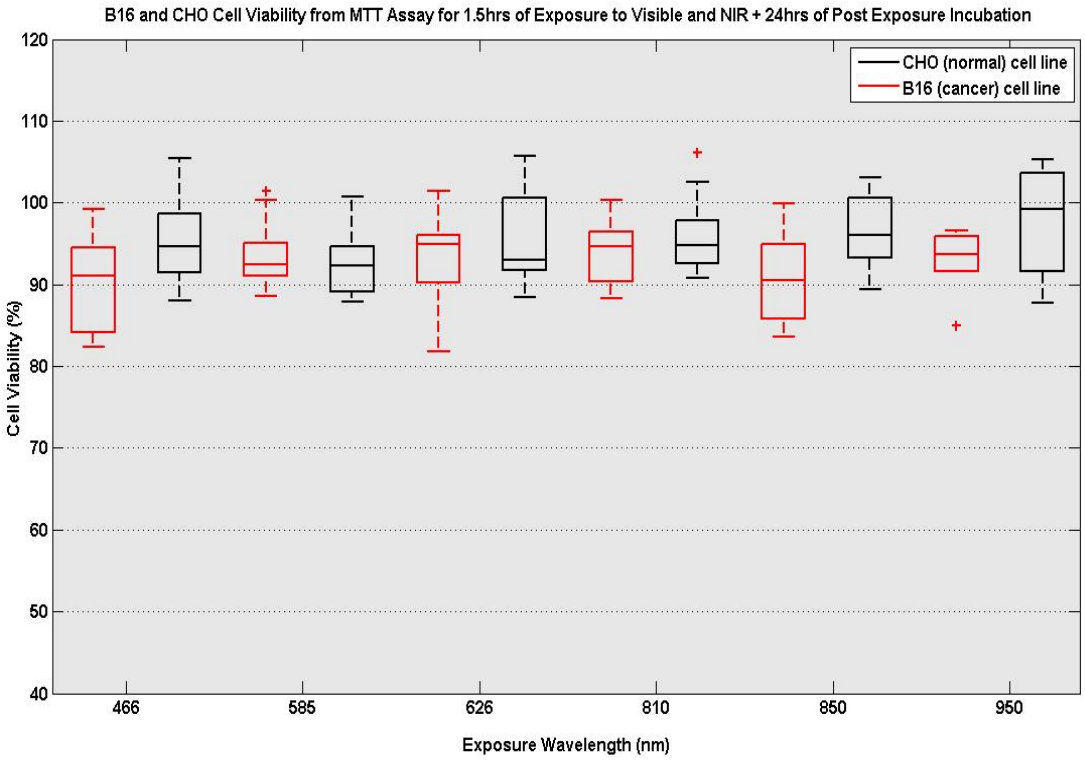

Figure 4.20: Cell proliferation measurements in B16F10 and CHO cells exposed for 1.5 hours at 466nm, 595nm, 626nm, 810nm, 850nm, and 950nm wavelength (visible and near infrared range) followed by 24 hours of post exposure incubation. The red color represents cell viability measured by MTT assay for animal cancer cell line, B16F10. The black color boxes represent cell viability measured by MTT assay for animal normal cell line, CHO. The horizontal line in the boxes indicates the mean values obtained from all repeats of that particular experiment.

clear indication of cell apoptosis or cytotoxicity is observed for the visible range irradiation (the first three wavelengths from right hand side of graph) in B16F10 and CHO cells. Analysis of near infrared range irradiation does not indicate any reportable effect on cell viability of either animal cancer or normal cells.

Finally, MTT evaluation of the third exposure regime for visible, near infrared and far infrared wavelength for B16F10 and CHO cells are shown in Figure 4.21 and 4.22.

Figure 4.21 shows the effects of 3 hours of exposures followed by 24 hours of post exposure incubation in terms of relative changes (%) in cell viability in B16F10 (shown in red color boxes). As evident from Figure 4.21, substantial reduction in cell viability is induced by irradiation at the selected far infrared LEDs. This range was predicted computationally by the RRM. As opposed to MTT results of this irradiation regime on B16F10, there are no changes in cell viability values do not reveal any noticeable changes in the exposed CHO cells (shown in black color boxes).

As it is apparent from Figure 4.22, cell proliferation of B16F10 and CHO cells do not show any cytotoxic effect after 3 hours of visible and near infrared wavelengths exposure and 24 hours of post exposure incubation. As it can be observed from both red box plots and black box plots MTT evaluation of B16F10 and CHO cells respectively, less than 10% change in the cell viability of these cells was induced

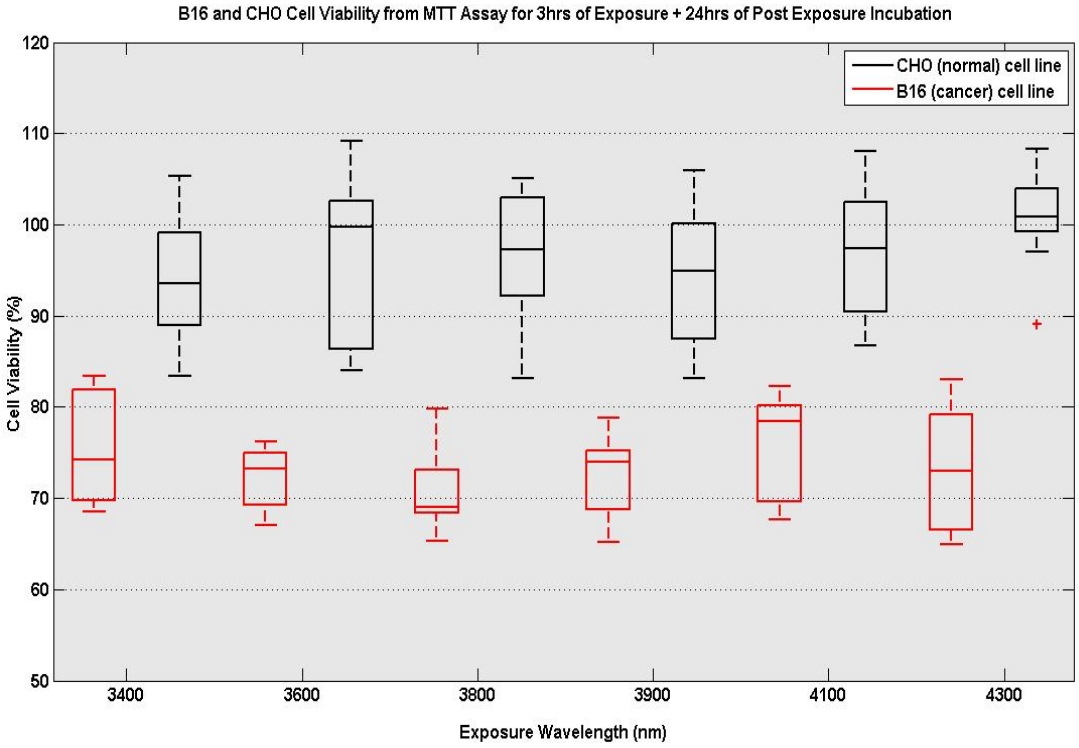

Figure 4.21: External electromagnetic radiation at far infrared wavelengths for the third regime of exposure. In this regime of exposure, cells are irradiated for 3 hours at the selected far infrared wavelength LEDs followed by 24 hours of post exposure incubation. In this box plot representation, each box represents the mean value (the middle box horizontal line) and standard errors (vertical lines outside the box) of the repeated MTT results. Data values that are at the significant levels are shown by +. The red color shows cell viability results from MTT assay for B16F10 cells. The black color demonstrates cell viability results for CHO cells.

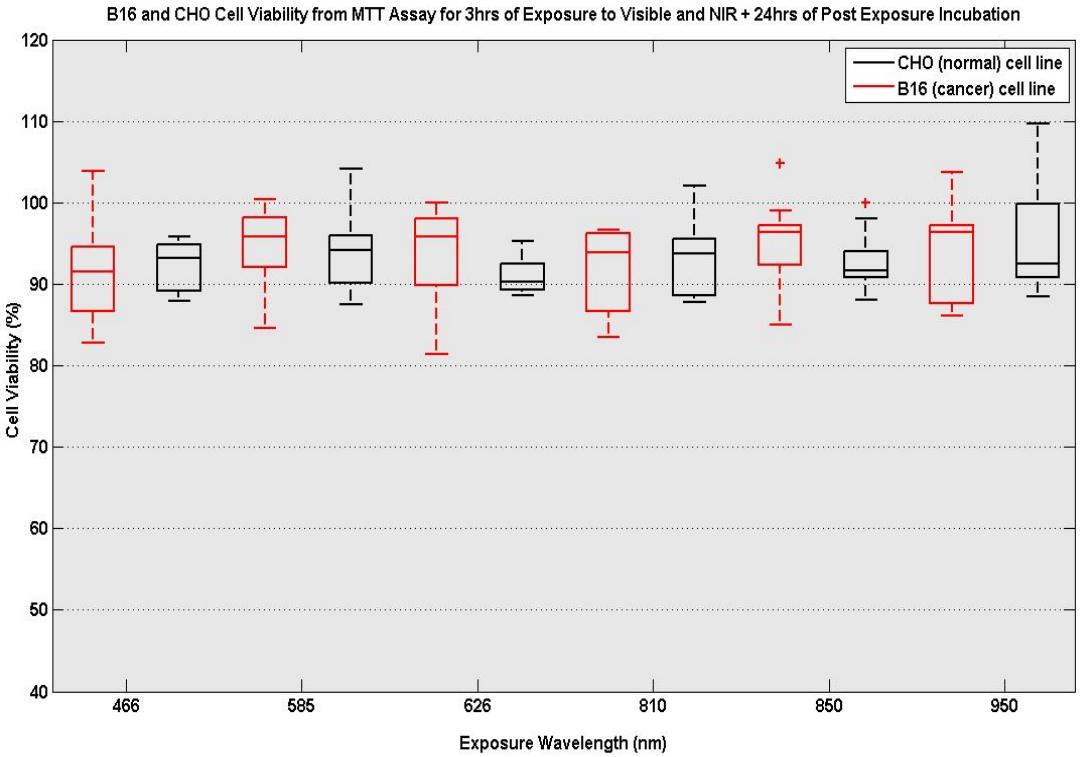

Figure 4.22: Cell proliferation measurements of B16F10 and CHO cells for 3 hours exposure at 466nm, 595nm, 626nm, 810nm, 850nm, and 950nm wavelengths (visible and near infrared range) followed by 24 hours of post exposure incubation. The red color represents cell viability measured by MTT assay for animal cancer cell line, B16F10. The black color represents cell viability measured by MTT assay for animal normal cell line, CHO. The horizontal line in the boxes indicates the mean value obtained from all repeats of that particular experiment.

by these exposures, which is not regarded as a significant effect.

MTT Assay of B16F10 and CHO Cells - Summary Remarks

From the three graphs presented in Figures 4.18, 4.20, and 4.22, it can be observed that external electromagnetic radiation at 466nm, 595nm, and 626nm wavelengths (visible light) does not induce any considerable effects on cell proliferation of B16F10 and CHO cells as measured by MTT assay. Moreover, similar results are obtained for external irradiation at near infrared wavelengths (810nm, 850nm, 950nm). No considerable cytotoxic effect is observed for both cell lines. Thus, it can be concluded that three different irradiation regime of visible and near infrared light did not induce changes in cell viability of both cancer and normal cell lines.

Figures 4.17, 4.19 and 4.21 show a substantial reduction in cell viability of B16F10 cells measured by MTT assay at the far infrared exposures and all three regimes of exposure and post exposure incubation. As opposed to the considerable effect of far infrared external irradiation on cell viability of B16F10 cells, MTT analysis of CHO cells for the same exposure regimes and wavelengths does not detect any noticeable cytotoxic effect. Hence, according to MTT assay analysis of different exposure wavelengths and regimes on B16F10 and CHO cells, it can be concluded that far infrared exposures induce significant cytotoxic effect on cancer cells (maximum 20% cell viability reduction), while normal cells are not affected

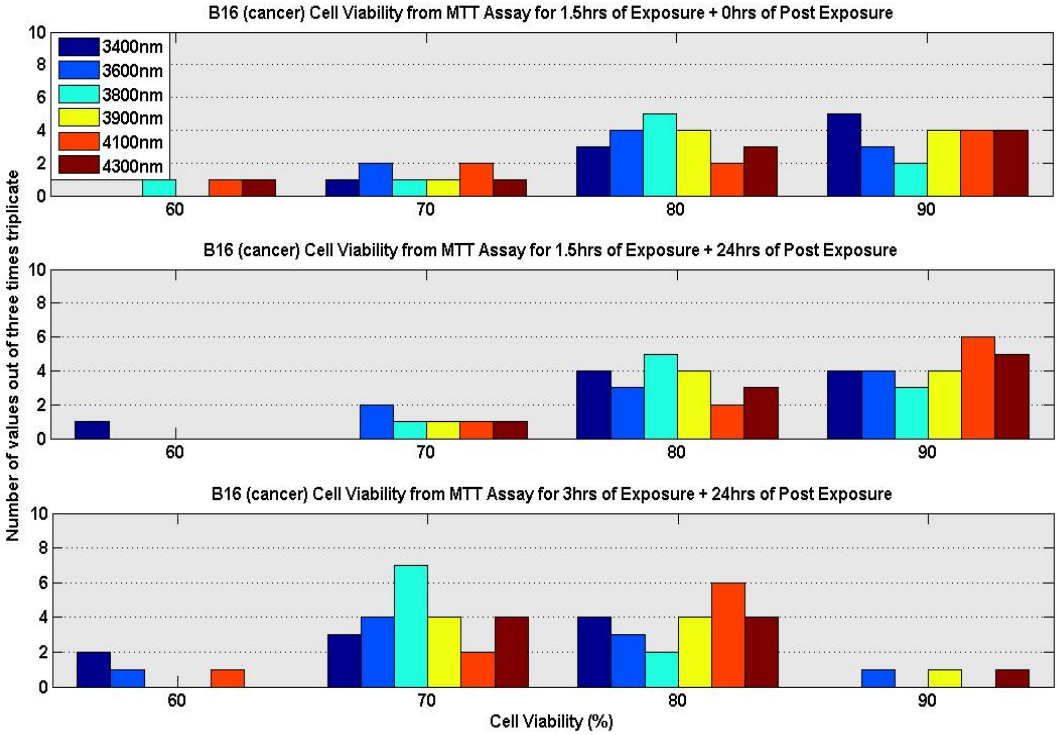

Figure 4.23: Histograms of all MTT assay data (cellular proliferation) for different exposure regimes on B16F10. The top histogram represents all evaluated far infrared wavelength for the first regime of exposure. The middle graph is the representation of the second regime of exposure. The bottom histogram demonstrates the results of the third regime of exposure on B16F10 cells.

by the same exposures.

To summarize the cytotoxic effects of visible, near infrared and far infrared exposures on B16F10 and CHO cells measured by MTT assay, the following Figures 4.23 and 4.24 are plotted to differentiate the exposure effect on these cell lines.

The subplots in Figure 4.23 show the changes in cell viability of B16F10 cancer cells for all three exposure regimes. The top plot illustrates the cell viability

results measured by MTT assay for the first exposure regime (1.5 hours of irradiation). As it is evident, cell viability of B16F10 cells is mainly around 80% and 90% compared to 100% cell viability of sham exposed B16F10 cells. The middle plot illustrates that the second regime of exposure (1.5 hours of exposure and 24 hours of post exposure) does not induce noticeable effect in cancer cells similar to the first regime of exposure. Majority of cell viability data shows cell viability around 80% and 90%. Finally, the bottom plot in Figure 4.23 shows a visibly different cell viability results achieved for the third regime of exposure (3 hours of exposure followed by 24 hours of post exposure incubation) compared to the first and second plot. In last plot, the results show cell viability is shifted toward 70% - 80% region. Thus, these findings clearly illustrate that the third regime of exposure induced the most significant cytotoxic effect in B16F10 cells compared to the other two regimes of exposure and post exposure incubation.

Figure 4.24 reveals the effects of different regimes of far infrared exposure on cell viability of B16F10 and CHO cells as measured by MTT assay. In Figure 4.24, two planes of green and purple color are shown: the green plane that spread on the 100% cell viability indicates that CHO cells are not substantially affected by far infrared exposures. In contrary, the purple plane intersects with z-plane in the range of 70%-80% cell viability indicates the significant effects of far infrared exposures on cell viability of B16F10 cancer cells.

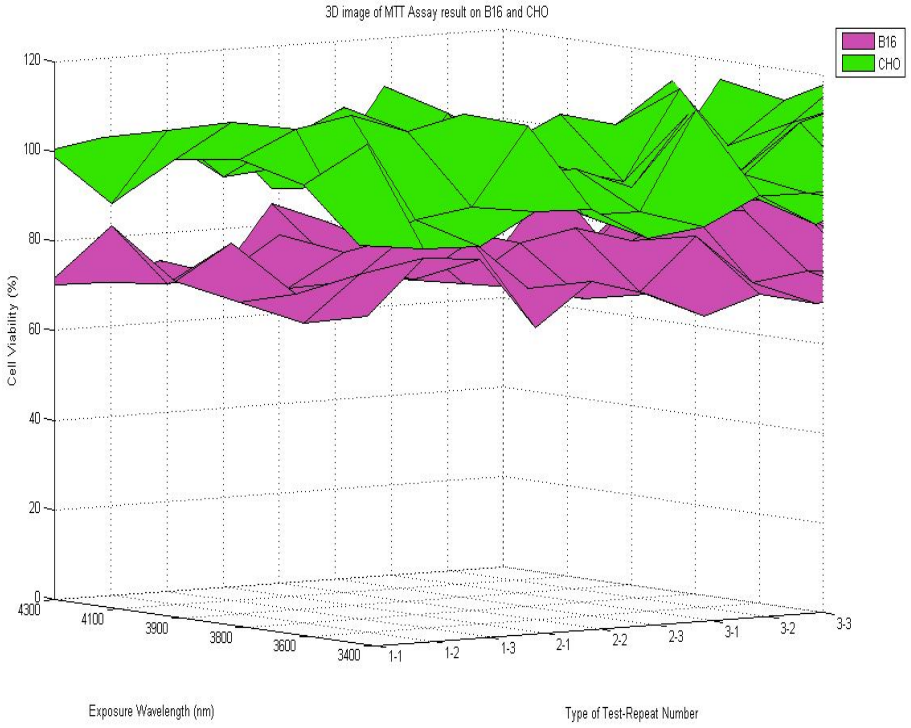

Figure 4.24: The cellular proliferation measurements by MTT assay shown for different regimes of far infrared exposures and post exposure incubations for both cancer (B16F10) and normal (CHO) animal cells.

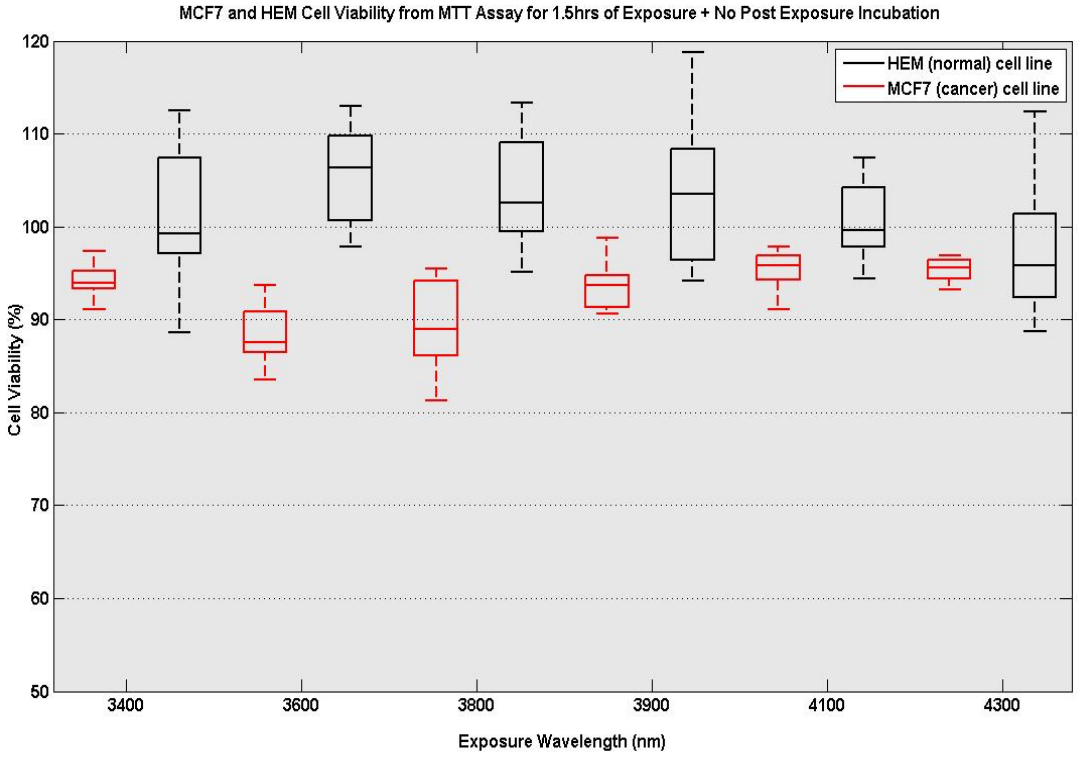

Figure 4.25: External electromagnetic radiation of far infrared wavelengths for the third regime of exposure. In this regime of exposure, cells are irradiated for 1.5 hours at the selected far infrared wavelength LEDs. In this box plot representation, each box represents mean (the middle box horizontal line) and standard errors (vertical lines outside the box) of the repeated MTT results. Data values at significantly higher levels are shown by +. The red color boxes show cell viability results from MTT assay for cancer MCF7 cells. The black color boxes demonstrate cell viability results for normal HEM cells.

4.2.2 Exposure of Human Cells - MCF7 vs. HEM Cells

Figure 4.25 and 4.26 illustrate the effects of external irradiation on cell viability of human cells by implementing MTT assay. In these experiments, cells are irradiated for 1.5 hours using visible, near infrared and far infrared light exposures.

Figure 4.25 provides insight into the effects of 1.5 hour light irradiation on MCF7

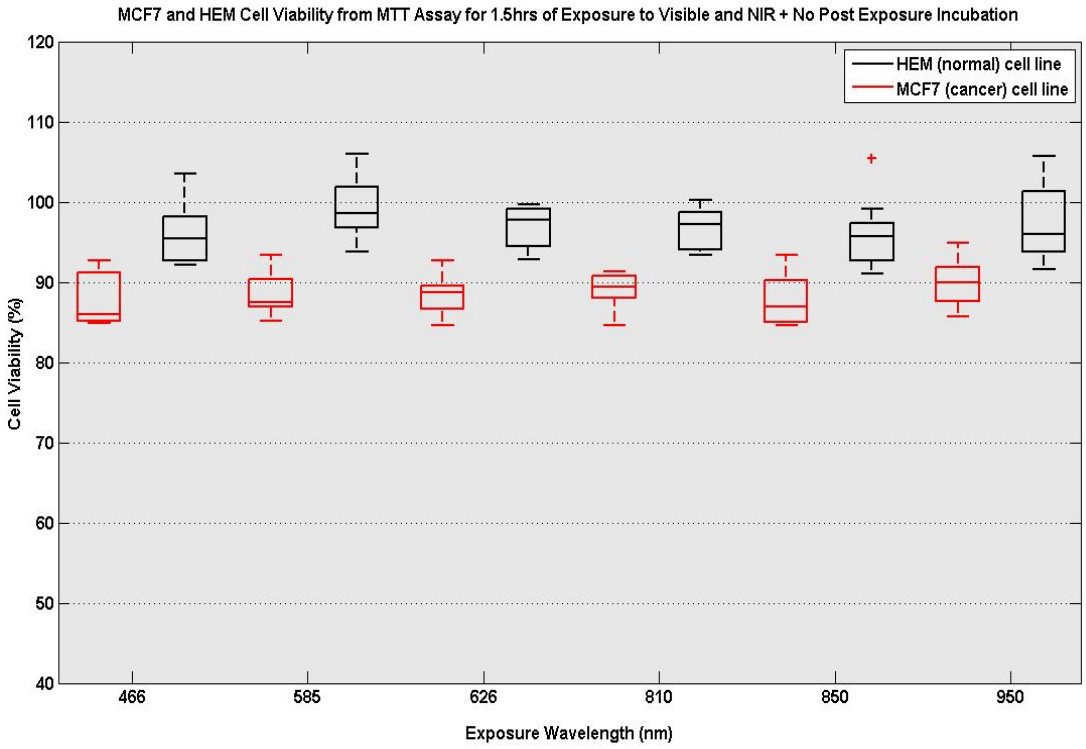

Figure 4.26: Cell proliferation measurements by MTT assay of MCF7 and HEM exposed for 1.5 hours at 466nm, 595nm, 626nm, 810nm, 850nm, and 950nm wavelengths (visible and near infrared range). The red color boxes signify cell viability measured by MTT assay for human MCF7 cancer cells. The black color boxes represent cell viability measured by MTT assay for human HEM normal cells. The horizontal lines in the boxes indicate the mean values obtained from all repeats of that particular experiment.

and HEM cells. The results demonstrated in the figure show a noticeable cellular apoptosis effect of exposures on MCF7 cells, when compared to the insignificant effects of such exposure on human HEM normal cell line.

The MTT assay results of MCF7 and HEM cells assessment for the first regime of exposure demonstrated in Figure 4.26 show minimal effects of irradiation on cellular viability of the MCF7 cancer cells but no effect is observed for HEM cells. Comparison of MTT analysis of both MCF7 cells and HEM cells for the first

three wavelengths (visible range) clearly demonstrate that MCF7 cells are affected slightly by these exposures. Figure 4.26 also shows similar effects from near infrared exposures (the last three wavelengths) of MCF7 and HEM cells, where a slight cell viability reduction is observed for MCF7 cells and no cell viability changes perceived for HEM cells. The changes observed in cellular proliferation of MCF7 at the selected visible light wavelengths are not very significant compared to that of far infrared exposure shown in Figure 4.25. Hence, it can be concluded that irradiation of different wavelengths in visible and near infrared range does not induce any considerable cytotoxicity on cultured cells.

Now, the MTT evaluation for the second regime of exposures (visible, near infrared and far infrared) of MCF7 and HEM cells is shown in Figure 4.27 and 4.28.

The effects of the second regime of exposure (1.5 hours of exposure and 24 hours of post exposure incubation) on two human cell lines are measured using MTT assay and represented in Figure 4.27. The cell viability changes in MCF7 cell induced by the exposures at the selected wavelengths in the far infrared range, are quiet visible in Figure 4.27. In contrary to the effects of the exposures on MCF7, no significant effects are identified for cell viability of normal HEM cells.

Apparently, visible and near infrared exposure of HEM cells, shown in Figure 4.28 do not indicate any significant cell proliferation effects, while a slight changes

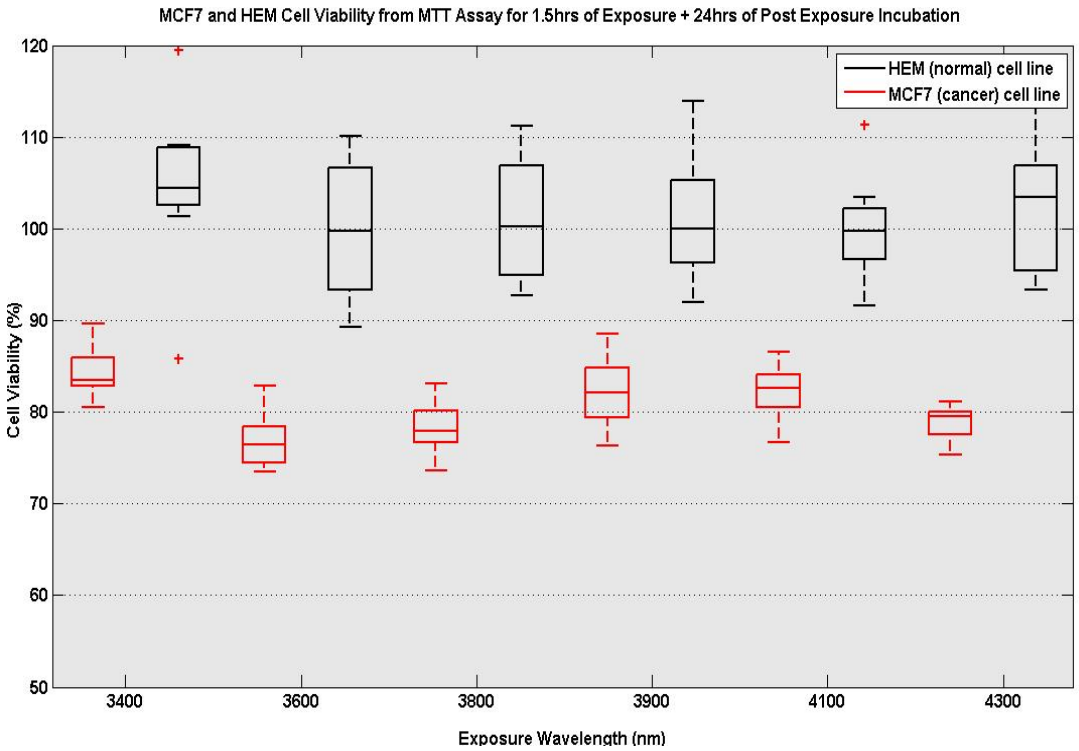

Figure 4.27: External electromagnetic radiation of far infrared light for the second regime of exposure. In this regime of exposure, MCF7 and HEM cells are irradiated for 1.5 hours with selected far infrared wavelengths followed by 24 hours of post exposure incubation. In this box plot representation, each box represents mean (the middle box horizontal line) and standard errors (vertical lines outside the box) of the repeated MTT results. Data values that are at the significant levels are shown by +. The red color boxes show cell viability results from MTT assay for MCF7 cells. The black color boxes demonstrate cell viability results for HEM cells.

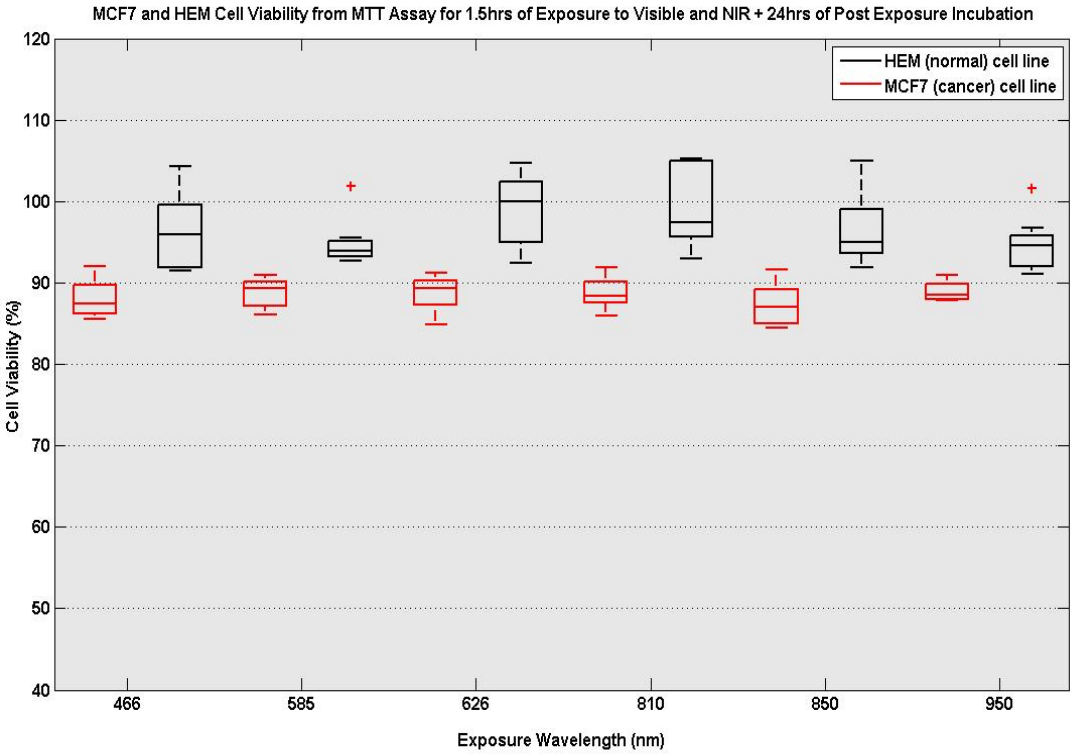

Figure 4.28: Cell proliferation measurements by MTT assay of MCF7 and HEM cells exposed for 1.5 hours at 466nm, 595nm, 626nm, 810nm, 850nm, and 950nm wavelengths (visible and near infrared range) followed by 24 hours of post exposure incubation. The MTT analysis results are evaluated by ELISA plate reader with OD reading of 595nm. The red color boxes represent cell viability measured by MTT assay for human cancer cell line, MCF7. The black color boxes represent cell viability measured by MTT assay for human normal cell line, HEM. The horizontal lines in the boxes indicate the mean values obtained from all repeats of that particular experiment.

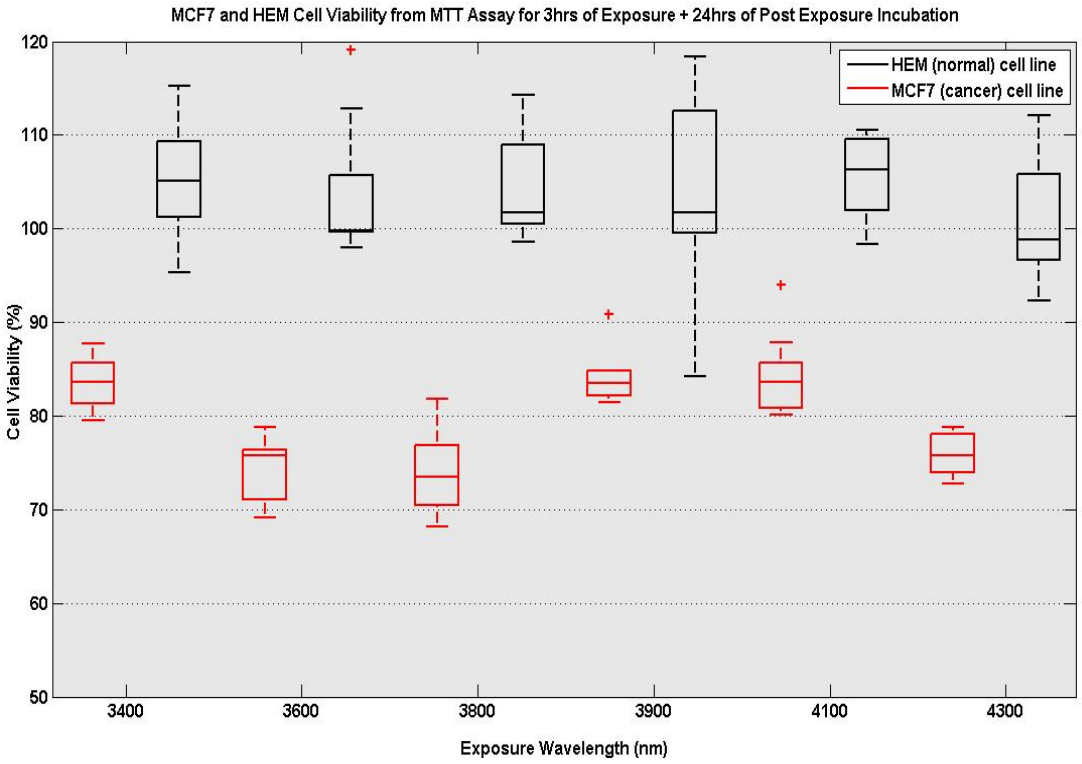

Figure 4.29: Cellular proliferation variation measurement by MTT assay of MCF7 and HEM cell exposed for 3 hours at the selected far infrared wavelengths followed by 24 hours of post exposure incubation. The MTT results were evaluated by ELISA plate reader with OD reading of 595nm.

in cell viability of MCF7 is visible. The changes in cell viability of MCF7 cells are not considered substantial since it is around 10% of reduction. Hence, it can be concluded that visible and near infrared wavelengths do not induce any considerable cellular apoptosis effect on MCF7 or HEM cells.

At the next step, the changes induced in cellular proliferation of MCF7 and HEM cells at the visible, near infrared and far infrared exposures are shown in Figure 4.29 and 4.30.

Figure 4.29 represents the MTT assessment of cellular proliferation changes of

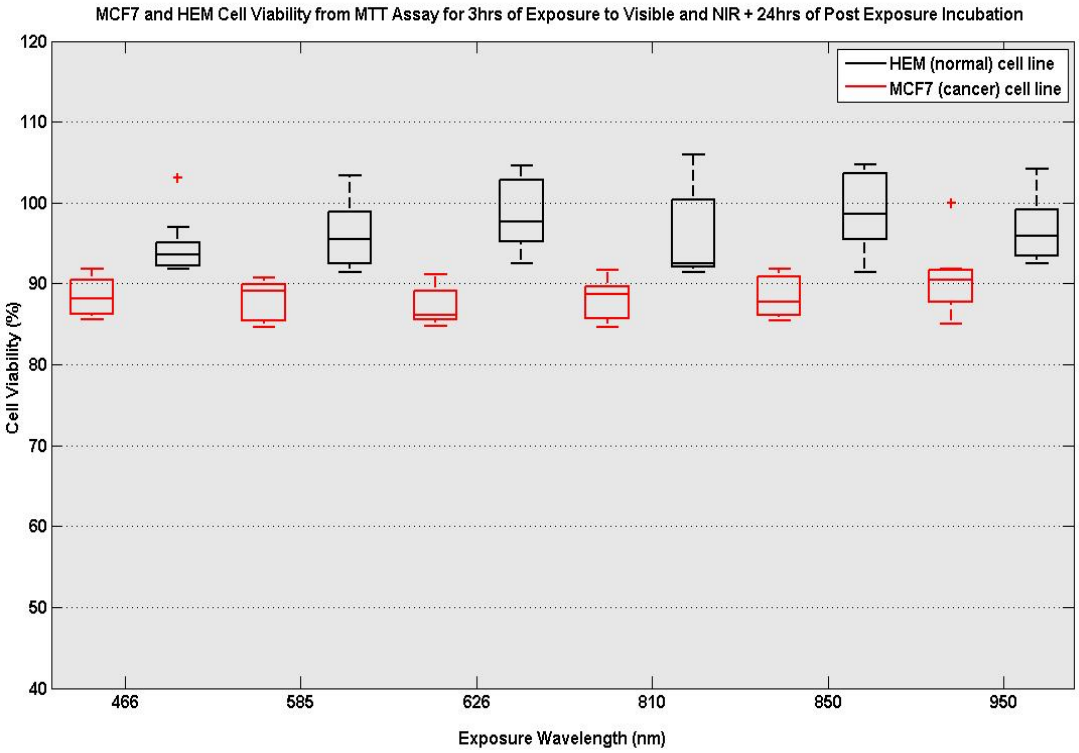

Figure 4.30: Cell proliferation measurements by MTT assay of MCF7 and HEM cells exposed for 3 hours at 466nm, 595nm, 626nm, 810nm, 850nm, and 950nm wavelengths (visible and near infrared range) followed by 24 hours of post exposure incubation. The MTT analysis results are evaluated by ELISA plate reader with OD reading of 595nm. The red color boxes represent cell viability measured by MTT assay for human cancer cells, MCF7. The black color boxes represent cell viability measured by MTT assay for human normal cells, HEM. The horizontal lines in the boxes indicate the mean value obtained from all repeats of that particular experiment.

MCF7 and HEM cells exposed at the far infrared wavelengths (range predicted computationally by the RRM). The effects of such exposure regime on MCF7 cells are easily identifiable. The cytotoxic effects induced in human cancer cells lead to cell viability reduction by approximately 20%. This cell viability reduction is in agreement with other quantitative results obtained from LDH analysis in Section 4.1.2.

Similar to other MTT results demonstrated in Figures 4.26 and 4.28, no considerable effects have been detected by MTT assessment for irradiation of HEM cells for 3 hours using visible and near infrared range LEDs and incubated for 24 hours after the exposures. Similarly, insignificant cell proliferation reduction in MCF7 cells of less than 10% is observed and demonstrated in Figure 4.30 at the visible and near infrared wavelengths.

MTT Assay on MCF7 and HEM Cells - Summary Remarks

To draw a final conclusion from the MTT assessment results on the effects of visible, near infrared and far infrared exposures on cell viability of human MCF7 cancer and HEM normal cells, the following Figures 4.31 and 4.32 are presented to depict dissimilarity of the induced effects in these two types of cells.

Three graphs displayed in Figure 4.31 provide a comprehensive illustration of cellular apoptosis effects of three different exposure regimes evaluated *in vitro* on human MCF7 cancer cells. The plots in this figure provide a clear demonstration of changes in cell viability (%) as a result of variation in exposure and post exposure incubation times. As it can be seen from the graphs, the cell viability obtained from the first regime of exposure is approximately around 90% viability, while the cellular viability obtained from the second regime of exposure shifts toward 80% viability. This 10% shift in cell viability can be due to extra 24 hours post exposure incubation of cells. Moreover, the bottom graph displays a further

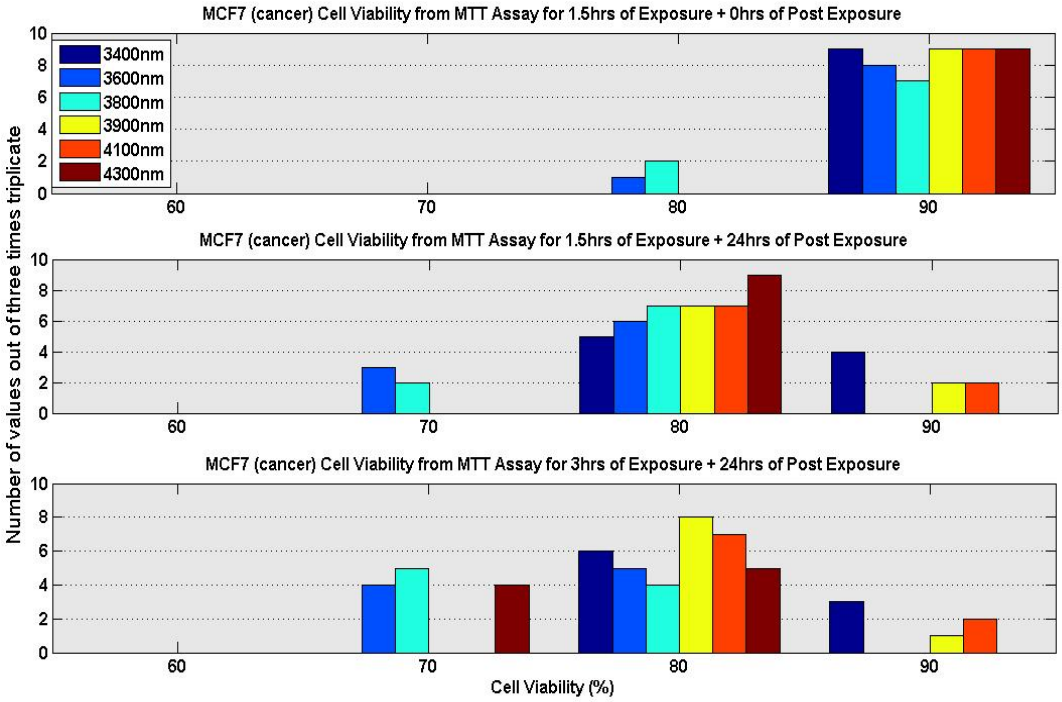

Figure 4.31: Histograms of MTT assessment results for triple triplicate of all three different exposure regimes on MCF7 cells. The first histogram from the top illustrates MTT evaluation of far infrared irradiation for the first regime of exposure. The middle graph displays MTT assessment for the second regime of exposure. At last, the bottom histogram demonstrates the results of the third regime of exposure on MCF7.

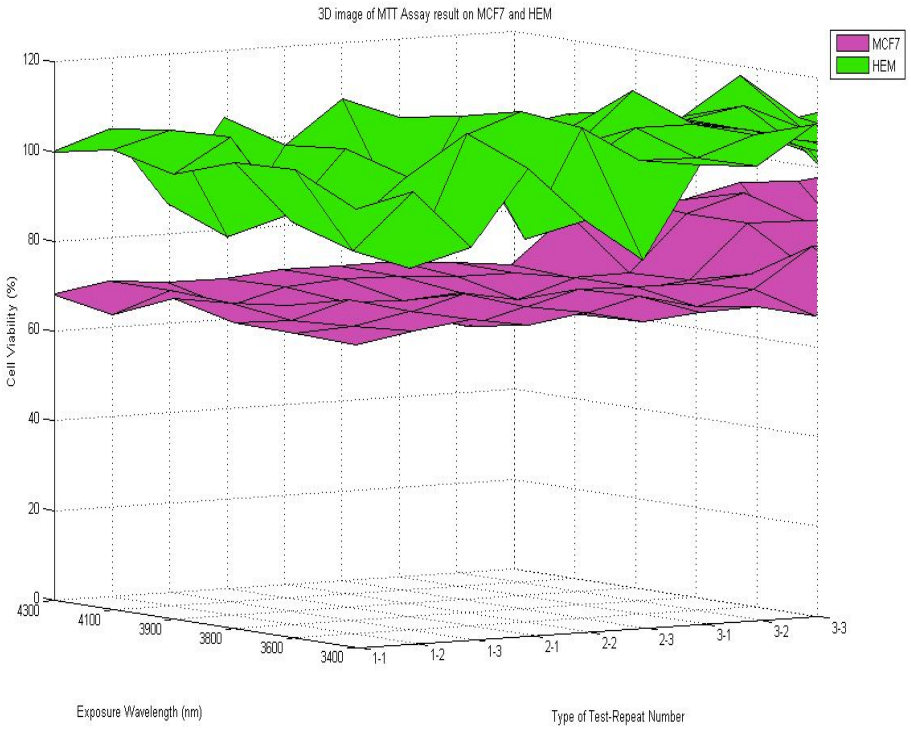

Figure 4.32: The proliferation results obtained from MTT assay are shown for different regimes of far infrared exposure and post exposure incubation for both cancer (MCF7) and normal (HEM) human cells.

reduction in cell viability compared to the above two graphs. The cell viability due to the third regime of exposure measured is shown in the last histogram. In this plot, the percentage of cellular viability appears to be shifted toward 70% and 80% by extension of exposure duration to 3 hours and post exposure incubation time to 24 hours compared to the first regime of exposure.

Figure 4.32 further clarifies and distinguishes the effects of different exposure regimes on both normal and cancer human cells. These two planes shown in Figure 4.32 illustrate the effect induced by the far infrared exposures on MCF7 cancer and HEM normal cells. The green plane represents the MTT assessment

of the induced effects on HEM normal cells. This plane generally is at z-plane of 100% cell viability, which means that no cytotoxic effects are observed in HEM cells. As oppose to HEM cells' MTT evaluation results, the effects of external irradiation on MCF7 cells are demonstrated by the purple plane that is on z-plane at 80% cell viability.

In conclusion, as proposed by the RRM hypothesis implementation, far infrared light in the range of 3500nm-6500nm predicted computationally by the RRM induces a significant cellular apoptosis on cancer cells only. MTT cellular proliferation analysis of MCF7 and HEM cells for three different exposure regimes in the visible and near infrared light wavelengths range demonstrates a slight, almost insignificant cytotoxic effect, while HEM cells are not affected by the same exposure regime and wavelengths.

Quantitative analysis of HEM normal cells irradiated by other wavelengths does not indicate any induced effect on their cell viability as measured by MTT assay. Although MCF7 cells are exposed by visible and near infrared wavelengths shows some induced cytotoxic effects which requires a further investigation. Another area that would require further analysis and experiments is the cell proliferation detected on a number of experiments on normal cell lines. These proliferation effects are shown in figures such as Figure 4.1, Figure 4.3, Figure 4.5, $\cdots$. Since the mechanism of such effects is not part of this thesis, it is not pursuit further here.

4.3 PrestoBlue^{TM} Cell Viability Assay

To conclusively evaluate and further clarify the quantitative results obtained from LDH and MTT assays for human cancer and normal cell lines, PrestoBlue^{TM} assay was also conducted on MCF7 and HEM cells. PrestoBlue^{TM} assay is used as reagent for rapid evaluation of viability and proliferation of MCF7 cells irradiated at three different regimes of exposure and post exposure incubation. The exposures are conducted using six selected LEDs in the far infrared wavelength range (as presented in previous sections). PrestoBlue^{TM} quantitatively measures any variation in cell viability of breast cancer cells due to external irradiation of these wavelengths at the far infrared (3400nm, 3600nm, 3800nm, 3900nm, 4100nm, 4300nm). Cells are seeded at the initial density of 1×10^4 cells per mL in a 96-well plate and incubated overnight before the start of experiments. The experiments are conducted in three times triplicate. The procedure and preparation of cells for evaluation of their cell viability by PrestoBlue^{TM} is closely followed by the accompanied manual (Invitrogen Technologies, Australia). Then, the results are measured at OD reading of 595nm using a 96 well ELISA plate reader (Thermo Electron Corporation, USA). The control is the mean absorption from the untreated (non-exposed) cells and the background is just the cell-less culture media.

Figure 4.33 demonstrates changes in cell viability of MCF7 cells irradiated at

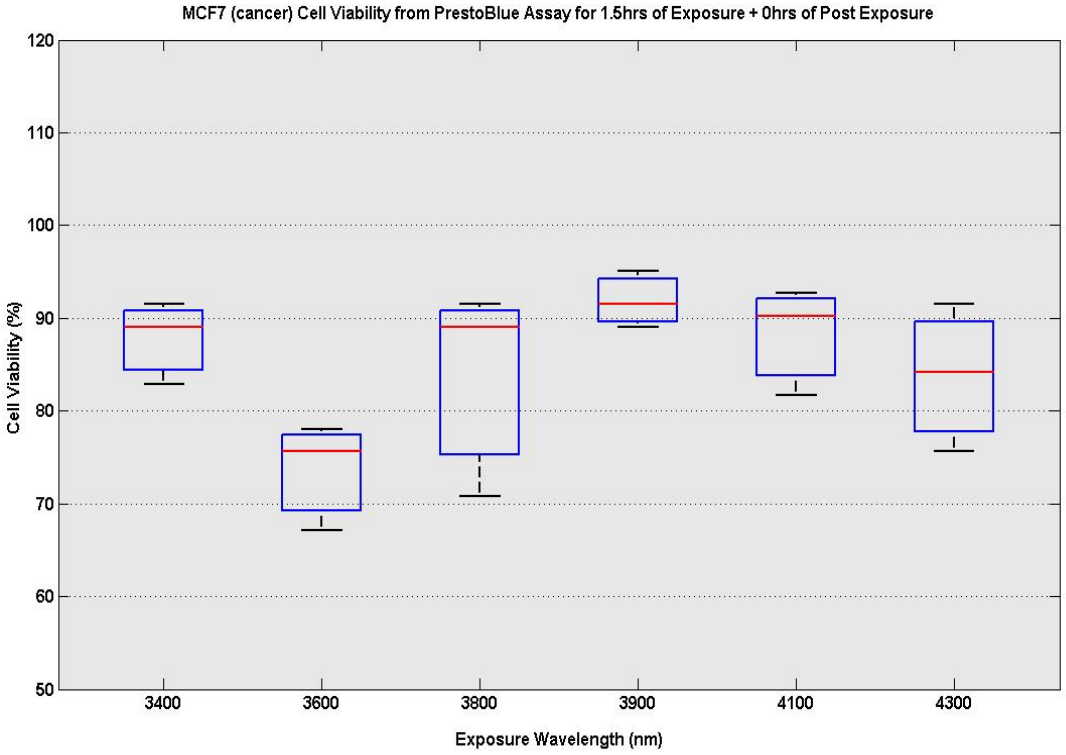

Figure 4.33: Cell viability measurements by PrestoBlue^{TM} assay of MCF7 cells exposed for 1.5 hours at the selected far infrared wavelengths. The horizontal lines in the boxes represent the mean value of all measurement repeats for that specific wavelengths and regime. The vertical lines indicate the range of the measurement values (the maximum value at the top end and the minimum value at the bottom end).

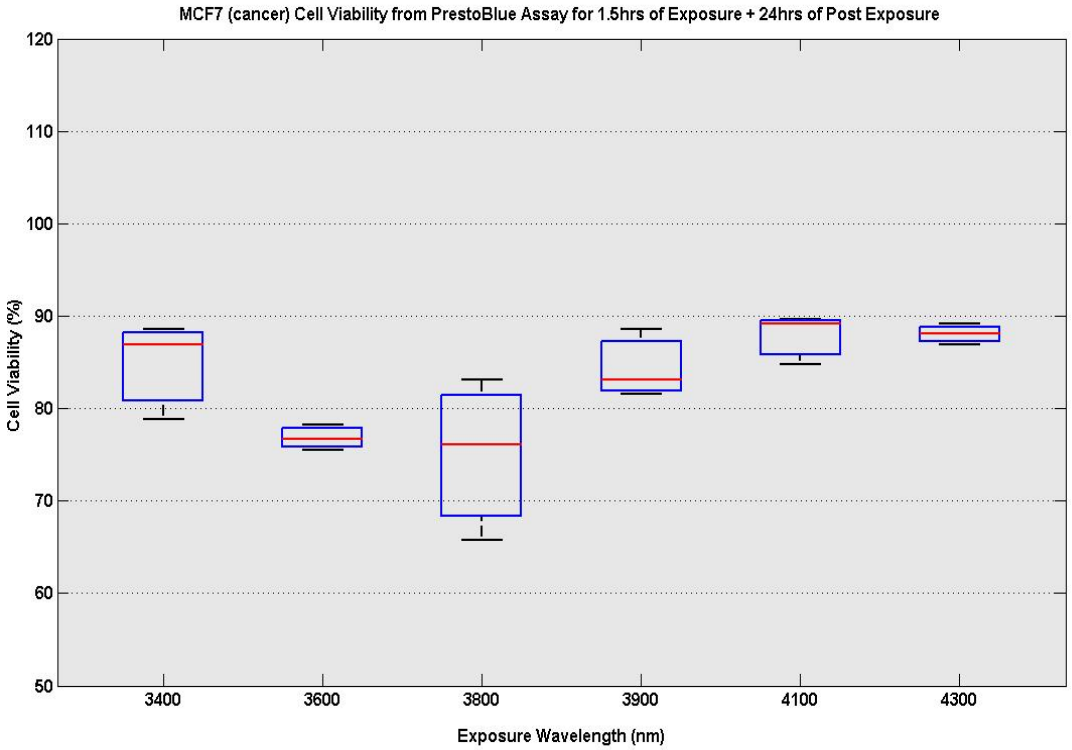

Figure 4.34: Cell viability measurements by PrestoBlue^{TM} assay of MCF7 cells exposed for 1.5 hours at the selected far infrared wavelengths with 24 hours of post exposure incubation. The horizontal lines in the boxes represent the mean value of all measurement repeats for that specific wavelengths and regime. The vertical lines indicate the range of the measurement values (the maximum value at the top end and the minimum value at the bottom end).

the first regime of exposure. In this regime, cells are irradiated for 1.5 hours at the selected far infrared wavelengths with no post exposure incubation after that. As demonstrated in Figure 4.33, visible reduction in cell viability of MCF7 cells is observed from PrestoBlue^{TM} analysis. The results obtained here further reaffirm the cytotoxic effects of the far infrared wavelengths on cancer cells.

The cell viability results evaluated by PrestoBlue^{TM} assay in Figure 4.34 demonstrate the effects induced by 1.5 hours irradiation at the selected far infrared

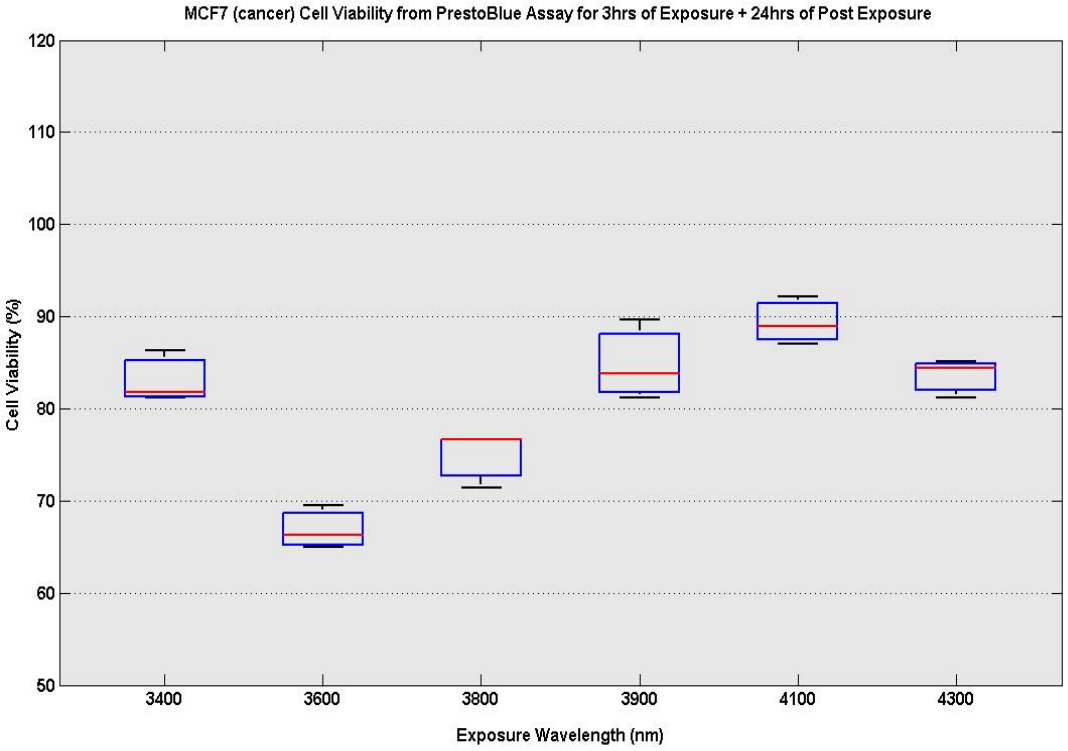

Figure 4.35: Cell viability measurements by PrestoBlue^{TM} assay on MCF7 cells exposed for 3 hours at the selected far infrared wavelengths followed by 24 hours of post exposure incubation. The horizontal lines in the boxes represent the mean value of all measurement repeats for that specific wavelengths and regime. The vertical lines indicate the range of the measurement values (the maximum value at the top end and the minimum value at the bottom end).

wavelengths followed by 24 hours of incubation on MCF7 cell line. Based on prediction by RRM approach, these far infrared light wavelengths are expected to induce resonant effects in biological activity of oncogenes and proto-oncogenes. As it can be seen here, the predicted far infrared wavelengths range demonstrate visible effect on cell viability of cancer cells as measured by PrestoBlue^{TM} assay.

The cell viability results of MCF7 cells shown in Figure 4.35 show the findings measured by PrestoBlue^{TM} assay, when cancer cells were exposed for 3 hours

at the selected far infrared wavelengths followed by 24 hours of post exposure incubation. The graph demonstrates the significant cell viability reduction due to external exposures at the third regime of exposure in MCF7 cells.

4.4 Discussion - Quantitative Analysis and Final Remarks

The quantitative results obtained from LDH assay for visible, near infrared and far infrared irradiation corroborate the computationally predicted far infrared light at the wavelengths in the range of 3500nm to 6500nm can induce cytotoxic effects on cell viability of animal and human cancer cells. LDH analysis confirms the significant cell viability reduction in B16F10 and MCF7 cells exposed to far infrared wavelengths. In contrary to responses of B16F10 and MCF7 cancer cells to far infrared irradiation, LDH analysis of normal CHO and HEM cells irradiated at the same far infrared wavelengths does not indicate any cytotoxic effects in their cell viability. Although irradiation by visible and near infrared exposures demonstrated insignificant cytotoxic effect on B16F10 and MCF7 cells, the underlying mechanism of that cytotoxic effect is not pursuit here, since it does not input any valuable contribution to the scope of this project. Furthermore, quantitative analysis of both animal and human cancer, and normal cell lines with the MTT assay leads to the similar conclusion obtained from the LDH assay. From the MTT evaluations, it can be deduced that the far infrared wavelength

exposures can induce the substantial cytotoxic effects in cell viability of cancer B16F10 and MCF7 cells, while normal CHO and HEM cells are not being affected by such exposures. The last quantitative test is conducted by PrestoBlue^{TM} on MCF7 cells to further elucidate the cytotoxic effects of far infrared wavelengths exposures. The result from PrestoBlue^{TM} assay reafirm the results obtained from LDH and MTT assays for human cancer MCF7 cells.

In addition, comparison of three different durations of exposures and post exposure incubations by LDH, MTT and PrestoBlue^{TM} assay analyses demonstrates that the cytotoxic effects of longer exposure time exceeds the cytotoxic effect of longer post exposure incubation time. As expressed in LDH, MTT and PrestoBlue^{TM} results obtained from three different exposure regimes differed from each other by exposure or post exposure incubation times, the effects of longer exposure time (3 hours) shows more significant cytotoxic effect. The results reveal that 3 hours of exposure and 24 hours of post exposure incubation induces the maximum cytotoxic effects compared to the other two exposure regimes. It is worth to mention that these optimum exposure regimes are proposed after a number of trial and error experiments with cancer B16F10 and MCF7 cells.

Chapter 5

Qualitative Analysis of *in vitro* Electromagnetic Radiation

As discussed in previous chapters, a recent theoretical hypothesis proposed in the RRM is being evaluated experimentally in this work. Based on this proposal, wavelength range between $\approx$ 3500nm and $\approx$ 6500nm is identified as activation wavelength range for oncogenes and proto-oncogenes. These genes play crucial role in unregulated growth of cancer cells. Hence, detrimental effect is expected to be induced on cellular proliferation of cancer cells upon exposure to external irradiation of these wavelengths.

In Chapter 4, quantitative analysis of RRM proposed theory is investigated through three standard cell-based quantitative assays of LDH, MTT and PrestoBlue^{TM}. Evaluations of selected far infrared wavelengths irradiation demonstrate visible cytotoxic effect on cell viability of animal and human cancer cells. The substantial cytotoxic effect of external far infrared irradiation on both B16F10 and MCF7

cells is shown by all quantitative assays. To further examine and verify the quantitatively obtained cytotoxic effect in Chapter 4, changes in cell morphology of cancer cells for far infrared external exposure is investigated through qualitative assays.

In this Chapter, the effect of far infrared irradiation on cell morphology is closely examined by phase contrast microscopy and confocal laser scanning microscopy (CLSM). Through phase contrast microscopy, the effect of three hours of external irradiation and 24 hours of post exposure incubation on cell morphology of B16F10 is conducted for wavelengths of 3400nm, 3600nm, 3800nm, 3900nm, 4100nm and 4300nm. The cell morphological effect of such irradiation is compare to untreated B16F10 cells. Then, the effect of same irradiation wavelength on CHO cells is explored to compare the effect of these external irradiation on CHO and B16F10 cells (Normal cells vs cancer cells). Subsequently, the effect of third regime of exposure for all 6 far infrared wavelengths on cell morphology of MCF7 and HEM cells is demonstrated. These images are then compared to sham exposed cells for further clarification of external exposure effect on cellular morphology. Investigation of HEM cells is conducted to provide a comparison benchmark for the effect of far infrared exposure on normal human and cancer human cells.

After qualitative analysis of B16F10 (cancer cell line) with phase contrast microscopy, the images from a more in-depth qualitative assay with confocal laser

scanning microscopy (CLSM) is presented. At first, the necrosis and apoptotic effect of far infrared irradiation on B16F10 cells is studied for two far infrared range LEDs of 3600nm and 4300nm as well as untreated B16F10 cells. Subsequently, the necrosis and opoptotic effect of external far infrared exposure on MCF7 cells is explored. This qualitative analysis on MCF7 is conducted on untreated MCF7 cells and cells exposed to wavelengths of 3600nm and 4300nm according to the third regime of exposure. Finally, the last section of this chapter provides a discussion of the two qualitative analysis conducted on human and animal cancer and normal cells.

5.1 Phase Contrast Microscopy

To measure any induced effects of the far infrared wavelengths on cell morphology of cancer and normal human and animal cells, phase contrast microscopy is used to analyze any effect qualitatively. For this assay, cells are seeded at the density of 2×10^5 cells per mL in 24-well plates and incubated overnight. Then, the cells are exposed to external irradiation of far infrared LEDs based on the third regime of exposure. Hence, cells are irradiated for 3 hours followed by 24 hours of post exposure incubation. It is worth to mention that one well in each plate is sham exposed and used as control for measurement of external exposure effects on cancer and normal cells. Upon elapse of post exposure incubation time, exposed cells are washed very carefully with cold phosphate-buffered saline (PBS) to remove

any cell detachment from the surface of the plates. After this step, the images are taken by phase contrast microscopy to elucidate any induced effects imposed on cell viability by the external exposures. These images for each wavelength are taken at 100X magnifications using Nikon Eclipse Ti-E microscope (Nikon Instruments Inc, Japan).

5.1.1 Animal Cell line - B16F10 vs. CHO cells

The effects of external irradiation of selected wavelengths (in the RRM computationally predicted far infrared range) are probed by phase contrast microscopy. In this qualitative assay, B16F10, and CHO cells are externally irradiated by the fabricated exposure device at the wavelengths of 3400nm, 3600nm, 3800nm, 3900nm, 4100nm, 4300nm. According to the experimental analysis from standard cell-based quantitative assays, cancer cells radiated with these LEDs in the far infrared range demonstrate to increase cellular death while normal cells are not affected.

Thus, this section further investigates the findings from quantitative analysis through qualitative assays conducted on both normal and cancer animal cell lines. The first graph is phase contrast microscopy images of untreated cell culture for B16F10 and CHO cells, respectively.

To comprehend and analytically assess any changes in cell morphology, a set

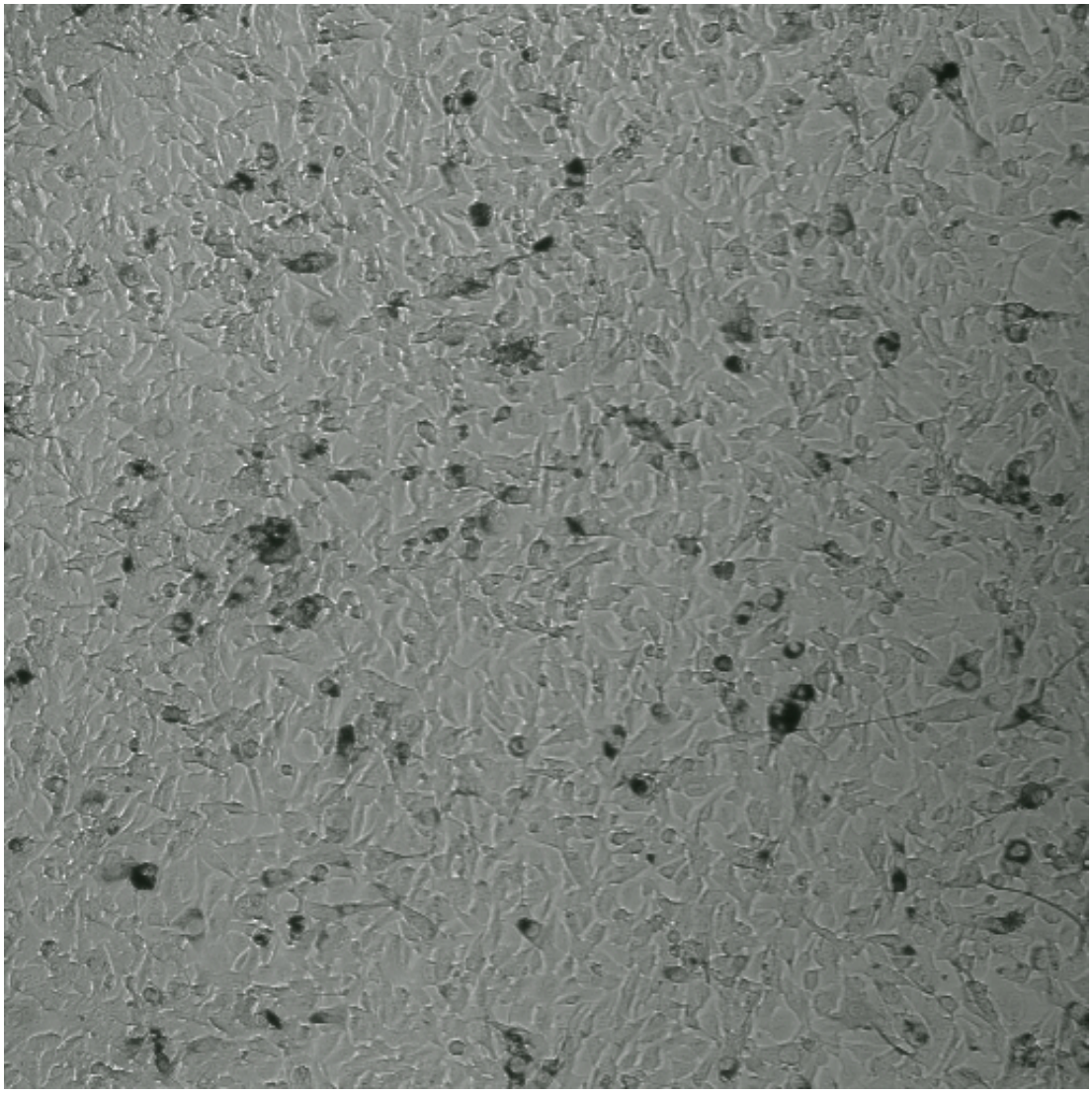

Figure 5.1: Untreated cultured B16F10 cell line.

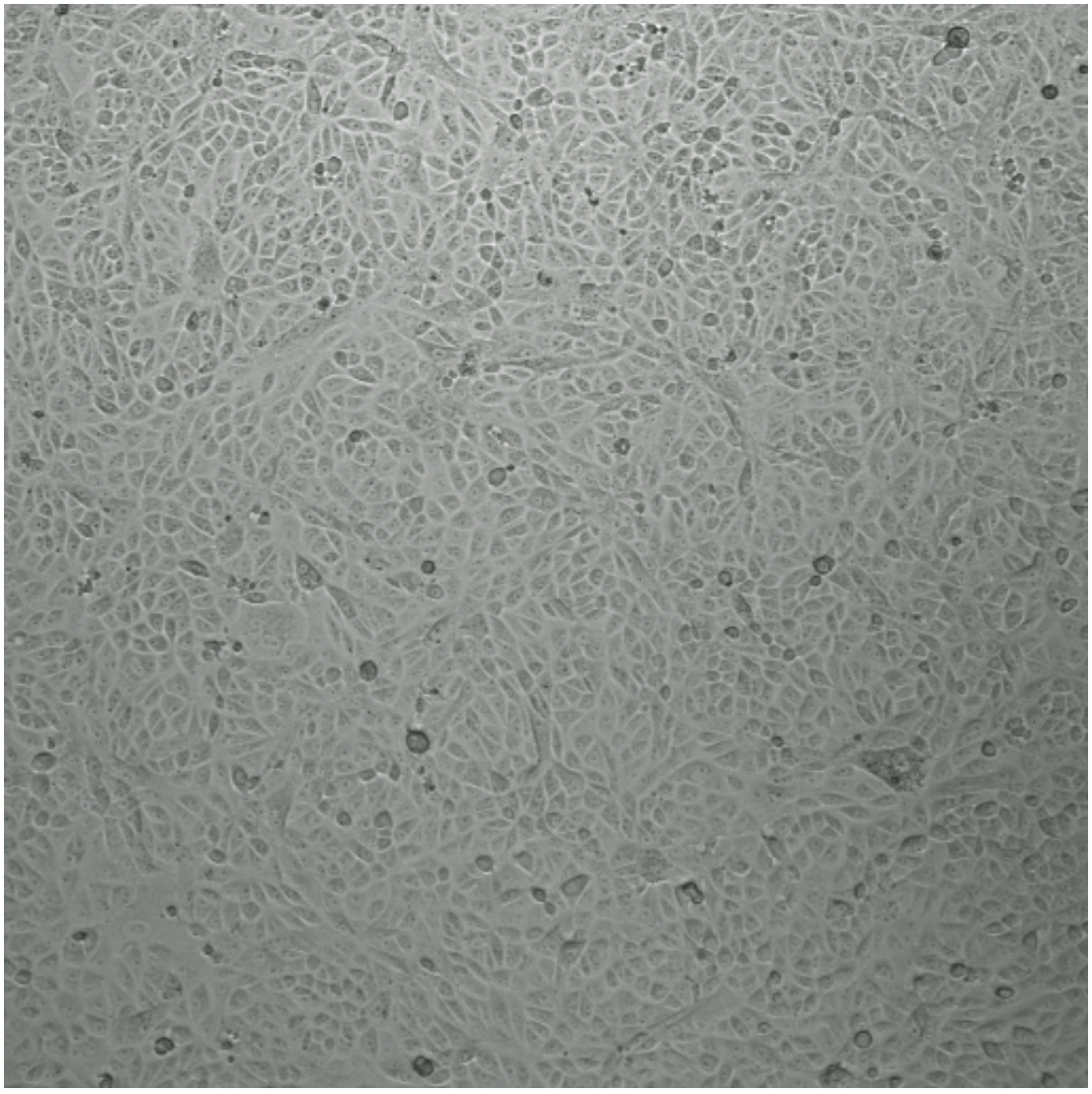

Figure 5.2: Untreated cultured CHO cell line.

of untreated cell culture from B16F10 as a cancer cell line and CHO cells as a normal cell line are examined by phase contrast microscopy and demonstrated in Figure 5.2 and 5.1. This set of microscopy images is used as a control to help us identify any morphology or significant confluency changes in cell morphology of B16F10 and CHO cells as a result of different external irradiation wavelengths.

Figure 5.3 and Figure 5.4 demonstrate the effect of 3400nm wavelength exposure on B16F10 and CHO cell lines. A close look at the image taken for B16F10 cells indicates the apparent cell detachment as a result of 3 hours of irradiation with 3400nm wavelength followed by 24 hours of incubation. When the images of both B16F10 and CHO cells are compared, no apparent cellular detachment or cell morphology changes are observed in CHO cells. Additionally, quantitative analysis of identical exposure regime on CHO cells in Chapter 4 does not indicate significant changes in cell viability of CHO cells.

Comparison of Figure 5.5 and 5.6 clearly demonstrate that far infrared wavelength of 3600nm causes cell apoptosis and cell detachment in B16F10 as cancer cells while CHO cells does not seem to be affected by this external electromagnetic irradiation. According to the RRM proposed hypothesis, the wavelength range of 3500nm to 6500nm is expected to induce resonant effects on the biological functionality of oncogene and proto-oncogene proteins. The results obtained from phase contrast microscopy for B16F10 cells compared to CHO cells not only corroborate the quantitative analysis demonstrated in Chapter 4 but also is

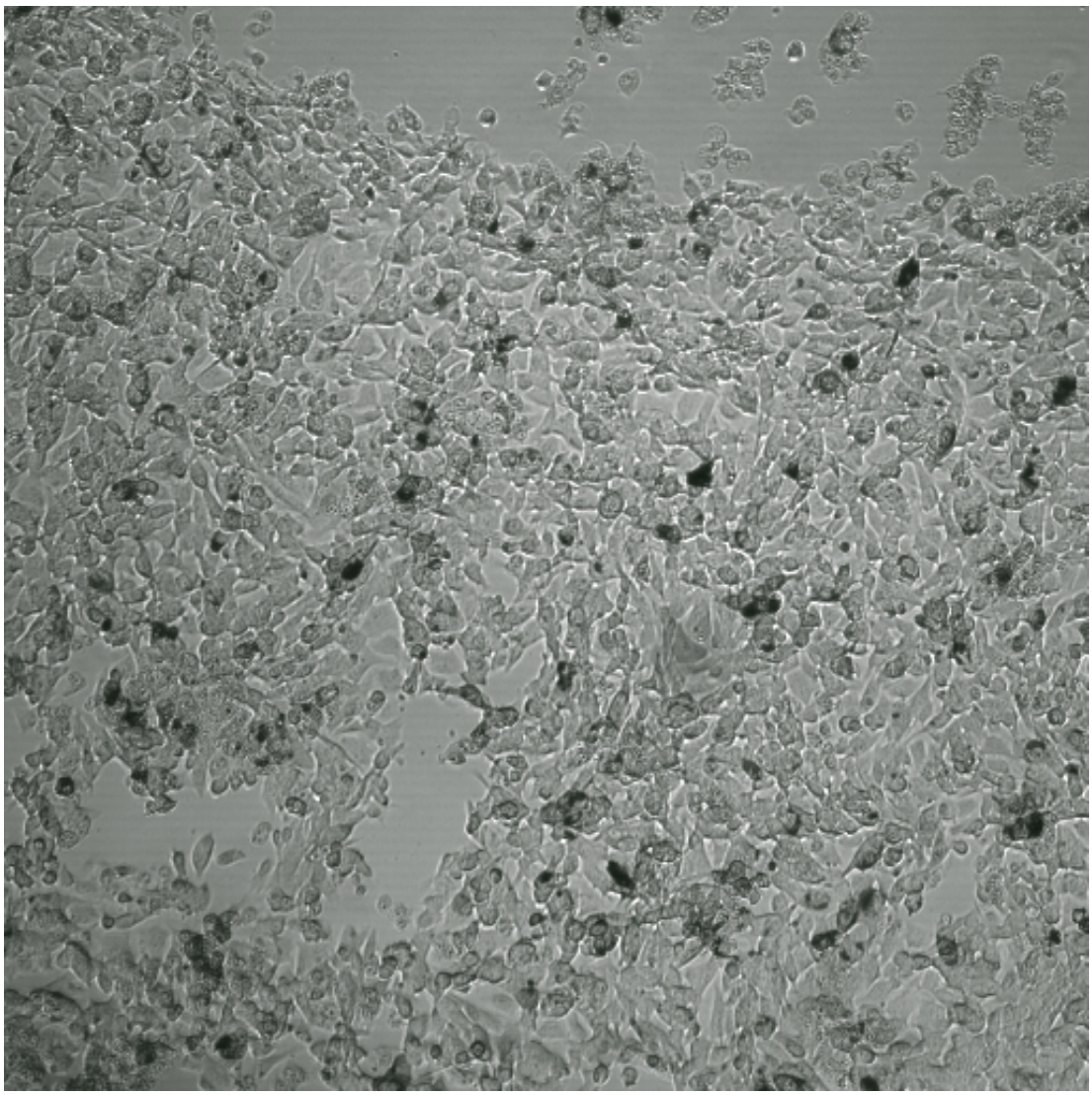

Figure 5.3: The effects of exposure irradiation of 3400nm wavelength on B16F10 as cancer cells. Cancer cells are exposed for 3 hours inside the incubator to 3400nm wavelength. The exposed cells are then incubated for 24 hours before phase contrast microscopy is conducted by Nikon Eclipse Ti-E microscope (Nikon Instruments Inc, Japan) with 100X magnification.

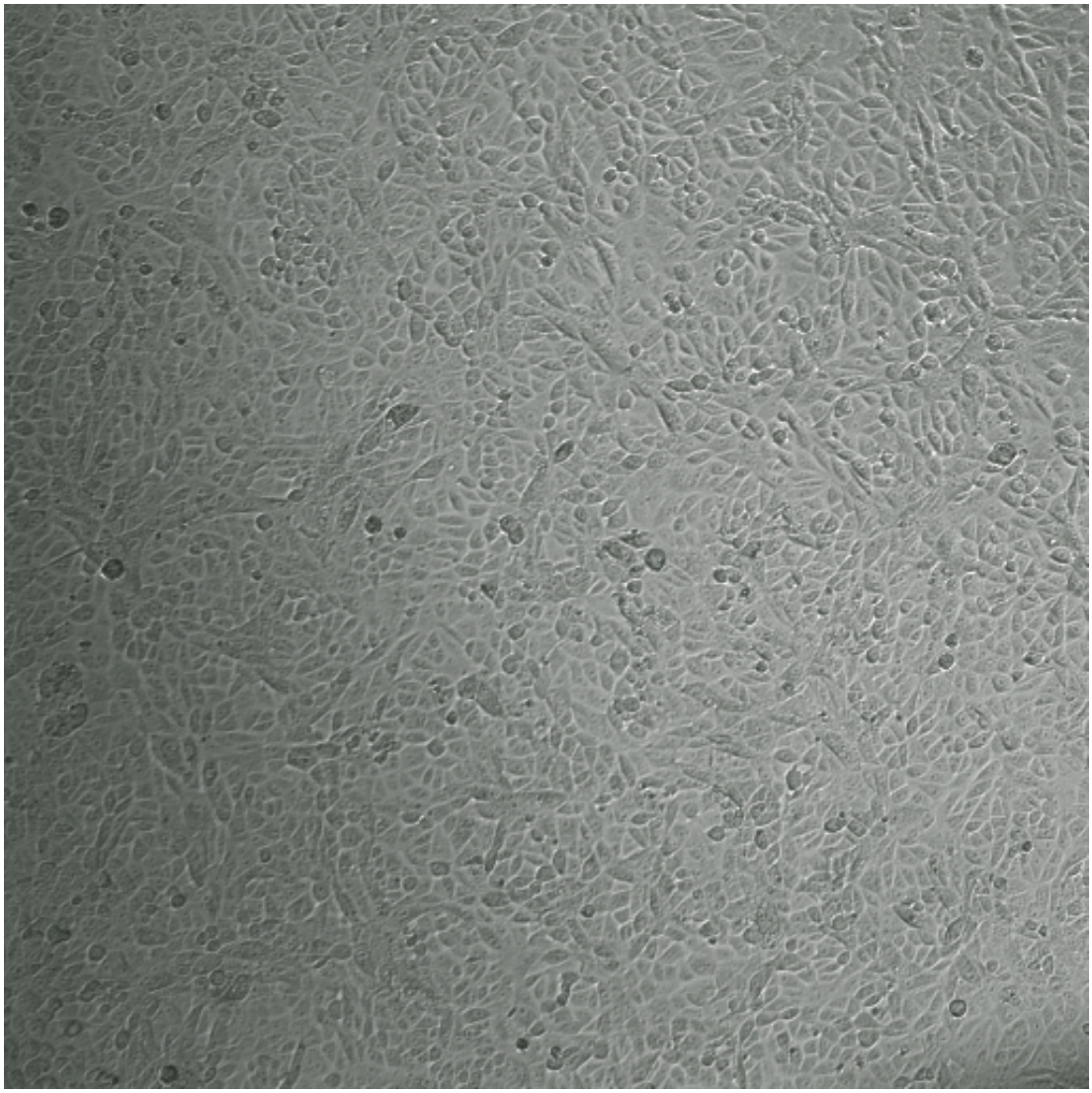

Figure 5.4: The effects of exposure irradiation of 3400nm wavelength on CHO as normal cell line candidate. Cells are exposed for 3 hours inside the incubator to 3400nm wavelength. The exposed cells are then incubated for 24 hours before phase contrast microscopy is conducted by Nikon Eclipse Ti-E microscope (Nikon Instruments Inc, Japan) with 100X magnification.

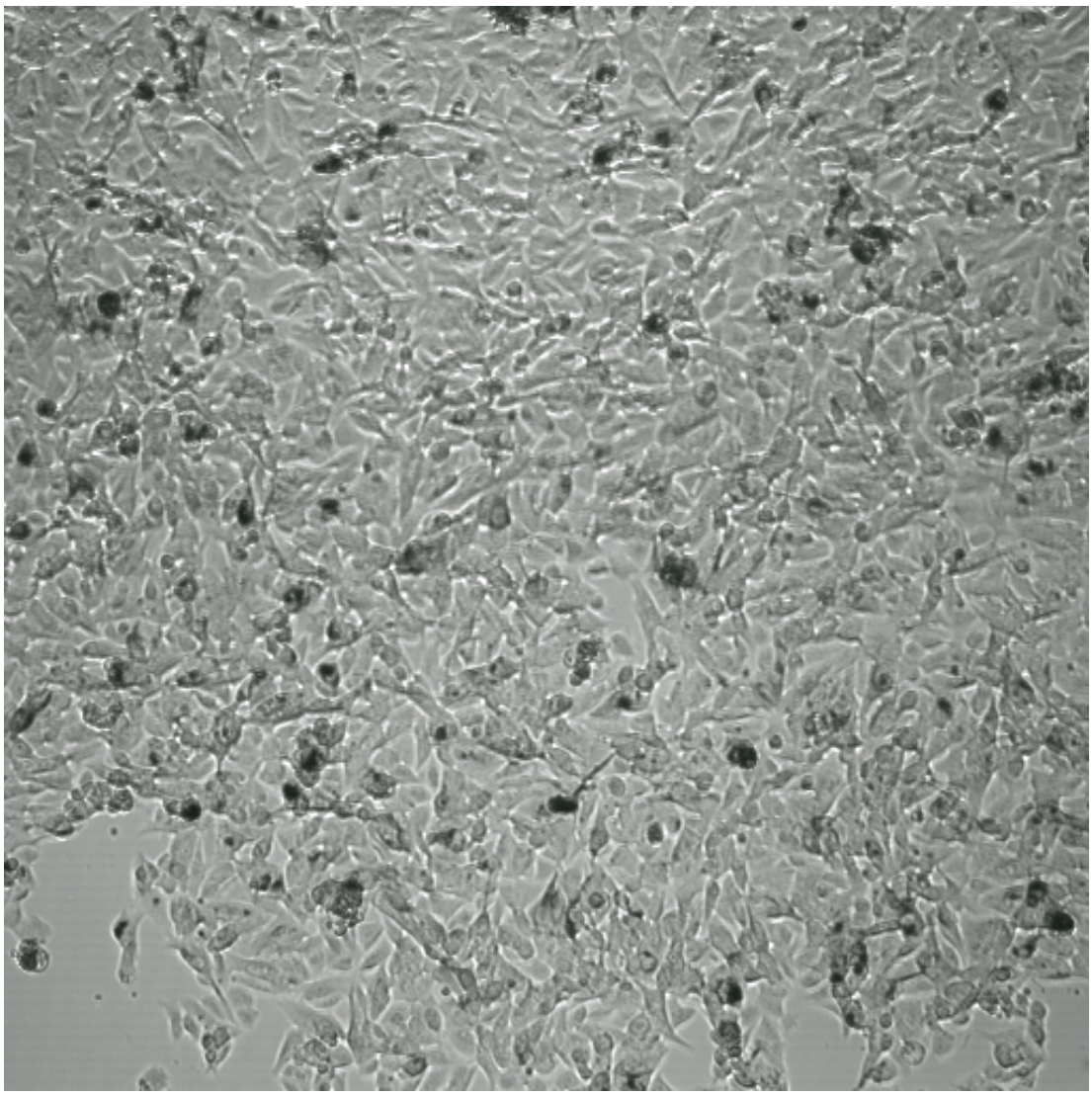

Figure 5.5: The effects of exposure irradiation of 3600nm wavelength on B16F10 as cancer cells. Cancer cells are exposed for 3 hours inside the incubator to 3600nm wavelength. The exposed cells are then incubated for 24 hours before phase contrast microscopy is conducted by Nikon Eclipse Ti-E microscope (Nikon Instruments Inc, Japan) with 100X magnification.

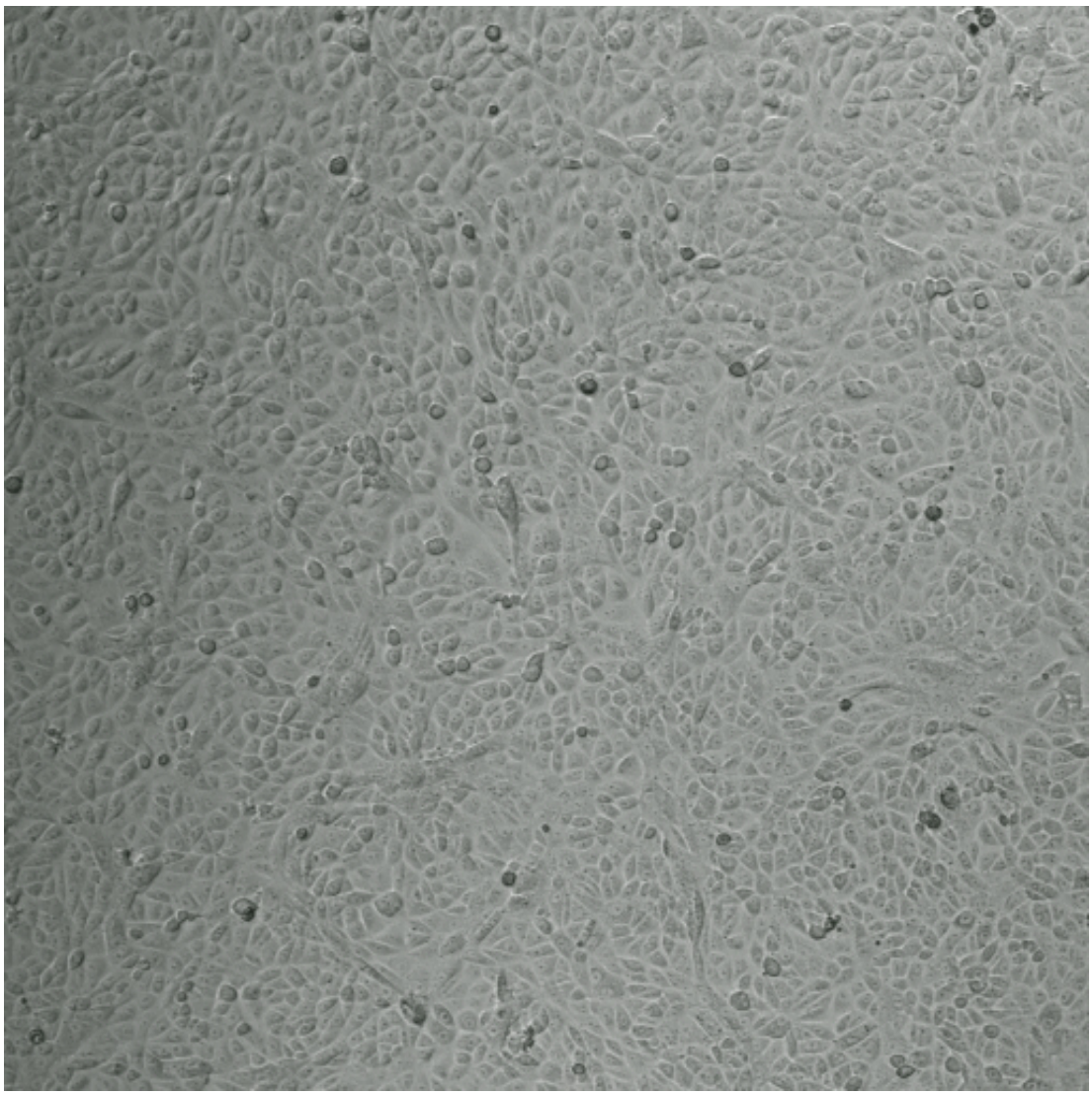

Figure 5.6: The effects of exposure irradiation of 3600nm wavelength on CHO as normal cell line candidate. Cells are exposed for 3 hours inside the incubator to 3600nm wavelength. The exposed cells are then incubated for 24 hours before phase contrast microscopy is conducted by Nikon Eclipse Ti-E microscope (Nikon Instruments Inc, Japan) with 100X magnification.

aligned with the RRM proposed hypothesis.

In Figure 5.7, visible cellular detachment in cell cultures irradiated externally with 3800nm wavelength is observed. In contrary, Figure 5.8 does not demonstrate any significant cytotoxic effects. Even though, CHO cells in Figure 5.8 and B16F10 cells in Figure 5.7 are irradiated at the same far infrared wavelengths and exposure regime, the cytotoxic effects are only observed on B16F10, which is a cancer cell line. According to the proposed hypothesis, wavelength range of 3500nm to 6500nm is related to the active site(s) of oncogene and proto-oncogene proteins. It has been proposed that external exposures at this wavelength range can induce changes in biological functionality of proteins that lead to therapeutic effect on cancer tumors.

Similarly, the external exposure of B16F10 as a cancer cell line in Figure 5.9 shows visible apoptotic effect while CHO as a normal cell line in Figure 5.9 does not demonstrate any visible sign of cellular death or cellular detachment. The visible cellular detachment in B16F10 cells corroborates the quantitative assays results which indicate increased cell apoptosis due to external far infrared exposures. It can be deducted from comparing the images of B16F10 and CHO cells that the external exposures at the selected far infrared wavelengths do not lead to any cell detachment or cell apoptosis in CHO cells, while its cytotoxic effects on B16F10 cells are apparent.

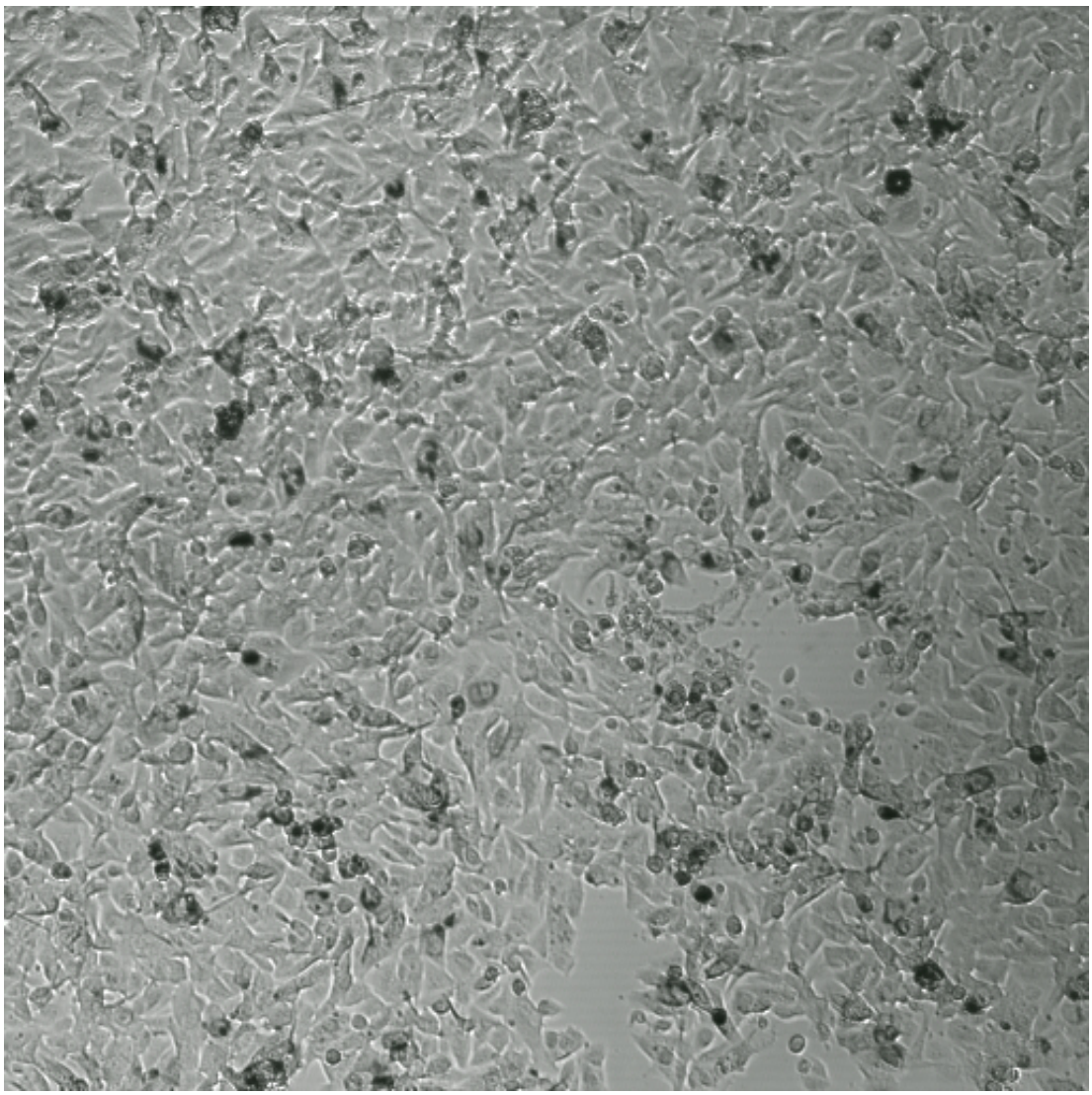

Figure 5.7: The effects of exposure irradiation of 3800nm wavelength on B16F10 as cancer cells. Cancer cells are exposed for 3 hours inside the incubator to 3800nm wavelength. The exposed cells are then incubated for 24 hours before phase contrast microscopy is conducted by Nikon Eclipse Ti-E microscope (Nikon Instruments Inc, Japan) with 100X magnification.

Figure 5.8: The effects of exposure irradiation of 3800nm wavelength on CHO as normal cell line candidate. Cells are exposed for 3 hours inside the incubator to 3800nm wavelength. The exposed cells are then incubated for 24 hours before phase contrast microscopy is conducted by Nikon Eclipse Ti-E microscope (Nikon Instruments Inc, Japan) with 100X magnification.

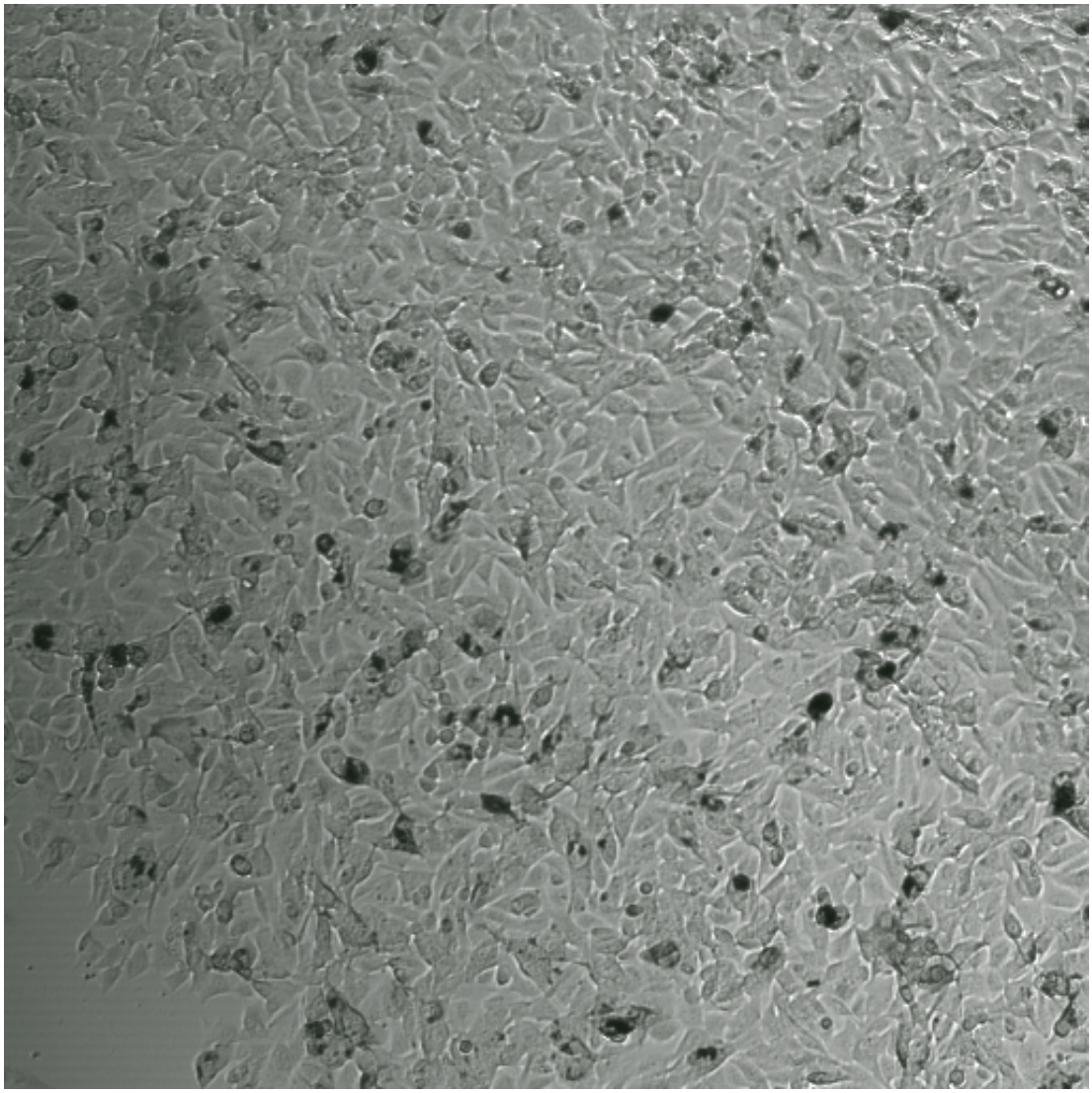

Figure 5.9: The effects of exposure irradiation of 3900nm wavelength on B16F10 as cancer cells. Cancer cells are exposed for 3 hours inside the incubator to 3900nm wavelength. The exposed cells are then incubated for 24 hours before phase contrast microscopy is conducted by Nikon Eclipse Ti-E microscope (Nikon Instruments Inc, Japan) with 100X magnification.

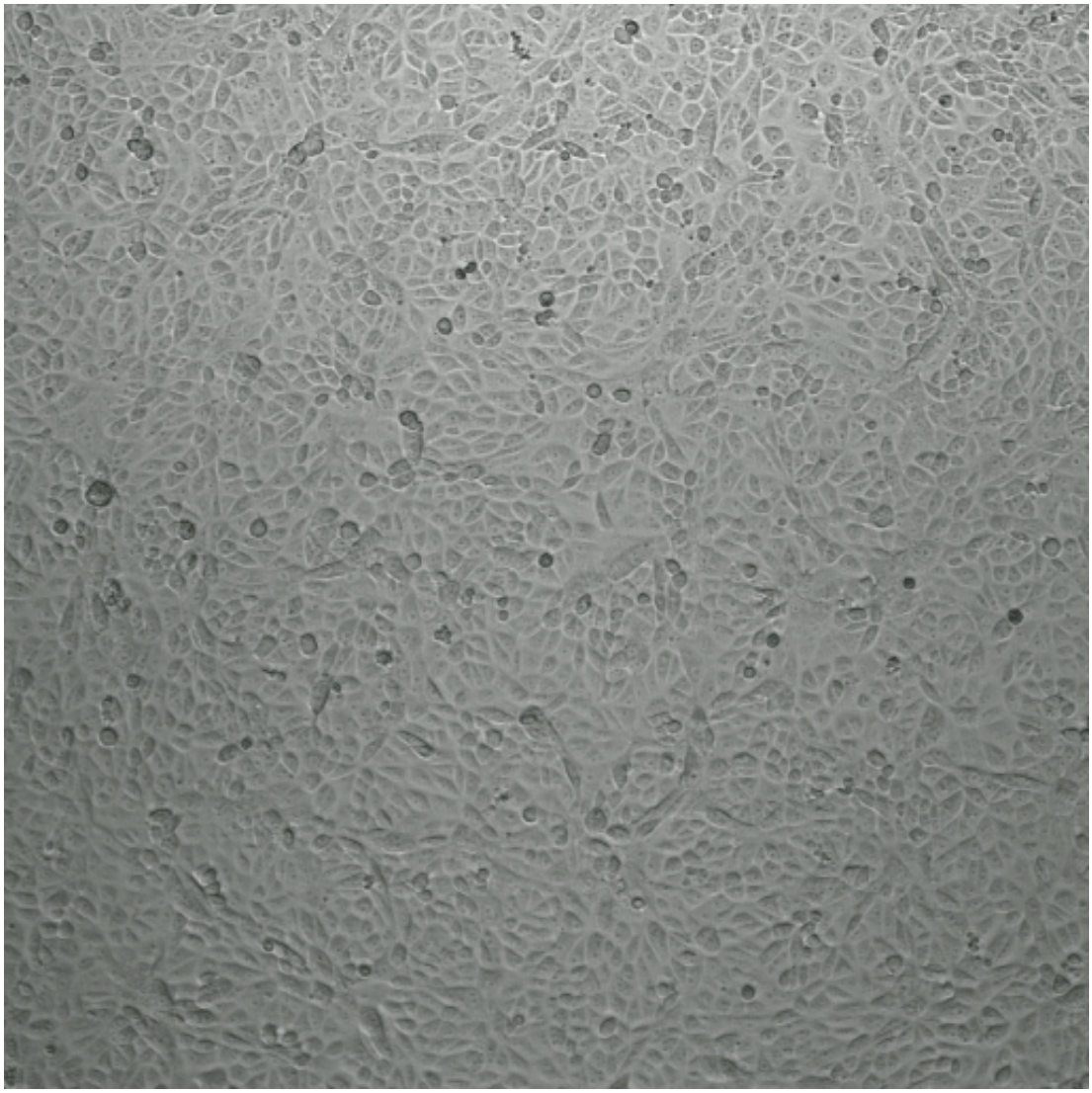

Figure 5.10: The effects of exposure irradiation of 3900nm wavelength on CHO as normal cell line candidate. Cells are exposed for 3 hours inside the incubator to 3900nm wavelength. The exposed cells are then incubated for 24 hours before phase contrast microscopy is conducted by Nikon Eclipse Ti-E microscope (Nikon Instruments Inc, Japan) with 100X magnification.

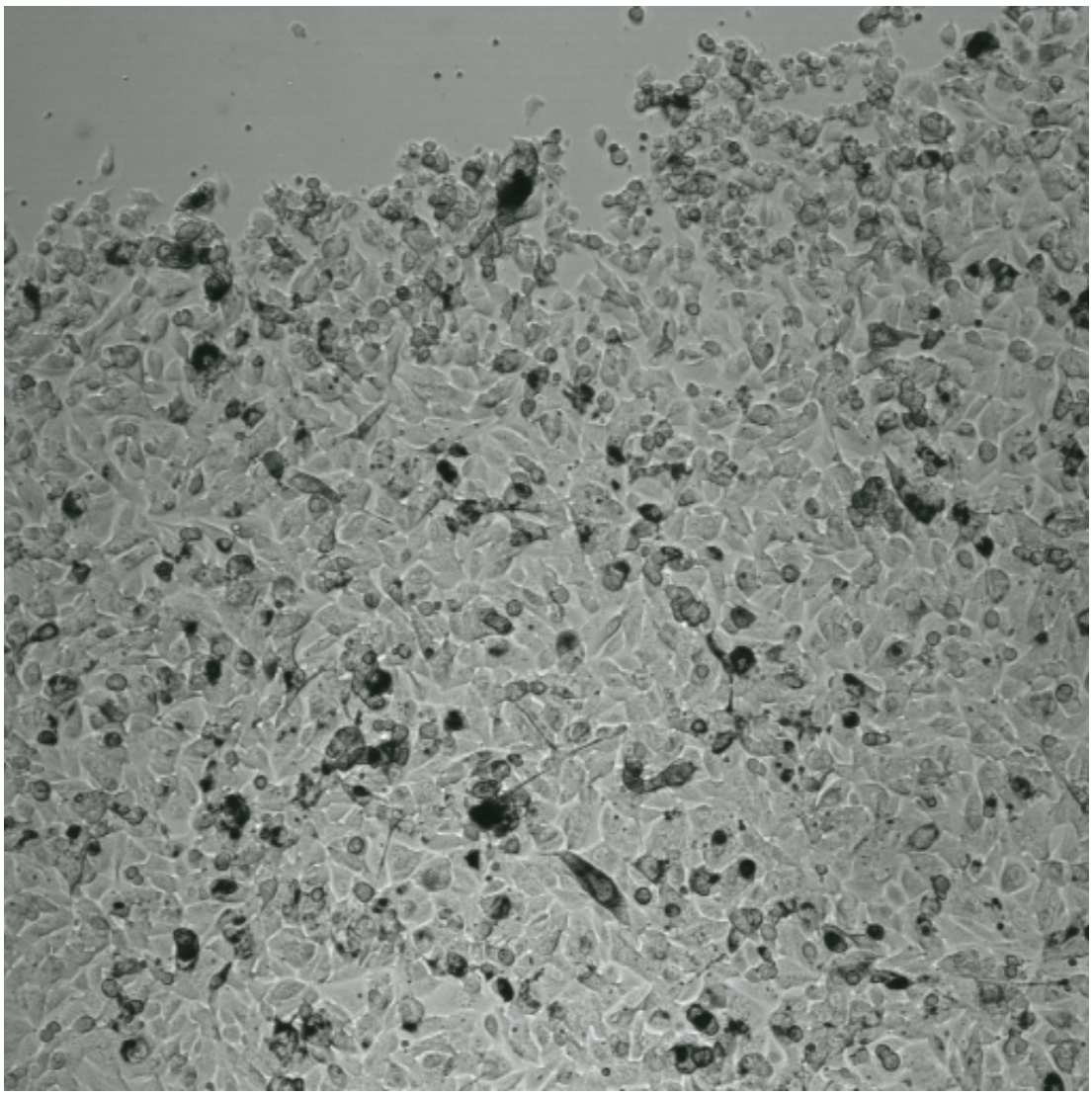

Figure 5.11: The effects of exposure irradiation of 4100nm wavelength on B16F10 cells. Cancer cells are exposed for 3 hours inside the incubator to 4100nm wavelength. The exposed cells are then incubated for 24 hours before phase contrast microscopy is conducted by Nikon Eclipse Ti-E microscope (Nikon Instruments Inc, Japan) with 100X magnification.

Figure 5.12: The effects of exposure irradiation of 4100nm wavelength on CHO as normal cell line candidate. Cells are exposed for 3 hours inside the incubator to 4100nm wavelength. The exposed cells are then incubated for 24 hours before phase contrast microscopy is conducted by Nikon Eclipse Ti-E microscope (Nikon Instruments Inc, Japan) with 100X magnification.

Images in Figure 5.11 and 5.12 qualitatively investigate any cytotoxic effect on *in vitro* culture of cancer and normal animal cells. These cytotoxic effects are studied through phase contrast microscopy for the level of cellular death and detachment of confluent layer indicating apoptosis and necrosis. According to these images, cellular detachment is observed for animal cell (B16F10) cultures exposed to 4100nm wavelength. In contrast to animal cancer cells, normal animal cells (CHO) do not exhibit any apparent cellular death or detachment, and hence no cytotoxic effect cannot be detected from the image. Since the same exposure regime and same wavelength were used in applied irradiation of both cells, the results reveal that far infrared exposure of 4100nm wavelength induces apoptotic effects on B16F10 cells, while CHO cells are not affected by such external exposures.

The phase contrast microscopy images in Figure 5.13 reveal significant cellular detachment upon 3 hours of external irradiation at 4300nm wavelength followed by 24 hours of post exposure incubation. On the other hand, the images of CHO cells in Figure 5.14 irradiated with the same regime of exposure and the same wavelength do not illustrate any sign of cytotoxicity induced in the normal animal cells. It can be deducted that external exposure of 4300nm wavelength induces the cytotoxic effects on B16F10 cells (which are animal cancer cells) and CHO cells are not affected by such exposures.

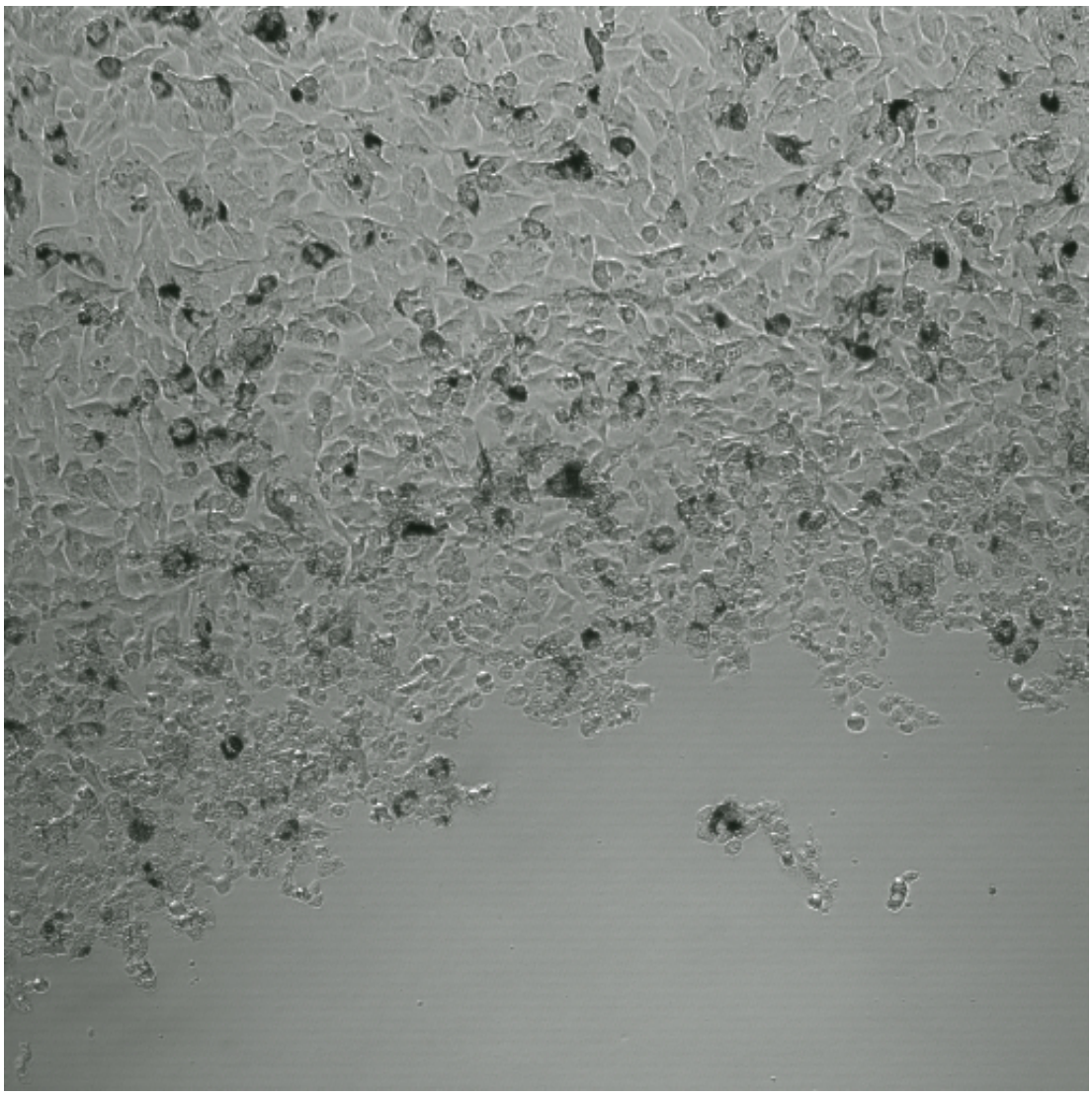

Figure 5.13: The effects of exposure irradiation of 4300nm wavelength on B16F10 cells. Cancer cells are exposed for 3 hours inside the incubator to 4300nm wavelength. The exposed cells are then incubated for 24 hours before phase contrast microscopy is conducted by Nikon Eclipse Ti-E microscope (Nikon Instruments Inc, Japan) with 100X magnification.

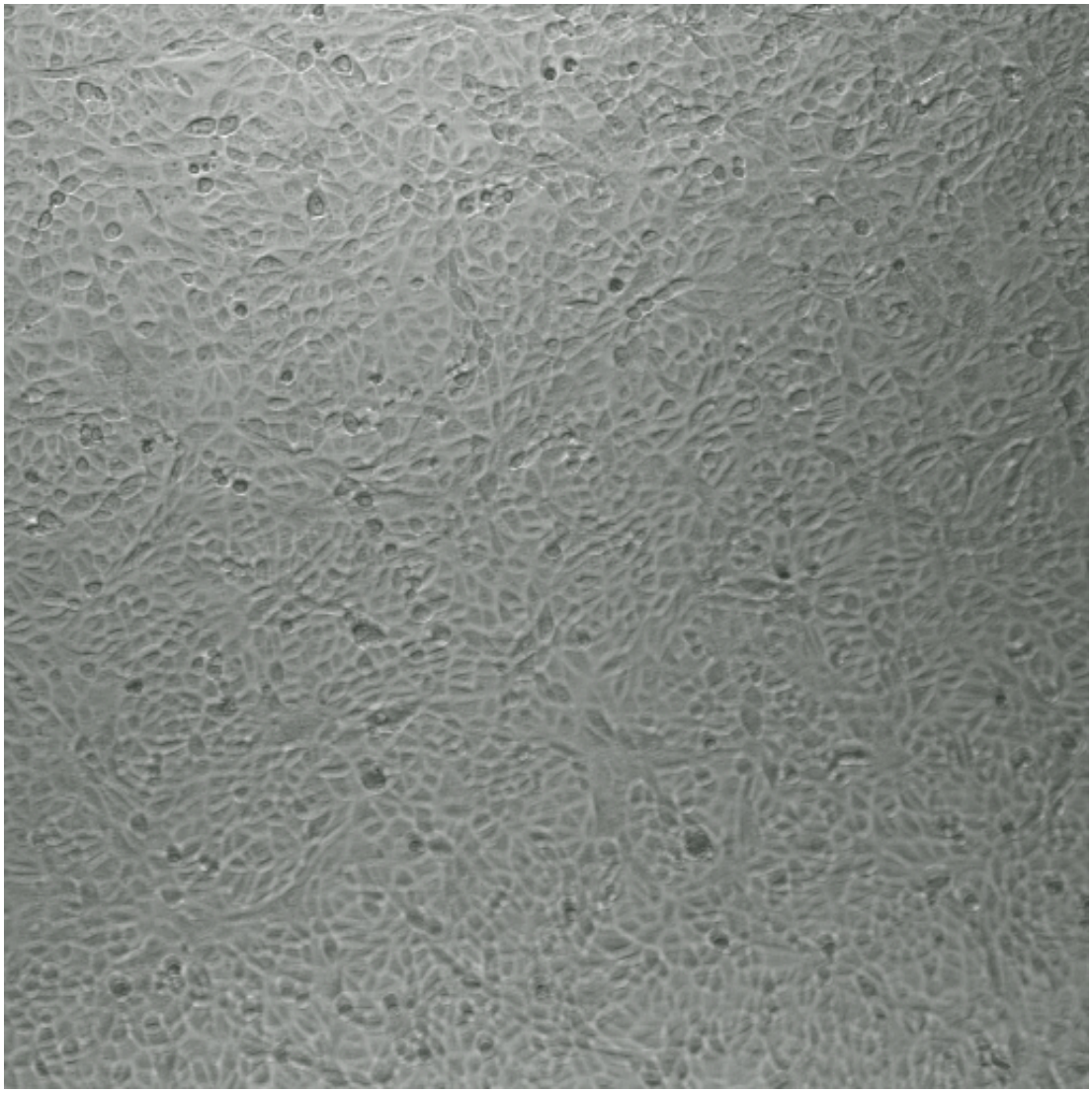

Figure 5.14: The effects of exposure irradiation of 4300nm wavelength on CHO as normal cell line candidate. Cells are exposed for 3 hours inside the incubator to 4300nm wavelength. The exposed cells are then incubated for 24 hours before phase contrast microscopy is conducted by Nikon Eclipse Ti-E microscope (Nikon Instruments Inc, Japan) with 100X magnification.

5.1.2 Human Cell Line - MCF7 Cells

This section is concerned with qualitative assessment of human cell lines. In the previous chapter (Chapter 4), measurement of standard cell-based quantitative assays demonstrate significant cell death or apoptotic for MCF7 cells as a result of external exposure at the selected wavelengths in the far infrared range, while no considerable changes in cell viability of HEM cells is observed through these quantitative assays. Thus, phase contrast microscopy is utilized to examine morphological changes of MCF7 cells since substantial changes in cell viability of this cell is observed from quantitative analyses.

This assay measures apopototic effects of external irradiation of selected wavelengths in far infrared range on MCF7 cells. The experimented wavelengths are 3400nm, 3600nm, 3800nm, 3900nm, 4100nm and 4300nm. These wavelengths are in the range that is proposed to have effect on the functionality of oncogenes and proto-oncogenes. The procedure that is conducted for imaging of MCF7 cells is identical to the protocol implemented for phase contrast microscopy of B16F10 and CHO cells. Cells are irradiated for 3 hours followed by 24 hours of post exposure incubation. Then, they are washed carefully with cold PBS to remove cells that are detached and floated in the media.

The first phase contrast image is from the untreated MCF7 cells. Then, the images are provided successively from 3400nm to 4300nm wavelength in increasing

order.

Obviously, untreated MCF7 cells does not indicated any cytotoxic effect on MCF7 cells as a human cancer cell line. Thus, no cytotoxic effect is observed from the phases contrast microscopy image of untreated MCF7 cells. Cells are suspended in 24-well plate with concentration of 2×10^5 for this qualitative assessment module.

The image shown in Figure 5.16 is obtained from MCF7 cells exposed to 3 hours of 3400nm external irradiation followed by 24 hours of post exposure incubation. Even though no significant cell detachment is observed from the image, a slight apoptotic effect is detectable to some extent. As it can be seen, morphology shape of a number of cells are changed into a circular form. These changes in cellular morphology of MCF7 cells indicate possible cell death or apoptotic. These morphological changes are formed in small patches and are not demonstrating any substantial cell death or detachment.

The phase contrast images presented in Figure 5.17 are taken after 3 hours irradiation of MCF7 with 3600nm LEDs followed by 24 hours of post exposure incubation. On the bottom left hand side of the image, a visible cellular detachment is noticeable upon the exposures. This cellular detachment indicates considerable cell apoptotis as a result of this external irradiation of far infrared wavelength on MCF7 cells. Thus, it can be deducted that 3600nm wavelength of

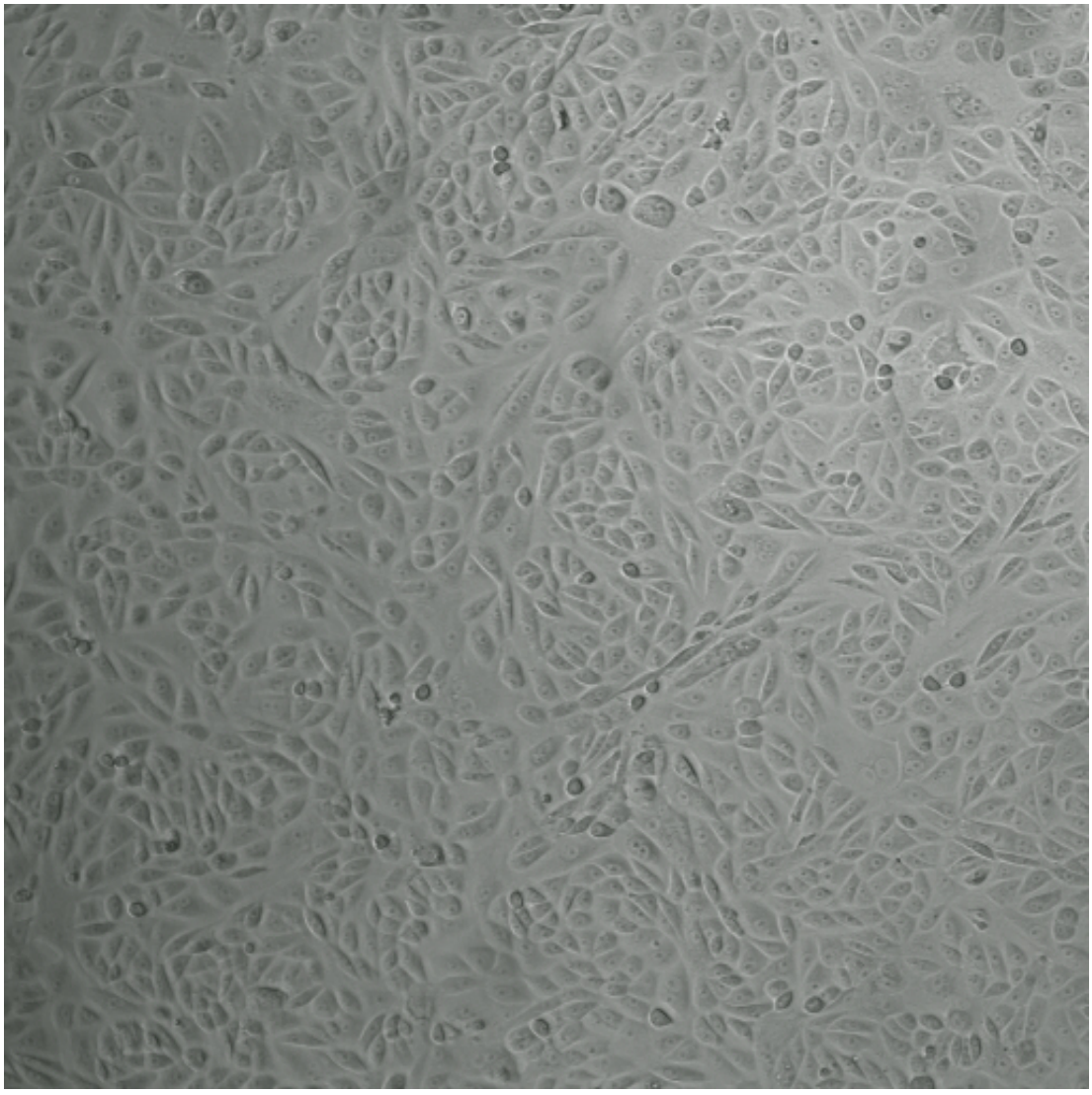

Figure 5.15: Sham exposed (untreated) MCF7 cells.

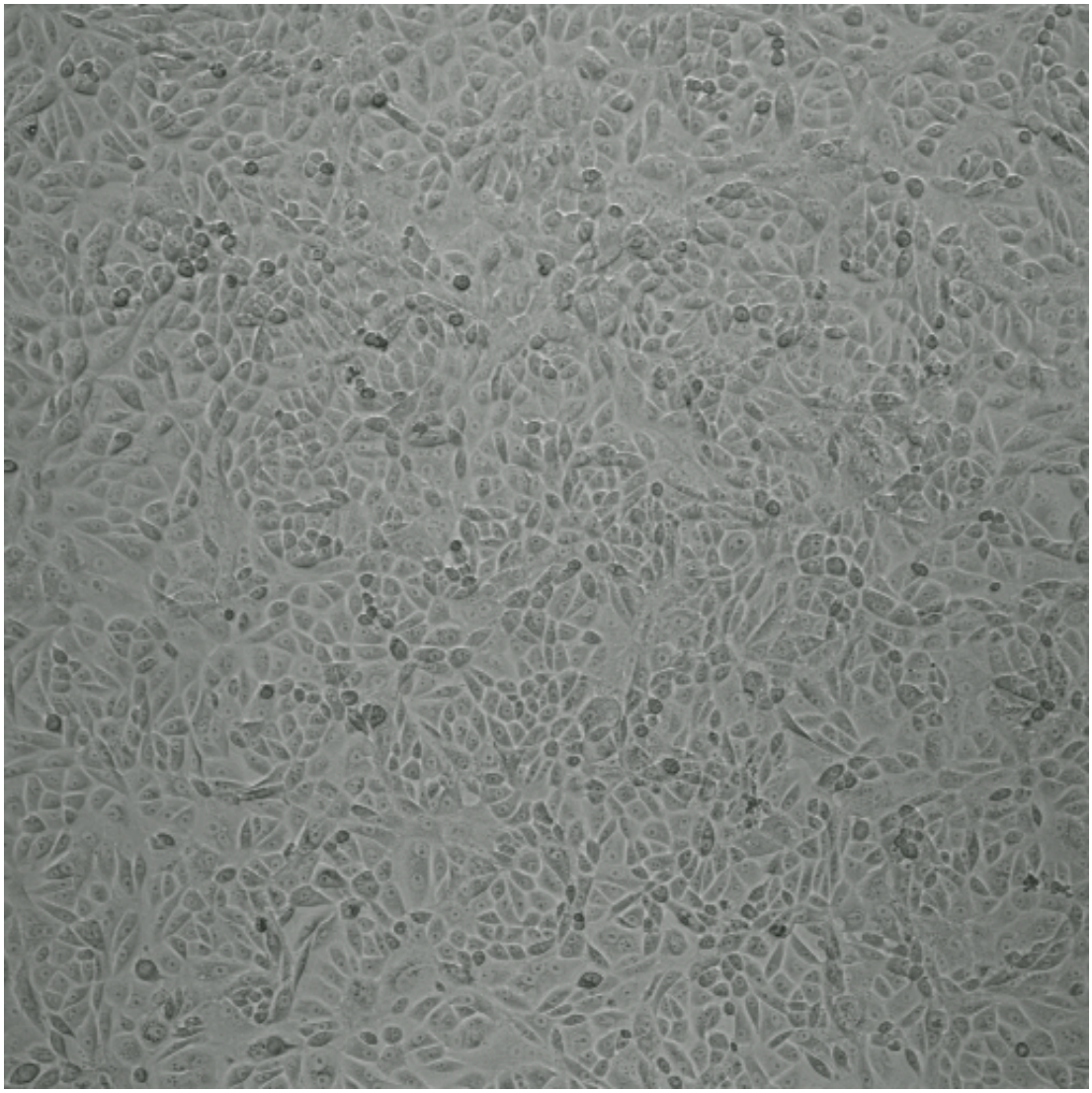

Figure 5.16: The effects of exposure irradiation of 3400nm wavelength on MCF7 cells. Cancer cells are exposed for 3 hours inside the incubator to 3400nm wavelength. Then, exposed cells are incubated for 24 hours before phase contrast microscopy imaging is conducted by Nikon Eclipse Ti-E microscope (Nikon Instruments Inc, Japan) with 100X magnification.

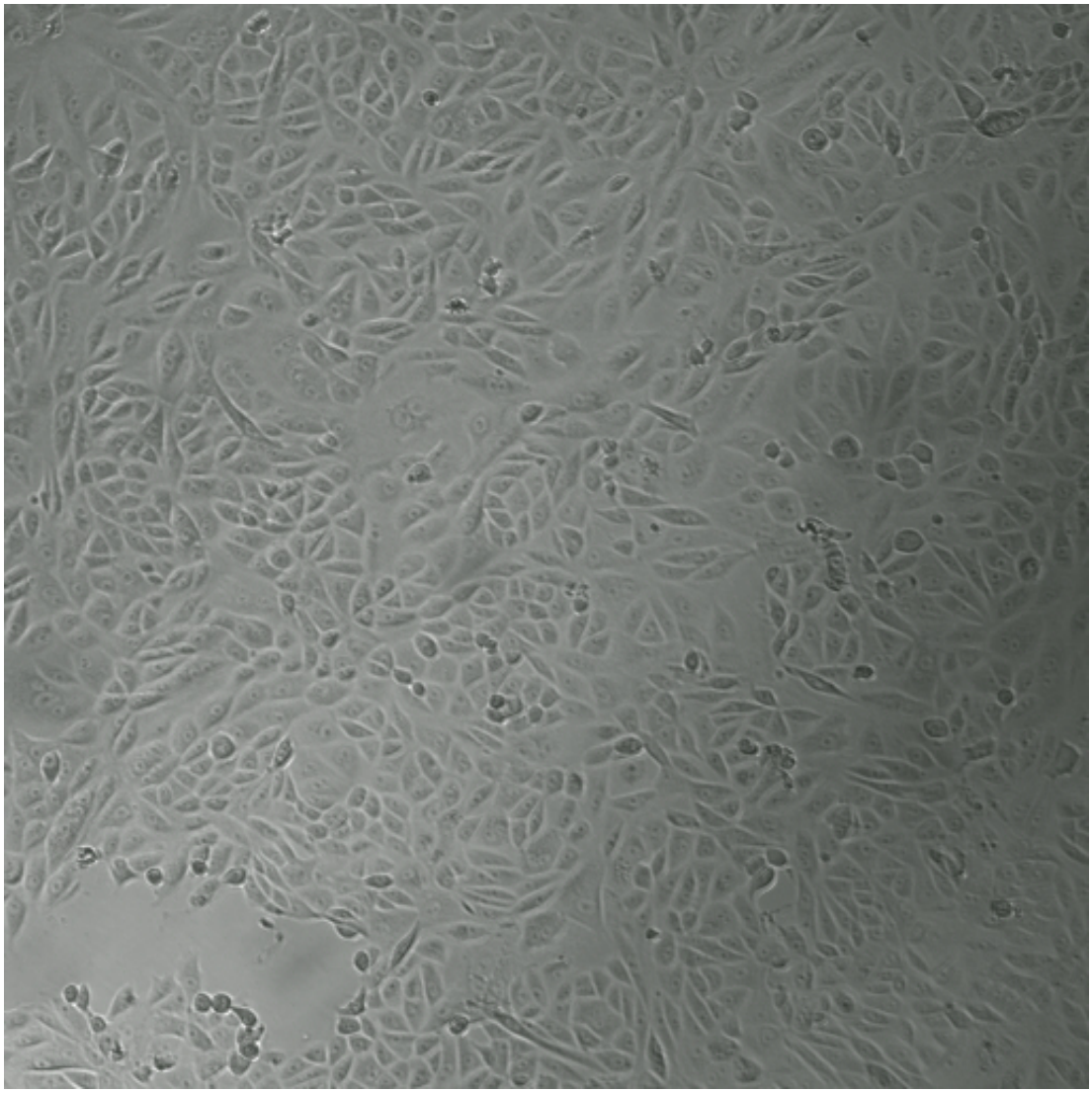

Figure 5.17: The effects of exposure irradiation of 3600nm wavelength on MCF7 cells. Cancer cells are exposed for 3 hours inside the incubator to 3600nm wavelength. Then, exposed cells are incubated for 24 hours before phase contrast microscopy imaging is conducted by Nikon Eclipse Ti-E microscope (Nikon Instruments Inc, Japan) with 100X magnification.

exposure induces significant cytotoxic effect on MCF7 cells as a cancer cell line.

Figure 5.18 shows any cytotoxic effect induced to MCF7 cell for 3 hours radiation of 3800nm wavelength and 24 hours post exposure incubation. From the image, cell free sections can be observed. These sections, when compared to sham exposed MCF7 cells, are the indication of cellular detachments that are induced from external exposures of far infrared wavelengths. Thus, it can be concluded that exposure of 3800nm wavelength causes cellular apoptosis in MCF7 cells as a cancer cell line. Comparison of the exposed and unexposed MCF7 cells further corroborates the cytotoxic effect of far infrared exposure on cancer cell viability.

The image in Figure 5.19 reflects similar cellular death effect as result of far infrared exposure as it is visibly shown in the far infrared range proposed by the RRM implementation. Phase contrast microscopy image in Figure 5.18 is from MCF7 cells exposed to 3900nm wavelength for 3 hours followed by 24 hours of post exposure incubation. The image clearly demonstrates cellular detachment on the bottom right hand corner of the image. Additionally, around the detachment area on the right hand side, there are visible signs of cell death on the cultured plate.

Similarly, Figure 5.20 shows sporadic cell detachment patches in the cultured plate resulted from 3 hours exposure of 4100nm wavelength with 24 hours of post exposure incubation. These detachments indicate that external far infrared light

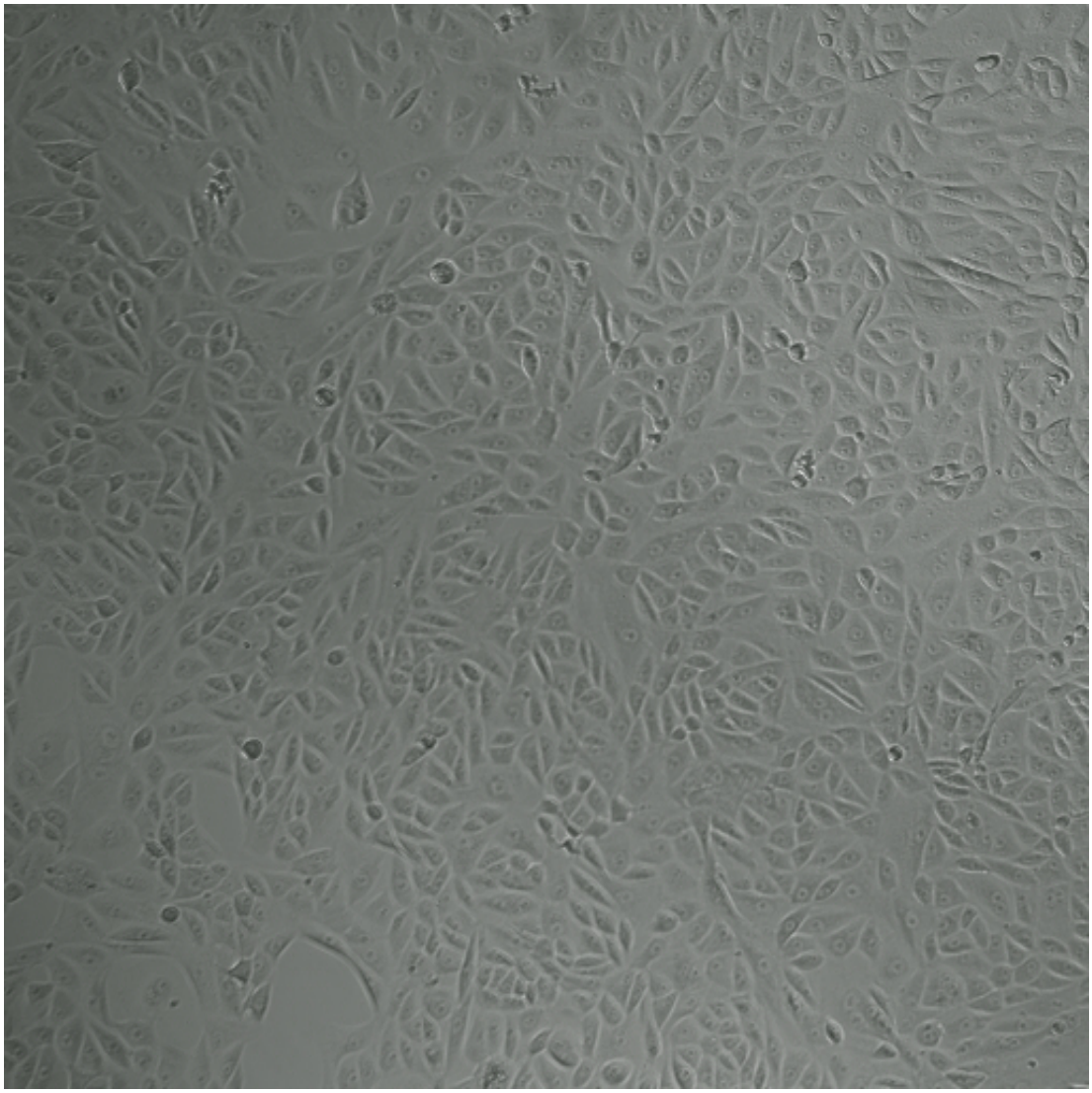

Figure 5.18: The effects of exposure irradiation of 3800nm wavelength on MCF7 cells. Cancer cells are exposed for 3 hours inside the incubator to 3800nm wavelength. Then, exposed cells are incubated for 24 hours before phase contrast microscopy imaging is conducted by Nikon Eclipse Ti-E microscope (Nikon Instruments Inc, Japan) with 100X magnification.

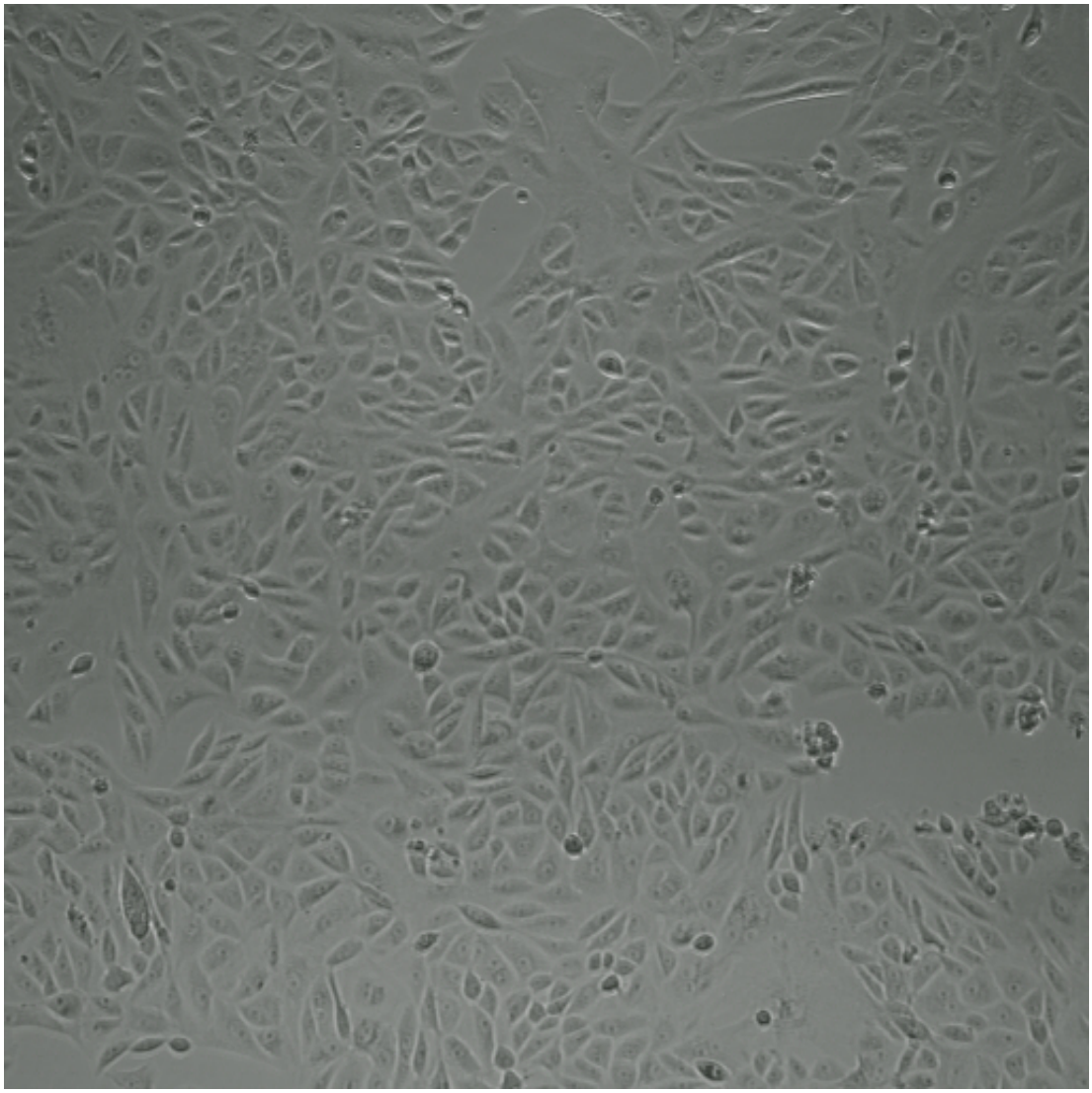

Figure 5.19: The effects of exposure irradiation of 3900nm wavelength on MCF7 cells. Cancer cells are exposed for 3 hours inside the incubator to 3900nm wavelength. Then, exposed cells are incubated for 24 hours before phase contrast microscopy imaging is conducted by Nikon Eclipse Ti-E microscope (Nikon Instruments Inc, Japan) with 100X magnification.

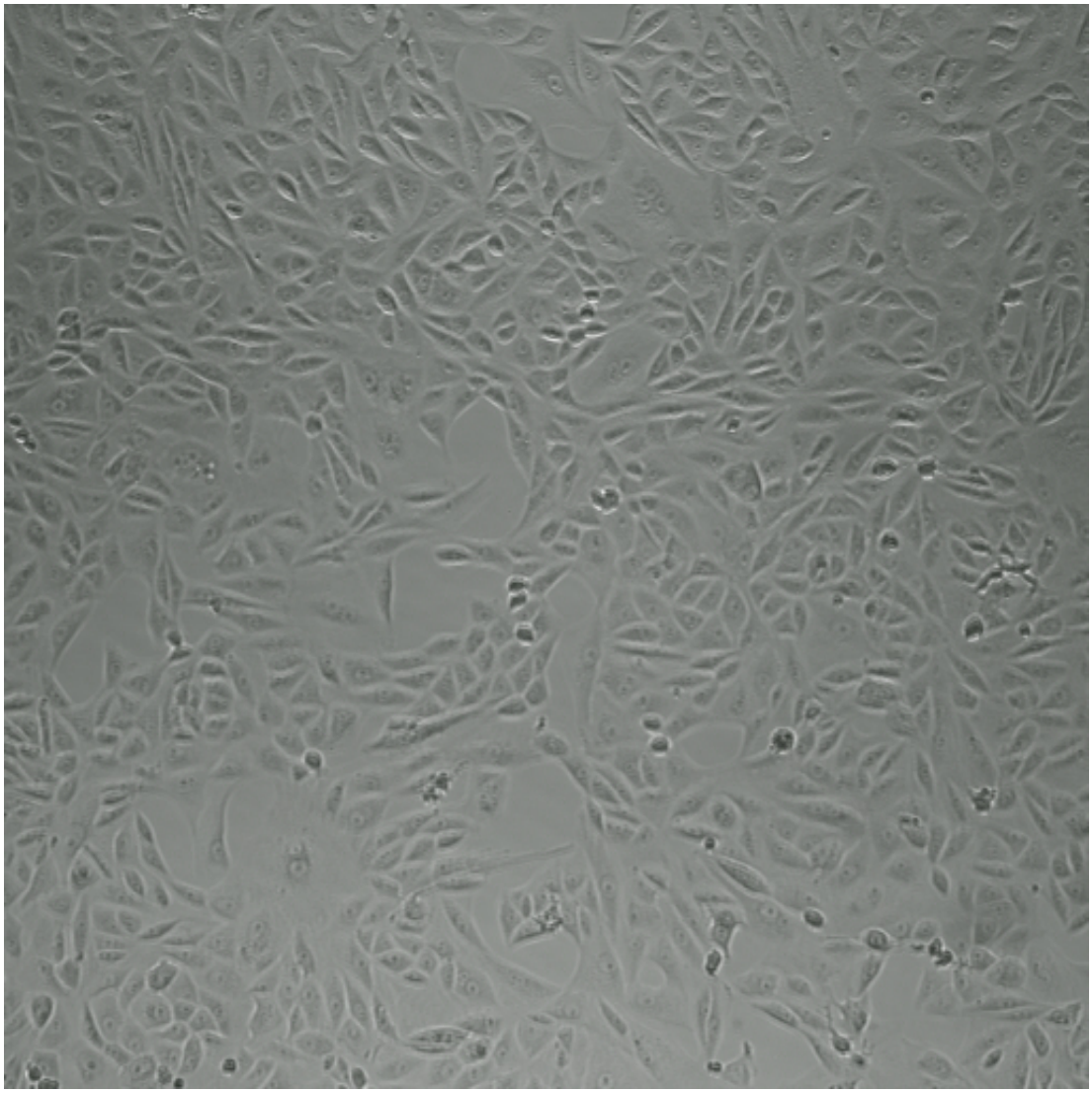

Figure 5.20: The effects of exposure irradiation of 4100nm wavelength on MCF7 cells. Cancer cells are exposed for 3 hours inside the incubator to 4100nm wavelength. Then, exposed cells are incubated for 24 hours before phase contrast microscopy imaging is conducted by Nikon Eclipse Ti-E microscope (Nikon Instruments Inc, Japan) with 100X magnification.

radiation induces cytotoxic effect on cell viability of MCF7 cancer cells when compared with sham exposed MCF7 cells. The untreated cancer cells in Figure 5.15 do not demonstrate any detrimental effect on cell viability of MCF7 cells while the induced cytotoxicity is visible in far infrared exposure through cell detachment and cell morphology forming a round shape (cell death indication).

The image in Figure 5.21 exhibits cellular detachment and cytotoxic effect. These cells are radiated for 3 hours followed by 24 hours of post exposure incubation by far infrared LED in 4300nm range. Like other images from the far infrared exposed MCF7 cells in this section, exposure of MCF7 cells with 4300nm range LED exposure demonstrates visible cellular detachment and cell death.

5.1.3 Phase Contrast Microscopy - Summary Remarks:

As predicted by the RRM approach, far infrared wavelength of 3500nm to 6500nm is expected to induce cytotoxic effect on cancer cells by affecting biological functionality of oncogene and proto-oncogene proteins. Quantitative cell-based assays in Chapter 4 show that external radiation of the proposed far infrared range induces detrimental effects on cell viability of cancer cells, while normal cell lines are not affected by such wavelengths exposures. To further investigate the quantitatively measured induce effects on cancer cells, phase contrast microscopy is utilized here.

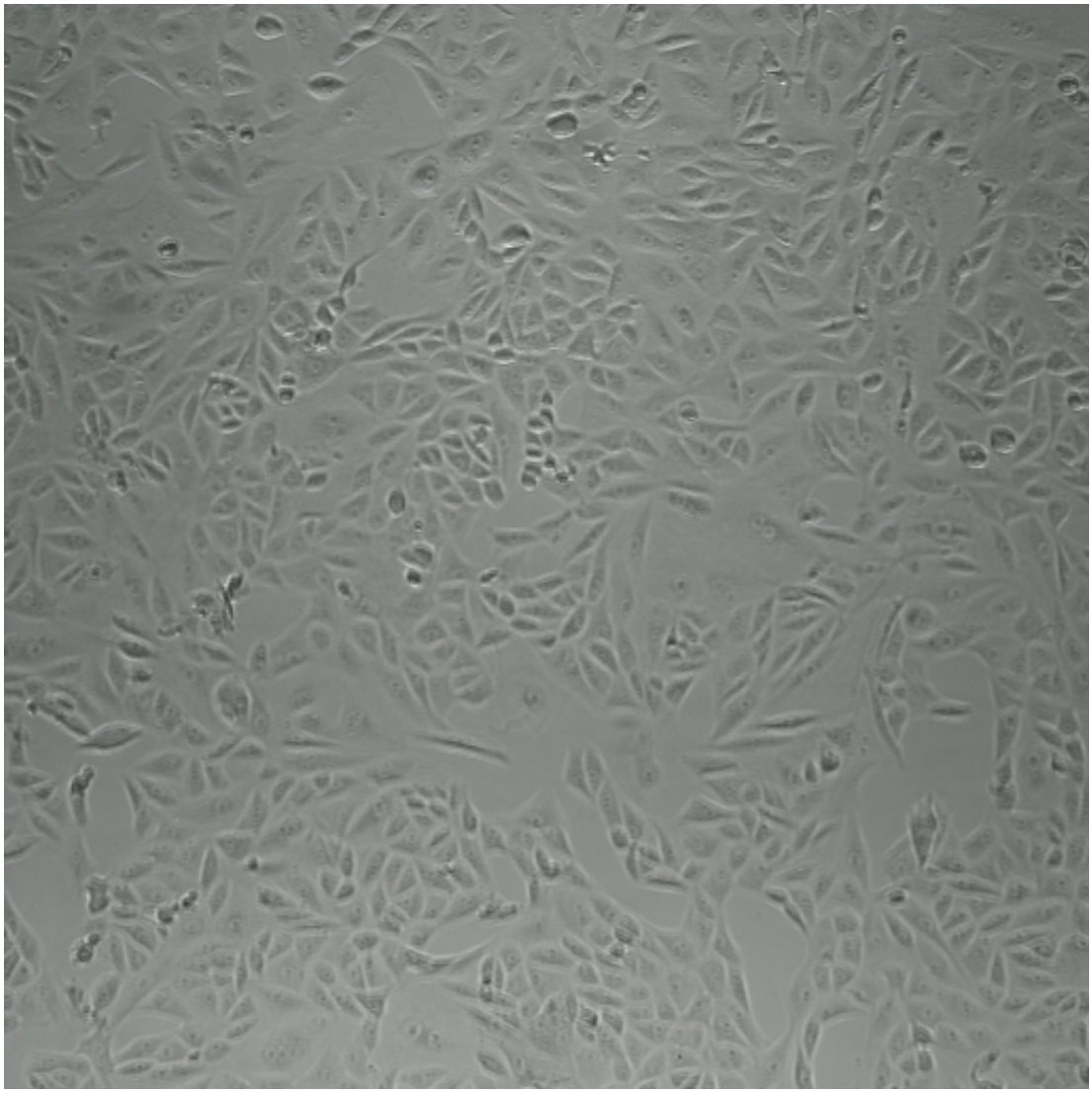

Figure 5.21: The effects of exposure irradiation of 4300nm wavelength on MCF7 cells. Cancer cells are exposed for 3 hours inside the incubator to 4300nm wavelength. Then, exposed cells are incubated for 24 hours before phase contrast microscopy imaging is conducted by Nikon Eclipse Ti-E microscope (Nikon Instruments Inc, Japan) with 100X magnification.

The images from both animal and human cancer cell lines clearly illustrates that radiation of selected wavelength in the proposed far infrared range induces detrimental effect on cell viability and cell morphology of cancer cells. This cytotoxic effect is more visible when the images of both exposed and sham exposed cancer cells are shown and compared with each other. In addition, no visible cytotoxic and morphological effects from the qualitative analysis of normal animal cells strongly imply that irradiation at these selected far infrared LEDs cause reduction in cell viability of cancer cells as proposed by the RRM hypothesis employed in this project.

5.2 Confocal Laser Scanning Microscopy (CLSM)

The results of the quantitative cell-based assays imply that external exposures of the far infrared wavelengths (proposed by the RRM hypothesis) induce cytotoxic effects on cell viability of cancer cells, while radiation of the same wavelengths and same exposure regimes on normal animal and human cells do not replicate the same observed cytotoxic effects on cancer cells. These experimental analyses and their measured effects urge for further qualitative analysis for a more reliable conclusion.

Hence, the apoptotic and necrotic effects of external far infrared radiation is explored qualitatively by confocal laser scanning microscopy (CLSM) in this sec-

tion. Cells are seeded at initial cell density of 2×10^5 cells per mL in 24-well plates and incubated overnight. Then, the cells are exposed to external irradiation of far infrared LEDs based on the third regime of exposure. Hence, cells are irradiated for 3 hours followed by 24 hours of post exposure incubation. After that, exposed cells are washed very carefully with cold phosphate-buffered saline (PBS) to remove any cell detachment from the surface of the plates. Then, CLSM protocol is conducted to capture any apoptotic or necrotic effects.

CLSM protocol conducted for CLSM imaging is that after 24 hours of incubation, cells are washed with cold phosphate-buffered saline (PBS) and labeled with V-AF 488 and PI according to the manufacturer's instructions with slight modifications. To each sample, 5 μL of AF488 and 1.5 μL of PI are added followed by 20 minutes incubation at room temperature before being washed twice and resuspended in a binding buffer (10 mM HEPES, 140 mM NaCl, 2.5 mM CaCl2 at pH 7.4). Afterward, stained cells are protected from the light by aluminum foil until they are examined by confocal laser scanning microscopy (CLSM).

5.2.1 Animal Cell Line - B16F10 Cells:

In this section, exposures at the far Infrared wavelengths on animal cancer cells are qualitatively investigated through confocal laser scanning microscopy (CLSM). These experiments conducted after 3 hour of exposure and 24 hours of incubation since the statistical results display a maximum effect for that regime of exposures.

The following figures illustrate CLSM images of the untreated B16F10 cells as well as cells exposed to 3600nm and 4300nm wavelengths.

The first figure is from the sham exposed B16F10 cells. These images are used as a benchmark for measuring the level of the induced effects on exposed animal cancer cells.

Figure 5.22 shows the CLSM images of untreated B16F10 cells. As it can be deducted from the confocal images, no apoptotic or necrotic effects are detected for the sham exposed cells. These images are used as a control to compare and identify any qualitative changes in exposed cancer B16F10 cells.

The CLSM analysis in Figure 5.23 is conducted after 3 hours irradiation at 3600nm wavelength followed by 24 hours of post exposure incubation. The CLSM images disclose the significant apoptotic effects measured by Annexin V, and the necrotic effects measured by Propidium Iodine. Apparently, the low intensity light exposure at the wavelength of 3600nm induces the apoptotic or necrotic effects on B16F10 cells despite the fact that untreated cells do not indicate any cellular toxicity as shown in Figure 5.22. The images from this figure imply that 3600nm exposure does not induce any noticeable cell detachment, while the induced cell toxicity is very apparent.

The analysis of the combined image of Annexin V and PI of the effect of the exposures at 4300nm reveals the apparent cell detachment as well as cell death.

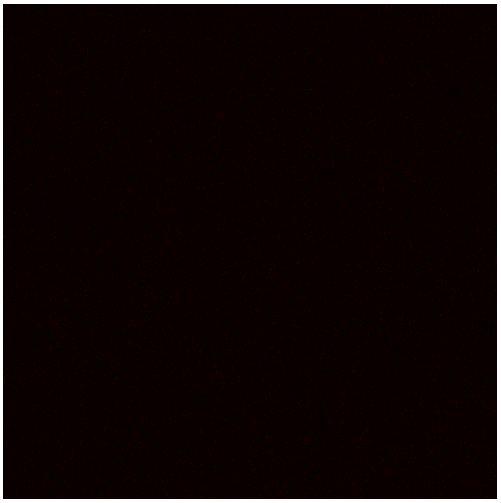

(a) Necrotic image of untreated B16F10 cells

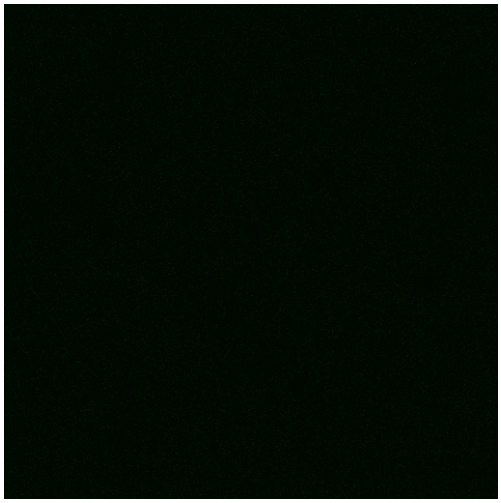

(b) Apoptotic image of untreated B16F10 cells

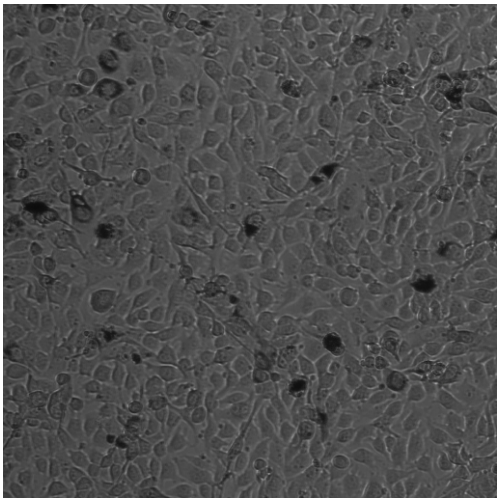

(c) Untreated B16F10 cells image with bright light microscopy

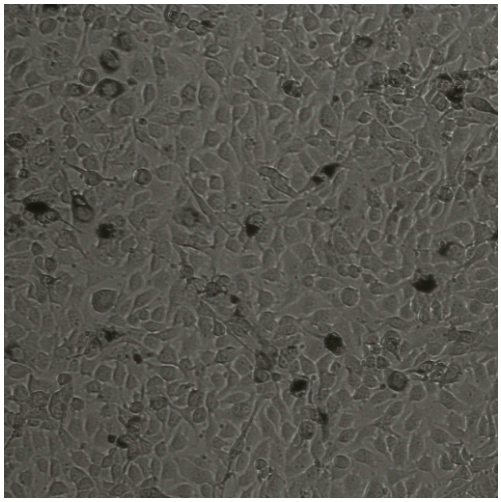

(d) Combination of necrotic and apoptotic image of untreated B16F10 cells

Figure 5.22: Apoptosis and necrosis measurements of untreated B16F10 cells. CLSM images were taken at 100X magnifications with the pinhole aperture set at 1 using Nikon Eclipse Ti-E A1 laser-scanning confocal system (Nikon Instruments Inc, Japan).

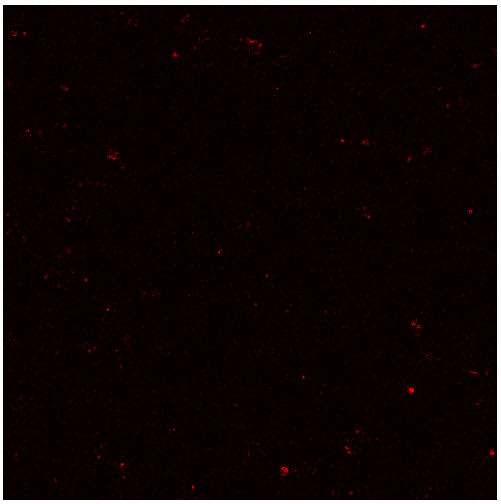

(a) Necrotic effects of far infrared wavelength exposure on B16F10 cells marked with red color

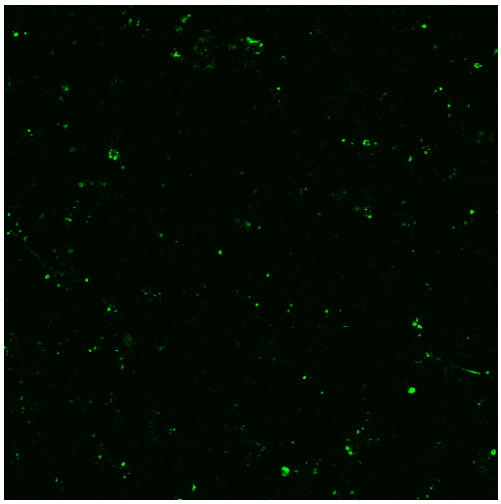

(b) Apoptotic effects of far infrared wavelength exposure on B16F10 cells marked with green color

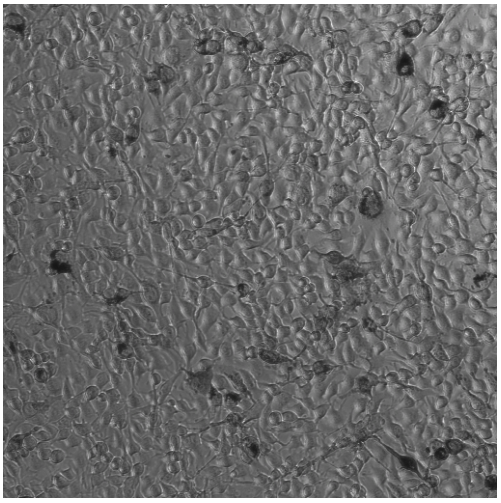

(c) Effects of far infrared exposure on B16F10 cells with bright light microscopy

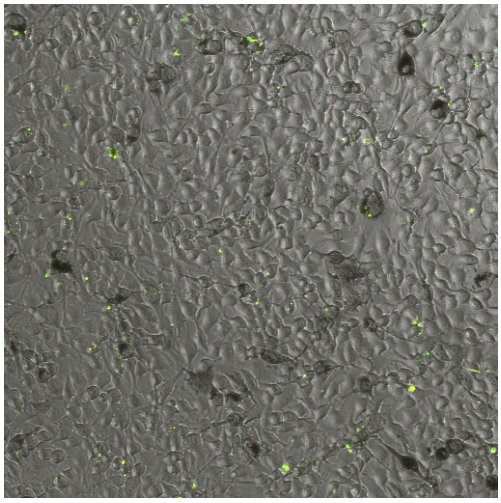

(d) Combination of necrotic and apoptotic effects on B16F10 cells

Figure 5.23: Apoptosis and necrosis effects of irradiation at 3600nm wavelength for 3 hours followed by 24 hours of post exposure incubation. CLSM images are taken at 100X magnifications with the pinhole aperture set at 1 using Nikon Eclipse Ti-E A1 laser-scanning confocal system (Nikon Instruments Inc, Japan).

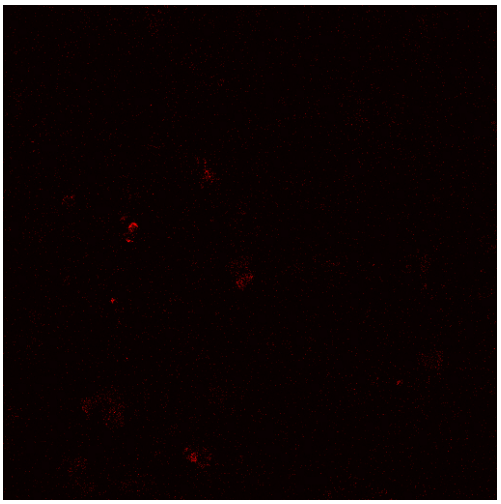

(a) Necrotic effects of far infrared wavelength exposure on B16F10 cells marked with red color

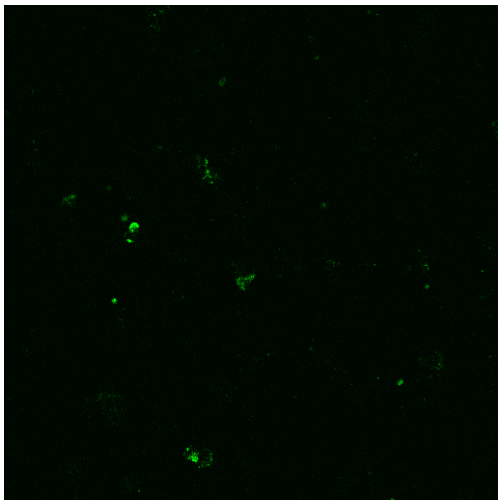

(b) Apoptotic effects of far infrared wavelength exposure on B16F10 cells marked with green color

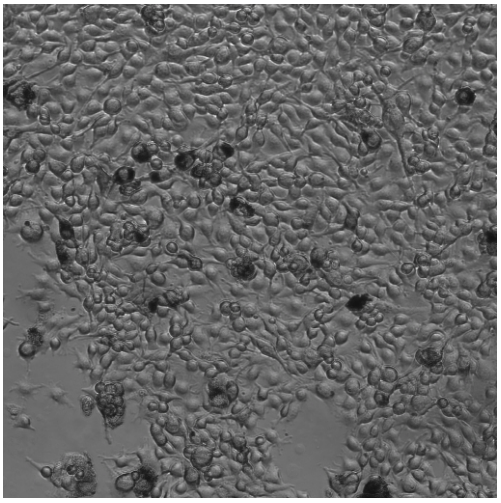

(c) Effects of far infrared exposure on B16F10 cells with bright light microscopy

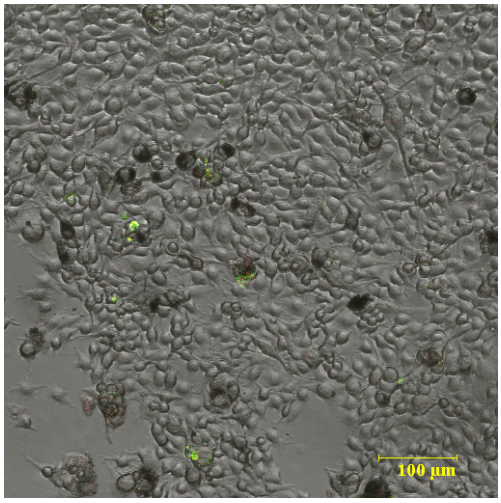

(d) Combination of necrotic and apoptotic effects on B16F10 cells

Figure 5.24: Apoptotic and necrotic effects of irradiation at 4300nm wavelength for 3 hours followed by 24 hours of post exposure incubation. CLSM images are taken at 100X magnifications with the pinhole aperture set at 1 using Nikon Eclipse Ti-E A1 laser-scanning confocal system (Nikon Instruments Inc, Japan).

The amount of cell detachment is visible in the images, though the cytotoxic activity induced by 4300nm exposure is not as significant as it is observed at 3600nm exposure. Comparison of confocal microscopy images shown in Figure 5.22, 5.23 and 5.24 lead to the conclusion that the exposures at far infrared wavelengths result in detrimental effects on cell viability of animal cancer cells.

5.2.2 Human Cell Line - MCF7 Cells

Apoptotic and necrotic effects induced by 3 hours of far infrared exposures along with 24 hours of post exposure incubation on human cancer cells are analyzed using CLSM technique. As no significant quantitative effect is detected for HEM cell line, the CLSM assay is used for MCF7 cells which is a human cancer cell line. The following CLSM images are taken at 100X magnifications with the pinhole aperture set at 1 using Nikon Eclipse Ti-E A1 laser-scanning confocal system (Nikon Instruments Inc, Japan). Images are then analyzed with the NISElement imaging software.

In this section, CLSM images from untreated MCF7 cells are provided as a benchmark for assessing the significance of exposure's effects on this human cancer cell line. Then, the effect of third exposure regime on MCF7 cells at 3600nm and 4300nm wavelengths are displayed.

Obviously, the images of sham-exposed MCF7 cells, shown in Figure 5.25, are

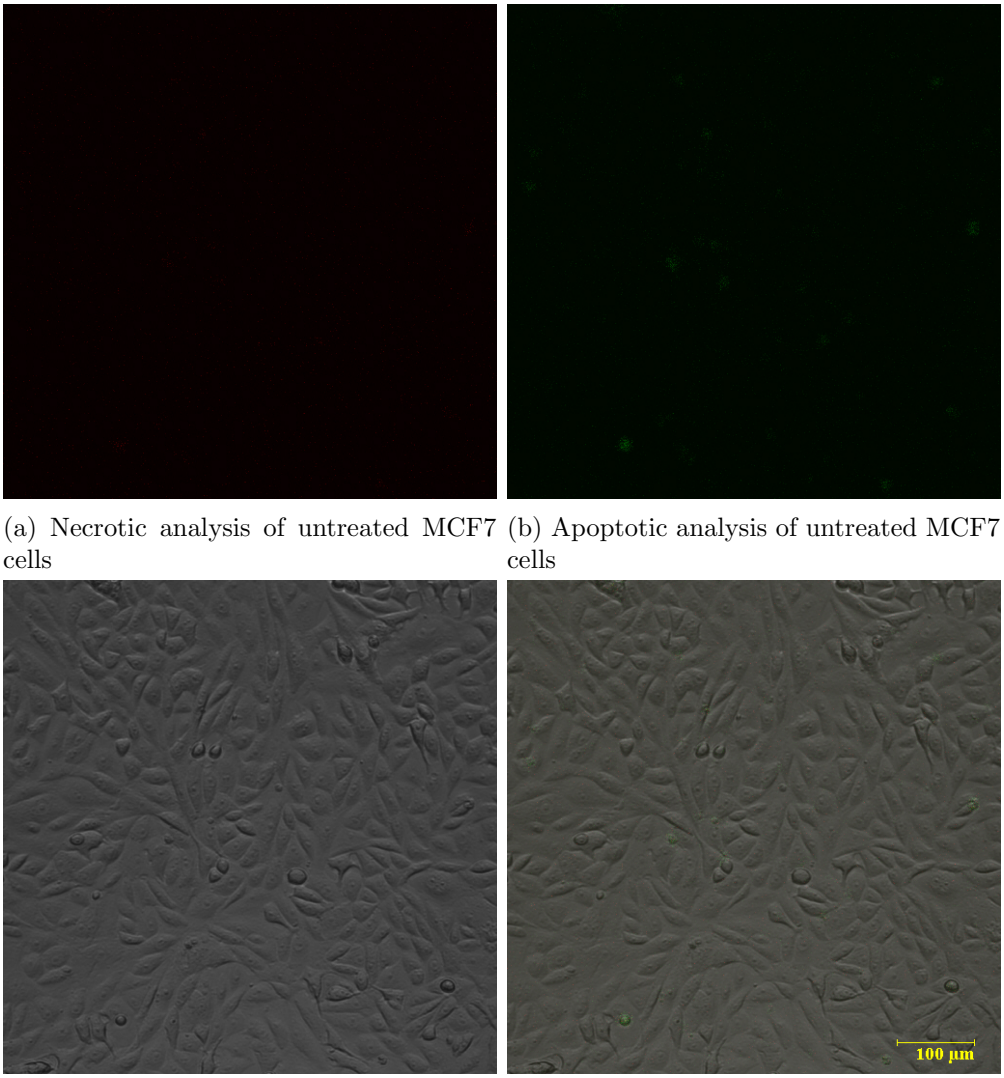

(a) Necrotic analysis of untreated MCF7 cells

(b) Apoptotic analysis of untreated MCF7 cells

(c) Analysis of untreated MCF7 with bright light microscopy

(d) Combination of necrotic and apoptotic analysis of untreated MCF7 cells

Figure 5.25: Apoptosis and necrosis detection of untreated MCF7 cells. CLSM images are taken at 100X magnifications with the pinhole aperture set at 1 using Nikon Eclipse Ti-E A1 laser-scanning confocal system (Nikon Instruments Inc, Japan).

not expected to reveal any necrosis, apoptotic or cell detachment effects as the untreated MCF7 cells have not demonstrated any negative cell viability effect in the previous quantitative and qualitative assays.

Figure 5.26 present CLSM images taken from Nikon Eclipse Ti-E A1 laser-scanning confocal microscope. The images are used as the second qualitative assessment assay for evaluation of necrotic and apoptotic effects that far infrared radiation induces in MCF7 cancer cells.

Fiugre 5.26a illustrates the necrotic effects that third regime of exposures induce on MCF7 cells. As it is apparent from PI stained cells, these necrotic effects are visible and shown by the red color dots. Figure 5.26b reveals apoptotic effects at 3600nm radiation wavelength through staining of MCF7 cells with Annexin V. The apoptotic cells marked with green color are substantially noticeable on MCF7 cells upon 3600nm radiation. Furthermore, the combination of necrotic and apoptotic effects are shown in Figure 5.26d, while bright light microscopy image (Figure 5.26c) exhibits a cell detachment as a result of 3600nm exposure. Despite no visible indication of cellular detachment is shown in Figure 5.26b, the significant cell apoptotic and necrotic effects are evident in PI and Annexin V images.

The CLSM images shown in Figure 5.27 are taken with Nikon Eclipse Ti-E A1 laser-scanning confocal system. They demonstrate the effects of 3 hours of

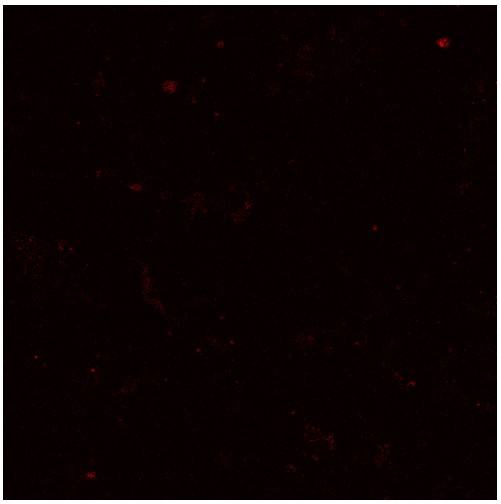

(a) Necrotic effects of far infrared exposure on MCF7 cells that is marked with red color

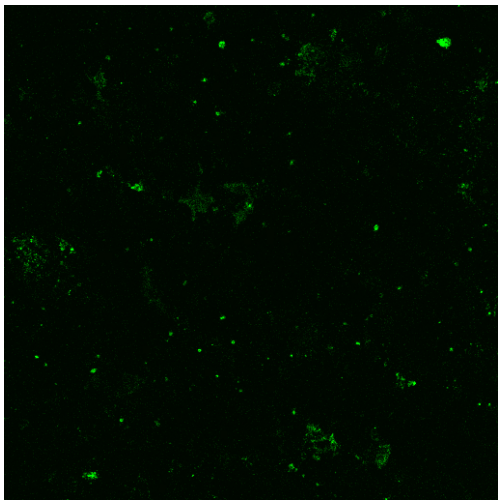

(b) Apoptotic effects of far infrared exposure on MCF7 cells that is marked with green color

(c) Effects of far infrared exposure on MCF7 with bright light microscopy

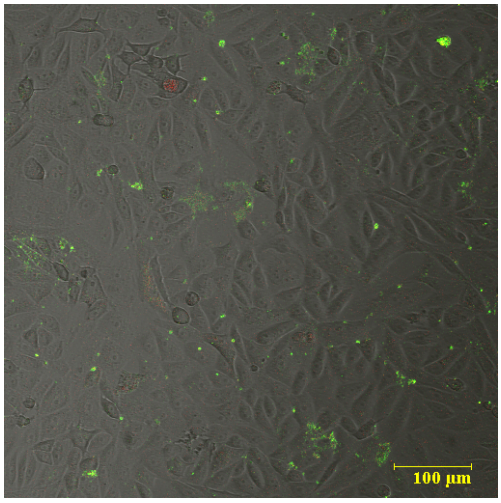

(d) Combination of necrotic and apoptotic effects on MCF7 cells

Figure 5.26: Apoptosis and necrosis effects of irradiation at 3600nm wavelength for 3 hours followed by 24 hours of post exposure incubation. CLSM images are taken at 100X magnifications with the pinhole aperture set at 1 using Nikon Eclipse Ti-E A1 laser-scanning confocal system (Nikon Instruments Inc, Japan).

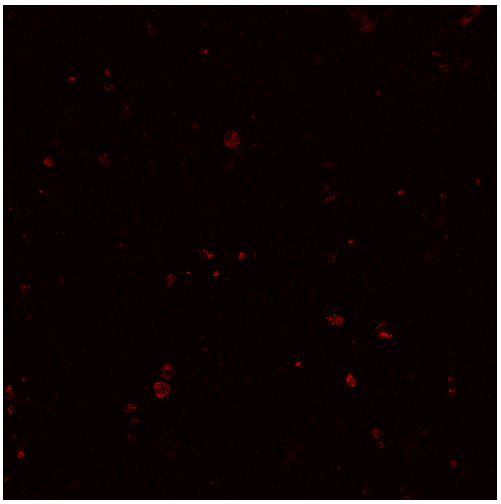

(a) Necrotic effects of far infrared exposure on MCF7 cells that is marked with red color

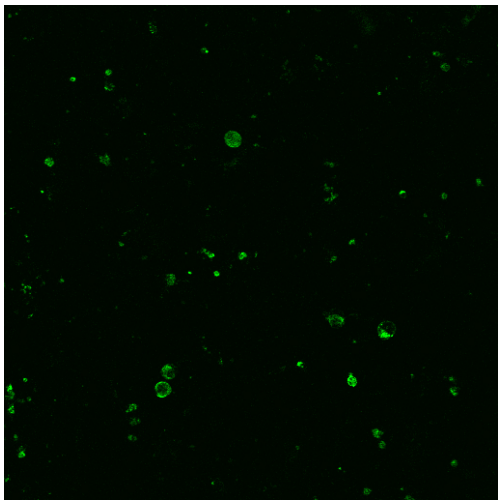

(b) Apoptotic effects of far infrared exposure on MCF7 cells that is marked with green color

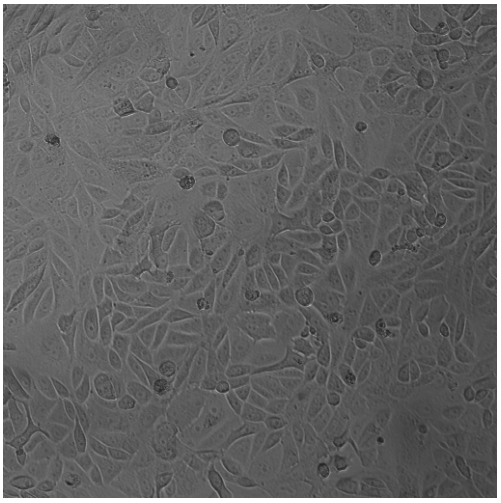

(c) Effects of far infrared exposure on MCF7 cells with bright light microscopy

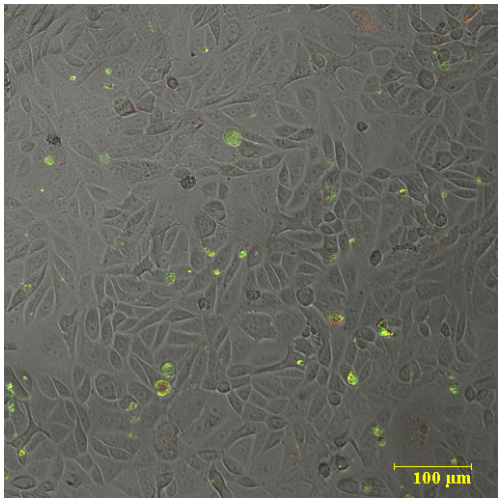

(d) Combination of necrotic and apoptotic effects on MCF7 cells

Figure 5.27: Apoptotic and necrotic effects of irradiation at 4300nm wavelength for 3 hours followed by 24 hours of post exposure incubation. CLSM images are taken at 100X magnifications with the pinhole aperture set at 1 using Nikon Eclipse Ti-E A1 laser-scanning confocal system (Nikon Instruments Inc, Japan).

irradiation at 4300nm wavelength LEDs followed by 24 hours of post exposure incubation. From Figure 5.27a, which shows cells stained with PI, necrotic activity of MCF7 cells is investigated. The image indicates a substantial necrotic effect as result of radiation at 4300nm wavelength. A close look at the image obtained from Annexin V staining in Figure 5.27a illustrates a significant level of cellular apoptosis in MCF7 cells exposed to 4300nm LEDs. The image in Figure 5.27c is used for analysis of any cellular detachment or cell death resulted from the far infrared exposure at 4300nm. Bright light microscopy image does not indicate a significant cellular detachment despite the observed cell apoptotic and necrotic effects shown in other images. Moreover, the image in Figure 5.27c displays the combination of necrotic and apoptotic effects from the far infrared exposure measured by PI and Annexin V staining of MCF7 cells.

5.2.3 Confocal Laser Scanning Microscopy - Summary Remarks:

CLSM is used in the previous section to qualitatively assess the effect of external far infrared exposures on cell viability of studied animal and human cancer cells. The confocal images of exposed and sham-exposed animal cancer cell line clearly imply that far infrared exposures at 3600nm and 4300nm wavelengths lead to a considerable apopototic and necrotic effects in B16F10 cells. Unlike the significant effects of exposures observed in B16F10 cells, sham-exposed cells do not show any effects as this unexposed cells are used for comparison of exposure effect.

Furthermore, images from MCF7 cells radiated with 3600nm and 4300nm strongly suggest that exposures of these cells at these particular far infrared LEDs induce necrotic and apoptotic effects measured by Propidium Iodine and Annexin V consecutively. Comparison of these exposed cell images to that of unexposed MCF7 cell denotes the scale of the induced effect as a result of the far infrared external radiation.

5.3 Discussion - Qualitative Analysis

Earlier comparison of the quantitative assessment of different exposure regimes on mouse cancer cells and human cancer cells revealed the significant increase in cell death as a result of different far infrared exposure regimes. These quantitative analysis of different exposure and post exposure incubation regimes did not establish a considerable increase in cell death in normal animal and human cell lines. According to the quantitative analysis of the different exposure regimes on cancer cell lines, a considerable cell apoptotic effect was observed for both human and animal cancer cell lines, while normal cell lines were not affected by such exposures.

Thus, this Chapter investigated qualitatively the effects of selected far infrared wavelengths radiation on B16F10 (Murine Melanoma cells) and CHO (Chinese Hamster Ovarian cells) MCF7 (Human Breast Cancer cells). These qualitative

analyses were based on phase contrast microscopy and confocal laser scanning microscopy (CLSM) and probed for any changes in cellular morphology or cell apoptotic as a result of such exposure.

At first, the apoptotic and necrotic effects of far infrared exposure on B16F10, CHO and MCF7 cells are explored and discussed by phase contrast microscopy. These cells are exposed to the far infrared light for 3 hours with 24 hours of post exposure incubation. Then, two LEDs in the RRM proposed far infrared wavelength range, one is in the lower range and another one is in the higher wavelength range, were used for necrotic and apoptotic study with CLSM microscopy. The exposure regime used for this qualitative assay was the same one used in phase contrast microscopy. *In vitro* qualitative analysis of human and animal cells suggested that external far infrared exposure induced considerable cell death in cancer cells only. This cell detachment and cell apoptosis and necrosis effect were more evident in animal cancer cell line (B16F10) compared to human cancer cell line (MCF7).

All in all, it can be deducted that external electromagnetic radiation of selected wavelengths in the far infrared range induces cytotoxic effects on cancer cells, while normal cells are not affected adversely by such irradiation. These selected far infrared wavelength LEDs are within the RRM computationally calculated range. Therefore, it can be concluded that the experimental evaluation of these far infrared exposures can induce detrimental effects on cell viability of cancer

cells as predicted by the RRM evaluations.

Chapter 6

Future Works

The RRM approach proposes that external electromagnetic radiation can induce or affect biological processes that are driven by proteins [253, 254]. Implementation of the RRM method for oncogene and proto-oncogenes proteins proposed that the external irradiation in the far infrared wavelengths ranging from 3500nm to 6500nm can induce resonant effects on biological function of these proteins [1–3]. These proteins play important role in uncontrolled growth of cancer cells. According to the RRM theory, the biological effects induced by external irradiation of particular wavelengths can possibly have detrimental effects on cancer cells. In this project, the main hypothesis, proposed by the RRM approach, has been studied *in vitro* on human and animal cancer cells. If this hypothesis is proven to be valid, it can revolutionize the treatment of surface or near the surface cancer tumors.

Thus, this research project aims to investigate experimentally the hypothesis

proposed within the computational RRM approach. The possibility of utilizing this innovative method as a ground breaking cancer treatment module has been investigated experimentally on B16F10 and MCF7 cells. *In vitro* analysis of the computationally calculated RRM far infrared wavelengths on B16F10 as animal cancer cell line and MCF7 as normal human cell line displayed apparent cytotoxic effects on cell viability of cancer cells, while the normal cells (CHO and HEM) used as controls did not demonstrate any significant effects upon irradiation. Although, the RRM hypothesis has been evaluated *in vitro* here on human and animal cell lines, the far infrared exposures have yet to be tested *in vivo* on animals and humans before it can be claimed as a cancer treatment method. Therefore, a number of possible future works closely related to this project can be defined and conducted.

A possible relevant topic can be a further *in vitro* investigation of the RRM hypothesis on other surface or near the surface cancer cells. *In vitro* investigation of other cancer cell lines can be considered as an immediate future work stemmed from this project.

Another possible future work can be *in vitro* analysis of human and animal primary cell lines. Since this project only evaluated non-primary cell lines, irradiation by the RRM-proposed far infrared wavelengths will be of importance, since the outcomes of exposures may not result in similar effects as observed and reported in this project.

Animal trials and clinical trials of cancer tumors treatment can be considered as the ultimate stages of the RRM hypothesiss evaluation. If the RRM concepts are proved to be valid, then the external irradiation of far infrared wavelengths can be accepted as an innovative, ground breaking cancer treatment module.

As it has been pointed out and discussed in Chapter 1, apart from oncogene and proto-oncogene proteins, tumor suppressor genes, pRb and p15, play an important role in development and spread of cancer tumors. Hence, the effects of exposures on these genes and their proteins should be also studied. Then, based on the RRM analysis of pRb and p15 proteins, the active wavelength range can be calculated, and a device for non-homogeneous LED exposures can be fabricated and tested of on the selected cancer cells.

Chapter 7

Conclusion

Cancer has been adversely affecting human life for a long period of time which dates back to early available recorded history of human existence on earth. Toxic effects of cancer can be viewed and discussed from different perspectives, since it impacts our life from different aspects. Statistically, cancer has devastating effects economically, socially and in terms of human toll. The economic loss due to cancer is the highest financial loss in the world. It is 20% higher than death toll caused by heart attack, which is recognized as a leading cause of death in developed countries. Moreover, disproportional socio-economic impact of cancer categorizes it as one of the main concerns of humankind in twenty first century.

As presented and discussed in Chapter 1, mutations in proto-oncogenes and tumor-suppressor genes play key roles in development and spread of cancer. The significant impacts of cancer on our day to day life and recent advancements in biological understanding of cancer have motivated scientists over the last decades

to combat cancer by developing effective treatment methods. Thus far, surgery, radiotherapy and chemotherapy, the so called conventional treatment methods, are established to be the most effective and widely used treatment methods. These conventional treatment methods, along with other alternative methods, were discussed comprehensively in Chapter 2. However, expensive employment and severe long-term and short-term side effects associated with these methods, as well as their inefficiency in treating some types of cancer as mentioned in Chapter 2, plea the need for a novel cost-effective and efficient treatment method.

In search for a better treatment method, several approaches have been proposed for cancer treatment. One approach would be the used of low intensity light therapy, which has proven to be successful for treatment of different medical conditions.

Each biological process involves a number of interactions between proteins and their targets, which are based on the energy transfer between the interacting molecules. Protein interactions are highly selective, and this selectivity is defined within the protein structure. The RRM is designed for analysis of protein (DNA) interactions and their interaction with EMR [3, 255, 256, 258–261]. A proteins biological function is "written" in its primary structure, i.e. a sequence of amino acids. The RRM is a physio-mathematical approach based on digital signal processing methods [253, 254]. The RRM theory states that an external EMF at a particular activation frequency would produce resonant effects on protein

biological activity [186, 255, 261, 262]. In this project, the RRM computational predictions have been tested experimentally on cancer and normal cells. It has been known that information laid in the amino acids sequence encodes information that determines the protein's biological functions and their 3D structure. The RRM is thriving to unravel the correlation between the amino acid sequence, proteins structural patterns, and their functional sites [1, 2, 258–261].

The RRM model (presented in Appendix B) is a physio-mathematical approach that is based on presentation of a protein primary structure as a numerical series. This numerical series is obtained by assigning a physical parameter value to each amino acid. The assigned number is related to the protein's biological activity [253, 254]. Implementation of this innovative approach proposed that the characteristic frequencies of oncogene and proto-oncogene proteins are within the range of 3500nm to 6400nm [1–3].

The aim of this experimental project was to evaluate the external radiation of light at the wavelength range predicted from the implementation of the RRM approach (3500nm - 6500nm). To conduct these experiments, an exposure device was designed and fabricated, and then used to irradiate cancer and normal cells. The experiments were conducted in three different regimes of exposure and post exposure incubation. Far infrared wavelengths used in these experiments were 3400nm, 3600nm, 3800nm, 3900nm, 4100nm and 4300nm. In addition to these far infrared wavelengths, three visible range LEDs (466nm, 585nm, 626nm) and

three near infrared LEDs (810nm, 850nm, 950nm) were used in the experimental study. Three standard quantitative cell-based assays along with two qualitative assays were used to evaluate the effects of different wavelengths on cancer and normal cells.

To optimize the control of experimental conditions and eliminate other factors, which could potentially affect the outcome of these *in vitro* experiments, certain considerations needed to be addressed. These issues mainly arise from certain limitations of conducting the experimentation *in vitro*. These concerns are described and my approach to addressing these issue is given below:

7.1 The issue related to transfer of energy to tissues and "hyperthermia" effect:

Human and animal cell lines, used in this project, are all adherent cell culture type. Thus, they would form a single layer at the bottom of the plates with 100μL of medium on top of it. In these *in vitro* experiments, irradiation of cells was not feasible outside the incubator or without a medium. This is because cells were dying quickly outside of their natural humid environment (simulated by incubator) or without their nutrition provided by medium.

For this reason, all experiments were conducted inside the incubator and with 100μL medium. LEDs, used in the experiments, are in μm range, with a parabolic

reflective angle of $10^{\circ C}$. These characteristics of LEDs indicate that most of the infrared energy is transferred into a small surface area. Thus, when cells are irradiated from the bottom of the plate, where irradiation source is very close to cells adhered to the plate, it would induce a local hyperthermia effect. To avoid this problem and prevent thermal/heating effects on cancer and normal cells, in my experiments cell cultures were irradiated from the top of the plate, where medium is considered as a barrier for far infrared energy transfer to the cultured cells located at the bottom of the plate. Energy absorption by water at infrared wavelengths is very high [263, 264]. Thus, most of the energy would be absorbed by the top layer of the medium and not by the cells at the bottom of the plate. Hence, the amount of energy transferred to cells would be minimal.

In my project, irradiation of cells was conducted with different exposure duration. Different time of exposure correspond to different doses of irradiation. Hence, the induced effects of different time exposures/doses were evaluated and compared in this study (the longest exposure time was 3 hours).

It is known, that longer exposure duration as well as absorption of infrared energy by a medium could induce heating/or hyperthermia effect which was not pursuit in this project. Of interest to this study, were non-thermal effects of infrared light on cancer and normal cells. Therefore, a heat shield cooling gel was purchased and used to reduce a possible hyperthermia effect. Cooling gel was placed around each well contained experimental cell culture to absorb a heat

generated from LEDs during longer exposure time that could induce heat in the medium and affect experiment results. These extra measures were applied to avoid heating effects on irradiated cells.

7.2 Issue of removing subconscious bias from CLSM imaging:

To avoid selection bias of the images, images were taken by another colleague, who was not aware which experimental regime of exposure or irradiation frequency/wavelength was used for each particular measurement.

In addition, to take the images from the same location for all experiments, 3 specific wells were selected for each plate. Images were taken from approximately a center of each well to avoid any selection bias based on the area chosen for imaging.

Images then were analyzed by NISElement imaging software since it was the only software available for the author of this thesis and any changes to other imaging analysis software was not possible. Moreover, the distance from the incubator to CLSM imaging machine was not long to cause unwanted effects on the experiments. The imaging process was conducted as fast as possible for a better accuracy of the results.

The conclusion remarks obtained from this project are outlined here:

- The significant reduction in cell viability is observed quantitatively for the external light radiation at the particular far infrared wavelengths on B16F10 animal cancer cells for three different regimes of exposure. The regime of exposure (3 hours of exposure followed by 24 hours of post exposure incubation) showed the most significant effects on cell viability of B16F10 animal cancer cells,

- No substantial changes in cell viability of normal CHO cells are observed quantitatively for 3 different regimes of light radiation at the far infrared wavelengths,

- External light radiation at the far infrared wavelengths induced considerable cytotoxic effects on MCF7 human cancer cells while no significant effect is detected on normal human HEM cells. The effects of the third regime of exposure (3 hours of exposure followed by 24 hours of post exposure incubation) on cell viability of MCF7 human cancer cells were the most significant effects compared to the first and second regimes of exposures,

- No significant cytotoxic effect was detected from external light irradiation at the visible and near infrared wavelengths on B16F10 animal cancer cells, MCF7 human cancer cells, CHO animal normal cells, and HEM human normal cells.

- Substantial cytotoxic effects, measured quantitatively for B16F10 animal

cancer cells and MCF7 human cancer cells as a result of different exposure regimes at the far infrared wavelengths, were corroborated in the qualitative assays. The observed cells detachment and changes in cell morphology of these cells indicate cell death and confirmed by both phase contrast microscopy and confocal laser scanning microscopy images.

In summary, this research project developed the exposure system and evaluated the applied visible, near infrared and far infrared (predicted by the RRM) exposures on selected human and animal cancer cell for three different exposure regimes. Extensive experimental evaluation of the external light radiation on the selected cancer and normal cells demonstrates that the RRM proposed wavelengths induce the significant cytotoxic effects in cancer cells for all three regimes of exposures and post exposure incubation, while normal cells were not affected significantly.

Appendix A

Cell Cycle

A.1 In-depth View of Cell Division Cycle

Cell division process generally consists of two consecutive stages of DNA replication followed by segregation of replicated chromosomes into two separate cells [25]. Originally, cell division comprises two stages of Mitosis (M), i.e. nuclear division process; and Interphase, interval between two M phases. Interphase stage provides DNA replication processes. Then, during mitosis the copied DNA is shared out equally between two cells. This means that all the chromosomes must be copied and divided into two full sets, one set at each end of cell that is splitting. The outcome of this split is two identical daughter cells [25].

These mitosis (M) and interphase stages are further divided into four and three stages consecutively. Mitosis is divided into four stages of prophase, metaphase, anaphase and telophase. Prophase is the stage where genetic material of the cell

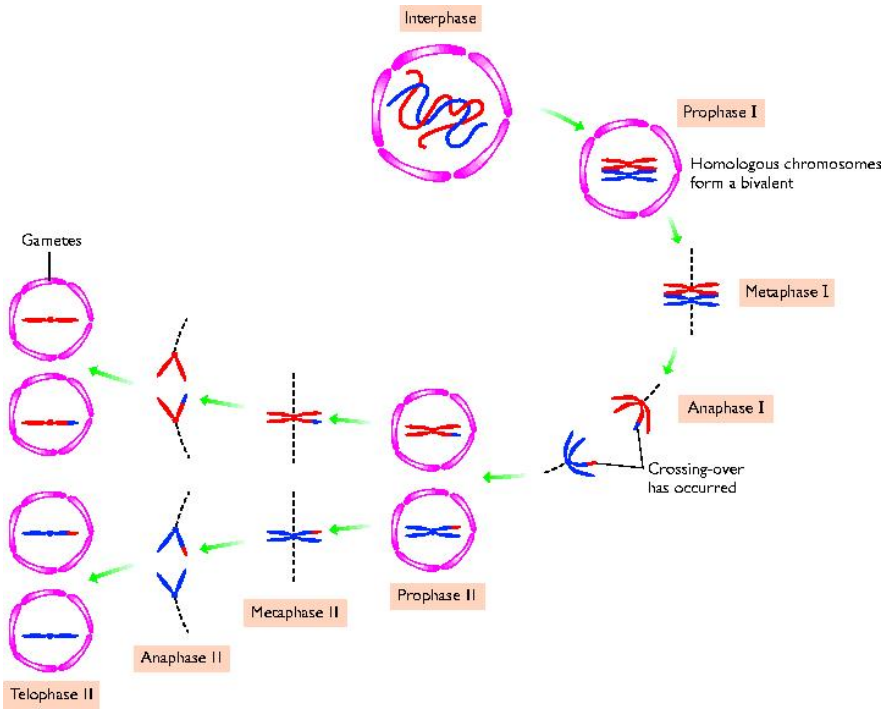

Figure A.1: Mitosis (M) Phase Stages [265]

is loosely bundled in the cell condenses to form chromosomes. At this stage, each chromosome is duplicated and has two sister chromatids. Then, within metaphase stage, the chromosomes aligns the cell spindle in the middle to prepare for cell splitting. After that, in the anaphase stage, those two sister chromatids formed during the prophase stage separate from each other and move to opposite end of the cell. Finally, in the telophase stage, cells prepare to split into two cells [266].

Traditionally, cell cycle division was divided into four stages of G_1, S, G_2 and M phases. This view has changed and the first three stages of cell cycle division are categorized as the interphase stage. Thus, the interphase stage consists of three stages: G_1, S and G_2 phases. In "Gap 1" or G_1 phase, cell grows in size

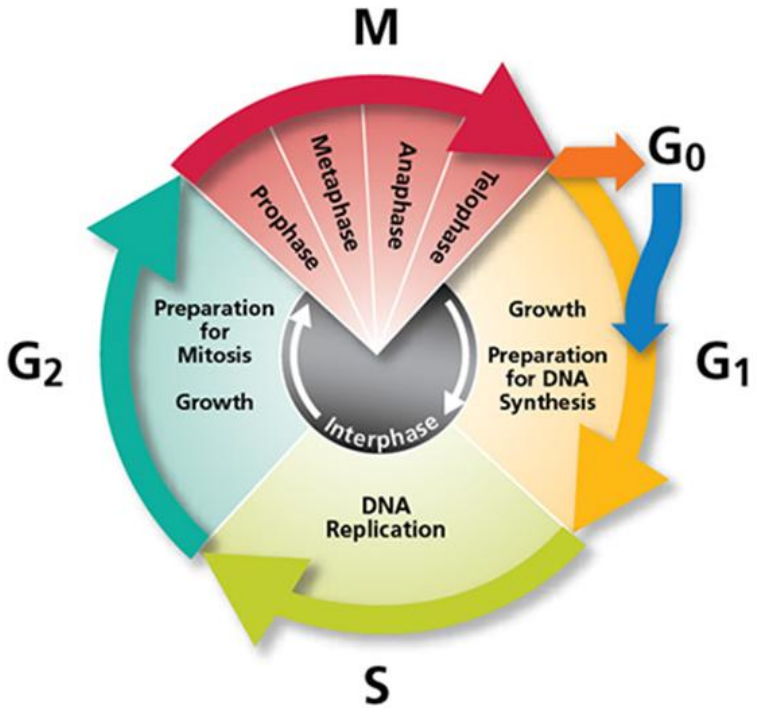

Figure A.2: The stages of cell cycle [266]

and checks everything to be OK for division [267]. Then, the replication of DNA occurs in "Synthesis" or S phase [267]. At last, "Gap 2" or G_2 phase checks whether DNA is correctly duplicated. If DNA duplication is correct, preparation of cell for mitosis is conducted at this phase [267]. However, prior to G_1 stage where commitment for DNA replication takes place, cells are considered to enter a resting stage called G_0. This state is responsible for the major non-growth, non-proliferation of cells in human body [25].

A.1.1 Cell Cycle Control

The process of replicating DNA for cell division is described as a series of coordinated events that follow a "cell division cycle". Two types of cell cycle control mechanisms are in place to ensure that the correct pathway for cell division is followed. These control mechanisms are Cyclic-Dependant Kinase regulation and a set of restriction points and checkpoints.

Cell Cycle Regulation: Cyclic-Dependent Kinase (CDK) regulation

This cell cycle mechanism is recognized as a cascade of protein phosphorylations that relay a cell from one stage to the next one. This regulation control involves a highly regulated kinase family. Kinase activation usually requires association with a second sub-unit called cyclin [25].

The transition from one cell division to another one is regulated and controlled by different cellular proteins. Cyclin-Dependent Kinases (CDK) are crucial regulatory proteins activated at specific points of the cell cycle. Among the nine CDKs that have been identified so far, five are active during cell cycles shown in Figure A.4 and Table A.1 [25].

One way to control cell cycle is through cyclin binding. CDKs are generally activated by their cyclin protein. CDKs are not known to play a critical role in normal cell cycle progression. They remain stable during the cell cycle in contrast

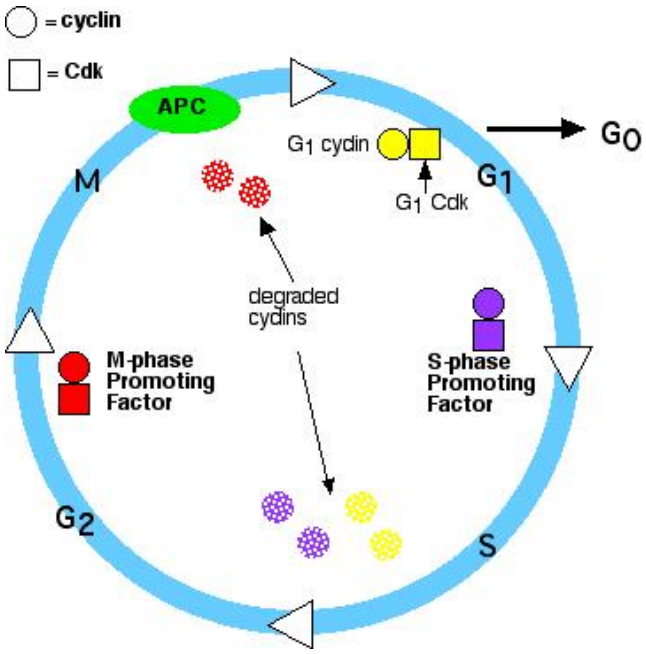

Figure A.3: Control of the Cell Cycle [268].

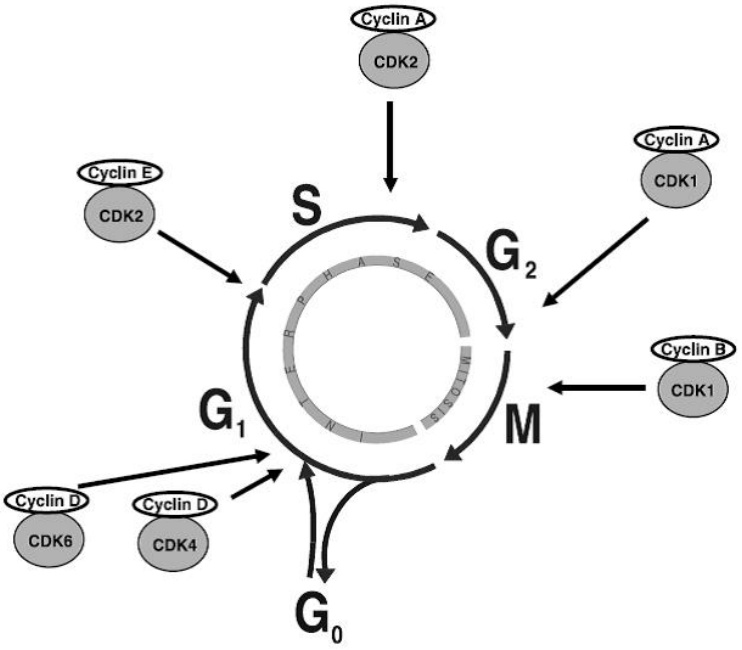

Figure A.4: The site activity of regulatory CDK [25].

to their activating proteins. Different cyclins are required at different phases of the cell cycle and each one of them is responsible for different functionality [25].

CDK	Cyclin	Cell cycle phase activity
CDK4	Cyclin D1,D2,D3	G_1 phase
CDK6	Cyclin D1,D2,D3	G_1 phase
CDK2	Cyclin E	G_1/S phase transition
CDK2	Cyclin A	S phase
CDK1 (cdc2)	Cyclin A	$G_2/Mphase$ transition
CDK1 (cdc2)	Cyclin B	Mitosis
CDK7	Cyclin H	CAK, all cell cycle phases

Table A.1: Cyclin-CDK complexes are activated at specific phases of the cell cycle [25].

One other way to control cell cycle is by regulating the activity of CDK by phosphorylation on conserved threonine and tyrosine residues. For instance, to fully activate CDK1, phosphorylation of threonine 161 is needed. This threonine is achieved by the release of threonine 172 in CDK4 and threonine 160 in CDK2 and is brought about by CDK7-cyclin H complex, called CAK [25].

Another way to control the activity of CDK and cell cycle is through inhibitory proteins called CDK Inhibitors (CKI) which has counteracting effect on cell cycle

[25]. To regulate CDK activity, CDK inhibitors bind to CDK or to the CDK-cyclin complex. Two discovered families of CDK inhibitors are INK4 family and Cip/Kip family [269]. INK4 family, consists of p15(INK4a), p16(INK4b), p18(INK4c), p19(INK4d), inactivates CDK 4 and CDK 6 in G_1 stage.

The second family of inhibitors, Cip/Kip, consists of p21(Wafl,Cip1), p27(Cip2), p57(Kip2). These inhibitors inactivate forming of CDK-cyclin complexes in G_1 stage and to a lesser extent CDK1-cyclin B complexes. Moreover, p21 inhibits DNA synthesis by binding to proliferating cell nuclear antigen (PCNA). The p21 expression is under transcriptional control of the p53 tumor suppressor gene. The p21 gene promoter consists of a p53-binding site, that allows p53 to dictate the activation of p21 gene [270]. The expression of p15 and activation of p27 promotes growth arrest in response to transforming growth factor $\beta(TGF-\beta)$.

CKI family	Function	Family members	
INK4 family	Inactivation of G_1 CDK (CDK4, CDK6)	p15	(INK4b)
		p16	(INK4a)
		p18	(INK4c)
		p19	(INK4d)
Cip/Kip family	Inactivation of G_1 cyclin-CDK complexes and cyclin B-CDK1	p21	(Waf1, Cip1)
		p27	(Cip2)
		p57	(Kip2)

Table A.2: Cyclin dependent kinases inhibitors (CKI) bind to CDK alone or to the CDK-cyclin complex and regulate CDK activity [25].

The intracellular localization of various proteins directing cell cycle-regulation leads to correct cell cycle progression. For instance, cyclin B sends out nuclear exclusion signal continuously until the beginning of the prophase stage. CDK inactivating kinases, Wee1 and Mytl in the nucleus and Golki complex, protect the cell from premature mitosis [25].

Cell Cycle Regulation: CDK Substrates

Activation of CDK turns the target proteins into phosphorylated one on the CDK consensus sites that result in physiological changes for cell cycle progression. The substrate of CDK4 and CDK6 binding with cyclin D are the most studied targets. Product of the retinoblastoma tumor suppressor gene (pRb) is one of these targets. At the early stages of G_1, pRb becomes phosphorylated and disrupts the complex with histone deacetylase protein (HDAC). This process is followed by the release of transcription factors, E2F-1 and DP-1. The release of E2F-1 and DP-1 regulates transcription of genes required for S phase progression, including cyclin A/E and Cdc25 [25].

Cell Cycle Quality Control: Restriction point and Checkpoints

Cell cycle control mechanisms monitor the completion of critical events and delay the progression to the next stage if necessary. These control mechanisms conduct a supervisory role and they are essential part of the cycle progression machinery.

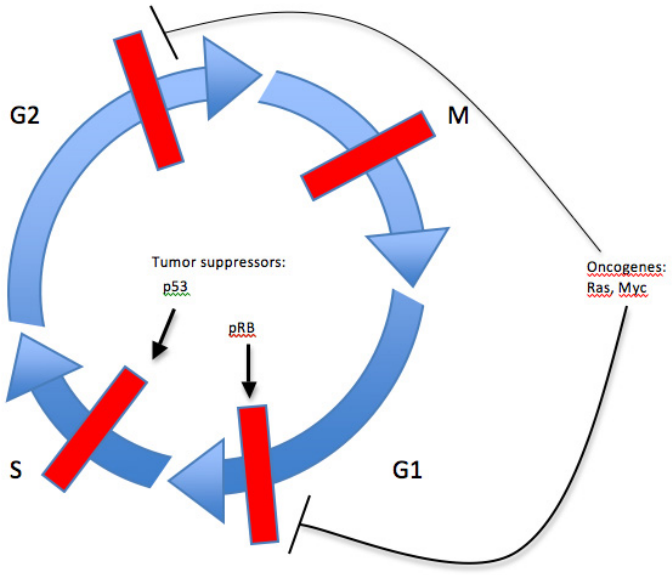

Figure A.5: Cell Cycle Checkpoints [31].

These checkpoints usually detect flaws in critical events such as DNA replication and chromosome segregation.

Apart from checkpoints, there is a Restriction point (R) at G_1 phase. Restriction point does not determine conditions for cell cycle progression but instead changes the course of the cell cycle initiation [25]. This point is called restriction point (R) in animals and Start point in yeast cells. This checkpoint is a critical point of no return in G_1. Following this stage, the commitment to start a cell cycle is determine. At G_1 checkpoint, just before entry to S phase, makes key decision to initiate cell division, delay division or enter a resting stage. If cells are starved from serum and cell division progression is not possible, they enter G_0 stage. Otherwise, cells progress to G_1 stage. Cell starvation at later stage does not affect progression to mitosis [25, 271].

There are three main checkpoints throughout the cell cycle process. These checkpoints are G_1-S or G_1 checkpoint, G_2 or G_2-M checkpoint and Metaphase or Mitotic spindle checkpoint [25, 29]. These checkpoints arrest the cell cycle to provide time for DNA repair in case of DNA disturbance. DNA damage checkpoints are situated before S phase (G_1-S) or after DNA replication (G_2-M) [25].

The first checkpoint is positioned before cell enters S phase and is called G_1-S checkpoint. At this checkpoint, cell cycle arrest induced by DNA damage is p53-dependent. Cellular level of p53 in normal condition is low but DNA damage leads to increased activity of p53. p53 activity stimulates *p21*, *Mdm2* and *Bax*. *p21* is a CKI that causes CDK inhibition and induces cell cycle arrest. Stimulation of *p21* prevents damaged DNA from replication and provides delay for DNA repair. Then, *Mdm2* regulates p53 release and works as a negative feedback loop. If the damage of DNA is severe and is not repairable, p53 induces cell apoptosis or cell death signal (e.g. *Bax*, *Fas*). DNA damage is detected by different protein kinases such as Ataxia Telangiectasia Mutated (ATM) and rad3 related (ATR). These protein kinases then phosphorelate p53 to block the cell cycle by p21 at G_1-S checkpoint [25].

It is understood that there is a DNA damage checkpoint in S phase between G_1 and G_2 checkpoints. Some studies indicate suppression of initiation and elongation phases of DNA replication. ATM-medicated phosphorylation of Nijmegen

Breakage Syndrome 1 (NBS1) is considered to induce S phase arrest during the S phase checkpoint [25, 271].

The second checkpoint after DNA replication is called G_2 or $G_2 - M$ checkpoint. This checkpoint ensures that cells with damaged DNA do not start mitosis process before they have had a chance to repair after replication process [272]. When DNA is damaged at G_2 stage, cell cycle arrest in absence or presence of p53 initiates. The nature of this checkpoint involves activation of phosphotase known as Cdc25. The progression of cell cycle into mitosis is prevented by maintaining CDK1 in its inhibited form through inhibitory phosphorylation or by removing components of CDK1-cyclin B complex outside the nucleus [25, 271]. Under this condition, the cell cycle is arrested through activation of Chk1 and Chk2 during ATM−dependent activity that phosphorylate Cdc25. Then, Cdc25 activity is inhibited, while its binding to 14-3-3 proteins is promoted. As a result, Cdc25 presence outside nucleus is removed and CDK1-cyclin B activation and mitotic entry is prevented. In addition to this process, p53 plays a regulatory role at $G_2 - M$ checkpoint. p53 increases transcription of p21 and 14-3-3σ. Then, the production of 14-3-3σ increases binding of cyclin B to 14-3-3σ which excludes it from the nucleus. p53 also facilitate the detachment of CDK1-cyclin B complexes by inducing Gadd45 (growth arrest and DNA damage inducible gene) [25, 271].

The third cell cycle checkpoint is called Metaphase or Mitotic Spindle checkpoint. At this checkpoint, proper alignment of chromosomes on mitotic spindle

is checked. In case of improper chromosome alignment at the mitotic plate, the cell cycle is stopped in metaphase [272]. Mitotic Arrest Defiant (Mad) and Budding uninhibited by benomyl (Bub) have recently been identified as mammalian spindle checkpoint-associated proteins. When defect in microtube attachment is detected, these spindle checkpoint-associated proteins are activated. The activation of these proteins inhibits the Cdc25 sub-unit of the anaphase-promoting complex (APC). This condition results in prevention of metaphase-anaphase transition [273, 274].

Appendix B

Resonant Recognition Model (RRM)

B.1 Protein Structure

Protein function can be the biochemical function of a molecule in isolation, or the cellular function as part of a complex structure with other molecules, or the phenotype it produces in an organism or the cell. Thus far, different aspects of proteins' functionality is studied including biochemical mechanism [275], molecular mechanism [276] and physiological mechanism [277], [278]. The most notable examples of biochemical functions of proteins are binding, catalysis, operating as molecular switches and serving as structure component of living organisms and cells.

Proteins may bind to other macromolecules such as DNA for gene regulatory proteins or DNA polymerases. They may bind to other proteins in case of a

transporter or receptor that binds a signalling molecule [279]. The latter functionality which is called catalysis ability enables proteins to interact with other molecules with high accuracy. This functionality requires not only the specific binding to substrate and sometimes to regulatory molecules but also specific chemical reactivity. Regulated enzymes and switches like signaling G proteins that are regulated enzymes for catalyzing the hydrolysis of GTP require large-scale conformational changes. These changes depend on the fragile balance that exists between structural stability and flexibility. Depending on their application and functionality, structural proteins can be very strong or extremely tough and durable as keratin such as the protein component of hair, horn and feature. Structural proteins may have complex dynamic properties which depend on nucleotide hydrolysis as it is in the case of actin and tublin. These functional diversity of proteins comes from the chemical diversity of their constituent amino acids, the flexibility of the polypeptide chain and the number of ways that polypeptide chains with amino acid sequences can fold [279].

Proteins are polymers of twenty diverse amino acids that are joined by peptide bonds. Protein structure consists of four levels including primary, secondary, tertiary and quaternary structure. The polypeptide chains of proteins fold into a globular form at physiological temperatures in aqueous solution. The sequence of different amino acids in a protein is determined by the sequence of nucleotides in the gene encoding it. This amino acid sequence is called the *primary structure*

of protein and it is shown in B.1a.

Then, the protein's primary structure determines how the protein folds into higher level structures. The form of polypeptide chain of protein is called its *secondary structure* and may have the form of either alpha helics, or beta strands that are shown in B.1b. The latter one formed through usual hydrogen bonding interaction between N-H groups and C=O groups in the invariant parts of the amino acids in the polypeptide backbone or main chain. Those elements of either alpha helix, or beta sheet or both as well as loops and links that have no secondary structure in the globular form are folded into a *tertiary structure* shown in B.1c. Many proteins are formed by conjunction of the folded chains of more than one polypeptide. This structure is called *quaternary structure* of a protein and it is demonstrated in B.1d [279].

In order for a polypeptide to function as a protein, it should be able to form a stable tertiary structure or fold under physiological conditions. At the same time, the protein function requires that the folded proteins not to be very rigid. As a result of these two constraints, there is a limited number of folds adopted by proteins [279]. The total number of proteins necessary for all living organism lies in the range of 4200 to 50,000 while the number of genes in higher organism is under debate.

In addition, the chemical characters of amino acid side chains also play an

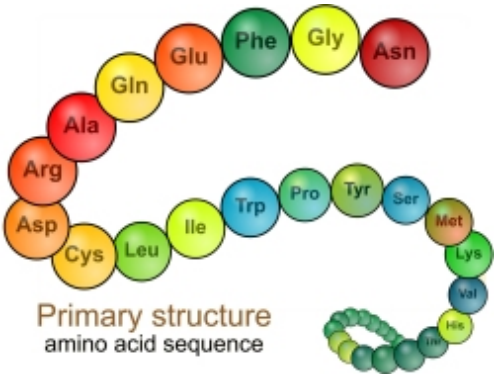

(a) Protein Primary Structure [48]

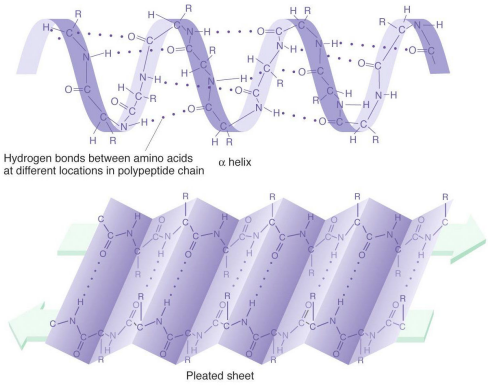

(b) Protein Secondary Structure [48]

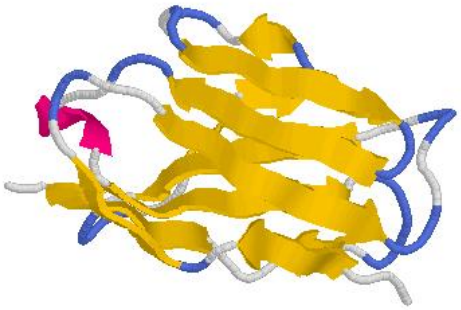

(c) Protein Tertiary Structure [48]

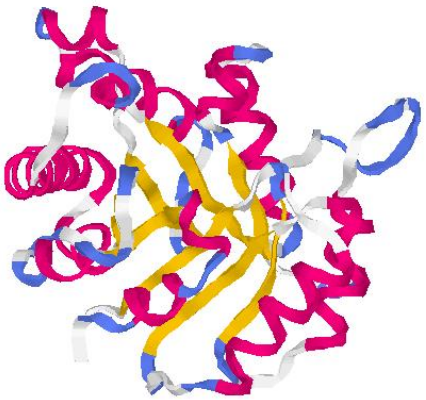

(d) Protein Quaternary Structure [48]

Figure B.1: Protein Structure Levels

important role in determining the way that they participate in the folding and function of proteins. The amino acid side chain has different tendency level to interact with each other and with water, which can have effect on their contributions to a protein stability and protein function. The various interaction tendency levels of amino acid residues include hydrophobic, hydrophilic, and amphipathic.

Proteins are linear polymers of amino acids that are linked together by amide bonds. The sequence of amino acid residues within the proteins dictates their biological functions and the specific amino acid sequence of proteins is specified by the genetic information in genome of the organisms. There is a strong correlation between the DNA sequence of gene and the amino acid sequence of the protein that DNA sequence encodes. The genetic codes pass the heredity information from genes into proteins. In order for proteins to fulfil their functionality, they would need to form a well-defined three dimensional structure. At this stage, the amino acid would have all the information required to order its final three dimensional structure or fold. In many small proteins, these 3D structures can be unfolded and refolded again *in vitro* without any losses of functionality. The procedure of unfolding and refolding again happens more often in more complex protein structures. These chaparones, proteins that assists these unfolding and reassembling, are used to allow a protein to reach its properly folded or correct three-dimensional state [280].

B.2 Protein Structure Prediction

Protein structure prediction is one of the most important and difficult problems in computational biology. According to the in-depth knowledge regarding the proteins structure, it should be possible to deduct the structure of a protein from its constituent amino acid sequence. Thus, there has been several attempts to discover the rules governing the coding of the biological function of protein by the amino acids sequences [281–293].

These approaches are mainly based on the homology characterization of specific feature of primary or secondary protein structures or they may deal with molecular modeling of protein tertiary structure. Though these approaches provide significant insight into protein structure and active location site(s), they are not able to provide sufficient knowledge about the informational, structural and physiochemical parameters that are crucial to the selectivity of protein interactions that can be used in de novo design for peptide or protein analogous with desired biological functionality. Despite the numerous efforts and research dedications, there are still different views and uncertainty surrounding the prediction and modeling of protein functionality based on their constituent amino acid sequence [253, 294].

Protein structure prediction is not only interesting from a *scientific* point of view but also from an *engineering* point of view. From engineering point of view,

protein structure prediction can be used to tackle de novo protein design. The objective is to identify amino acid sequences that would fold into proteins with desired functions. De novo protein design can be viewed as design problem at the molecular level. Since design problem starts with the structure and looks for sequences that will fold into such structure. De novo protein design problem is the "inverse" of protein folding problem that is followed by scientific community. This problem has been tackled computationally and also by experimentalists with mutagenesis, rational design, and directed evolution. However, comparison of these methods and computational protein design methods reveal the fact that the experimentalist methods can screen a limited number of structure [295].

One of the pioneer computational approaches in investigating the correlation between amino acid sequence of protein and their biological functionality is that of Anfinsen in 1973. It was proposed that proteins are not assembled into their native structure by a biological process but rather folding is a purely physical process. This approach believes that protein structure depends only on specific amino acid sequence of the protein and the surrounding solvent. This physics based method attempt to minimize the free energy and derive structure from first principles. It allows deducting macroscopic structure of proteins from their microscopic interactions between the protein's constituents. Anfinsen's thermodynamic approach became the dominant principle used in computational protein structure prediction over the last decade [295].

Then, in recent years another computational structure prediction approach has been developed for determining the protein structure. This alternative approach is called knowledge-based as opposed to anfinsen's physics based approach. These knowledge-based approaches search databases of known structures to infer information about an amino acid sequence of unknown three-dimensional structure.

Thus far, the research effort for protein structure prediction can broadly be categorized into two categories of mathematical or knowledge-based approach and physical-based approach. The first approach is based on mathematical analysis of amino acid or nucleotide arrangement aimed at searching for information on biological function. The second approach analyses the physical processes inside the macromolecule that could contribute to its biological function [253].

The existing knowledge in the field of computer-aided molecular modeling and protein structure analysis use to be divided into primary, secondary and tertiary protein structure analysis that is described in details in [253, 254]. The primary structure analysis is mainly concern with homologies among amino acid sequences. The most common method used in this approach is homology searching. The main idea of this approach is that amino acid sequences with the same biological functions do have sequence homology and carry the main information about function. This approach is very effective in conserved sequences including histones, haemoglobins, and insulin as well as DNA regulatory sequences where existence of core sequence of nucleotides has been validated [254, 295]. Some of

the examples of using primary structure analysis includes [281–283, 296].

In secondary structure analysis and prediction, various empirical, computer-aided algorithms are used when the primary structure of the protein is known but there is no experimental knowledge regarding protein secondary structure. Majority of these algorithms are based on the average probability that any particular amino acid residue can be found in an α-helical, β-sheet or random coil conformation [284, 285, 297]. The protein's secondary structure prediction improved substantially in 1990s. This prediction method has improved for correct residue prediction from 60%-70% more than a decade ago to around 76% in recent years. The improvement in accuracy of prediction which is due to the larger databases available has boosted this method's popularity substantially [298, 299].

Tertiary structure analysis is another prediction method which is based on the folding of the linear, primary polymer chain of a protein into a defined 3D structure. The increasing data based on experimentally obtained protein primary structure in conjunction with computer algorithms to perform molecular mechanics and dynamics provide an opportunity to establish computational algorithms as a powerful tool to examine protein's tertiary structure and predict protein active conformations. This technique has been utilized in the [288, 289].

In recent years, new classification for protein structure prediction has been emerged due to advancement in biology science and computer aided chemical

engineering. This new approach classification of protein structure prediction are based on different analysis method including protein structure prediction, loop structure prediction [300–302], and the first principle method, ASTROFOLD [303–307]. A comprehensive review of protein folding structure prediction requires the review of recent advances on different structure prediction method that can be divided into four groups:

1. comparative modeling,
2. fold recognition,
3. first principle methods with database information, and
4. first principle methods without database information.

In comparative modeling the structure prediction of a protein is conducted by comparing its amino acid sequence to a known native three-dimensional structure [308–311]. The method is based on the observation that similarity in amino acid sequence of two proteins implies similarity in their structure. While little progress in homology template of this method has been done, continuous improvement in sequence comparison technique has broaden the scope of homology modeling.

Fold recognition methods aim to predict three-dimensional folded structure of amino acid sequences when there is no reliable comparative is available. This method contains different approaches within itself that have demonstrated to be

based on fold recognition method [312–315]. Then, we have the first principle prediction with database information which is used for structure predictions that do not used experimentally known structures [316–320]. Finally, first principle prediction without database information make direct use of Anfinsen's thermodynamic hypothesis by attempting to find the minimum of the free energy of the protein in its environment [321–323].

B.2.1 Resonant Recognition Model (RRM) Approach

Use of conventional cancer treatment methods often negatively affects healthy tissues or organs of the body in the process of treating cancer. Thus, development of a targeted treatment module can lead to the optimum treatment method. However, such drugs or treatment methods should be designed in a way that they would not adversely affect the functionality of key molecules in human body. Sequence homology can provide a solution to avoid such similarities between drugs and important molecules.

Significant efforts of scientific community in solving the problem of finding a cure for cancer has led to development of new and advanced drug and methodologies with some degree of success; however this battle with cancer is still an ongoing issue. There is an urgent need for theoretical approaches that can analyze protein and DNA structure-functional relationships that can lead to a novel cancer treatment methodology. The RRM provides a non-conventional computational

approach for analysis of protein and deoxyribonucleic acid (DNA) sequences and their interactions.

The functionality of proteins is derived from the properties of twenty amino acid side chains that may exist in a protein molecule. This property of proteins molecule and its constituent amino acid side chains is reflected in the wide range of bioactivity of the formed protein molecules. However, the biological functionality of proteins can only be expressed when a certain active native conformation is achieved. This is called three dimensional structure (3D). Thus, the particular function of a given protein and it active 3D structure is determined by the sequence of amino acid conforming this particular protein molecule. It can be said that protein's biological function is encoded within proteins primary structure.

With rapid identification of protein databases, the revelation of biological activity of these newly identified sequenced protein or their contribution on functional families of protein becomes crucial for advancement in biology science. These advancements in biology science further confirms the fact that information laid in the amino acids sequence encodes the protein's biological functions and its 3D structure.

The RRM is thriving to unravel the correlation between the amino acid sequence, proteins structural patterns, and functional sites. This method provides a novel engineering analysis of linear macromolecules: protein and DNA

sequence [253,294]. The basis of biological function of a protein or DNA is related to the ability of macromolecule to interact selectively with other proteins, DNA regulatory segments, or small macromolecules. This method uses amino acid sequences and dopxyribonucleic acid (DNA) to predict the protein's functional and structural information. The RRM represents protein's primary structure as a numerical series by assigning a parameter value to each amino acid in the sequence. This parameter value is relevant to protein's biological activity.

According to the RRM, there is a substantial correlation between spectra of numerical presentation of amino acid and their biological function. It has been validated that proteins with similar biological functions share a common distinctive frequency in their numerical spectra that is associated with their biological function or interaction [253, 254]. That is, if the frequency of interaction or biological function is known, the RRM can determine the constituent amino acids that correlate to that particular frequency which led to that specific function or interaction. The reverse of this process is possible by designing peptides that would have the desired frequency.

The RRM identifies these constituent amino acids by implementing inverse Fourier transform (IFT) [253, 294]. After that, wavelet transformation, the new signal processing tool, is used to extract the local feature of the numerical series correspond to non-stationary signals that have obtained from IFT. In [324–326] continuous wavelet transform (CWT) has been used successfully to determine

the functional active sites of different protein families. The application of different wavelets have been investigated in scalogram of mouse epidermal growth factor (EGF), human β hemoglobin, prolactin, and tuna heart cytochrome c [324, 327]. For these applications, different wavelet functions such as Morley, Meyer, Daubechies, Simlets, Coiflets and Mexican hat have been used to determine different proteins' active site(s). The study of these protein types demonstrated that the combination of Fourier and Wavelet method were useful analytical tool in determining the active site(s) of these proteins. The analysis also established the sensitivity of these proteins to the wavelet functions used in the analysis. Among the Wavelet (WT) functions Morely/Meyer wavelets were providing better approximate of the active site(s).

The novelty of this model is the new view of biologically relevant intermolecular interactions, which is suggested to consist in the transfer of resonant energy between molecules. The successful implementation of this model can have significant impact on molecular biology and consequently on medicine, pharmacology and agriculture. When the nature of protein interactions and their selectivity is understood, this knowledge can be used for different application in molecular biology. The proposed application of RRM includes

1. defining a particular function of a protein or DNA fragment,

2. predicting functionally crucial amino acids within the protein sequence to

propose effective mutations,

3. predicting the feasibility of macromolecular interactions in specific protein-DNA interactions, and

4. designing sequences with desired spectra and functional characteristics.

These different applications were used in a variety of research studies shown in [253, 262, 294, 328]. All of these publications demonstrate the concept and implementation of RRM method for modeling of different biological functions.

The most notable application of RRM is in de novo peptides and protein design that can mimic the biological functionality of a natural protein or peptide. This model has been utilized successfully in a number of de novo design peptides [1, 186, 255, 261, 262, 328]. These experimental publications demonstrated the applicability of the RRM theory in peptide design. In addition, RRM is used to predict locations of a protein's biological active site(s) binding utilizing digital signal processing methods.

One of these investigations into implementation of RRM is presented in [328]. In fact, the study outcome and its hypothetical concepts were used as the basis for this work. This study incorporates the continuous wavelet transform (CWT) into the RRM method to predict the active site(s) of a chosen protein. The study investigated the oncogenes functional group by utilizing digital signal processing

techniques. In other words, the relationship between oncogene structure and its function is explored.

Thus, the main focus of this work is to solve the problem of functional and structural relationships of oncogene proteins using the RRM method with the incorporated CWT. Oncogenes are generally categorized as growth factors since they promote uncontrolled cell proliferation. These proteins derived from normal cellular growth factors (so-called proto-oncogenes) by having modifications such as mutations, deletions or insertions. As a result of this implementation, the characteristic frequency and functional active sites of oncogene obtained [1–3]. After that, the design of the peptide analogous was performed.

The results reported in [1, 3] provide novel insight into the structure-function relation of oncogene protein family. The concepts and computational analysis reported in study [1–3] were used in this PhD project for design of the exposure system and *in vitro* experimental irradiation of cells at the frequencies predicted computationally by the RRM.

Another, topic that is very relevant to cancer treatment is RRM implementation for interaction analysis of Viral and tumor suppressor proteins [1–3]. This study was motivated by other research studies that demonstrated the correlation between T-antigen, common virus, and brain tumor in children. Hence, the structure-function relation of T-antigen, p53 and pRb proteins have been exten-

sively studied using RRM approach. They found that interestingly these three proteins have a very prominent frequency component that is shared by all three analyzed sequences.

B.2.2 Application of the Resonant Recognition Model for analysis of oncogene and proto-oncogene proteins

The RRM theory also states that an external electromagnetic field (EMF) at a particular activation frequency would produce resonant effects on protein biological activity [255]. This hypothesis has successfully evaluated experimentally in literature [3]. In earlier related studies [256], the effects of visible light radiation in a range of 550-850nm and infrared light in the wavelengths ranging from 1140 up to 1200 nm on enzyme kinetics of L-Lactate Dehydrogenase (LDH) enzyme [3] has been investigated. Previous experimental evaluation also demonstrated that external irradiation of the certain frequencies, which were computationally determined using the RRM, can modulate a protein activity.

Each biological process involves a number of interactions between proteins and their targets, which are based on the energy transfer between the interacting molecules. The RRM is designed for analysis of protein (DNA) interactions and their interaction with EMR [3, 256, 258–261].

The application of the RRM involves two stages of calculation. The first is the transformation of the amino acid sequence into a numerical sequence. Each

amino acid is represented by its Electron-Ion Interaction Potential (EIIP) value which describes the average energy states of all valence electrons in a given amino acid [329]. These EIIP values are calculated from the general model of pseudo-potentials [329]:

$$\langle k+q|w|k\rangle = 0.25\frac{Z\ \sin(1.04\times\pi Z)}{2\pi} \tag{B.1}$$

where q is the momentum change of delocalized electron when interacting with potential w, while

$$Z = \sum \frac{Z_i}{N} \tag{B.2}$$

where Z_i is the number of valence electrons of the i-th components of each amino acids and N is the total number of atoms in amino acids.

Amino Acid	EIIP
Leu	0
Ile	0
Asn	0.0036
Gly	0.0050
Val	0.0057
Glu	0.0058
Pro	0.0198
His	0.0242
Lys	0.0371
Ala	0.0373
Tyr	0.0516
Trp	0.0548
Gln	0.0761
Met	0.0823
Ser	0.0829
Cys	0.0829
Thr	0.0941
Phe	0.0946
Arg	0.0959
Asp	0.1263

Table B.1: EIIP Values of 20 Amino Acids

A unique number can thus represent each amino acid or nucleotide, irrespective of its position in a sequence. Then the numerical series obtained are analyzed by digital signal analysis methods, Fourier and Wavelet transform, in order to extract information pertinent to the biological function. A multiple cross-spectral function is defined and calculated to obtain the common frequency components from the spectra of a group of proteins. Peaks in such function denote common frequency components for all sequences analyzed. Peak frequencies in such a multiple cross-spectral function denote common frequency components for all

sequences analyzed.

Prior to this work in [3, 256, 258–260], a relationship between the RRM spectra of some protein groups and their interaction with visible light was established. It has been shown that all protein sequences with a common biological function have a common frequency component in the free energy distribution of electrons along the protein backbone. This characteristic frequency was shown to be related to protein biological function [3, 256, 258–260].

Furthermore, it was also shown that proteins and their targets share a characteristic frequency. Thus, it can be further postulated that RRM frequencies characterize not only a general function but also a recognition/interaction between the particular proteins and their target at a distance. Thus, protein interactions can be viewed as a resonant energy transfer between the interacting molecules. This energy can be transferred through oscillations of a physical field, possibly electromagnetic in nature [253, 258].

A strong linear correlation exists between the predicted and experimentally determined frequencies corresponding to the absorption of electromagnetic radiation of such proteins [253, 256]. It is inferred that approximate wavelengths in real frequency space can be calculated from the RRM characteristic frequencies for each biologically related group of sequences. These calculations can be used to predict the wavelength of the light irradiation, which might affect the biological

activity of exposed proteins [253, 256]. The frequency range predicted for protein interactions is from 10^{13}Hz to 10^{15}Hz. This estimated range includes IR, visible and UV light.

These computational predictions were confirmed by comparison of:

a) Absorption characteristics of light absorbing proteins and their characteristic RRM frequencies [253, 259].

b) Frequency selective light effects on cell growth and characteristic RRM frequencies of growth factors [253, 261].

c) Activation of enzymes by laser radiation [253, 256, 258].

All these results indicate that the specificity of protein interaction is based on a resonant electromagnetic energy transfer at the frequency specific for each interaction observed. A linear correlation between the absorption spectra of proteins and their RRM spectra with a regression coefficient of $K = 201$ has been established. Using RRM postulates, a computationally identified characteristic frequency for a protein functional group can be used to calculate the wavelength of applied irradiation, λ , which assumingly would activate this protein sequence and modify its bioactivity [253]:

$$\lambda = \frac{201}{f_{RRM}} \tag{B.3}$$

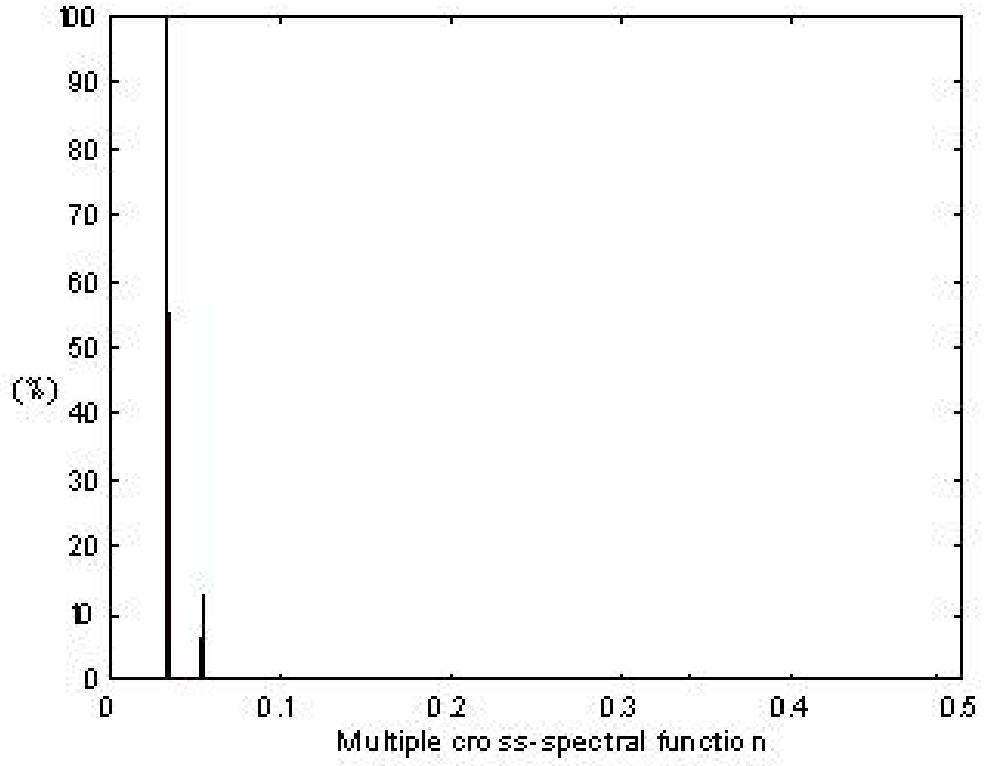

Figure B.2: Activation frequency of transforming proteins. x axis being frequency of transforming proteins.

In previous study, the RRM approach has been used to determine the characteristic frequencies of oncogene and proto-oncogene proteins [1,3]. The frequency range obtained from this analysis is presented in Figure B.2 and B.3.

By identifying computationally the difference between oncogene and proto-oncogene proteins and designing the peptide analogues, the new field of investigation of oncogenic activity is opened.

These frequencies were determined as follow: Activation frequency of transforming proteins is at $f_1 = 0.0322$ (oncogene proteins) and the activation frequency

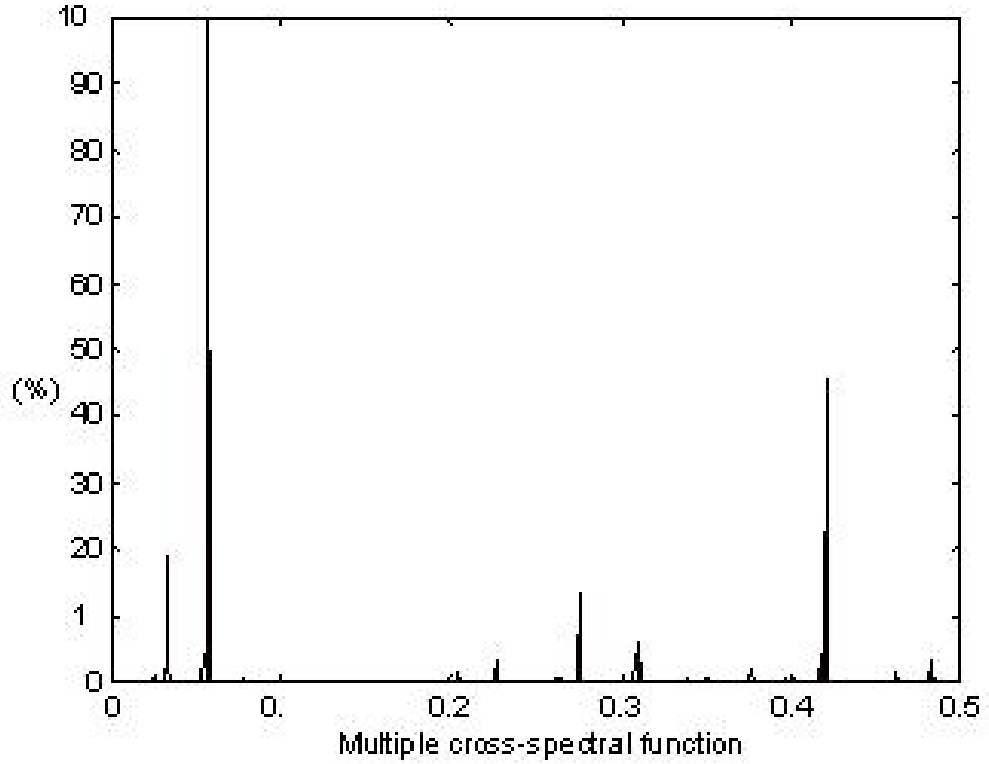

Figure B.3: Activation frequency of non-transforming proteins. x axis being frequency of transforming proteins.

of non-transforming proteins is at $f_2 = 0.0576$ (proto-oncogene proteins).

Using the equation B.3, these frequencies can be converted into a real space wavelength of applied irradiation: $\lambda_1 = 6242$nm and $\lambda_2 = 3490$nm respectively. Therefore, the proposed light emitting exposure system will have the operating range of 3500nm-6400nm.

Bibliography

[1] E. Pirogova, M. Kay, and I. Cosic, "Investigating the interaction between oncogene and tumor suppressor protein," *IEEE Trans. on Info. Tech. in Biomed.*, vol. 13, pp. 10–15, January 2009.

[2] E. Pirogova, Q. Fang, M. Kay, and I. Cosic, "Investigation of the structural and functional relationships of oncogene proteins," *Proc. of IEEE*, vol. 90, pp. 1859–1867, December 2002.

[3] V. Vojisavljevic, E. Pirogova, and I. Cosic, "Influence of electromagnetic radiation on enzyme kinetics," in *IEEE Proc. of Inter. of EMBS, Lyon*, vol. 2, pp. 317–324, August 2007.

[4] Lightbulb Press, Inc, "Conventional treatment." `http://www.cancercompass.com/cancer-guide/conventional-treatment.html`, 2008.

[5] Stanford Medicine, "Cancer treatment methods." `http://cancer.stanford.edu/information/cancerTreatment/methods.html`, 2013.

[6] Cancer Research United Kingdom, "Treatment." http://www.cancerresearchuk.org/cancer-help/about-cancer/treatment, 2013.

[7] G. Karp, *Cell and Molecular Biology: Concepts and Experiments*. John Wiley & Sons, third edition ed., 1996, 1999, 2002.

[8] American Society of Cancer, "Evolution of cancer treatments: Chemotherapy." http://www.cancer.org/cancer/cancerbasics/thehistoryofcancer/the-history-of-cancer-cancer-treatment-chemo, 2012.

[9] R. Jorgenson and F. Carness, "Cancer genes, proto-oncogenes." http://www.healthopedia.com/oncogenes/, 2001.

[10] S. Freeman, *Biological Science*. Prentice Hall, 2005.

[11] J. Slonczewski, "Kap genetics and development." http://biology.kenyon.edu/courses/biol114/biol114_fall_sec0.html\#dates, 2006.

[12] International Agency for Research on Cancer, World Health Organization (WHO), "Globocan 2012." http://www.wcrf.org/cancer_statistics/cancer_facts/millions_new_cancer_worldwide.php, 2008.

[13] American Cancer Society, "Cancer facts and figures." http://www.cancer.org/research/cancerfactsfigures/cancer-facts-figures-2008, 2008.

[14] W. H. Organization, "Cancer mortality and morbidity," tech. rep., Global Health Observatory (GHO), 2014.

[15] E. Hatzimichael and T. Crook, "Cancer epigentics: New therapies and new challenges," *Journal of Drug Delivery*, vol. 2013, pp. 1–9, 2013. Article ID 529312.

[16] American Cancer Society, "Economic impact of cancer," 2013.

[17] J. Rijo and H. Ross, "American Cancer Society and LIVESTRONG Global Economic Cost of Cancer." `http://www.cancer.org/acs/groups/content/@internationalaffairs/documents/document/acspc-026203.pdf`, 2010.

[18] J. Seffrin, "The global economic cost of cancer." `http://pressroom.cancer.org/index.php?s=43&item=262`, 2010.

[19] L. Woods, B. Rachet, and M. Coleman, "Origins of socio-economic inequalities in cancer survival: a review," *Annals of Oncology Oxford Journals*, vol. 17, pp. 5–19, 2006.

[20] Melanoma Institute Australia, "Melanoma facts and statistics." `www.melanoma.org.au/about-melanoma/melanoma-skin-cancer-facts.html`, 2012.

[21] Cancer Council Australia, "Melanoma." `http://www.cancer.org.au/about-cancer/types-of-cancer/skin-cancer/melanoma.html`, 2012.

[22] D. Hanahan and R. Weinberg, "The hallmark of cancer," *Cell*, vol. 100, no. 1, pp. 57–70, 2000.

[23] R. Weinberg, *The Biology of Cancer*. Garland Science, 2006.

[24] E. McDonald and W. El Deiry, "Cell cycle control as a basis for cancer drug development," *International Journal of Oncology*, vol. 16, p. 871, 2000.

[25] K. Vermeulen, D. Van Bockstaele, , and Z. Berneman, "The cell cycle: a review of regulation, deregulation and therapeutic targets in cancer," *Cell Proliferation*, vol. 36, pp. 131–149, 2003.

[26] Cancerquest, "Introduction to cancer biology." `http://www.cancerquest.org/cancer-genes-overview.html`, 2012.

[27] K. Collins, T. Jacks, and N. Pavletich, "The cell cycle and cancer," *Proceedings of the National Academy of Sciences of USA*, vol. 94, no. 7, pp. 2776–2778, 1997.

[28] W. E. Foundation, "Background essay: How cancer cells grow and divide." `http://www.pbslearningmedia.org`.

[29] H. Niida and M. Nakanishi, "Dna damage checkpoints in mammals," *Mutagenesis*, vol. 21, no. 1, pp. 3–9, 2006.

[30] P. McClean and BioChemWeb.org, "The virtual library of biochemistry, molecular biology and cell biology." `http://www.biochemweb.org/cell_cycle.shtml`, 1997, 2013.

[31] W. Lim, "Designing customized cell signalling circuits," *Nature Reviews Molecular Cell Biology*, vol. 11, pp. 393–403, 2010.

[32] C. Sherr, "Cancer cell cycles," *Science*, vol. 274, pp. 1672–1677, December 1996.

[33] E. Adamson, "Oncogenes in development," *development*, vol. 99, pp. 449–471, 1987.

[34] R. Thomas, "High-throughput oncogene mutation profiling in human cancer," *Nature Genetics*, vol. 39, pp. 347–351, 2007.

[35] L. Jiang and E. P. Encyclopedia, "The discovery of p53 protein." `http://embryo.asu.edu/pages/discovery-p53-protein`, 2011.

[36] T. Tsai, S. Davalath, C. Rankin, J. Radich, D. Head, F. Appelbaum, and D. Boldt, "Tumor suppresoor gene alteration in adult acute lymphobalstic leukemia (all). analysis of retinoblastoma (rb) and p53 gene expression in lymphoblasts of patients with de novo, relapsed or refractory all treated in southwest oncology group studies," *Leukemia*, vol. 10, p. 1906, 1996.

[37] G. Peter and M. Hall, "Genetic alterations of cyclin, cyclin-dependent kinases and cdk inhibitor in human cancer," *Advanced Cancer Research*, vol. 68, p. 67, 1996.

[38] Cancer Institute NSW Government, "Cancer treatment." `http://www.cancerinstitute.org.au/patient-support/what-i-need-to-know/cancer-treatment`, 2012.

[39] C. Powell, "Conventional, complementary, and alternative approaches to healing." `http://enrichmentjournal.ag.org/200702/200702_118_Healing.cfm`, 2013.

[40] C. Creighton, X. Li, M. Landis, J. Dixon, V. Neumeister, A. Sjolund, D. Rimm, H. Wong, A. Rodriguez, J. Herschkowitz, C. Fan, X. Zhang, X. He, A. Pavlick, M. Gutierrez, L. Renshaw, A. Larionov, D. Faratian, S. Hilsenbeck, C. Perou, M. Lewis, J. Rosen, and J. Chang, "Residual breast cancers after conventional therapy display mesenchymal as well as tumor-initiating features," *Proceedings of National Academy of Science*, vol. 106, no. 33, pp. 13820–13825, 2009.

[41] F. Frame and N. Maitland, "Cancer stem cells, models of study and implications of therapy resistance mechanisms.," *Advances in Experimental and Medical Biology*, vol. 720, no. 105-118, 2011.

[42] C. Eyler and J. Rich, "Survival of the fittest: cancer stem cells in therapeutic resistance and angiogenesis," *Journal of Clinical Oncology*, vol. 26, no. 17, 2008.

[43] P. Newman and M. Gibb, "Electromagnetic spectrum - introduction." `http://imagine.gsfc.nasa.gov/docs/science/know_l1/emspectrum.html`, 2013.

[44] N. Patel, K. Vo, and M. Hernandez, "Electromagnetic radiation." `http://chemwiki.ucdavis.edu/Physical_Chemistry/Spectroscopy/Electromagnetic_Radiation`, 2010.

[45] X. Meng, G. He, J. Zhang, Z. Han, M. Yu, M. Zhang, Y. Tang, L. Fan, and X. Zhou, "A comparative study of fibroid ablation rates using radio frequency or high-intensity focused ultrasound," *CardioVascular and Interventional Radiology*, vol. 33, no. 4, pp. 794–799, 2010.

[46] L. Guo, N. Kubat, and R. Isenberg, "Pulsed radio frequency energy (prfe) use in human medical applications," *Electromagnetic Biology and Medicine*, vol. 30, no. 1, pp. 21–45, 2011.

[47] I. Belyaev, V. Shcheglov, E. Alipov, and V. Ushakov, "Nonthermal effects of extremely high-frequency microwaves on chromatin conformation in cells in vitrodependence on physical, physiological, and genetic factors," *IEEE*

Tranactions On Microwave Theory and Techniques, vol. 48, pp. 2172–2179, November 2000.

[48] Google, "Google.com." `https://www.google.com/search`, 2013.

[49] T. Karu, A. Tiphlova, G. Lukpanova, and I. Parkhomenko, "Effect of irradiation with monochromatic visible light on camp content in chinese hamster fibroblasts," *IlNuovo Cimento D*, vol. 9, no. 10, pp. 1245–1251, 1987.

[50] S. Banik, S. Bandyopadhyay, and S. Ganguly, "Bioeffects of microwave - a brief review," *Science, Bioresource Technology*, vol. 87, no. 2, pp. 155–159, 2003.

[51] N. Shupak, "Therapeutic uses of pulsed magnetic-field exposure: A review," *The Radio Science Bulletin*, 2003.

[52] C. Vallbona and T. Richards, "Evolution of magnetic therapy from alternative to traditional medicine," *Physical Medicine and Rehabilitation Clinics of North America*, vol. 10, no. 3, pp. 729–754, 1997.

[53] M. Markov, "Expanding use of pulsed electromagnetic field therapies," *Electromagnetic Biology and Medicine*, vol. 26, no. 3, pp. 257–274, 2007.

[54] H. Schwan and K. Foster, "Rf-field interactions with biological systems: Electrical properties and biophysical mechanisms," *Proceedings of the IEEE*, vol. 68, no. 1, pp. 104–113, 1980.

[55] B. Rubik, "Bioelectromagnetics and the future of medicine," *Administrative Radiology Journal*, vol. 16, no. 8, pp. 38–46, 1997.

[56] X. Grifn, M. Costa, N. Parsons, and N. Smith, *Electromagnetic field stimulation for treating delayed union or non-union of long bone fractures in adults*. John Wiley and Sons, Ltd., 2011.

[57] C. Bassett, "The development and application of pulsed electromagnetic fields (pemfs) for ununited fractures and arthrodeses," *Clinical Plastic Surgery*, vol. 12, pp. 259–277, 1985.

[58] I. Goudarzi, S. Hajizadeh, M. Salmani, and K. Abrari, "Pulsed electromagnetic fields accelerate wound healing in the skin of diabetic rats," *Bioelectromagnetics*, vol. 31, no. 4, pp. 318–323, 2010.

[59] W. Pawluk, "Pain management with pulsed electromagnetic field (pemf) treatment." `http://www.curatronic.com/pdf/Pain\%20management\%20with\%20PEMF.pdf`, 2003.

[60] H. Siadat, S. Bassir, M. Alikhasi, Y. Shayesteh, A. Khojasteh, and A. Monzavi, "Effect of static magnetic fields on the osseointegration of immediately placed implants: A randomized controlled clinical trial," *Implant Dentistry*, vol. 21, no. 6, pp. 491–495, 2012.

[61] P. Stavroulakis, *Biological Effects of Electromagnetic Fields*. Springer-Verlag Berlin Heidelberg New York, 2003.

[62] C. Bassett, "Fundamental and practical aspects of therapeutic uses of pulses electromagnetic fields (pemfs)," *Critical Reviews in Biomedical Engineering*, vol. 17, no. 5, pp. 451–529, 1989.

[63] V. DiLazzaro, F. Capone, F. Apollonio, P. Boread, R. Cadossie, L. Fassinaf, C. Grassig, M. Libertic, A. Paffic, M. Parazzinih, K. Varanid, and P. Ravazzanih, "A consensus panel review of central nervous system effects of the exposure to low-intensity extremely low-frequency magnetic fields," *Brain Stimulation*, pp. 1–8, 2013.

[64] C. Miha, G. Vochita, F. Brinza, and P. Rotinberg, "Extremely low-frequency electromagnetic fields cause dna strand breaks in normal vero cells," *Quantitative Biology*, 2013.

[65] G. del Vecchio, A. Giuliani, M. Fernandez, P. Mesirca, F. Bersani, R. Pinto, L. Ardoino, G. Lovisolo, L. Giardino, and L. Calz, "Continuous exposure to 900 mhz gsm-modulated emf alters morphological maturation of neural cells," *Neuroscience Letters*, vol. 455, no. 3, pp. 173–177, 2009.

[66] R. Girgert, H. Schimming, W. Körner W, C. Grndker, and V. Hanf, "Induction of tamoxifen resistance in breast cancer cells by elf electromagnetic fields," *Biochemical Biophysical Research Community*, vol. 336, no. 4, pp. 1144–1149, 2005.

[67] A. Evangelou, I. Toliopoulos, C. Giotis, A. Metsios, I. Verginadis, Y. Simos, K. Havelas, G. Hadziaivazis, and S. Karkabounas, "Functionality of natural killer cells from end-stage cancer patients exposed to coherent electromagnetic fields," *Electromagnetic Biology and Medicine*, vol. 30, no. 1, pp. 46–56, 2011.

[68] M. Jiménez-García, J. Arellanes-Robledo, D. Aparicio-Bautista, M. Rodrguez-Segura, S. Villa-Trevio, and J. Godina-Nava, "Antiproliferative effect of extremely low frequency electromagnetic field on preneoplastic lesions formation in the rat liver," *Biomed Central Cancer*, vol. 10, p. 159, 2010.

[69] P. Galloni and C. Marino, "Effects of 50 hz magnetic field exposure on tumor experimental models," *Bioelectromagnetics*, vol. 21, no. 8, pp. 608–614, 2000.

[70] M. Yasui, T. Kikuchi, M. Ogawa, Y. Otaka, M. Tsuchitani, and H. Iwata, "Carcinogenicity test of 50 hz sinusoidal magnetic fields in rats," *Bioelectromagnetics*, vol. 18, no. 8, pp. 531–540, 1997.

[71] R. Seze, S. Tuffet, J. Moreau, and B. Veyret, "Effects of 100 mt time varying magnetic fields on the growth of tumors in mice," *Bioelectromagnetics*, vol. 21, no. 2, pp. 107–111, 2000.

[72] A. Barbault, F. Costa, B. Bottger, R. Munden, F. Bomholt, N. Kuster, and B. Pasche, "Amplitude-modulated electromagnetic fields for the treatment of cancer: discovery of tumor-specific frequencies and assessment of a novel therapeutic approach," *Journal of Experimental Clinical Cancer Research*, vol. 28, p. 51, 2009.

[73] S. Tofani, M. Cintorino, D. Barone, M. Berardelli, M. De Santi, A. Ferrara, R. Orlassino, P. Ossola, K. Rolfo, F. Ronchetto, S. Tripodi, and P. Tosi, "Increased mouse survival, tumor growth inhibition and decreased immunoreactive p53 after exposure to magnetic fields," *Bioelectromagnetics*, vol. 23, no. 3, pp. 230–238, 2002.

[74] S. Lange, I. Viergutz, and M. Simko, "Modifications in cell cycle kinetics and in expression of g1 phase-regulating proteins in human amniotic cells after exposure to electromagnetic fields and ionizing radiation," *Cell Proliferation*, vol. 37, no. 5, pp. 337–349, 2004.

[75] W. Jian, Z. Wei, C. Zhiqiang, and F. Zheng, "X-ray-induced apoptosis of bel-7402 cell line enhanced by extremely low frequency electromagnetic field in vitro," *Bioelectromagnetics*, vol. 30, no. 2, pp. 163–165, 2009.

[76] S. Tofani, D. Barone, M. Cintorino, M. de Santi, A. Ferrara, R. Orlassino, P. Ossola, F. Peroglio, K. Rolfo, and F. Ronchetto, "Static and elf magnetic

fields induce tumor growth inhibition and apoptosis," *Bioelectromagnetics*, vol. 22, no. 6, pp. 419–428, 2001.

[77] J. Zimmerman, M. Pennison, I. Brezovich, N. Yi, C. Yang, R. Ramaker, D. Absher, R. Myers, N. Kuster, F. Costa, A. Barbault, and B. Pasche, "Cancer cell proliferation is inhibited by specific modulation frequencies," *British Journal of Cancer*, vol. 16, pp. 307–313, 2012.

[78] M. Daniell and J. Hill, "A history of photodynamic therapy," *Austalia and NZ Journal of surgery*, vol. 61, no. 5, pp. 340–348, 1991.

[79] D. Dolmans, D. Fukumra, and R. Jain, "Photodynamic therapy for cancer," *Nature Reviews Cancer*, vol. 3, no. 5, pp. 380–387, 2003.

[80] B. Wilson, "Photodynamic therapy for cancer: principles," *Canadian Journal of Gastroenterology*, vol. 16, no. 6, pp. 393–396, 2002.

[81] M. Vrouenraets, G. Visser, G. Snow, and G. Van Dongen, "Basic principles, applications in oncology and improved selectivity of photodynamic therapy," *Anticancer Research*, vol. 23, no. 1B, pp. 505–522, 2003.

[82] T. Dougherty, C. Gomer, B. Henderson, G. Jori, D. Kessel, M. Korbelik, J. Moan, and Q. Peng, "Photodynamic therapy," *Journal of the National Cancer Institute*, vol. 90, no. 12, pp. 889–905, 1998.

[83] E. Dickson, R. Goyan, and P. R., "New directions in photodynamic therapy," *Cellular and Molecular Biology*, vol. 48, no. 8, pp. 939–954, 2002.

[84] L. Kwasniak, E. Schweiger, and V. Tonkovic-Capin, "A patient with neviod basal cell carcinoma syndrome treated successfully with photodynamic therapy: case report and review of the literature," *Journal of Drugs in Dermatology*, vol. 9, no. 2, pp. 167–168, 2010.

[85] R. Saager, D. Cuccia, S. Saggese, K. Kelly, and A. Durkin, "A light emitting diode (led) based spatial frequency domain imaging system for optimization of photodynamic therapy of nonmelanoma skin cancer: Quantitative reflectance imaging," *Lasers in Surgery and Medicine*, vol. 45, pp. 207–215, 2013.

[86] Z. Huang, "A review of progress in clinical photodynamic therapy," *Technol Cancer Research Treatment*, vol. 4, pp. 283–293, 2005.

[87] N. Idris, M. Gnanasammandhan, J. Zhang, P. Ho, R. Mahendran, and Y. Zhang, "In vivo photodynamic therapy using upconversion nanoparticles as remote-controlled nanotransducers," *Nature Medicine*, vol. 18, pp. 1580–1585, 2012.

[88] S. Brown, E. Brown, and I. Walker, "The present and future role of photodynamic therapy in cancer treatment," *Lancet Oncology*, vol. 5, no. 497-508, 2004.

[89] P. Juzenas and A. Juzeniene, "Reduction of cutaneous photosensitivity by application of ointment containing ferrous or cobaltous ions concomitant with the use of topical protoporphyrin ix precursors," *Photodiagnosis of Photodynamic Therapy*, vol. 7, no. 3, pp. 152–157, 2010.

[90] N. Idris, M. Gnanasammandhan, J. Zhang, P. Ho, R. Mahendran, and Y. Zhang, "In vivo photodynamic therapy using upconversion nanoparticles as remote-controlled nanotransducers," *Nature Medicine*, vol. 18, pp. 1580–1585, 2012.

[91] M. Capella and L. Capella, "A light in multidrug resistance: photodynamic treatment of multidrug-resistant tumors," *Journal of Biomedical Science*, vol. 10, no. 4, pp. 361–366, 2003.

[92] National Cancer Institute, "Photodynamic therapy for cancer." `http://www.cancer.gov/cancertopics/factsheet/Therapy/photodynamic`, 2011.

[93] P. Kaur, M. Hurwitz, S. Krishnan, and A. Asea, "Combined hyperthermia and radiotherapy for the treatment of cancer," *Cancers*, vol. 3, no. 4, pp. 3799–3823, 2011.

[94] G. Hegyi, G. Szigeti, and A. Szász, "Hyperthermia versus oncothermia: Cellular effects in complementary cancer therapy," *Evidence-Based Com-*

plementary and Alternative Medicine, vol. 2013, pp. 1–12, 2013. Article ID 672873.

[95] S. Azeemi and S. Raza, "A critical analysis of chromotherapy and its scientific evolution," *Evidence-Based and Complementary Alternative Medicine*, vol. 2, no. 4, pp. 481–488, 2005.

[96] R. Roelandts, "The history of phototherapy: something new under the sun?," *Journal of American Academy of Dermatology*, vol. 46, no. 6, pp. 926–930, 2002.

[97] M. Terman, "Evolving applications of light therapy," *Sleep Medicine Reviews*, vol. 11, pp. 497–507, 2007.

[98] R. Golden, B. Gaynes, R. Ekstrom, R. Hamer, F. Jacobsen, T. Suppes, K. Wisner, and G. Nemeroff, "The efficacy of light therapy in the treatment of mood disorders: a review and meta-analysis of the evidence," *American Journal of Psychiatry*, vol. 162, pp. 656–662, 2005.

[99] S. Campbell, M. Terman, A. Lewy, D. D., E. C., and B. Z., "Light treatment for sleep disorders: consensus report. v. age related disturbances," *Journal of Biology Rhythms*, vol. 10, pp. 151–154, 1995.

[100] M. Terman and J. Terman, "Light therapy for seasonal and nonseasonal depression: efficacy, protocol, safety and side effects," *CNS Spectroscopy*, vol. 10, pp. 647–663, 2005.

[101] F. Benedetti, B. Barbini, M. Fulgosi, C. Colombo, S. Dallaspezia, A. Pontiggia, and E. Smeraldi, "Combined total sleep deprivation and light therapy in the treatment of drug-resistant bipolar depression: acute response and longterm remission rates," *Journal of Clinical Psychiatry*, vol. 66, pp. 1535–1540, 2005.

[102] Y. Rybak, H. McNeely, B. Mackenzie, U. Jain, and R. Levitan, "An open trial of light therapy in adult attention-deficit/hyperactivity disorder," *Journal of Clinical Psychiatry*, vol. 67, pp. 1527–1535, 2006.

[103] G. Dowling, E. Hubbard, J. Mastick, J. Luxenberg, R. Burr, and E. Van Someren, "Effect of morning bright light treatment for rest-activity disruption in institutionalized patients with severe alzheimers disease," *Internal Journal of Psychogeriatry*, vol. 17, pp. 221–236, 2005.

[104] P. Fontana-Gasio, K. Kräuchi, C. Cajochen, E. Someren, I. Amrhein, M. Pache, E. Savaskan, and A. Wirz-Justice, "Dawndusk simulation light therapy of disturbed circadian restactivity cycles in demented elderly," *Exp Gerontol*, vol. 38, pp. 207–216, 2003.

[105] E. Mester, B. Szende, and P. Gärtner, "The effect of laser beams on the growth of hair in mice," *Radiobiology Radiotherapy (Berl)*, vol. 9, no. 5, pp. 621–626, 1968.

[106] J. Jones and J. Dang, "The plant immune system," *Nature*, vol. 444, pp. 323–329, 2006.

[107] J. Dang and J. Jones, "Plant pathogens and integrated defence responses to infection," *Nature*, vol. 411, pp. 826–833, 2001.

[108] S. Shimizu-Sato, E. Huq, J. Tepperman, and P. Quail1, "A light-switchable gene promoter system," *Nature Biotechnology*, vol. 20, pp. 1041–1044, 2002.

[109] R. Bhattacharyya, A. Reményi, B. Yeh, and W. Lim, "Domains, motifs, and scaffolds: the role of modular interactions in the evolution and wiring of cell signaling circuits," *Annual Review Biochemistry*, vol. 75, pp. 655–680, 2006.

[110] T. Pawson and P. Nash, "Assembly of cell regulatory systems through protein interaction domains," *Science*, vol. 300, pp. 445–452, 2003.

[111] J. Chin, "Programming and engineering biological networks," *Current Opinion in Structural Biology*, vol. 16, no. 4, pp. 551–556, 2006.

[112] P. Pryciak, "Designing new cellular signaling pathways," *Chemical Biology*, vol. 16, no. 3, pp. 249–254, 2009.

[113] A. Levskaya, O. Weiner, W. Lim, and C. Voigt, "Spatiotemporal control of cell signalling using a light-switchable protein interaction," *Nature*, vol. 461, pp. 997–1001, September 2009.

[114] J. Mettetal, D. Muzzey, C. Gómez-Uribe, and A. van Oudenaarden, "The frequency dependence of osmo-adaptation in saccharomyces cerevisiae," *Science*, vol. 319, no. 5862, pp. 482–484, 2008.

[115] R. Neira, J. Arroyave, H. Ramirez, C. Ortiz, E. Solarte, F. Sequeda, and M. Gutierrez, "Fat liquefaction: Effect of low-level laser energy on adipose tissue," *Plast Reconstr Surg*, vol. 110, no. 3, pp. 912–922 discussion 923–925, 2002.

[116] R. Niera, E. Solarte, and M. Reyes, "Low level assisted lipoplasty: A new technique," in *In Proceedings of the World Congress on Liposuction, Dearborn, MI*, pp. 13–15, 2000.

[117] P. King, "Low level laser therapy: A review," *Laser Med Sci*, vol. 4, no. 3, pp. 141–150, 1989.

[118] G. Baxter, A. Bell, J. Allen, and J. Ravey, "Low level laser therapy: Current clinical practice in northern ireland," *Physiotherapy*, vol. 77, no. 3, pp. 171–178, 1991.

[119] J. Oschmann, *Energy medicine: The scientific basis*. Edinburgh: Churchill Livingstone, 2000.

[120] A. Fonseca, T. Moreira, L. Paixão, F. Farias, O. Guimaraes, S. de Paoli, M. Geller, and F. de Paoli, "Effect of laser therapy on dna damage," *Lasers in Surgery and Medicine*, vol. 42, no. 6, pp. 481–488, 2010.

[121] A. Fonseca, M. Geller, M. Filho, S. Valenca, and F. de Paoli, "Low-level infrared laser effect on plasmid dna," *Lasers in Medical Science*, 2011.

[122] A. Fonseca, A. Teixeira, G. Presta, M. Geller, S. Valenca, and F. Paoli, "Low intensity infrared laser effects on escherichia coli cultures and plasmid dna," *Laser Physics*, vol. 22, no. 10, pp. 1635–1641, 2012.

[123] C. Oliveira, F. Basso, R. dos Reis, L. Parreiras-e Silva, E. Lins, C. Kurachi, J. Hebling, V. Bagnato, and C. deSouza Costa, "In vitro transdentinal effect of low-level laser therapy," *Laser Physics*, vol. 23, no. 3, pp. 288–297, 2013.

[124] J. Kujawa, I. Zavodnik, A. Lapshina, M. Labieniec, and M. Bryszewska, "Cell survival, dna, and protein damage in b14 cells under low-intensity near-infrared (810 nm) laser irradiation," *Photomedicine and Laser Surgery*, vol. 22, no. 6, pp. 504–508, 2004.

[125] T. Sasaki, K. Beppu, K. Tanaka, Y. Fukazawa, R. Shigemotoa, and K. Matsuia, "Application of an optogenetic byway for perturbing neuronal activity via glial photostimulation," *PNAS, Proceedings of the National Academy of Sciences*, vol. 109, no. 50, pp. 20720–20725, 2012.

[126] A. Vazquez, M. Fukuda, J. Crowley, and S. Kim, "Neural and hemodynamic responses elicited by forelimb- and photo-stimulation in channelrhodopsin-2 mice: Insights into the hemodynamic point spread function," *Oxford Journals*, 2013.

[127] K. Dittmann, C. Mayer, B. Fehrenbacher, M. Schaller, U. Raju, L. Milas, D. Chen, R. Kehlbach, and H. Rodemann, "Radiation-induced epidermal growth factor receptor nuclear import is linked to activation of dna-dependent protein kinase," *Journal of Biological Chemistry*, vol. 280, pp. 31182–31189, 2005.

[128] J. Kujawa, L. Zavodnik, I. Zavodnik, V. Buko, A. Lapshyna, and M. Bryszewska, "Effect of low-intensity (3.75-25 j/cm2) near-infrared (810nm) laser radiation on red blood cell atpase activities and membrane structure," *Journal of Clin Laser Med Surg*, vol. 22, no. 2, pp. 111–117, 2004.

[129] T. Kameya, S. Ide, and J. Acorda, "Effect of different wavelengths of low level laser therapy on wound healing in mice," *Laser Therapy*, vol. 7, pp. 33–36, 1995.

[130] H. Frohlich, "Long-range coherence and energy storage in biological systems," *International Journal of Quantum Chemistry*, vol. 2, no. 5, pp. 641–649, 1968.

[131] H. Frohlich, "Long range coherence and the action of enzymes," *Nature*, vol. 228, no. 5276, p. 1093, 1970.

[132] H. Frohlich, "The extraordinary dielectric properties of biological materials and the action of enzymes," *Proceeding of National Academy of Science*

USA, vol. 72, no. 11, pp. 4211–4215, 1975.

[133] R. Sroka, M. Schaffer, C. Fuchs, T. Pongratz, U. Schrader-Reichard, M. Busch, P. Schaffer, E. Dühmke, and R. Baumgartner, "Effects on the mitosis of normal and tumor cells induced by light treatment of different wavelenghts," *Lasers Surgery Medicine*, vol. 25, no. 3, pp. 263–271, 1999.

[134] H. van Breugel and P. Bar, "Power density and exposure time of hene laser irradiation are more important than total energy dose in photo-biomodulation of human fibroblasts in vitro," *Lasers Surgery Medicine*, vol. 12, no. 5, pp. 528–537, 1992.

[135] F. Al-Watban and X. Zang, "Comparison of the effects of laser therapy on wound healing using different laser wavelengths," *Laser Therapy*, vol. 8, no. 2, pp. 127–135, 1996.

[136] W. Posten, D. Wrone, J. Dover, K. Arndt, S. Silapunt, and M. Alam, "Low-level laser therapy for wound healing: Mechanism and efficacy," *Dermatology Surgery*, vol. 31, pp. 334–340, 2005.

[137] D. Hawkins, N. Hourld, and H. Abarahamse, "Low level laser therapy (lllt) as an effective therapeutic modality for delayed wound healing," *New York Academy of Science*, vol. 1056, pp. 486–493, 2005.

[138] S. Roberts, "Led light therapy." `heelspurs.comLLC`, 2008.

[139] E. Mester, A. Korenyi-Both, and T. Spiry, "Stimulation of wound healing by means of laser rays. clinical and electron microscopical study," *Acta Chir Acad Sci Hung*, vol. 14, no. 4, pp. 347–356, 1973.

[140] A. Lowe, M. Walker, M. O'Byrne, G. Baxter, and D. Hirst, "Effect of low intensity monochromatic light therapy (890 nm) on a radiation-impaired, wound-healing model in murine skin," *Lasers in Surgery and Medicine*, vol. 23, pp. 291–298, 1998.

[141] S. Kasai, T. Kono, Y. Yamamoto, H. Kotani, T. Sakamoto, and M. Mito, "Effect of low-power laser irradiation on impulse conduction in anesthetized rabbits," *Journal of Clinical Laser Medicine Surgery*, vol. 14, no. 3, pp. 107–109, 1996.

[142] T. Ohno, "Pain suppressive effect of low power laser irradiation. a quantitative analysis of substance p in the rat spinal dorsal root ganglion," *Nihon Ika Daigaku Zasshi*, vol. 64, no. 5, pp. 395–400, 1997.

[143] K. Saber, N. Chiniforush, and S. Shahabi, "The effect of low level laser therapy on pain reduction after third molar surgery," *Minerva Stomatol*, vol. 61, no. 7-8, pp. 319–322, 2012.

[144] M. Miloro, L. Halkias, S. Mallery, S. Mallery, S. Travers, and R. Rashid, "Low-level laser effect on neural regeneration in gore-tex tubes," *Oral Surg Oral Med Oral Pathol Oral Radiol Endod*, vol. 93, pp. 27–34, 2002.

[145] K. Byrnes, R. Waynant, I. Ilev, X. Wu, L. Barna, K. Smith, R. Heckert, H. Gerst, and J. Anders, "Light promotes regeneration and functional recovery and alters the immune response after spinal cord injury," *Lasers Surgery Medicine*, vol. 36, pp. 171–185, 2005.

[146] Y. Fujimaki, T. Shimoyama, Q. Liu, T. Umeda, S. Nakaji, and K. Sugawara, "Low-level laser irradiation attenuates production of reactive oxygen species by human neutrophils," *Journal of Clinical Laser Medicine Surgery*, vol. 21, pp. 165–170, 2003.

[147] Y. Chen, S. Hsu, C. Chiu, J. Lin, C. Chen, and C. Yao, "Effect of low-power pulsed laser on peripheral nerve regeneration in rats," *Microsurgery*, vol. 25, pp. 83–89, 2005.

[148] V. Poon, L. Huang, and A. Burd, "Biostimulation of dermal fibroblast by sublethal q-switched nd:yag 532 nm laser: collagen remodeling and pigmentation," *Journal of Photochemical Photobiology B 81*, vol. 81, pp. 1–8, 2005.

[149] A. Medrado, L. Pugliese, S. Reis, and Z. Andrade, "Influence of low level laser therapy on wound healing and its biological action upon myofibroblasts," *Lasers Surgery Medicine*, vol. 32, pp. 239–244, 2003.

[150] A. Hussein, A. Alfars, M. Falih, and A. Hassan, "Effects of a low level laser on the acceleration of wound healing in rabbits," *American Journal*

of Medical Science, vol. 3, no. 4, pp. 193–197, 2011.

[151] R. Carvalho, P. Alcantara, F. Kamamoto, M. Cressoni, and R. Casarotto, "Effects of low-level laser therapy on pain and scar formation after inguinal herniation surgery: A randomized controlled single-blind study," *Photomedicine in Laser Surgery*, vol. 28, no. 3, pp. 417–422, 2010.

[152] A. Medrado, L. Pugliese, R. Reis, and Z. Andrade, "Influence of low level laser therapy on wound healing and its biological action upon myofibroblasts," *Lasers Surgery Medicine*, vol. 32, no. 3, pp. 239–244, 2003.

[153] R. Neira, L. Toledo, J. Arroyave, E. Solarte, C. Isaza, O. Gutierrez, W. Criollo, H. Ramirez, M. Gutierrez, and C. Ortiz-Neira, "Low level laser-assisted liposuction: The neira 4 l technique," *Clin Plast Surg*, vol. 33, no. 1, pp. 117–127, 2006.

[154] S. Brown, R. Rohrich, J. Kenkel, V. Young, J. Hoopman, and M. Coimbra, "Effect of low-level laser therapy on abdominal adipocytes before lipoplasty procedures," *Plastic Reconstruction Surgery*, vol. 113, no. 6, pp. 1796–1806, 2004.

[155] R. Neira and C. Ortiz-Neira, "Low-level laser-assisted liposculpture: Clinical report of 700 cases," *Journal of Aesthetic Surgery*, vol. 22, no. 5, pp. 451–455, 2002.

[156] T. Fukuda, M. Tanji, S. Silva, M. Sato, and H. Plapler, "Infrared low-level diode laser on inflammatory process modulation in mice: pro- and anti-inflammatory cytokines," *Lasers in Medical Science*, vol. 28, no. 5, pp. 1305–1313, 2012.

[157] L. Assis, A. Moretti, T. Abrahao, V. Cury, H. Souza, M. Hamblin, and N. Parizotto, "Low-level laser therapy (808 nm) reduces inflammatory response and oxidative stress in rat tibialis anterior muscle after cryolesion," *Lasers Surgery Medicine*, vol. 44, no. 9, pp. 726–735, 2012. doi: 10.1002/lsm.22077.

[158] W. Lim, S. Lee, I. Kim, M. Chung, M. Kim, H. Lim, J. Park, O. Kim, and H. Choi, "The anti-inflammatory mechanism of 635 nm light-emitting-diode irradiation compared with existing cox inhibitors," *Lasers in Surgery and Medicine*, vol. 39, no. 7, pp. 614–621, 2007.

[159] J. Hashmi, Y. Huang, B. Osman, S. Sharma, M. Naeser, and M. Hamblin, "Role of low-level laser therapy in neurorehabilitation," *PM R*, vol. 2, no. 12 Suppl. 2, pp. S292–S305, 2010.

[160] B. Ivandic and T. Ivandic, "Low-level laser therapy improves vision in patients with age-related macular degeneration," *Photomedicine Laser Surgery*, vol. 26, no. 3, pp. 241–245, 2008.

[161] H. Tuby, L. Maltz, and U. Oron, "Induction of autologous mesenchymal stem cells in the bone marrow by low-level laser therapy has profound beneficial effects on the infarcted rat heart," *Lasers Surgery Medicine*, vol. 43, no. 5, pp. 401–409, 2011.

[162] C. Rhee, P. He, J. Jung, J. Ahn, P. Chung, and M. Suh, "Effect of low-level laser therapy on cochlear hair cell recovery after gentamicin-induced ototoxicity," *Lasers Medicine Science*, vol. 27, no. 5, pp. 987–992, 2012.

[163] M. Hamblin and T. Demidova, "Mechanism of low level light therapy," *Proc. of SPIE*, vol. 6140, no. 614001, 2006.

[164] S. Ganji, *Effect of light-emitting diode curing light on human buccal mucosa.* PhD thesis, Karolinska Institute, Nr114, Stokholm, 2006.

[165] J. Eells, M. Wong-Riley, J. VerHoeve, M. Henry, E. Buchman, M. Kane, L. Gould, R. Das, M. Jett, B. Hodgson, D. Margolis, and H. Whelan, "Mitochondrial signal transduction in accelerated wound and retinal healing by near-infrared light therapy," *Mitochondrion*, vol. 4, pp. 559–567, 2004.

[166] D. Barolet, "Light-emitting diodes (leds) in dermatology," *Lasers and Lights*, vol. 27, no. 4, pp. 227–238, 2008.

[167] A. Schindl, H. Merwald, L. Schindl, C. Kaun, and J. Wojta, "Direct stimulatory effect of low-intensity 670 nm laser irradiation on human endothelial cell proliferation," *Journal of Dermatology*, vol. 148, pp. 334–336, 2003.

[168] R. Weiss, D. McDaniel, R. Geronemus, and M. Weiss, "Clinical trial of a novel non-thermal led array for reversal of photoaging: Clinical, histologic, and surface profilometric results," *Lasers in Surgery and Medicine*, vol. 36, no. 2, pp. 85–91, 2005.

[169] F. Jackson, R. Gregory, and T. Mangione, "Low-level laser therapy effectiveness for reducing pain after breast augmentation," *American Journal of Cosmetic Surgery*, vol. 26, no. 3, pp. 144–148, 2009.

[170] P. Avci, T. Nyame, G. Gupta, M. Sadasivam, and M. Hamblin, "Low-level laser therapy for fat layer reduction: A comprehensive review," *Lasers in Surgery and Medicine*, vol. 45, no. 6, pp. 349–357, 2013.

[171] A. Sterodimas, F. Boriani, E. Magarakis, B. Nicaretta, L. Pereira, and Y. Illouz, "Thirty four years of liposuction: Past, present and future," *Eur Rev Med Pharmacol Sci*, vol. 16, no. 3, pp. 393–406, 2012.

[172] B. Katz and J. McBean, "Laser-assisted lipolysis: A report on complications," *Journal of Cosmetic Laser Therapy*, vol. 10, no. 4, pp. 231–233, 2008.

[173] N. Sadick, "Overview of ultrasound-assisted liposuction, and body contouring with cellulite reduction," *Semin Cutan Med Surg*, vol. 28, no. 4, pp. 250–256, 2009.

[174] H. Jalian and H. Avram, "Body contouring: The skinny on noninvasive fat removal," *Semin Cutan Med Surg*, vol. 31, no. 2, pp. 121–125, 2012.

[175] G. Sasaki, K. Oberg, B. Tucker, and B. Gaston, "The effectiveness and safety of topical photo actif phosphatidylcholine-based anti-cellulite gel and led (red and near-infrared) light on grade iiiii thigh cellulite: A randomized, double-blinded study," *Journal of Cosmetic Laser Therapy*, vol. 9, no. 2, pp. 87–96, 2007.

[176] E. Lach, "Reduction of subcutaneous fat and improvement in cellulite appearance by dual-wavelength, low-level laser energy combined with vacuum and massage," *Journal of Cosmetic Laser Therapy*, vol. 10, no. 4, pp. 202–209, 2008.

[177] R. Jackson, F. Stern, R. Neira, C. Ortiz-Neira, and J. Maloney, "Application of low-level laser therapy for noninvasive body contouring," *Laser Surgery Medicine*, vol. 44, no. 3, pp. 211–217, 2012.

[178] M. Caruso-Davis, T. Guillot, V. Podichetty, N. Mashtalir, N. Dhurandhar, O. Dubuisson, Y. Yu, and F. Greenway, "Efficacy of low-level laser therapy for body contouring and spot fat reduction," *Obes Surgery*, vol. 21, no. 6, pp. 722–729, 2011.

[179] M. Nestor, M. Zarraga, and H. Park, "Effect of 635 nm low-level laser therapy on upper arm circumference reduction: A double-blind, randomized,

sham-controlled trial," *Journal of Clinical Aesthetic Dermatology*, vol. 5, no. 2, pp. 42–48, 2012.

[180] M. Gold, K. Khatri, K. Hails, R. Weiss, and N. Fournier, "Reduction in thigh circumference and improvement in the appearance of cellulite with dual-wavelength, low-level laser energy and massage," *Journal of Cosmet Laser Therapy*, vol. 13, no. 1, pp. 13–20, 2011.

[181] V. Podichetty and D. Bourassa, "Effects of low-level laser therapy in subcutaneous fat reduction and improvement in body contour," *Lasers Surgery Medicine*, vol. 42, no. Suppl.22, p. 62, 2010.

[182] M. Nestor, J. Newburger, and M. Zarraga, "Body contouring using 635-nm low level laser therapy," *Semin Cutan Med Surg*, vol. 32, no. 1, pp. 35–40, 2013.

[183] F. Jackson, G. Roche, and K. Wisler, "Reduction in cholesterol and triglyceride serum levels following low-level laser irradiation: A non-controlled, nonrandomized pilot study," *American Journal of Cosmetic Surgery*, vol. 27, no. 4, pp. 177–184, 2010.

[184] A. Rushdi, "Effect of low-level laser therapy on cholesterol and triglyceride serum levels in icu patients: A controlled, randomized study," *EJCTA*, vol. 4, pp. 96–99, 2010.

[185] C. Creighton, M. Landis, J. Chang, M. Dixonb, V. Neumeisterc, A. Rimmc, H. Wonga, A. Rodrigueza, J. Herschkowitza, C. Fand, X. Zhanga, X. Hec, A. Pavlicka, M. Gutierreza, L. Renshawb, A. Larionovb, D. Faratianb, S. Hilsenbecka, C. Peroud, M. Lewisa, J. Rosena, and C. Changa, "Residual breast cancers after conventional therapy display mesenchymal as well as tumor-initiating features," *Proceedings of the National Academy of Sciences of the United States of America*, vol. 106, no. 33, pp. 13820–13825, 2009.

[186] E. Pirogova, V. Vojisavlejevic, T. Istivan, P. Coloe, and I. Cosic, "Review study: Influence of electromagnetic radiation on enzyme activity and effects of synthetic peptides on cell transformation," *Medical Data*, vol. 2, no. 4, pp. 317–324, 2010.

[187] C. Lin and W. Yang, "Prognostic factors influencing the patency of hemodialysis vascular access: Literature review and novel therapeutic modality by far infrared therapy," *J Chin Med Assoc*, vol. 72, no. 3, pp. 109–116, 2009.

[188] T. Karu, "Molecular mechanism of the therapeutic effect of low-intensity laser radiation," *Lasers in the Life Sciences*, vol. 2, no. 1, pp. 53–74, 1988.

[189] E. Vinck, B. Cagnie, M. Cornelissen, H. Declercq, and D. Cambier, "Increased fibroblast proliferation induced by light emitting diode and low

power laser irradiation," *Lasers in Medical Science*, vol. 18, no. 2, pp. 95–99, 2003.

[190] J. Eells, M. Wong-Riley, J. VerHoeve, M. Henry, E. Buchman, M. Kane, L. Gould, R. Das, M. Jett, B. Hodgson, D. Margolis, and H. Whelan, "Mitochondrial signal transduction in accelerated wound and retinal healing by near-infrared light therapy," *Mitochondrial Medicine*, vol. 4, no. 5-6, pp. 559–567, 2004.

[191] K. Smith, "Laser (and led) therapy is phototherapy," *Photomedicine and Laser Surgery*, vol. 23, no. 1, pp. 78–80, 2005.

[192] E. Vinck, B. Cagnie, M. Cornelissen, H. Declercq, and D. Cambier, "Green light emitting diode irradiation enhances fibroblast growth impaired by high glucose level," *Photomedicine and Laser Surgery*, vol. 23, no. 2, pp. 167–171, 2005.

[193] M. Rosenbaum, V. Prieto, J. Hellmer, M. Boschmann, J. Krueger, R. Leibel, and A. Ship, "An exploratory investigation of the morphology and biochemistry of cellulite," *Plast Reconstr Surg*, vol. 101, no. 7, pp. 1934–1939, 1998.

[194] K. Ball, P. Castell, and R. Poyton, "Low intensity light stimulates nitrite-dependent nitric oxide synthesis but not oxygen consumption by cytochrome c oxidase: Implications for phototherapy," *Journal of Photochemistry and Photobiology B: Biology*, vol. 102, no. 3, pp. 182–191, 2011.

[195] K. Desmet, D. Paz, J. Corry, J. Eells, M. Wong-Riley, M. Henry, E. Buchmann, M. Connelly, J. Dovi, H. Liang, D. Henshel, R. Yeager, D. Millsap, J. Lim, L. Gould, R. Das, M. Jett, B. Hodgson, D. Margolis, and H. Whelan, "Clinical and experimental applications of nir-led photobiomodulation," *Photomedicine and Laser Surgery*, vol. 24, no. 2, pp. 121–128, 2006.

[196] R. Jeffrey and M. Basford, "Low intensity laser therapy: Still not an established clinical tool," *Lasers in Surgery and Medicine*, vol. 16, no. 4, pp. 331–342, 2005.

[197] A. Renno, P. McDonnell, N. Parizotto, and E. Laakso, "The effects of laser irradiation on osteoblast and osteosarcoma cell proliferation and differentiation in vitro," *Journal of Photomedicine for Laser Surgery*, vol. 25, no. 4, pp. 275–280, 2007.

[198] Y. Huang, A. Chen, S. Sharma, Q. Wu, and M. Hamblin, "Comparison of cellular responses induced by low level light in different cell types," in *Proc. SPIE 7552*, vol. 75520A, 2010.

[199] T. Karu, "Mitochondrial signaling in mammalian cells activated by red and near-ir radiation," *Photochem. Photobiol*, vol. 84, no. 5, pp. 1091–1099, 2008.

[200] T. Karu, L. Pyatibrat, and G. Kalendo, "Photobiological modulation of cell attachment via cytochrome c oxidase," *Photochem. Photobiol. Sci*, vol. 3,

no. 2, pp. 211–216, 2004.

[201] T. Karu, "Mitochondrial mechanisms of photobiomodulation in context of new data about multiple roles of atp," *Photomedicine Laser Surgery*, vol. 28, no. 2, pp. 159–160, 2010.

[202] T. Karu and S. Kolyakov, "Exact action spectra for cellular responses relevant to phototherapy," *Photomed Laser Surg*, vol. 23, no. 4, pp. 355–361, 2005.

[203] S. Wu, D. Xing, X. Gao, and W. Chen, "High fluence low-power laser irradiation induces mitochondrial permeability transition mediated by reactive oxygen species," *Journal of Cellular Physiology*, vol. 218, no. 3, pp. 603–611, 2009.

[204] T. Karu, L. Pyatibrat, and N. Afanasyeva, "A novel mitochondrial signaling pathway activated by visible-to-near infrared radiation," *Journal Photochemical and Photobiological*, vol. 80, no. 2, pp. 366–372, 2004.

[205] R. Lubart, M. Eichler, R. Lavi, H. Friedman, and A. Shainberg, "A low-energy laser irradiation promotes cellular redox activity," *Journal of Photomedicine Laser Surgery*, vol. 23, no. 1, pp. 3–9, 2005.

[206] W. Yang, X. Xiao, J. Tan, and Q. Cai, "In situ evaluation of breast cancer cell growth with 3d atr-ftir spectroscopy," *Vib. Spec.*, vol. 49, no. 1, pp. 64–67, 2009.

[207] J. Tafur and P. Mills, "Low-intensity light therapy: Exploring the role of redox mechanisms," *Photomedicine and laser surgery*, vol. 26, no. 4, pp. 323–328, 2008.

[208] Y. Tanaka, K. Matsuo, S. Yuzuriha, H. Yan, and J. Nakayama, "Non-thermal cytocidal effect of infrared irradiation on cultured cancer cells using specialized device," *Cancer Science*, vol. 101, no. 6, pp. 1396–1402, 2010.

[209] I. Coutinho, M. Correia, V. Thiagarajan, G. Gajula, S. Petersen, and M. Neves-Petersen, "Photonic cancer therapy modulating cellular metabolism with light," *Proceeding of SPIE*, vol. 8568 856806-5, 2013.

[210] M. Lima, J. Lima, M. de Andrade, and A. Bergmann, "Low-level laser therapy in secondary lymphedema after breast cancer: systematic review.," *Lasers in Medical Science*, 2012.

[211] A. Simões, F. Eduardo, A. Luiz, L. Campos, P. Sá, M. Cristófaro, M. Marques, and C. Eduardo, "Laser phototherapy as topical prophylaxis against head and neck cancer radiotherapy-induced oral mucositis: Comparison between low and high/low power lasers," *Lasers in Surgery and Medicine*, vol. 41, no. 4, pp. 264–270, 2009.

[212] A. Schindl, M. Schindl, H. Pernerstorfer-Schön, U. Mossbacher, and L. Schindl, "Low intensity laser irradiation in the treatment of recalcitrant radiation ulcers in patients with breast cancer -long-term results of 3 cases,"

Photodermatology Photoimmunology Photomedicine, vol. 16, no. 1, pp. 34–37, 2000.

[213] G. Lyman, D. Dale, and J. Crawford, "Incidence and predictors of low dose-intensity in adjuvant breast cancer chemotherapy: a nationwide study of community practices," *Journal Clinical Oncology*, vol. 21, no. 24, pp. 4524–4531, 2003.

[214] A. Sommer, D. Zhu, and T. Scharnweber, "Extraordinary anticancer effect of green tea and red light," *Photomedicine and Laser Surgery*, vol. 28, no. 3, pp. 429–430, 2010.

[215] A. Pinheiro, N. Carneiro, A. Vieira, A. Brugnera, F. Zanin, R. Barros, and P. Silva, "Effects of low-level laser therapy on malignant cells: In vitro study," *Journal of Clinical Laser Medicine and Surgery*, vol. 20, no. 1, pp. 23–26, 2004.

[216] C. Migliorati, I. Hewson, R. Lalla, H. Antunes, C. Estilo, B. Hodgson, N. Lopes, M. Schubert, J. Bowen, and S. Elad, "Systematic review of laser and other light therapy for the management of oral mucositis in cancer patients," *Support Care Cancer*, vol. 21, pp. 333–341, 2013.

[217] L. Frigo, J. Luppi, G. Favero, D. Maria, S. Penna, J. Bjordal, R. Bensadoun, and R. Lopes-Martins, "The effect of low-level laser irradiation (in-ga-al-

asp- 660 nm) on melanoma in vitro and in vivo," *BioMed Central Cancer*, vol. 9, pp. 404–413, 2009.

[218] T. Magrini, N. Villa dos Santos, M. Milazzotto, G. Cerchiaro, and H. da Silva Martinho, "Low-level laser therapy on mcf-7 cells: a micro-fourier transform infrared spectroscopy study," *Journal of Biomedical Optics*, vol. 17, no. 10, p. 101516, 2012.

[219] G. Maiya, M. Sagar, and D. Fernandes, "Effect of low level helium-neon (he-ne) laser therapy in the prevention and treatment of radiation induced mucositis in head and neck cancer patients," *Indian Journal of Medical Research*, vol. 124, pp. 339–402, 2006.

[220] Y. Tanaka, N. Tatewaki, H. Nishida, T. Eitsuka, N. Ikekawa, and J. Nakayama, "Non-thermal dna damage of cancer cells using near-infrared irradiation," *Cancer Science*, vol. 103, no. 8, pp. 1467–1473, 2012.

[221] Y. Tanaka, K. Matsuo, and S. Yuzuriha, "Differential long-term stimulation of type i versus type iii collagen after infrared irradiation," *Dermatology Surgery*, vol. 35, pp. 1099–1104, 2009.

[222] Y. Tanaka, K. Matsuo, and S. Yuzuriha, "Long-term evaluation of collagen and elastin following infrared (1100 to 1800 nm) irradiation," *Journal of Drugs Dermatology*, vol. 8, pp. 708–712, 2009.

[223] Y. Tanaka, K. Matsuo, and S. Yuzuriha, "Long-term histological comparison between near-infrared irradiated skin and scar tissues," *Clinical Cosmetic Investigation Dermatology*, vol. 3, pp. 143–149, 2010.

[224] Y. Tanaka, K. Matsuo, and S. Yuzuriha, "Objective assessment of skin rejuvenation using near-infrared 1064-nm neodymium:yag laser in asians," *Clinical Cosmetic Investigation Dermatology*, vol. 4, pp. 123–130, 2011.

[225] B. Saleh, *Fundamentals of photonics*. John Wiley and Son Inc., 1991.

[226] S. Kasap, *Optoelectronics and Photonics*. Prentice Hall, 2001.

[227] G. Keiser, *Optical Fiber Communications*. McGraw Hill, 2000.

[228] T. Karu, "Cellular mechanism of low power laser therapy: new questions," *Lasers in Medicine and Dentistry*, 2003.

[229] A. M. Encyclopedia, "Light therapy." `http://www.answers.com`.

[230] A. Lowe, M. Walker, M. O'byrne, G. Baxter, and D. Hirst, "Effect of low intensity monochromatic light therapy (890 nm) on a radiation-impaired, wound-healing model in murine skin," *Lasers in Surgery and Medicine*, vol. 23, pp. 291–298, 1998.

[231] T. Vo-Dinh, ed., *Biomedical Photonics Handbook*. CRC Press, 2003.

[232] Y. Vladimirov, "Photobiological principles of therapeutic applications of laser radiation," *et al in Biochemestry (Moscow)*, vol. 69, 2004.

[233] LED Microsensor, "Leds data sheet." http://www.ledmicrosensor.com/2750led.htm, 2012.

[234] OPTEK Technology INC., "Converting radiant intensity in units of mw/cm^2 to mw/sr." www.optekinc.com, 2003.

[235] P. H. Society, "The international commission on non-ionizing radiation protection (icnirp)," 2011.

[236] L. Hode, "Penetration of light into living tissue." http://www.laser.nu/, 2012.

[237] I. Therapies, "Depth of penetration." http://nirtherapy.com/penetration.php, 2006.

[238] V. Setnicka, "Ft-ir reflection technique." http://www.vscht.cz/anl/vibspec/FTIR\%20Reflection\%20Techniques.pdf, 2011.

[239] Public Health England, "General cell collection: B16 melanoma." http://www.hpacultures.org.uk/products/celllines/generalcell/detail.jsp?refId=94042254&collection=ecacc_gc, 2013.

[240] ATCC, "Mcf7, essentials of science research." http://www.atcc.org/products/all/HTB-22.aspx, 2012.

[241] Invitrogen life technology, "Products." www.invitrogen.com, 2013.

[242] G. Haslam, D. Wyatt, and P. Kitos, "Estimating the number of viable animal cells in multi-well cultures based on their lactate dehydrogenase activities," *Cytotechnology*, vol. 32, no. 63-75, 2000.

[243] H. Wolterbeek and A. Meer, "Optimization, application, and interpretation of lactate dehydrogenase measurements in microwell determination of cell number and toxicity," *Assay and Drug Development Technologies*, vol. 3, 2005.

[244] R. A. Science, "Cytotoxicity detection kit (ldh)." `https://cssportal.roche.com/LFR_PublicDocs/ras/11644793001_en_07.pdf`, 2005.

[245] T. Mosmann, "Rapid colorimetric assay for cellular growth and survival: Application to proliferation and cytotoxicity assays," *Journal of Immunological Methods*, vol. 65, no. 55-63, 1983.

[246] Invitrogen, Life Technologies, "Vybrant mtt cell proliferation assay kit." `http://www.invitrogen.com/site/us/en/home/References/protocols/cell-culture/mtt-assay-protocol/vybrant-mtt-cell-proliferation-assay-kit.html`, 2002.

[247] Wallert and P. Lab, "Proliferation assay." `http://web.mnstate.edu/provost/mtt%20proliferation%20assay%20protocol.pdf`, 2007.

[248] N. Almansour, E. Pirogova, P. Coloe, I. Cosic, Istivan, and T., "A bioactive peptide analogue for myxoma virus protein with a targeted cytotoxicity for

human skin cancer *in vitro*," *Journal of Biomedical Science*, vol. 19, no. 65, pp. 1–13, 2012.

[249] I.-L. Technologies, "Prestoblue cell viability reagent frequently asked questions." `http://tools.invitrogen.com/content/sfs/manuals/PrestoBlueFAQ.pdf`, 2012.

[250] S. Ruzin, *Plant Microtechnique and Microscopy*. Oxford University Press, 1999.

[251] J. Murray, K. Spring, I. Johnson, W. Metcalfe, A. Lerant, K. Riddle, H. Bass, P. Fajer, A. Cusma, M. Parry-Hill, and M. Davidson, "Laser scanning confocal microscopy." `http://micro.magnet.fsu.edu/primer/virtual/confocal/`, 2006.

[252] C. C. Company, *Annexin V FITC Assay Kit(Cayman)*.

[253] I. Cosic, *The Resonant Recognition Model of Macromolecular Bioactivity*, vol. 8 of *BioMethods*. Birkhäuser Verlag, 1997.

[254] I. Cosic, "Macromolecular bioactivity: Is it resonant interaction between molecules?theory and applications," *IEEE Trans. Biomed. Eng.*, vol. 41, pp. 1101–1114, 1994.

[255] E. Pirogova, V. Vojisavlejevic, and I. Cosic, "Biological effects of electromagnetic radiation," review report, RMIT university, Australia, 2001.

[256] V. Vojisavljevic, E. Pirogova, and I. Cosic, "The effect of electromagnetic radiation (550nm-850nm) on l-lactate dehydrogenase kinetics," *Radiation Biology*, vol. 83, no. 4, pp. 221–230, 2006.

[257] P. Peidaee, I. Cosic, and E. Pirogova, "Low intensity light therapy exposure system," *World Congress on Medical Physics and Biomedical Engineering(IFMBE Proceedings)*, vol. 39, pp. 1648–1651, May 2012.

[258] G. Biscar, "Photon enzyme activation," *Bull. Math. Biology*, vol. 38, pp. 29–38, 1986.

[259] I. Cosic and S. Birch, "Photoreceptors having similar structure but different absorptions can be distinguished using the resonant recognition model," *Proc. IEEE EMBS*, vol. 16, pp. 265–266, 1994.

[260] I. Cosic, "Virtual spectroscopy for fun and profit," *Biotechnology*, vol. 13, pp. 236–238, 1995.

[261] I. Cosic, V. Vojisavlejevic, and M. Pavlovic, "The relationship of the resonant recognition model to effects of low-inensity light on cell growth," *International Journal of Radiation Biology*, vol. 56, no. 2, pp. 179–191, 1998.

[262] I. Cosic and E. Pirogova, "Bioactive peptide design using the resonant recognition model," *Nonlinear Biomedical Physics*, vol. 1, no. 7, pp. 1–17, 2007.

[263] Harvard University Taken from The Optical Absorption of Water Compendium, "Absorption spectra of water," 2014.

[264] M. Chaplin, "Water structure and science," 2014.

[265] T. Brown, *Genomes*. Department of Biomolecular Sciences, UMIST, Manchester, UK: Oxford: Wiley-Liss, Garland Science, 2nd edition ed., 2002.

[266] BD Biosciences, "Apoptosis, cell cycle, and cell proliferation." `http://www.bdbiosciences.com/research/apoptosis/analysis/index.jsp`, 2013.

[267] Cancer Research UK, "Cancer and research." `http://www.cancerresearchuk.org`, 2010.

[268] Kimball's Biology Pages, "The cell cycle." `http://users.rcn.com/jkimball.ma.ultranet/BiologyPages/C/CellCycle.html`, 2013.

[269] C. Sherr and J. Roberts, "Inhibitors of mammalian g1 cyclin-dependent kinases," *Genes Device*, vol. 9, p. 1149, 1995.

[270] W. el Deiry, T. Tokino, V. Velculescu, D. Levy, R. Parsons, J. Trent, D. Lin, W. Mercer, K. Kinzler, and B. Vogelstein, "Waf1, a potential mediator of p53 tumor suppression," *Cell*, vol. 75, no. 4, pp. 817–825, 1993.

[271] Nature, *Cell Cycle and Cell Division*. Nature, 2013.

[272] V. Smits and R. Medema, "Checking out the g2/m transition," *Biochimica et Biophysica Acta*, vol. 1519, pp. 1–12, 2001.

[273] M. Kirsch-Volders, E. Cundari, and B. Verdoodt, "Towards a unifying model for the metaphase/anaphase transition," *Mutagenesis*, vol. 13, no. 4, pp. 321–335, 2004.

[274] N. Cahuzac, A. Studenya, K. Marshall, I. Versteege, K. Wetenhall, B. Pfeiffer, S. Leonce, J. Hickman, A. Pierre, and R. Golsteyn, "An unusual dna binding compound, s23906, induces mitotic catastrophe in cultured human cells," *Cancer Letters*, vol. 289, no. 2, pp. 178–187, 2010.

[275] E. Stadtman, "Metal ion-catalyzed oxidation of proteins: Biochemical mechanism and biological consequences," *Radical Biology and Medicine*, vol. 9, no. 4, pp. 315–325, 1990.

[276] B. Levine and D. Klionsky, "Development by self-digestion: Molecular mechanisms and biological functions of autophagy," *Developmental Cell*, vol. 6, no. 4, pp. 463–477, 2004.

[277] T. Brown and S. McKnight, "Specificities of protein-protein and protein-dna interaction of gabp alpha and two newly defined ets-related proteins," *Genes and Development*, vol. 6, pp. 2502–2512, 1992.

[278] C. Brändén, *Introduction to Protein Structure*. Garland Publishing, second edition ed., 1999.

[279] G. Petsko and D. Ringe, *Protein Structure and Function*. New Science Press Ltd, 2004.

[280] I. Rayment, "Protein structure," *Encyclopedia of Physical Science and Technology*, vol. 13, pp. 191–218, 2003.

[281] J. Devereux, P. Haeberly, and O. Smithies, "A comprehensive set of sequence analysis programs for the vax," *Nucl. Acids Res.*, vol. 12, pp. 387–395, 1984.

[282] R. Doolottle, "Similar amino acid sequences: Chance or common ancestry?," *Science*, vol. 214, pp. 149–159, 1981.

[283] J. Breg, J. Opheusden, M. Burgering, R. Boelens, and R. Kaptein, "Structure of arc repressor in solution: evidence for a family of β-sheet dna-binding proteins," *Nature*, vol. 346, pp. 586–589, 1990.

[284] J. King, "Deciphering the rules of protein folding," *Chem. Eng. News*, vol. 67, pp. 32–54, 1989.

[285] G. Fasman, *Prediction of Protein Structure and the Principles of Protein Conformation*. Plenum Press, New York, 1989.

[286] C. DeLisi and J. Berzofsky, "T-cell antigenic sites tend to be amphipatic structures," *Proc. Natl. Acad. Sci. USA*, vol. 82, pp. 7048–7052, 1985.

[287] E. Schmid, F. Schneider, and F. Siebert, *Spectroscopy of Biological Molecules: New Advances*. John Wiley & Sons, 1988.

[288] D. Mackay, A. Cross, and A. Hagler, *The role of energy minimisation in simulation strategies of biomolecular systems*. No. 317-357, Plenum Press, New York, 1989.

[289] J. Maple, U. Dinur, and A. Hagler, "Derivation of force field for molecular mechanics and dynamics from ab initio energy surfaces," *Proc. Natl. Acad. USA*, vol. 85, pp. 5350–5354, 1988.

[290] R. Schultz, "Proteins and protein structure," *Brenner's Encyclopedia of Genetics*, pp. 496–500, 2013.

[291] M. Eftink and S. Pedigo, "Protein folding," *Encyclopedia of Physical Science and Technology (Third Edition)*, pp. 179–190, 2003.

[292] I. Rayment, "Protein structure and function," in *Encyclopedia of Physical Science and Technology* (R. Meyers, ed.), pp. 191–218, Elsevier Science Ltd, 2003.

[293] R. Kretsinger, R. Ison, and S. Hovmöller, "Prediction of protein structure," *Methods in Enzymology*, vol. 383, pp. 1–27, 2004.

[294] I. Cosic, A. Drummond, J. Underwood, and M. Hearn, "In vitro inhibition of the actions of basic fgf by a novel 16 amino cid peptide," *Molecular Cell Biochemistry*, vol. 130, pp. 1–9, 1994.

[295] C. Floudas, H. Fung, S. McAllister, M. Mnnigmann, and R. Rajgaria, "Advances in protein structure prediction and de novo protein design: A review," *Chemical Engineering Science*, vol. 61, pp. 966–988, 2006.

[296] M. Dayhoff, "Atlas of protein sequence and structures," *Nat. Biomed. Res. Fund*, vol. 3, pp. 345–352, 1978.

[297] Y. Chou and G. Fasman, "The conformation of glucagon: Predictions and consequences," *Bioc.her7r*, vol. 14, pp. 2536–2540, 1975.

[298] B. Rost, "Review: Protein secondary structure prediction continues to rise," *Journal of Structural Biology*, vol. 134, no. 2-3, pp. 204–218, 2001.

[299] G. Rose, "Secondary structure in protein analysis," *Encyclopedia of Biological Chemistry*, pp. 1–6, 2004.

[300] M. Jacobson, D. Pincus, C. Rappa, T. Day, B. Honig, D. Shaw, and R. Friesner, "A hierarchical approach to all-atom protein loop prediction," *Proteins: Structure, Function, and Bioinformatics*, vol. 55, pp. 351–367, 2004.

[301] X. Li, M. Jacobson, and R. Friesner, "High-resolution prediction of protein helix positions and orientations," *Proteins: Structure Function and Bioinformatics*, vol. 55, pp. 368–382, 2004.

[302] L. Forrest and T. Woolf, "Discrimination of native loop conformations in membrane proteins: decoy library design and evaluation of effective energy scoring functions," *Proteins: Structure, Function, and Bioinformatics*, vol. 52, pp. 491–509, 2003.

[303] J. Klepeis and C. Floudas, "Ab-initio prediction of helical segments in polypeptides," *Journal of Computational Chemistry*, vol. 23, pp. 245–266, 2002.

[304] J. Klepeis and C. Floudas, "Astro-fold: a combinatorial and global optimization framework for ab initio prediction of threedimensional structures of proteins from the amino acid sequence," *Biophysical Journal*, vol. 85, pp. 2119–2146, 2003.

[305] C. Adjiman, I. Androulakis, C. Maranas, and C. Floudas, "A global optimization method, αbb, for process design," *Computers and Chemical Engineering*, vol. 20, pp. S419–S424, 1996.

[306] C. Floudas, *Deterministic Global Optimization: Theory, Methods and Applications, Nonconvex Optimization and its Applications*. Kluwer Academic Publishers, Dordrecht., 2000.

[307] J. Klepeis and C. Floudas, "Astro-fold: Ab-initio secondary and tertiary structure prediction in protein folding," *Computer Aided Chemical Engineering*, vol. 10, pp. 97–102, 2002.

[308] J. Kopp and T. Schwede, "Automated protein structure homology modeling: a progress report," *Pharmacogenomics Journal*, vol. 5, no. 4, pp. 405–416, 2004.

[309] A. Tramontano and V. Morea, "Assessment of homologybased predictions in casp5," *Proteins: Structure, Function, and Bioinformatics*, vol. 53, pp. 352–368, 2003.

[310] J. Liu, H. Hegyi, T. Acton, G. Montelione, and B. Rost, "Automatic target selection for structural genomics on eukaryotes.," *Proteins: Structure, Function, and Bioinformatics*, vol. 56, pp. 188–200, 2004.

[311] A. Fiser, M. Feig, C. Brooks-III, and A. Sali, "Evolution and physics in comparative protein structure modeling," *Accounts of Chemical Research*, vol. 35, pp. 413–421, 2002.

[312] D. Przybylski and B. Rost, "Improving fold recognition without folds," *Journal of Molecular Biology*, vol. 341, pp. 255–269, 2004.

[313] D. Kim, D. Xu, J. Guo, K. Ellrott, and Y. Xu, "Prospect ii: protein structure prediction program for genome-scale applications," *Protein Engineering*, vol. 16, no. 9, pp. 641–650, 2004.

[314] D. Jones, W. Taylor, and J. Thornton, "A new approach to protein fold recognition," *Nature*, vol. 358, pp. 86–89, 1992.

[315] J. Xu, M. Li, D. Kim, and Y. Xu, "Raptor: optimal protein threading by linear programming," *Journal of Bioinformatics and Computational Biology*, vol. 1, pp. 95–117, 2003.

[316] J. Lee, D. Ripoll, C. Czaplewski, J. Pillardy, W. Wedemeyer, and H. Scheraga, "Optimization of parameters in macromolecular potential energy functions by conformational space annealing," *Journal of Physical Chemistry B*, vol. 105, pp. 7291–7298, 2001.

[317] Y. Xia, E. Huang, M. Levitt, and R. Samudrala, "Ab initio construction of protein tertiary structure using a hierarchical approach," *Journal of Molecular Biology*, vol. 300, pp. 171–185, 2000.

[318] J. Lee, S. Kim, K. Joo, I. Kim, and J. Lee, "Prediction of protein tertiary structure using profesy, a novel method based on fragment assembly and conformational space annealing," *Proteins: Structure Function and Bioinformatics*, vol. 56, pp. 704–714, 2004.

[319] Y. Zhang and J. Skolnick, "Spicker: a clustering approach to identify near-native protein folds," *Journal of Computational Chemistry*, vol. 25, pp. 865–871, 2004.

[320] Y. Shao and C. Bystroff, "Predicting interresidue contacts using templates and pathways," *Proteins: Structure, Function, and Bioinformatics*, vol. 53, pp. 497–502, 2003.

[321] R. Srinivasan and G. Rose, "Ab initio prediction of protein structure using linus," *Proteins: Structure, Function, and Bioinformatics*, vol. 47, pp. 489–495, 2002.

[322] C. Czaplewski, S. Oldziej, A. Liwo, and H. Scheraga, "Prediction of the structures of proteins with the unres force field, including dynamic formation and breaking of disulfide bonds," *Protein Engineering Design and Selection*, vol. 17, pp. 29–36, 2004.

[323] J. Klepeis, Y. Wei, M. Hecht, and C. Floudas, "Ab initio prediction of the three-dimensional structure of a de novo designed protein: a double blind case study," *Proteins: Structure, Function, and Bioinformatics*, vol. 58, pp. 560–570, 2005.

[324] I. Cosic, C. deTrad, Q. Fang, and M. Akay, "Protein sequences analysis using the rrm model and wavelet transform methods: A comparative study analysis," *Proc. IEEE-EMBS Asia-Pacific Conf. Biomed. Eng.*, pp. 405–406, 2000.

[325] M. Akay, *Time Frequency and Wavelets in Biological Signal Processing*. Piscataway, IEEE Press, 1998.

[326] C. Trad, Q. Fang, and I. Cosic, "The resonant recognition model (rrm) predicts amino acid residues in highly conservative regions of the hormone prolactin (prl)," *Biophys. Chem.*, vol. 84, no. 2, pp. 149–157, 2000.

[327] I. Cosic and Q. Fang, "Prediction of different wavelet constructions (designs) for analysis of protein sequence," In Proceeding of the 14th International Conference on DSP, 2002.

[328] E. Pirogova, Q. Fang, M. Akay, and I. Cosic, "Investigation of the structure and function relationships of oncogene proteins," *Proceeding of IEEE*, vol. 90, no. 12, pp. 1859–1868, 2002.

[329] L. Veljkovic and M. Slavic, "General model of pseudopotentials," *Physical Review Let.*, vol. 29, pp. 105–108, 1972.